UNIVERSITÄT OSNABRÜCK

The role of Rho5 in oxidative stress response and glucose signalling in *Saccharomyces cerevisiae*

Dissertation
Zur Erlangung des akademischen Grades
Doctor rerum naturalium
(Dr. rer. nat.)

vorgelegt von
Carolin Christin Sterk
Osnabrück, Juli 2020

Fachbereich Biologie/Chemie

Prof. Dr. rer. nat. Jürgen Heinisch
Prof. Dr. rer. nat. Joost Holthuis

Table of contents

1. Introduction 1
1.1 Rho-GTPases 3
1.2 Rho-GTPases in *S. cerevisiae* and other fungi 4
1.3 Regulation of subcellular localization and spatial organization of Rho-GTPases via auxiliary proteins 5
1.3.1 RhoGEFs 5
1.3.2 Rho-GAPs 8
1.3.3 Rho-GDIs 9
1.3.4 Adaptor proteins 11
1.4 Intrinsic structural features of Rho-GTPases that regulate subcellular localization 13
1.4.1 Nucleotide binding state 13
1.4.2 Prenylation 14
1.4.3 Phospholipids and the polybasic region (PBR) 15
1.4.4 Phosphorylation 17
1.5 Aim of this thesis 18

2. Materials & Methods 19
2.1 Materials 19
2.1.1 Chemicals 19
2.1.2 Electronic equipment 19
2.1.3 Enzymes 20
2.1.4 Buffers, solutions and gels 20
2.1.5 Media 21
2.1.5.1 Yeast media 21
2.1.5.2 *E. coli* media 21
2.1.6 Yeast strains used in this study 21
2.1.7 Bacterial strain 25
2.1.8 Oligonucleotides used in this study 25
2.1.9 Pre-existing plasmids used in this study 26
2.1.10 Plasmids constructed in this study 26
2.2 Methods 28
2.2.1 Handling of *Escherichia coli* 28
2.2.1.1 Growth conditions and preparation of over-night culture 28
2.2.1.2 Competent *Escherichia coli* and Transformation with plasmid DNA 28
2.2.2 Handling of yeast strains 28
2.2.2.1 Handling of *Saccharomyces cerevisiae*, preparation of an over-night culture 28
2.2.2.2 Construction of deletion mutants and gene tagging in *Saccharomyces cerevisiae* 29
2.2.2.3 Sporulation, determination of the mating type and crossing 29
2.2.2.4 Tetrad analysis 30
2.2.2.5 Growth and sensitivity analysis by serial drop dilution assay 30
2.2.2.6 Growth analysis and sensitivity in a microwell plate scanner 30
2.2.3 Analysis of DNA 31
2.2.3.1 Polymerase chain reaction (PCR) 31
2.2.3.2 Separation of DNA fragments via agarose gel electrophoresis 31
2.2.3.3 Extraction of DNA fragments from an agarose gel 32
2.2.3.4 Plasmid extraction 32
2.2.3.4.1 From *E. coli* 32

2.2.3.4.2 From *S. cerevisiae* ... 32
2.2.3.5 Sequencing of plasmid DNA ... 32
2.2.3.6 Restriction of DNA with endonucleases ... 33
2.2.3.7 Ligation of DNA fragments ... 33
2.2.3.8 Chromosomal DNA extraction from *Saccharomyces cerevisiae* ... 33
2.2.3.8.1 "Quick-and-dirty" DNA extraction ... 33
2.2.3.8.2 Pure DNA Extraction ... 33
2.2.3.9 Gene synthesis ... 34
2.2.4 Cell Imaging and life-cell fluorescence microscopy ... 34
2.2.5 Abbreviations ... 34

3. Results ... 36
3.1 Importance of the C-terminal region for intracellular distributions of Rho5 ... 36
3.1.1 *In silico* analysis of the primary sequence of Rho5 and its homologues ... 37
3.1.2 Intracellular distribution of wild type Rho5 ... 37
3.1.3 Importance of Rho5's hypervariable region for its intracellular distribution under different growth conditions ... 39
3.1.4 Role of Rho5's extension in signalling and cellular distribution ... 42
3.1.4.1 Rho5's extension is essential for its function in the oxidative stress response and vegetative growth ... 42
3.1.4.2 Inclusion of five amino acids partly re-establishes the PM localization of Rho5 ... 44
3.1.5 The hypervariable region determines function and distribution of yeast Rho5 ... 45
3.1.5.1 Investigations of the hexa-lysine polybasic region of Rho5 ... 46
3.1.5.2 Role of the serine 326 for Rho5 function and distribution ... 49
3.1.5.3 The role of the CAAX motif for Rho5 function ... 52
3.1.6 Constitutively active Rho5 ... 55
3.1.7 Intracellular location of a dominant negative Rho5 variant ... 58
3.2 Artificial recruitment of a GFP-tagged Rho5 and the components of its dimeric GEF to specific membranes ... 59
3.2.1 GFP-recruitment to mitochondria ... 59
3.2.2 Trapping of GFP-Rho5 to mitochondria by stably inherited GFP-binder ... 61
3.2.3 *In vivo* trapping of GFP-Rho5 at the mitochondrial surface results in a hyper-resistance towards hydrogen peroxide ... 62
3.2.4 *In vivo* trapping of GFP-tagged, constitutively active Rho5 exhibits wild-type sensitivity towards oxidative stress ... 63
3.2.5 Trapping of Dck1 and Lmo1, the subunits of the dimeric GEF, to mitochondria ... 64
3.3 Dck1 and Lmo1 relocation ... 66
3.4 *POR1*, encoding the main VDAC in *S. cerevisiae*, genetically interacts with *RHO5* ... 68
3.5 Human Rac1 in the yeast *Saccharomyces cerevisiae* ... 71
3.5.1 Wild-type *HsRAC1* does not complement a *rho5* deletion and does not associate with the plasma membrane ... 71
3.5.2 GFP-*Hs*Rac1 localizes in the cytosol and at intracellular structures ... 73
3.5.3 Function and localization of chimeric *Hs*Rac1 constructs ... 74
3.5.4 The C-terminal half of yeast Rho5 improves peripheral distribution of *Hs*Rac1 ... 76

4. Discussion ... 80
4.1 Role of Rho5's extension in signalling and cellular distribution as compared to human Rac1 in *Saccharomyces cerevisiae* ... 80
4.2 GTPase activity and nutrient signalling ... 83
4.3 The CAAX motif ... 88

4.4 The polybasic region 89
4.5 *In vivo* trapping of Rho5, Dck1 and Lmo1 92
4.6 Interaction of Rho5 with the VDAC Por1 94

5. Summary 96

6. References 97

7. Acknowledgements/Danksagung 110

8. Statutory declaration 111

9. Curriculum vitae 112

1. Introduction

Organisms are constantly exposed to an environment with a multitude of immanent drastic changes. The ability to adapt to these changes is an essential characteristic of every living being in order to thrive and ensure survival. On a cellular level this means the sensing, transport and execution of signals which is achieved by a plethora of proteins. External signals first arrive at the cell's plasma membrane where different sensors are integrated. They consist of domains extending into the extracellular medium with at least one transmembrane domain anchoring them into the lipid bilayer and an intracellular domain that transmits the stimulus perceived by the extracellular domain. Thus, sensors represent a connector between the cytoplasm and the environment. The process of signal sensing can either happen via ligand binding or through a structural change of the receptor itself as a reaction to altered mechanical forces. Either way, in many cases the intracellular domain undergoes conformational changes resulting in the recruitment of signalling molecules to further transmit the stimulus. A highly conserved superfamily of membrane embedded sensors are the G-Protein-coupled receptors (GPCR) that are only found in eukaryotes. They cover a wide variety of signalling pathways ranging from basic processes like glucose sensing and fungal mating response (reviewed in (Xue et al. 2008)) to complex ones like chemosensory perception in multicellular organisms as part of the olfactory and optical system (Buck and Axel 1991, Palczewski 2006). GPCRs are usually activated by ligand binding which initiates a GDP-to-GTP exchange and thus the activation of a G_α subunit. This subunit is bound to the cytosolic section of the receptor and part of a heterotrimeric G-protein complex, consisting of the subunits G_α, G_β and G_γ. The nucleotide exchange triggers the dissociation of the trimeric complex into a monomeric G_α and a dimeric $G_{\beta,\gamma}$ subunit that interacts with downstream effectors to further transmit the respective signal (reviewed in (Hilger et al. 2018)). However, the sensing of disturbances is not restricted to the perception of external changes in the surrounding medium. Internal control mechanisms are also vital to induce the appropriate countermeasures and thus guarantee the continued meticulous execution of subcellular processes.

The receptor-coupled G proteins are structurally related to members of the small GTPases superfamily (also "small G-proteins"). They act as independent signalling factors and constitute a large group of monomeric regulatory proteins. Their independence grants a higher degree of versatility within signalling networks. Small GTPases usually have a size of around 21 Kilodalton and function as so called "molecular switches" due to their ability to cycle between an active, GTP-bound and an inactive, GDP bound state. To do so, all members of this family rely on a set of auxiliary proteins to switch the current state, namely guanine nucleotide exchange factors (GEFs) for activation and GTPase activating proteins (GAPs) for inactivation. Each small GTPase possesses an own set of multiple, highly specific auxiliary proteins.

The Gpr1 and the Ras branch of the Ras/cAMP/PKA pathway in *S. cerevisiae* serve as an attractive example for a GPCR working in parallel with monomeric GTPases on the same essential glucose sensing pathway (Figure 1). The G protein-coupled receptor Gpr1 senses external glucose which leads to the activation and subsequent dissociation of the G_{α} subunit Gpa2 that in turn activates the adenylate cyclase Cyr1. This stimulates the production of the important second messenger cAMP from ATP and triggers downstream effects through the heterotetrameric protein kinase A (PKA). Cyr1 is also regulated by the monomeric GTPases Ras1 and Ras2 and thus represents the congregation point of the Gpr1 and Ras branch. Both Ras-GTPases are activated by their GEF Cdc25 via a signal from glycolytic catabolites and stimulate the same PKA downstream effects, like cell proliferation and developmental pathways (reviewed in (Santangelo 2006)).

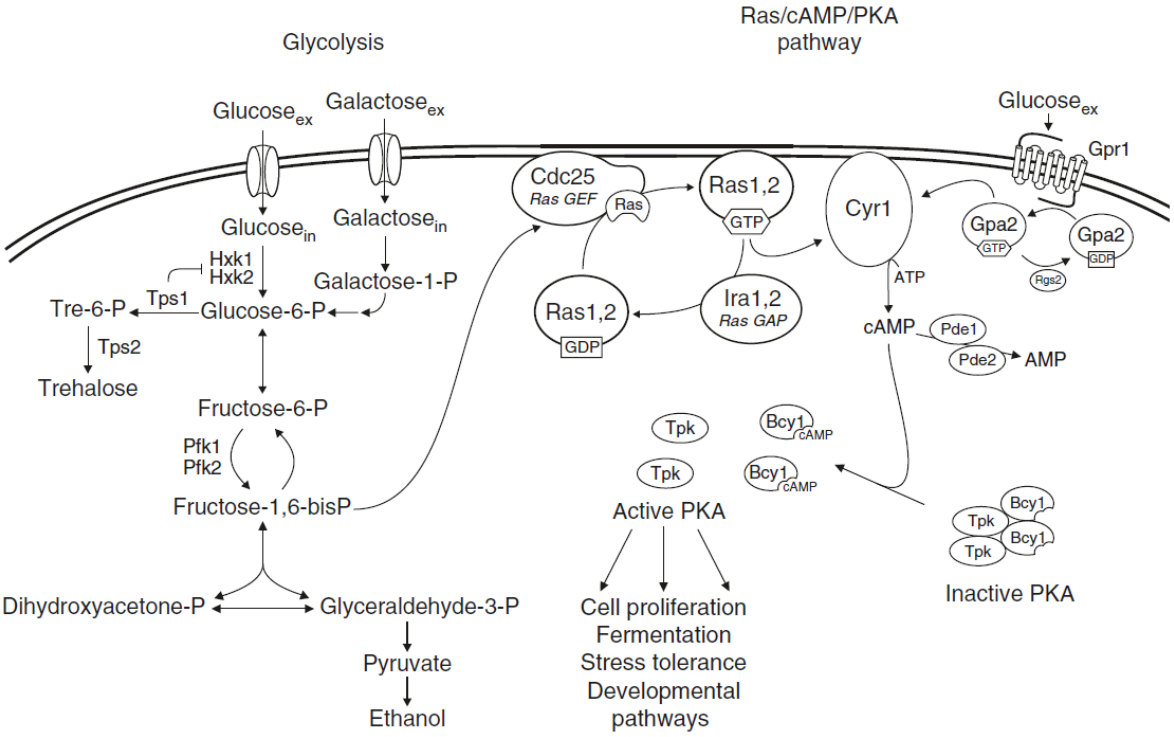

Figure 1: Schematic overview of initial glucose metabolism in yeast and its connection to the activation of the Ras/cAMP/PKA pathway (Peeters et al. 2017)

The large group of small G-proteins can be divided into the five subfamilies Rho, Ras, Rab, Arf and Ran that are conserved amongst eukaryotes (Wennerberg and Der 2004). Each of these Rho family members exerts a function at distinct subcellular localization which is coordinated and controlled by regulators as well as distinct structural components that affect their biochemical properties. The members of the Rho subfamily are particularly interesting because of their involvement in a variety of human diseases linked to aberrant Rho signalling, including neurodegenerative disorders, cardiovascular afflictions and cancer. This makes it a competitive field of research and a potential pharmaceutical target with a proper understanding of regulatory mechanisms as a prerequisite (Olson 2018).

1.1 Rho-GTPases

The first Ras homologues (Rho)-GTPase were identified in 1985 by Madaule and Axel (Madaule and Axel 1985). Subsequent studies showed that Rho proteins play a central role in actin cytoskeleton assembly which became a hallmark function (Ridley and Hall 1992). The following decades revealed that they are also involved in a variety of other fundamental cellular processes including vesicle trafficking, cell cycle progression, cell polarity (Bustelo et al. 2007) and redox regulation (Mitchell et al. 2013). In order to cycle between the active, GTP-bound and inactive, GDP-bound state, Rho-GTPases employ three types of proteins that will be described below in further detail. Based on their structure, motifs and function, Rho-GTPases can be further divided into six subfamilies: The Rac1-related, RhoA-related, Cdc42-related, Rnd, RhoBTB and Miro subfamily (Figure 2). Each member of this subfamily possesses structural core components including the G-domain, the insert region and the carboxyterminal hypervariable region. The G-domain is situated at the amino terminus and consists of five conserved sequence motifs (G1-G5). The G1 motif is also called P-loop and is involved in binding to the β-phosphate of the guanine nucleotide. The switch I and switch II region are also part of the G-domain and both cooperate to recognize whether the GTPase holds a guanine di- or triphosphate which specifically modifies the section's conformation in what is called the 'loading-spring' mechanism: Conserved residues of both switch I and switch II interact with the γ-phosphate of GTP which is released when the guanosine triphosphate is hydrolysed (reviewed in (Schaefer et al. 2014)). The "Rho family insert" is an α-helical sequence of usually 10 to 13 amino acids and can normally be found after residue 122 (Valencia et al. 1991, Feltham et al. 1997). Numerous analyses have proven this region to be essential for activation as well as regulation, making it a central region for Rho function. Furthermore, the variation in length and sequence of the Rho insert seems to ensure the specificity of different Rho-GTPases (Freeman et al. 1996, Feltham et al. 1997, Karnoub et al. 2001, Zong et al. 2001).

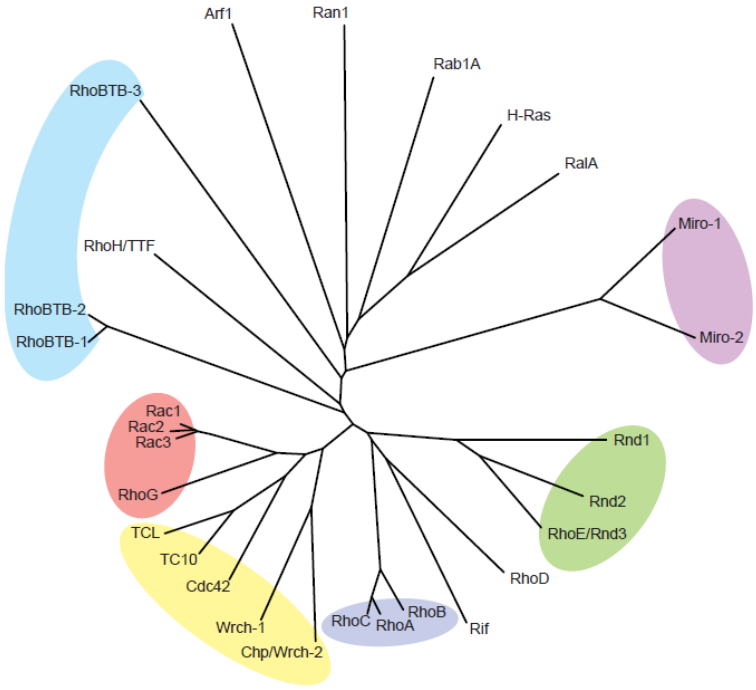

Figure 2: Phylogenetic tree of the Rho family GTPases and representatives of other Ras-superfamily GTPases. Color-coded subfamilies: Cyan = RhoBTB, red = Rac-like, yellow = Cdc42-like, blue = Rho-like, green = Rnd, purple = Miro (Wennerberg and Der 2004)

1.2 Rho-GTPases in *S. cerevisiae* and other fungi

An invaluable tool to obtain knowledge about Rho-GTPases and their regulators are fungal model organisms. Especially the baker's yeast *Saccharomyces cerevisiae* contributed tremendously to the understanding of molecular interactions and components of Rho-GTPases. It was thus chosen as model organism in this work. The genome of the *S. cerevisiae* encodes six Rho proteins: Rho1 to 5 and Cdc42. Cdc42 is an essential Rho-GTPase and highly conserved from yeast to mammals. It was first identified in *S. cerevisiae* as an essential protein and is responsible for bud site assembly. To do so, Cdc42 transfers to a small cortical patch where it regulates the subsequent trafficking and deposition of cell components for the emerging daughter cell. The high degree of conservation is impressively demonstrated by the fact that the expression of the human *CDC42* allele in *S. cerevisiae* can complement the lethality of a *ScCDC42* deletion (Shinjo et al. 1990).

The well-studied Rho-GTPase Rho1 is a central signalling molecule in the cell wall integrity (CWI) pathway. Upon cell wall stress, cell wall embedded sensors undergo a mechanically induced conformational change which leads to the recruitment and activation of the GEF Rom2 which in turn activates Rho1. This is followed by a phosphorylation cascade of a MAPK module and ultimately results in the transcription of specific stress responsive genes in order to adapt to the new environment (reviewed in (Heinisch et al. 1999)). Secondly, Rho1 localizes to sites of polarized growth and regulates actin organization by activating the formin Bni1 (Dong et al. 2003). Rho2 is a non-essential Rho-GTPase in *S. cerevisiae* and currently little is known about its precise role. Epistatic analysis indicate that it appears to cooperate with Rho1 to regulate actin organization (Park and Bi 2007). This notion is supported by results from the closely related filamentous cotton pathogen *Ashbya gossypii*, where the homologue *Ag*Rho2 seems to be involved in polarizing the actin cytoskeleton at the hyphal tip (Nordmann et al. 2014). Rho3 localizes to the plasma membrane with a slightly increased abundance at buds (Wu and Brennwald 2010). The Rho protein regulates exocytosis crucial for polarized bud growth (Imai et al. 1996, Adamo et al. 1999) and also actin organization by activating two formins (Dong et al. 2003). Yet, detailed studies about the exact mechanisms are still pending. In these processes, Rho3 shares functions with Rho4 (Matsui and Tohe 1992). Rho5 is also a non-essential Rho protein and one of the last characterized of the six Rho-GTPases. It was initially identified as a negative regulator of the cell wall integrity (CWI) pathway (Schmitz et al. 2002). However, subsequent investigations uncovered that Rho5 participates in a multitude of pathways including the oxidative stress induced apoptosis (Singh et al. 2008), the high osmolarity glycerol (HOG) pathway (Annan et al. 2008) and glucose signalling (Schmitz et al. 2018). There is evidence suggesting that Rho5 is involved in even more cellular processes like the selective digestion of mitochondria, which is termed mitophagy (Schmitz et al. 2015, Singh et al. 2019). These studies point to Rho5 as a central hub that integrates signals from a variety of pathways. Furthermore, Rho5 was shown to relocate from the plasma

membrane to the mitochondrial surface under certain stress conditions (Schmitz et al. 2015, Schmitz et al. 2018). While the factors involved in this redistribution remain elusive, Rho-GTPases are known to possess a variety of external and intrinsic mechanisms to allow a precise spatio-temporal regulation of their subcellular localization, which will be presented in the next sections.

1.3 Regulation of subcellular localization and spatial organization of Rho-GTPases via auxiliary proteins

Rho-GTPases are part of a complex regulatory network highlighting the importance of this protein family and the need for a tight control. As with many signalling proteins, the spatio-temporal control of Rho-GTPases is crucial for the correct function and subsequent signal transduction. A remarkable example is illustrated by the bud site assembly during the budding process in *S. cerevisiae* which requires the precisely orchestrated sequential action of at least four of the six yeast Rho proteins: After the selection of the bud site, Cdc42 is a key player for polarity establishment by regulating actin organization, septin organization, and exocytosis. Following the septin ring formation, bud growth is promoted by polarized vesicle transport supported by Rho1 and Rho3 that interact with components of the exocyst complex, providing additional polarization signals. Rho4 acts as redundant factor to Rho3 (reviewed in (Park and Bi 2007)). To ensure this high-level precision, Rho proteins employ a set of tools, some of which are encoded in the GTPase's intrinsic structure. Others are mediated by additional components that regulate the recruitment to other compartments or target the protein's activity.

1.3.1 RhoGEFs

The human genome encodes for approximately 80 GEFs compared to 22 Rho family members. Each Rho-GTPase has multiple GEFs allowing a remarkably complex tissue-specific regulation (Hodge and Ridley 2016). Rho proteins with multiple GEFs are not restricted to humans but are a rather common occurrence in eukaryotes. This points to a conserved principle albeit in a less complex manner in lower organisms. *S. cerevisiae* for example possesses six RhoGEFs for the six described Rho-GTPases and the fission yeast *Schizosaccharomyces pombe* harbours at least seven GEFs (Wang et al. 2015). RhoGEFs are categorized into two unrelated families that can be categorized by the presence of a catalytic Dbl-homology (DH) domain or a DOCK homology region 1 (DHR1) domain (Rossman et al. 2005). Despite the fact that the two RhoGEF families are non-related, the process of GDP-to-GTP exchange itself is executed in a fairly similar way and requires a multistep reaction. In the first step a low-affinity Rho/GEF dimer is established. Members of the Dbl RhoGEF family associate with the switch I and II region of the Rho-GTPase via their DH-PH module while this is adopted in the DOCK family by the DHR2

(also “docker”) domain (Rossman et al. 2005, Cote and Vuori 2007). The binding process triggers a remodelling of the regions and encourages the discharge of GDP leading to a nucleotide-free, high-affinity intermediate complex that can bind either GTP or again GDP. Because of the ten times higher intracellular concentration of GTP compared to GDP, it is statistically more likely that GTP will be incorporated. The GTP-Rho-GEF complex is now in a low-affinity state and the dissociation of the dimeric composite ensues followed by the correspondent downstream effects.

The RhoGEF family carrying the characteristic DH domain is represented by at least 70 members in mammalian cells. The DH domain is invariantly followed by the regulatory pleckstrin homology (PH) domain and this DH-PH module works in coordination to exert the catalytic activity on the Rho-GTPase as described above (Chhatriwala et al. 2007). The module is flanked by a diversity of other domains that eventually contribute considerably to the subcellular localization and function by associating with lipids or other proteins (reviewed in (Rossman et al. 2005)). One of the first identified Dbl proteins three decades ago was Cdc42’s GEF Cdc24 from *S. cerevisiae*. It serves as an excellent example for the spatio-temporal control of Cdc42 depending on the subcellular localization of its GEF (Hart et al. 1991, Ron et al. 1991): Cdc24 associates with the scaffold protein Bem1 thereby augmenting the polarized localization of the GTPase Cdc42 to the emerging bud site and thereby locally restricting its signalling (Butty et al. 2002). The interaction of the Cdc24 and the scaffold protein was evidenced to be an essential prerequisite for the GEF’s activity and its concentration at the incipient bud site. A uniform, non-polarized distribution of Cdc24 at the plasma membrane failed to sustain viability due to abolished polarized growth (Woods et al. 2015). This incisively exemplifies the important role of GEFs in guiding certain Rho-GTPase to a specific site-of-action. The second family of RhoGEFs is the “dedicator of cytokinesis” (DOCK). Although first characterizations of DOCK proteins in fungi have been conducted after their identification in mammalian cells, the last decade has experienced an increasing knowledge of this protein family in fungal organisms. This includes the identification and characterization of DOCK proteins in the opportunistic human pathogen *C. albicans* (Hope et al. 2008) and the budding yeast *S. cerevisiae* (Brugnera et al. 2002, Schmitz et al. 2015), but also filamentous fungi like the ergot plant pathogen *Claviceps purpurea* (Herrmann et al. 2014) and the cotton pathogen *Ashbya gossypii* (Nordmann et al. 2014). However, most of the knowledge regarding structure and regulation was obtained from mammalian DOCK homologues. At basal state, DOCK proteins are subordinated to autoinhibition which is achieved by the interaction of the GEF’s amino terminal SH3 with the DHR2 domain establishing a “closed” confirmation (Figure 3, left). This abrogates the association of the DHR2 domain with the Rho protein and the subsequent GTP loading due to steric inhibition (Lu et al. 2005). The exact mechanism leading to the relief from the autoinhibitory state is still not fully understood. Yet, there are two models which could provide explanations: In the first one, upon stimulation the autoinhibitory state of the scaffold protein “engulfment and motility” (ELMO) is dissolved allowing the

protein to bind to DOCK. This disrupts its SH3-DHR2 interaction, opening the confirmation and subsequently allowing Rac-binding. In the second model, ELMO and DOCK are constitutively connected and autoinhibition is mutually lifted by a specific signal (Patel et al. 2011). Upstream of the signature DHR2 domain, DOCK proteins harbour a DHR1 domain. It mediates the binding to certain phosphoinositides via a pocket lined with basic amino acids providing membrane specificity (Cote and Vuori 2007). This is particularly important for the DOCK protein to orchestrate the spatio-temporal localization at the membrane for the proper activation and positioning of its effectors to specific sites (Cote et al. 2005). The first indications for DOCK family proteins in fungi were obtained from a study investigating the DOCK180-ELMO1 complex.

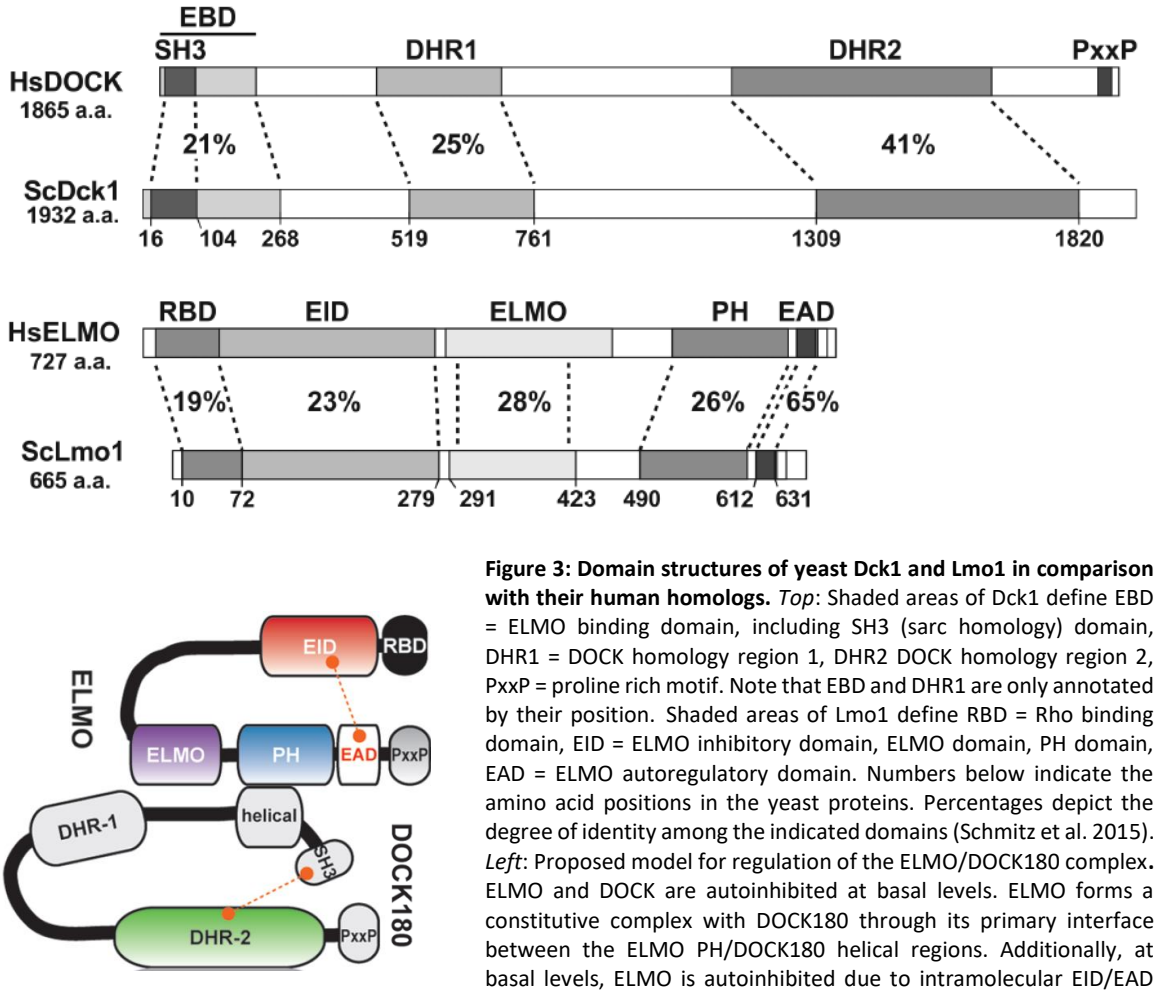

Figure 3: Domain structures of yeast Dck1 and Lmo1 in comparison with their human homologs. *Top*: Shaded areas of Dck1 define EBD = ELMO binding domain, including SH3 (sarc homology) domain, DHR1 = DOCK homology region 1, DHR2 DOCK homology region 2, PxxP = proline rich motif. Note that EBD and DHR1 are only annotated by their position. Shaded areas of Lmo1 define RBD = Rho binding domain, EID = ELMO inhibitory domain, ELMO domain, PH domain, EAD = ELMO autoregulatory domain. Numbers below indicate the amino acid positions in the yeast proteins. Percentages depict the degree of identity among the indicated domains (Schmitz et al. 2015). *Left*: Proposed model for regulation of the ELMO/DOCK180 complex**.** ELMO and DOCK are autoinhibited at basal levels. ELMO forms a constitutive complex with DOCK180 through its primary interface between the ELMO PH/DOCK180 helical regions. Additionally, at basal levels, ELMO is autoinhibited due to intramolecular EID/EAD interactions. Also proposed here is that, in unstimulated conditions, DOCK180 GEF activity is hindered through a DHR2/SH3 interaction. Picture and description taken from (Patel et al. 2011).

The authors discovered that the DHR2 domain from *Sc*Dck1 showed *in vitro* interaction with Rac1 (Brugnera et al. 2002). The first characterization of a DOCK protein in a yeast was gathered from *Candida albicans*. For this human pathogen, the switch from budding to invasive filamentous growth is important for the organism's pathogenicity. In this process, *Ca*Rac1 was shown to cooperate with the DOCK homologue *Ca*Dck1 acting upstream of two MAP kinases involved in morphogenesis and cell

wall formation (Hope et al. 2008, Hope et al. 2010). Several years later the subsequent characterization of Dck1 in the yeast *S. cerevisiae* was accomplished alongside the identification of Lmo1, the homologue of ELMO1. It revealed a participation of all three proteins in the cell wall integrity (CWI) pathway, oxidative stress response (Schmitz et al. 2015) and in glucose signalling (Schmitz et al. 2018). Similar to the mammalian counterparts, both proteins seem to act as a bipartite GEF for Rho5. Dck1 and Lmo1 localize to distinct puncta at the cell periphery. But when exposed to oxidants redistribute to mitochondria analogous to their Rho protein (Schmitz et al. 2015). Dck1 seems to have a surprisingly low impact on the actin cytoskeleton in normal budding growth, which is in stark contrast to the homologous from higher eukaryotes (Schmitz et al. 2018). It appears as if the more relevant function of Dck1 during budding growth is the oxidative stress response and glucose signalling. However, in a screen for defects in pseudohyphal growth mutated *DCK1* was identified (Brugnera et al. 2002). This agrees with polarity disturbances in other filamentous fungi deprived of homologues of this GEF. In *A. gossypii*, for instance, the Dck1 homologue is involved in septin ring formation and depletion resulted in severely reduced mycel diameter (Herrmann et al. 2014, Nordmann et al. 2014). This suggests that in fungi Dck1 homologues fulfil a conserved role in actin remodelling during polar growth.

1.3.2 Rho-GAPs

Due to their low intrinsic activity of GTP hydrolysation, Rho-GTPases need a second class of regulatory factors to re-establish the inactive, GDP-bound state and avoid hyper stimulation. This task is carried out by RhoGAPs that are characterized by the catalytic GAP domain of about 190 amino acids. This domain harbours a conserved arginine residue called the “arginine finger”. To stimulate the intrinsic hydrolytic activity, the arginine finger inserts into the catalytic side of Rho proteins thereby stabilizing the transition state that is needed to effectively remove the γ phosphate. As a result, GTP hydrolysis is enhanced by an order of several magnitudes (Boguski and McCormick 1993, Scheffzek et al. 1997). Similar to RhoGEFs, in any given organism the RhoGAPs outnumber their targets. The human genome is predicted to encode between 59 and 70 proteins with a RhoGAP domain while only encoding 20 Rho-GTPases (Amin et al. 2016, Hodge and Ridley 2016). Similarly, *S. cerevisiae* harbours ten predicted RhoGAPs which act on the six Rho-GTPases (Tcherkezian and Lamarche-Vane 2007, Perez and Rincon 2010). Typically, a single RhoGAP acts on multiple Rho proteins, like *Sc*Bem2 which is a GAP for the Rho protein Cdc42 but also regulates Rho1. In the baker’s yeast, Cdc42 additionally has three Cdc42-specific GAPs, Rga1, Rga2 and Bem3. The biological relevance of the redundancy finds an explanation in the fact that depletion of a certain GAPs exhibited specific phenotype. This implies that they each regulate a specific aspect of the Cdc42 (Smith et al. 2002) and supports the notion that GAPs act to integrate different signals and influence Rho-GTPase activity on multiple levels. The catalytic GAP domain itself seems to be rather non-selective and in some cases even ineffective in promoting GTP hydrolysis (Amin

et al. 2016). In order to confer the required versatility, each RhoGAP is equipped with a varying composition of functional regions corresponding to the physiological role it fulfils. For example, Rgd1 from *S. cerevisiae* is a Rho-GAP for Rho3 and Rho4 and harbours an F-BAR domain which binds phosphoinositides. By associating with these lipids, the F-BAR domain enables the Rho-GAP to discriminate between the two Rho proteins. Furthermore, this region seems to be responsible for subcellular targeting of the GAP Rgd1 (Prouzet-Mauleon et al. 2008).

1.3.3 Rho-GDIs

Rho proteins possess a third regulatory level conferred by the guanine dissociation inhibitors (GDIs). They are named after their ability to inhibit the dissociation of the bound guanine nucleotide from the Rho-GTPase (Sasaki et al. 1993, Michaelson et al. 2001, Boulter et al. 2010). The N‑terminal domain of RhoGDIs interacts with the switch regions of the Rho-GTPase thereby preventing both the intrinsic and the GAP-stimulated hydrolysis of GTP and impeding the Rho protein's downstream effects. In consequence, the Rho protein is locked in the current guanine nucleotide state. GDIs have a significantly higher affinity for the GDP-bound state thereby tending to stabilize the inactive Rho protein. Thus, RhoGDIs are considered negative regulators for Rho proteins (reviewed in (Garcia-Mata et al. 2011)). In contrast to GEFs and GAPs, the number of individual RhoGDIs in a given organism is low, usually ranging from one in yeast (*S. cerevisiae*, *C. albicans* Rdi1) to three in mammalian cells (RhoGDI1-3). An intriguing feature of RhoGDIs is the concealment of the prenyl residue from the hydrophilic environment in a hydrophobic pocket so that it forms a soluble complex with certain Rho-GTPases. This acts as a reservoir that resides in the cytosol until needed (Isomura et al. 1990). The mechanism for the mobilisation and re-activation of this pool is still under debate but it is speculated to involve phosphorylation of either RhoGDIs or the Rho protein. The interaction with membrane lipids was also shown to decrease the affinity of RhoGDIs for their GTPases (Chuang et al. 1993, DerMardirossian and Bokoch 2005). In any case, after mobilization a two-step process is implicated for a Rho-GTPase to be recruited from the inactive cytosolic pool to its intended site-of-action: First, the Rho protein needs to dissociate from the complex. In the budding yeast, association of Rdi1 with Cdc42 and Rho1 is disrupted by the PAK-family kinase Cla4. This supports the model of regulation through phosphorylation and is similar results obtained from human cells: The kinase PAK1, Cla4's human homologue, phosphorylates RhoGDI *in vivo* at two serine residues adjacent to the binding site for the GTPase prenyl group. As a result, it selectively releases bound Rac1 (DerMardirossian et al. 2004). In the second step of Rho mobilization, the hydrophobic tail of the GTPase inserts into the correspondent membrane and resumes the normal regulatory cycle with GEFs and GAPs ((Abo et al. 1994, Robbe et al. 2003), Figure 4e+g). Afterwards, the GTPase can return to its reservoir state (Figure 4f). In *S. cerevisiae* for instance Cdc42 is recycled from the polar cap of the emerging bud site via two parallel-

working pathways: A slower recycling by endocytosis and a rapid recycling mediated by Rdi1 (Slaughter et al. 2009). Another function of RhoGDIs was shown to be the global regulation of the homeostasis of Rho proteins. At steady-state, the level of a RhoGDI roughly equals that of all their Rho-GTPases (Michaelson et al. 2001). Thus, any change in the interaction levels of a distinct Rho protein by altered affinity, expression or degradation level has an impact on the other Rho proteins creating a competition for GDI-interaction and allowing a crosstalk on multiple levels. Beyond storage of Rho proteins in the cytosol, RhoGDIs are also responsible for the transport of Rho family members. Certain newly matured RhoGTPases are transported from the ER to their designated membrane by RhoGDIs (Michaelson et al. 2001). This is impressively supported by the fact that depleting cells of RhoGDIs

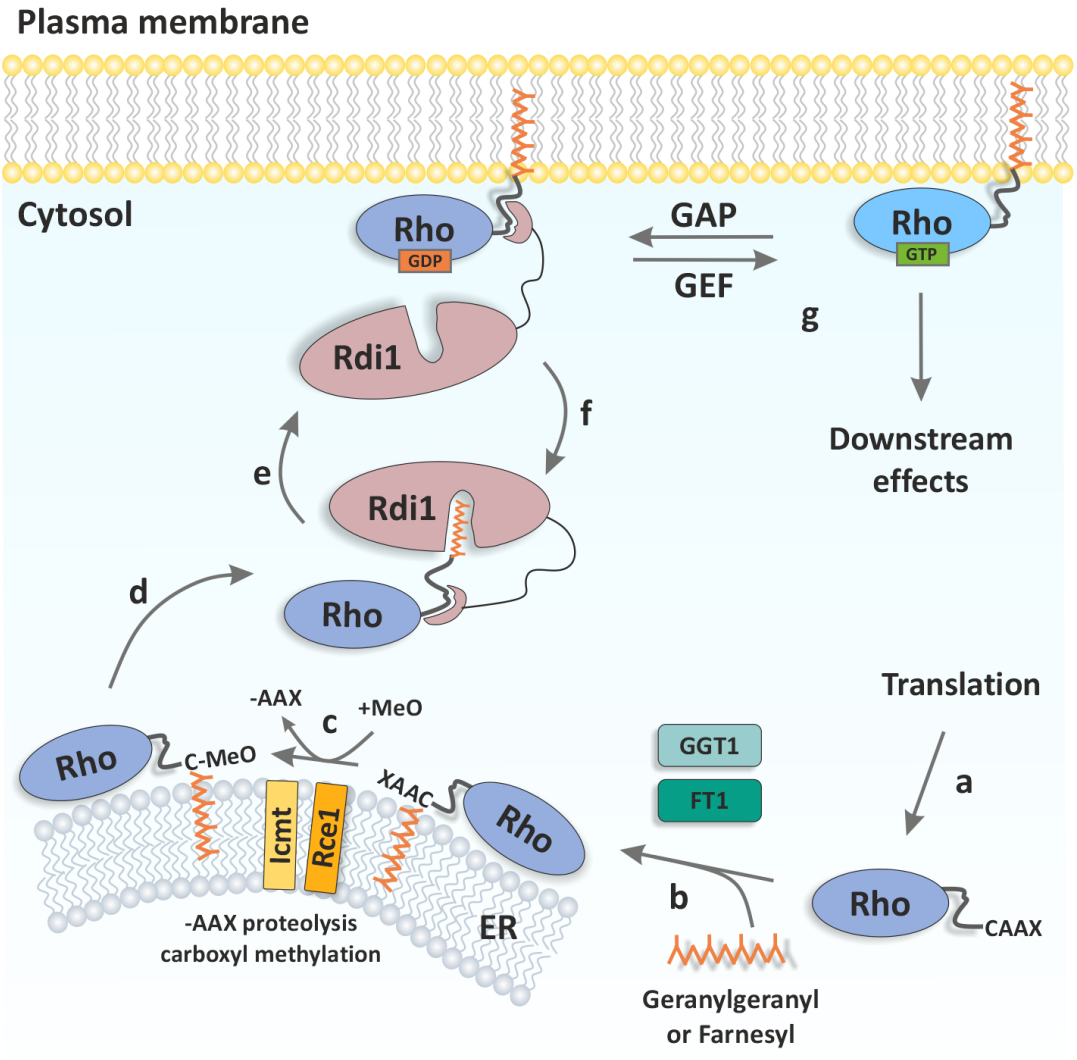

Figure 4: The Rho cycle a – After translation, the Rho-GTPase is released into the cytosol in an unprocessed soluble form. b – The native Rho-GTPase is modified by either the geranylgeranyl-transferase or the farnesyl-transferase which adds geranylgeranyl or a farnesyl moiety to the cysteine of the CAAX motif and is then transported to the outer leaflet of the endoplasmic reticulum (ER). c – On the ER surface, the two enzymes Rce1 and Icmt further process the Rho protein by cleaving off the AAX tripeptide and adding a methyl group to the cysteine. d – A RhoGDI extracts the fully processed Rho-GTPase from the ER membrane. e – The RhoGDI releases the Rho protein at the plasma membrane. f – RhoGDI extracts Rho from the membrane for storage in a cytosolic pool. g – The membrane-bound GTPase can be activated by GEFs.

results in their accumulation at the ER, the compartment where they are posttranslationally modified ((Boulter et al. 2010), Figure 4c). Curiously, *in vitro* assays with cell lysates from *S. cerevisiae* suggest that Rdi1 only interacts with Cdc42, Rho1 and Rho4. This implies that Rho2, Rho3 and Rho5 may be subjected to other transport mechanisms (Tiedje et al. 2008). Nevertheless, a loss of Rdi1 in *S. cerevisiae* cells causes the proteasomal breakdown of both Cdc42 and Rho1 while simultaneously maintaining a high level of activity (Tiedje et al. 2008). Interestingly, the same proteasomal breakdown was observed in mammalian cells where exogenous overexpression of RhoA, Rac1 or Cdc42 removed endogenous RhoA from its complex with RhoGDI1, respectively, condemning it for proteasomal degradation (Boulter et al. 2010). Considering the involvement in these different processes, it comes as a surprise that Rdi1 seems to be of a minor significance for *S. cerevisiae* as evident from Rdi1-depleted cells that show a distinctively mild phenotype (Tiedje et al. 2008). This inconsistency might be explained by the fact that all basic functions of Cdc42, like polarized localization, were exerted in a Rdi1-independent way (Woods et al. 2015). Thus, Rdi1 is regarded as a fine-tuning tool with compensatory mechanisms that secure vital processes. Ultimately, these functions make RhoGDIs versatile factors in Rho-GTPase regulation.

1.3.4 Adaptor proteins

Adaptor proteins are essential components in signal transduction and drive signalling through spatial localization. They lack any inherent catalytic activity and rather function as scaffolds for multi-protein complexes and enable a crosstalk between different signalling pathways. A prominent example is the scaffold protein Bem1 which in cooperation with the GEF Cdc24 ensures a stable and polar localization of the GTPase Cdc42. In *S. cerevisiae* the conserved PB domain of Bem1 connects to Cdc24 via a special peptide repeat motif. Together they recruit activated Cdc42 to the incipient bud site to initiate and maintain the bud emerge (Butty et al. 2002). Furthermore, a recently published study assessed the factors involved in the targeting of this complex for locally restricted Cdc42 activation: Bem1 harbours a cluster of basic amino acids that drive the interaction with anionic membrane lipids. This leads to a local accumulation of Bem1-Cdc24 which subsequently stimulates nanoclustering of Cdc42 (Meca et al. 2019).

Another class of adaptor protein that is involved in Rho-GTPase recruitment is the ELMO protein family. It ensures the correct positioning of the DOCK-Rho-GTPase complex for efficient GDP displacement. ELMO is subjected to autoinhibition by the interaction of the N-terminal ELMO Inhibitory Domain (EID) and the C-terminal ELMO Autoregulatory Domain (EAD) creating a “closed” conformation when inactive ((Patel et al. 2010), Figure 3, left). Upon stimulation, ELMO transitions to an “open” conformation, now acting, together with DOCK, as a heterodimeric GEF on Rho-GTPases like Rac1 (Cote and Vuori 2007). In this complex, ELMO ensures efficient signalling due to its ability to

localize the trimeric complex to distinct subcellular compartments which leads to the subsequent downstream effects (Brugnera et al. 2002, Grimsley et al. 2004). As the hallmark of this protein family, ELMO harbours a highly conserved ELM domain in its central region. Surprisingly, the exact function is yet to be uncovered (Figure 3, top). At the C-terminus there is an atypical PH domain which is anticipated to bind phosphoinosites and thus being involved in subcellular location. The C-terminal region also harbours a proline rich domain which mediates DOCK binding. The interface for Rho binding is provided by the Ras-Binding Domain (RBD) on the far N-terminus (Patel et al. 2011). The ELMO family seems to be highly conserved and can be found throughout the fungal kingdom. Homologues have been identified in many model organisms including *Cryptococcus neoformans, Aspergillus fumigatus, Ustilago maydis, C. albicans* and *S. cerevisiae* (Brzostowski et al. 2009, Hope et al. 2010). Yet, only limited studies have been conducted to this date to characterize the role in the respective organism. Nevertheless, there is a low overall identity to human ELMO1 with 15 % from both *C. albicans' Ca*Lmo1 and *S. cerevisiae's Sc*Lmo1. Slightly higher values seem to be restricted to functional domains with the values surpassing 23 % (Hope et al. 2010, Schmitz et al. 2015). In *C. albicans*, the DOCK homologue *Ca*Dck1 and the ELMO homologue *Ca*Lmo1 cooperate to establish the invasive filamentous growth as part of the yeast's pathogenicity. In this process, the ELM and PH domain are both critical and sufficient for the co-operational function with *Ca*Dck1 on *Ca*Rac1 (Hope et al. 2010). In *S. cerevisiae*, Lmo1 was shown to be part of the oxidative stress and glucose response and is likely working with Dck1 as a bipartite GEF on Rho5 (Schmitz et al. 2015, Schmitz et al. 2018). A rough mapping of the functional domains based on homologies and interaction studies unveiled that the putative EBD of Dck1 is essential for Lmo1 interaction. Furthermore, the two proteins seem to form a stable constitutive interaction as indicated by the fact that the punctuate location of the two proteins colocalize in the fluorescence microscope and that this pattern depends on the presence of the respective other (Schmitz et al. 2015). However, it is yet to be clarified what significance the respective domains have in the cellular and physiological context. Ste50 acts as an adaptor protein in three different MAPK signalling pathways in *S. cerevisiae* namely filamentous growth, osmotic stress and mating response. Together with the kinase Ste11, Ste50 participates in all three MAPK cascades by mediating component overlap where the three pathways share elements. Pathway specificity and thus distinct physiological responses are moderated by varying interactions with its Ras association (RA) domain (Sharmeen et al. 2019). Intriguingly, in *S. cerevisiae* the small GTPase Rho5 seems to be involved in the hyperosmotic stress response by interacting with the RA domain of Ste50 (Annan et al. 2008).

1.4 Intrinsic structural features of Rho-GTPases that regulate subcellular localization

Auxiliary proteins are not the only factors that influence subcellular distribution of GTPases. Posttranslational modifications, interaction with lipids and biochemical properties are central factors that influence the subcellular location of GTPases. For this, Rho proteins possess distinct structural features that considerably contribute to their correct spatio-temporal behaviour which will be outlined in the following chapter.

1.4.1 Nucleotide binding state

The fact that the nucleotide binding state influences the subcellular destination of the signalling proteins is not only a logical but vital mechanism considering the requirement to restrict signal transmission to a specific site. This circumstance is strikingly demonstrated with the Rho protein Cdc42 which represents a key component of regulating polarity in all eukaryotic organisms. Excellent model organisms to investigate the components that orchestrate the complex process of polarity establishment are provided by the fungal kingdom. In *S. cerevisiae*, the anisotropic location of Cdc42 to the growing bud depends on its nucleotide binding state and it is the GTP-bound variant that preferably accumulates at sites of polarized growth (Meca et al. 2019). Similarly, in the fission yeast *S. pombe Sp*Cdc42 is subjected to a tightly controlled spatio-temporal activation. While preferentially locating to the plasma membrane, the activated Rho protein accumulates at sites of growth. Intriguingly, the dynamics of constitutively active *Sp*Cdc42 at the plasma membrane was severely impeded compared to the wild type or a dominant negative mutant as evinced by FRAP experiments. The authors attribute this to a possible formation of large complexes slowing down the lateral diffusion (Estravis et al. 2017). A permanent GTP-bound state can also have a negative effect on localization as demonstrated with Rho1 which failed to be targeted to the bud neck. Consequently, formation of the cytokinetic actomyosin ring was abrogated. The authors provided evidence that the failed targeting could be caused by an impeded interaction of Cdc42 and its GEF (Yoshida et al. 2009).

Another example for the influence of the nucleotide state on Rho localization can be found in the human pathogen *C. albicans*: A GTP-locked *Ca*Rac1 exhibits a uniform distribution along the plasma membrane in exponentially growing cells which coincides with the wild type. By contrast, a dominant negative mutant demonstrates a peculiar patch-like dispersion implying a clustering of the protein. Furthermore, FRAP assays proved a severely altered dynamic of the dominant negative *Ca*Rac1 with a tenfold deceleration of the recovery half time. This suggests that the high mobility of *Ca*Rac1 depends on GTPase cycling (Vauchelles et al. 2010). All these examples demonstrate that the nucleotide binding state of Rho-GTPases has an influence on the subcellular distribution and behaviour in order to secure a correct signalling output.

1.4.2 Prenylation

An important posttranslational modification (PTM) of Ras- and Rho-type GTPases is a carboxy-terminal lipid-modification. After translation, a 15-carbon (farnesyl) or a 20-carbon (geranylgeranyl) isoprenoid lipid, termed farnesylation or geranylgeranylation, respectively, is added to most proteins of this family (Figure 4a+b). As the first of a three-step process, a cytosolic farnesyl transferase (FTase) or geranylgeranyl transferase (GGTase-I) covalently adds the respective isoprenoid moiety to the cysteine of the CAAX motif which is the corresponding peptide recognized by the enzymes (Figure 4b). The "C" representing the cysteine that is to be lipidated and the "A" for two aliphatic residues. The "X" stands for a variable amino acid that is the major determinant which of the enzymes bind to the unprocessed protein with methionine resulting in farnesylation and a leucine in geranylgeranylation. While the subcellular distribution itself seems to be unaltered by either of the lipid modifications, geranylgeranylated proteins appear to be more tightly anchored in the PM. Due to the longer C20 chain the moiety protrudes farther into the membrane's lipid phase compared to the shorter C15-farnesyl (Hancock et al. 1991). The last three amino acids (-AAX) of the motif are now enzymatically cleaved off by the ER-resident endoprotease Ras-converting enzyme 1 (Rce1), and the second enzyme isoprenylcysteine-O-carboxyl methyltransferase (Icmt) catalyses the addition of a methyl group to the cysteine ((Clarke 1992, Ashby 1998), Figure 4c). The process is called prenylation and is an irreversible protein modification. Mutations of the essential cysteine of the CAAX motif as well as pharmaceutical inhibition of prenylation result in an unmodified and biologically inactive molecule emphasizing the importance of this PTM (Hancock et al. 1991, Kato et al. 1992).

In yeast, the membrane localization of the Ras-type proteins Ras1 and Ras2 is an important feature for their regulatory inputs in glucose signalling (Figure 1), namely for the nucleotide exchange mediated by their GEF Cdc25 (Crechet et al. 2000). A similar significance was found for Rho-GTPases which are often mislocalized to the cytosol when prenylation was disrupted (Roberts et al. 2008). This is typically accompanied by a loss-of-function as demonstrated by non-prenylatable Rho1 in yeast which failed to interact with its effector. In higher eukaryotes Rho proteins like Rac1 and Cdc42 are sequestered from the cytoplasmatic leaflet of the ER after their translation by the lipid binding protein RhoGDI for storage in the cytosol or induced extraction ((Garcia-Mata et al. 2011), Figure 4e+f). RhoGDIs also seem to be responsible for the transport of these Rho-GTPases to the plasma membrane where the hydrophobic residue of Rho-GTPases is integrated into biological membranes to anchor the protein by interacting with the lipid phase of the bilayer (Boulter et al. 2010). However, the significance of this process remains under debate.

Besides the role in anchoring the Rho protein to its biological membrane, the lipid modification also seems to be involved in the transport to organelles including endosomes, the nucleus, and mitochondria. Generally, mitochondria have been overlooked as sites for Rho GTPase signalling but

over the last decade ample evidence was gathered that showed this organelle to be a platform assembling different pathways (reviewed in (Phuyal and Farhan 2019)). The first evidence was provided by the systematic investigation of central Rho-GTPases following their subcellular location in different tissues where *Hs*Rac1 was predominantly detected in the mitochondrial fraction (Boivin and Beliveau 1995). Intriguingly, in alveolar macrophages from patients suffering from asbestosis, *Hs*Rac1 locates to mitochondria and is imported into the intermembrane space where it ultimately increases mitochondrial H_2O_2 generation. This subcellular translocation depends on the geranylgeranylation of the CAAX motif. The authors reasoned that the PTM may be important for *Hs*Rac1's activation and association with other proteins (Osborn-Heaford et al. 2012). Rho5, the Rac1 homologue in *S. cerevisiae*, was shown to relocate from the plasma membrane to mitochondria under oxidative stress and glucose starvation. This redistribution depends on the presence of both components of the dimeric GEF Dck1/Lmo1 which also relocate to this organelle (Schmitz et al. 2015, Schmitz et al. 2018).

1.4.3 Phospholipids and the polybasic region (PBR)

Many members of the Rho and the Ras family display a conspicuous sequence at their C-terminus adjacent to the CAAX box comprising of a series of basic amino acids – the polybasic region (PBR). It was characterized as a second membrane targeting signal that enables the protein to recognize specific membranes of subcellular compartments (Michaelson et al. 2001, Williams 2003). In *S. cerevisiae*, the PBR of the essential Rho-GTPase *Sc*Rho1 binds to the phospholipid phosphatidylinositol-4,5-bisphosphate (PIP_2) which is used to concentrate the Rho protein at late stages of the division site where PIP_2 usually accumulates (Yoshida et al. 2009). The ability to bind phosphoinosites seems to be a characteristic feature of the PBR and it is evolutionary conserved: The membrane specificity of mammalian Rho proteins derives from the interaction of the negatively charged residues of the PBR with specific positively charged phospholipids (Heo et al. 2006). Organelle identity and even cellular subdomains can be encoded by phosphoinosites and thus working as guides for Rho proteins (Fairn and Grinstein 2012). This is distinctively demonstrated by the fact that a forced enrichment or depletion of one type of phosphoinosites causes a reorganization of GTPases which follow the new lipid distribution even to other organelles (Miller et al. 2019, Yang et al. 2019). This has a central physiological significance as in *S. cerevisiae* for instance the concentrated localization of the Rho-GTPase Cdc42 at the emerging bud tip depends on the accumulation of phosphatidylserine (PS). It is the main charge contributor at the plasma membrane and its polarized accumulation is an essential step in the establishment and maintenance of polar growth (Leventis and Grinstein 2010, Fairn et al. 2011). A mutational analysis strongly indicates that the polybasic region of Cdc42 is the main driver of its PS-mediated concentration since the exchange of all four C-terminal lysines leads to a loss of anisotropic placement and a lethal phenotype (Meca et al. 2019). A similar PBR-dependency on

function was observed in the *S. pombe*: The rod-shaped model organism exhibits a phosphatidylserine gradient that emanates from the cell tip. This is implicated as an orientation to coordinate polarized subcellular location of Rho-GTPases like *Sp*Rho1 and *Sp*Cdc42 in a charge-dependant manner. The authors imply that the PBR of the proteins is likely to be the driving component for this process (Haupt and Minc 2017). This also seems to be conserved in mammalian Rho-GTPases as demonstrated by Yeung and colleagues who followed the subcellular distribution of different small GTPases by using fluorescently labelled surface charge biosensors. They could show that the net positive charge was responsible for the distribution to certain subcellular membranes. These locations corresponded with the examined Rho-GTPases including *Hs*Rac1 and *Hs*Cdc42 and the net positive charge in their PBR. They also demonstrated that phosphatidylserine (PS) contributes to the recruitment of these signalling molecules in yeast as well as mammalian cells (Yeung et al. 2008). These findings remarkably demonstrate how electrostatic attraction works as a key factor for the correct localization of signalling proteins with the PBR as its protein counterpart.

Within the C-terminal sequence of basic residues scientists have identified a canonical nuclear localization sequence (NLS) with the consensus sequence K-K/R-x-K/R which is necessary for nuclear accumulation of some members of the Rho family (Lanning et al. 2003, Lanning et al. 2004). Analyses subsequently identified NLSs in other members of the Ras and Rho family suggesting it to be an inherent aspect of these molecular switches (Williams 2003). Ensuing studies in three mammalian cell types unveiled that Rac1 shuttles between nucleus and cytoplasm following the cell cycle and thus promoting cell division. Surprisingly, prenylation interferes with this shuttling as proven by the fact that prenylation-defective Rac1 is completely transferred to the nucleus. This tempts the assumption that only newly synthesized, non-prenylated Rac1 is transported to the nucleus. However, a significant portion of nuclear Rac1 was demonstrated to be prenylated. The physiological significance remains to be uncovered (Michaelson et al. 2008). This phenotype is analogous to *Ca*Rac1's behaviour in *C. albicans*: Its PBR also harbours an NLS which is required for nuclear accumulation and the cycling in and out of the nucleus in non-agitated cells. Mutating the cysteine of the CAAX motif to serine resulted in a constant nuclear residence of *Ca*Rac1 (Vauchelles et al. 2010). When searching for an appropriate transport chaperone, surprisingly, Rac1-shuttling in both Mammalia and *C. albicans* was independent of RhoGDI. Hence, an alternative transport protein was postulated for *Ca*Rac1 in *C. albicans,* but results are pending. In higher eukaryotes, the armadillo chaperone small G-protein dissociation stimulator (SmgGDS) is assigned to this function (Lanning et al. 2003). While the role of the prenylation in the nuclear transport remains cryptic, the accumulation appears to be a conserved mechanism, nonetheless.

1.4.4 Phosphorylation

Protein phosphorylation is a widely used posttranslational modification of proteins. In higher eukaryotes phosphorylation sites have been characterized in many Rho-GTPases and were shown to modulate activity, subcellular distribution and altered affinity to interaction partners (Hodge and Ridley 2016). A compelling phosphorylation site in some Rho proteins can be found within their PBR and has been reported to be similar to the "farnesyl electrostatic switch" described for KRas-4B. In this proposed model, the net positive charge of the PBR causes an electrostatic interaction with negatively charged headgroups of membranes. The addition of a negatively charged phosphate residue partly neutralizes this association by repulsion triggering the detachment of the Ras protein from the plasma membrane and relocalization to intracellular membranes. In case of KRas-4B these include the endoplasmic reticulum (ER), Golgi apparatus and mitochondria, where the Ras protein engages in a variety of signalling pathways (Bivona et al. 2006). An illustrative example for the alternations caused by phosphorylation of Rho proteins is RhoA: It harbours a serine at position 188 situated within the PBR which is recognized by the kinase PKA and when phosphorylated has a triple effect: The phosphorylation causes an enhanced binding of RhoA to its RhoGDI which subsequently protects the protein from ubiquitin-mediated proteasomal degradation (Forget et al. 2002, Rolli-Derkinderen et al. 2005). Secondly, when RhoA is in its GTP-bound state, phosphorylated serine 188 causes a reduced downstream output due to decreased affinity of the Rho protein to its target ROK (Rho-associated kinase) whereas unphosphorylated GTP-bound RhoA did not negatively influence the binding. This is suggested to serve as a secondary switch to overwrite RhoA's GTP-induced effector binding (Nusser et al. 2006). Furthermore, as a downstream effect of the enhanced complex formation of RhoA and RhoGDI, Rac1 is competitively removed from RhoGDI, causing the Rho protein to locate to the PM which subsequently induces Rac-mediated stimulation of migration and adhesion. This is an example of how a crosstalk of two Rho-GTPases can be executed (Rolli-Derkinderen et al. 2005).

Studies about phosphorylation of Rho proteins in lower eukaryotes, like fungi, are virtually absent. Despite the knowledge gap, it is likely that Rho-GTPases are at least partly subjected to such regulations. One of the few studies examined the Rac1 homologue in *S. cerevisiae*, Rho5. It revealed that the kinase Npr1 seems to associate and phosphorylate the Rho protein, as demonstrated in *in vitro* studies. The authors propose that Rho5 may act as an inhibitor of HOG pathway signalling similarly to its role as negative regulator of the CWI pathway. Hence, phosphorylation may suppress Rho5 signalling (Annan et al. 2008). However, individual phosphorylation sites as well as the physiological significance for Rho5's activity, subcellular distribution or altered protein-protein interaction are pending. Nevertheless, the results obtained from Rho5 are highly interesting because its human counterpart Rac1 is also phosphorylated and ubiquitylated (Hodge and Ridley 2016). Combining these findings with global phosphoproteome analyses encourage the idea that other fungal

Rho-GTPases are regulated by phosphorylation as well. Additional studies in lower eukaryotes could contribute valuable knowledge to answer some open questions in Rho phosphorylation. For example, to suspend the phosphorylation-induced effects described above, it would be expected to require a phosphatase to remove the respective phosphate group from the Rho protein. Until now, the factors involved in this step remain to be elucidated. Also, due to the hydrophobic isoprenyl moiety of Rho-GTPases it is likely that auxiliary proteins are needed for the extraction from the resident membrane and subsequent transport throughout the hydrophilic cellular environment.

1.5 Aim of this thesis

The structural aspects described above prove once more that the C-terminal region of Rho-GTPases harbour a multitude of sites involved in regulation, modification and subcellular localization. They are densely packed on a relatively short stretch of protein with a high degree of versatility, similar to a "swiss pocketknife". The aim of this work was the characterization of structural components that determine the spatio-temporal behaviour of the GTPase *Sc*Rho5 in *Saccharomyces cerevisiae* and assess how they contribute to its functionality in the oxidative stress response and glucose signalling, with a focus on the carboxy-terminal region. These elements include the CAAX motif, the polybasic region, a potential phosphorylation site at serine 326 and a specific "extension" from proline 221 to aspartate 320. To unveil the physiological role of these components, mutants either carrying specific point mutations or lacking the corresponding region of *Sc*Rho5 were analysed by employing automatized growth assays and serial drop dilution assays. The effect on glucose signalling was investigated by complementation assays of the synthetic lethality of a *sch9 rho5* double deletion.

To study the spatio-temporal distribution, the subcellular localization of GFP-tagged *Sc*Rho5 and its mutants was followed in life-cell fluorescence microscopy both under standard growth conditions and after exposure to hydrogen peroxide as oxidant. The latter was employed to reveal any deviations in the mitochondrial translocation. Moreover, GFP-tagged *Sc*Rho5 and the subunits of the dimeric GEF *Sc*Dck1/*Sc*Lmo1, were trapped at the mitochondrial surface via a construct consisting of a GFP-recognizing antibody fused to a membrane anchored mitochondrial protein. The physiological effects of this artificial *in vivo* trapping were to reveal the specific roles of Rho5 after its association with the organelle as opposed to those exerted at the plasma membrane.

2. Materials & Methods

2.1 Materials

2.1.1 Chemicals

Chemicals and consumables used in this work were obtained from the following suppliers: Applichem (Darmstadt, Germany), BD (Franklin Lakes, USA), Bio-Rad (Munich, Germany), Biozym (Hessisch Oldendorf, Germany), Boehringer Ingelheim (Ingelheim, Germany), Brand (Gießen, Germany), Difco (Heidelberg, Germany), Eppendorf (Hamburg, Germany), Fluka (Steinheim, Germany), Formedium (Hunstanton, UK), GE Healthcare (Freiburg, Germany), Greiner BioOne (Solingen, Germany), Invitrogen (Darmstadt, Germany), Merck (Darmstadt, Germany), MP Biomedicals (Illkirch, France), New England Biolabs (Ipswich, MA, USA), Neolab (Heidelberg, Germany), Omnilab (Bremen, Germany), Riedel-de Haën (Seelze, Germany), Roche (Mannheim, Germany), Roth (Karlsruhe, Germany), Sarstedt (Nümbrecht, Germany), Schott (Mainz, Germany), Serva (Heidelberg, Germany), Sigma (Steinheim, Germany), Süd-Laborbedarf (Gauting, Germany), Thermo Scientific (Waltham, USA) and Trefflab (Degersheim, Switzerland)

2.1.2 Electronic equipment

Function	Model	Manufacturer
Agarose gel documentation	GelDoc-It Imaging System	UVP, LLC, Upland, California, USA
Autoclaves	3870 EL	Systec GmbH, Linden, Germany
	Fedegari autoclave	ibs | tecnomara GmbH
Centrifuges	EBA 8S	Andreas Hettich GmbH & Co.KG, Tuttlingen, Germany
	Heraeus Pico 17	Thermo Scientific, Waltham, Massachusetts, USA
	Micro centrifuge	Carl Roth, Karlsruhe, Germany
	Mikro 22R	Andreas Hettich GmbH & Co.KG, Tuttlingen, Germany
Magnetic stirrer	MAG RH	IKA-Werke GmbH & CO. KG, Staufen, Germany
Micromanipulator	MSM system series 300	Singer Instrument Company Limited, Roadwater, Watchet, Somerset, UK
Microscopic setup	See “Cell Imaging and Life Cell Fluorescence Microscopy”	
pH meter	Labor pH meter 766	Knick Elektronische Messgeräte GmbH & Co. KG, Berlin, Germany
Photometer	Amersham Biosciences Ultrospec 2100 pro	GE Healthcare Europe GmbH, Freiburg, Germany
	NanoPhotometer NP80	Implen, Inc., California, USA
Plate reader	Varioscan Lux plate reader	Thermo Scientific, Waltham, Massachusetts, USA

Power source	Biometra Standard Power Pack P25	Biometra GmbH, Göttingen, Germany
Scanner	Scanjet 3500c	HP Inc., Palo Alto, California
Shaker	Duomax 1030	Heidolph Instruments GmbH & Co.KG, Schwabach, Germany
	Innova 2300 platform shaker	Eppendorf AG, Hamburg, Germany
	TC-7 roller drum	Eppendorf AG, Hamburg, Germany
	Vibrax VXR basic	IKA-Werke GmbH & CO. KG, Staufen, Germany
	Vortex-Genie 2	Scientific Industries, Inc., Bohemia, New York, USA
Thermoblock	ThermoStat plus	Eppendorf AG, Hamburg, Germany
Thermocycler	Tpersonal, Tgradient	Biometra GmbH, Göttingen, Germany
UV transilluminator	Ultraviolet Transilluminator BioImaging Systems	UVP, LLC, Upland, California, USA

2.1.3 Enzymes

For the restriction of DNA, endonucleases were used either from the Fast-Digest series of Thermo Scientific or the High-Fidelity series of New England Biolabs. DreamTaq™ and Phusion™ for PCR, T4 DNA-ligase for ligation, Fast-AP as thermosensitive alkaline phosphatase for removal of phosphate groups off of the 5'-ends of DNA were also supplied by Thermo Scientific. For the enzymatic digestion of the ascus wall for tetrad analyses, Zymolyase-20T from MP Biomedicals (LLC, USA) was used.

2.1.4 Buffers, solutions and gels

Name	Instruction
50x TAE buffer	24,2 % (m/v) Tris, 10 % (v/v) 0,5 M EDTA (pH 8,0), 5,72 % (v/v) acetic acid
Agarose gel	1 % (m/v) agarose in 1x TAE buffer
Ampicillin stock solution	100 µg in 1 ml 50 % (v/v) ethanol
G418 stock solution	200 µg in 1 ml H_2O and sterile filtrated
RF1	100 mM RbCl, 50 mM MnCl, 30 mM KAc, 10 mM CaCl2, 15 % (v/v) glycerine, adjusting pH value with acetic acid to 5,8
RF2	10 mM MOPS, 10 mM RbCl, 75 mM CaCl2, 15 % (v/v) glycerine, adjustment of pH value with acetic acid to 6,8
MPI1	50 mM Tris-HCl (pH 8,0), 10 mM EDTA, 0,1 mg/ml RNase, adjustment of pH value with HCl to 8,0
MPI2	200 mM NaOH, 1 % SDS
MPI3	4 M Guanidinium-HCl, 0,5 M potassium acetate, adjusting pH value with HCl_{conc} to 4,2
Spheroblast buffer	0,9 M Sorbitol, 0,1 M EDTA
Washing buffer	20 mM NaCl, 2 mM Tris-HCl, 80 % (v/v) ethanol
X-Gal	20 mg per 1 ml DMSF

2.1.5 Media

All media and solutions were either steam autoclaved (121 °C, 20 minutes) or sterilized via filtration. For YEP, SC and LB plates, 1.5 % (m/v) Select Agar was added before autoclaving and 3 % (m/v) for sporulation plates. Antibiotics and stressors were added after autoclaving and cooling to 50 °C. If needed, 2 % (v/v) of the corresponding carbon source was added after autoclaving.

2.1.5.1 Yeast media

Rich medium (YEP)	1 % (m/v) Bacto Tryptone, 2 % (m/v) yeast extract
Synthetic medium (SC)	0.06 % (m/v) CSM (-His, -Leu, -Ura, -Trp), 0.67 % (m/v) yeast nitrogen base, 10 % (v/v) 100x stock solution amino acids and nucleotide bases, 6.7 g YNB w/o amino acids w/ $(NH_4)_2SO_4$ amino acids and uracil stock solutions were added for preparation of dropout media, as required, in the following concentrations: 20 mg/l uracil, 20 mg/l L-histine, 20 mg/l tryptophan, 100 mg/l leucine pH was adjusted to 6.2 with NaOH
Sporulation medium	1 % (m/v) potassium acetate

2.1.5.2 *E. coli* media

LB_0	1 % (m/v) Bacto Tryptone, 5 % (m/v) yeast extract, 1 % (m/v) NaCl

2.1.6 Yeast strains used in this study

All yeast strains used in this study are listed below. Strains were all isogenic, except for the mutant allele as indicated, and derived from HD56-5A and its isogenic diploid DHD5. HD56-5A is one of the parental strains of the CEN.PK series (Schacherer et al. 2007) and was first described in (Arvanitidis and Heinisch 1994). DHD5 is an isogenic diploid derived from HD56-5A described in (Kirchrath et al. 2000).

Pre-existing strains used in this work

Strain	Modifications compared to HD56-5A[1] or DHD5[2] background	Source
DAJ138	*sch9::SkHIS3/SCH9 rho5::KanMX/RHO5*	(Schmitz et al. 2018)
DHD5/dL+5	*RHO5Δ222–314-SkHIS3/RHO5*	J. J. Heinisch
HAJ03-B	*dck1::kanMX*	(Schmitz et al. 2018)
HAJ152-A	*MATa; DCK1-3GFP-SkHIS3*	(Schmitz et al. 2018)

HAJ201-B	*lmo1::kanMX*	(Schmitz et al. 2018)
HAJ216-A	*MATα; rho5::kanMX*	(Schmitz et al. 2015)
HD56-R2	*RHO5Δ222–319*	J. J. Heinisch
HD56-R7	*RHO5S328E-SkHIS3*	J. J. Heinisch
HD56-R8	*RHO5G12V-SkHIS3*	J. J. Heinisch
HD56-R8D	*RHO5G12VC328L-SkHIS3*	J. J. Heinisch
HD56-RHC328L#4	*RHO5C328L-SkHIS3*	J. J. Heinisch
HD56-RHC328L#5	*RHO5C328L-SkHIS3*	J. J. Heinisch
HD56-RHS326A #9	*RHO5S326A-SkHIS3*	J. J. Heinisch
HD56-RHwt #2	*RHO5-SkHIS3*	J. J. Heinisch
HJH11-2B	*IDP1-mCherry SkHIS3*	Julia Hühn
HOD266-1B	*por1::SkHIS3*	J. J. Heinisch
HOD295-7D	*rho5::SkHIS3*	J. J. Heinisch
HOD337-7D	*RHO5pbrK6A-SkHIS3*	J. J. Heinisch
HOD348-4D	*MATα; sch9::kanMX*	J. J. Heinisch
HOD354-RHG	*MATα; GFP-RHO5G12V-SkHIS3*	J. J. Heinisch
HOD365-7B	*GFP-RHO5-SkHIS3*	J. J. Heinisch
HOD365-9A	*MATα; GFP-RHO5-SkHIS3*	J. J. Heinisch
HOD370-2A	*MATα; GFP-RHO5-SkHIS3 leu2-3,112::pLAO12 (GB-FIS1TMD-LEU2)*	J. J. Heinisch
HOD370-3B	*GFP-RHO5-SkHIS3 leu2-3,112::pLAO12 (GB-FIS1TMD-LEU2)*	J. J. Heinisch
HOD371-4A	*MATα GFP-RHO5-SkHIS3 leu2-3,112::pLAO12 (GB-FIS1TMD-LEU2)*	J. J. Heinisch
HOD388-1C	*RHO5Δ222–314*	J. J. Heinisch
HOD388-2D	*RHO5Δ222–314*	J. J. Heinisch
HOD405-3A	*leu2-3,112::pLAO12 (GB-FIS1TMD-LEU2)*	J. J. Heinisch
HOD405-3C	*leu2-3,112::pLAO12 (GB-FIS1TMD-LEU2); DCK1-3GFP-SkHIS3*	J. J. Heinisch
HOD405-3D	*leu2-3,112::pLAO12 (GB-FIS1TMD-LEU2)*	J. J. Heinisch
HOD406-8C	*MATα leu2-3,112::pLAO12 (GB-FIS1TMD-LEU2); DCK1-3GFP-SkHIS3*	J. J. Heinisch
HOD410-1A	*leu2-3,112::pLAO12 (GB-FIS1TMD-LEU2)*	J. J. Heinisch
HOD410-1B	*MATα*	J. J. Heinisch
HOD410-1C	*MATα; GFP-RHO5G12V-SkHIS3*	J. J. Heinisch
HOD410-1D	*GFP-RHO5G12V-SkHIS3 leu2-3,112::pLAO12 (GB-FIS1TMD-LEU2)*	J. J. Heinisch
HOD410-3A	*leu2-3,112::pLAO12 (GB-FIS1TMD-LEU2)*	J. J. Heinisch
HOD410-3B	*MATα; GFP-RHO5G12V-SkHIS3*	J. J. Heinisch
HOD410-3C	*GFP-RHO5G12V-SkHIS3 leu2-3,112::pLAO12 (GB-FIS1TMD-LEU2)*	J. J. Heinisch
HOD410-3D	*MATα*	J. J. Heinisch
HOD415-11C	*LMO1-3GFP-kanMX*	J. J. Heinisch
HOD415-11D	*LMO1-3GFP-kanMX; leu2-3,112::pLAO12 (GB-FIS1TMD-LEU2)*	J. J. Heinisch

[1] *MATα ura3-52 leu2-3,112 his3-11,15.*

[2] *MATα/MATα; ura3-52/ura3-52 leu2-3,112/leu2-3,112 his3-11,15/his3-11,15*

Strains constructed in the course of this work

Strain	Modifications compared to HD56-5A[1] or DHD5[2] background	Construction
DAFO1	*MATa/MATα; rho5::KanMX/RHO5; por1::SkHIS3/POR1*	Crossing of HOD266-1B (*por1::SkHIS3*) and HAJ216-A (*rho5::KanMX*). BSc Aileen Faist
HAFO1	*rho5::KanMX; por1::SkHIS3*	Sporulation and tetrad dissection of DAFO1.
DCSO20	*rho5::KanMX/RHO5; DCK1-3GFP-SkHIS/DCK1*	Crossing of HAJ216-A (*rho5::KanMX*) and HAJ152-A (*DCK1-3GFP-SkHIS3*)
HCSO20	*rho5::KanMX; DCK1-3GFP-SkHIS*	Sporulation and tetrad dissection of DCSO20.
DCSO25	*rho5::KanMX/RHO5; LMO1-3GFP-SkHIS/LMO1*	Crossing of HAJ216-A (*rho5::KanMX*) and HMZ31-A (*LMO1-3GFP-SkHIS3*)
HCSO25	*rho5::KanMX; LMO1-3GFP-SkHIS*	Sporulation and tetrad dissection of DCSO25.
DCSO26	*lmo1::KanMX/LMO1; DCK1-3GFP-SkHIS3/DCK1*	Crossing of HAJ201-A (*lmo1::KanMX*) and HAJ152-B (*DCK1-3GFP-SkHIS3*)
HCSO26	*lmo1::KanMX; DCK1-3GFP-SkHIS3*	Sporulation and tetrad dissection of DCSO26.
DCSO33	*dck1::KanMX/DCK1; LMO1-3GFP-SkHIS3/LMO1*	Crossing of HAJ03-B (*dck1::KanMX*) and HMZ31-A (*LMO1-3GFP-SkHIS3*),
HCSO33	*dck1::KanMX; LMO1-3GFP-SkHIS*	Sporulation and tetrad dissection of DCSO33.
DCSO67	*MATa/MATα; SkHIS3-GAL1p-POR1/POR1*	Amplification *SkHIS3-GAL1p* cassette from pFA6a *SkHIS3 GAL1p* with 17.180 + 17.179, transformation into DHD5. Control PCR with 16.237 + 16.238.
HCSO67-1A	*SkHIS3-GAL1p-POR1*	Sporulation and tetrad dissection of DCSO67.
HCSO67-1D	*MATa; SkHIS3-GAL1p-POR1*	Sporulation and tetrad dissection of DCSO67.
DCSO72	*MATa/MATα; rho5::KanMX/ RHO5; SkHIS3-GAL1p-POR1/ POR1*	Crossing of HAJ216-A (*rho5::KanMX*) and HCSO67-1D (*GAL1p POR1 SkHIS3*)
HCSO72-1C	*rho5::KanMX; SkHIS3-GAL1p-POR1*	Sporulation and tetrad dissection of DCSO72.
DCSO76	*MATa/MATα; rho5::kanMX/ RHO5; IDP1::mCherry-SkHIS3/ IDP1*	Crossing of HAJ216-A (*rho5::KanMX*) with *IDP1-mCherry SkHIS3* 5E (J. Hühn)
HCSO76-1A	*MATa; rho5::kanMX IDP1::mCherry-SkHIS3*	Sporulation and tetrad dissection of DCSO76.
DCSO80	*MATa/MATα; por1::KlURA3/ POR1*	Amplification of *KlURA3*-deletion cassette for *POR1* from pJJH1286 with oligos 16.240 + 16.241, transformation into DHD5, control PCR with 16.237 + 16.238
HCSO80-2A	*por1::KlURA3*	Sporulation and tetrad dissection of DCSO80.
DCSO87	*MATa/MATα; por1::KlURA3/ POR1; rho5::SkHIS3/ RHO5*	Crossing of HCSO80-2A (*por1::KlURA3*) with HOD295-7B (*rho5::SkHIS3*).
HCSO87-1A	*por1::KlURA3*	Sporulation and tetrad dissection of DCSO87.
HCSO87-1B	*rho5::SkHIS3*	Sporulation and tetrad dissection of DCSO87.
HCSO87-2B	like HD56-5A	Sporulation and tetrad dissection of DCSO87.
HCSO87-2D	*rho5::SkHIS3; por1::KlURA3*	Sporulation and tetrad dissection of DCSO87.
HCSO87-4A	*por1::KlURA3*	Sporulation and tetrad dissection of DCSO87.
HCSO87-6A	*rho5::SkHIS3*	Sporulation and tetrad dissection of DCSO87.
HCSO87-7A	*rho5::SkHIS3; por1::KlURA3*	Sporulation and tetrad dissection of DCSO87.
DCSO90	*MATa/MATα; bxi1::KanMX; RHO5S326A-SkHIS3*	Crossing of HCSO68-9A (*bxi1::KanMX*) and HD56-RHS326A #8 (*RHO5S326A SkHIS3*).
HCSO90wt	*MATa*	Sporulation and tetrad dissection of DCSO90.

HCSO90-3D	*RHO5S326A-SkHIS3*	Sporulation and tetrad dissection of DCSO90.
HCSO90-5A	*MATa; RHO5S326A-SkHIS3*	Sporulation and tetrad dissection of DCSO90.
HCSO90-7B	*RHO5S326A-SkHIS3*	Sporulation and tetrad dissection of DCSO90.
DCSO91	*MATa/MATα; sch9::KanMX/ SCH9; RHO5wt SkHIS3/RHO5*	Crossing of HD56-RHwt #2 (*RHO5wt-SkHIS3*) and HOD348-4D (*sch9::KanMX*)
HCSO91-1A	*RHO5-SkHIS3*	Sporulation and tetrad dissection of DCSO91.
HCSO91-3C	*MATa; RHO5-SkHIS3*	Sporulation and tetrad dissection of DCSO91.
HCSO91-5A	*RHO5-SkHIS3*	Sporulation and tetrad dissection of DCSO91.
HCSO91-7A	*RHO5-SkHIS3*	Sporulation and tetrad dissection of DCSO91.
HCSO92-3A	*RHO5S326A-SkHIS3*	Sporulation and tetrad dissection of DCSO91.
HCSO92-5A	*RHO5S326A-SkHIS3*	Sporulation and tetrad dissection of DCSO91.
DCSO94	*MATa/MATα; sch9::KanMX/SCH9; RHO5Δ222–319 SkHIS3/RHO5*	Crossing of HD56-R2 (*rho5::KanMX::[YIp RHO5p RHO5dLoop]*) and HOD348-4D (*sch9::KanMX*).
HCSO94-1A	*RHO5Δ222–319-SkHIS3*	Sporulation and tetrad dissection of DCSO94.
HCSO94-11B	*RHO5Δ222–319-SkHIS3*	Sporulation and tetrad dissection of DCSO94.
DCSO95	*MATa/MATα; sch9::kanMX/SCH9 RHO5S328E-SkHIS3/RHO5*	Crossing of HD56-R7 (*rho5::KanMX::[YIp RHO5p RHO5S326E]*) and HOD348-4D (*sch9::KanMX*).
HCSO95-1C	*MATa; RHO5S326E-SkHIS3*	Sporulation and tetrad dissection of DCSO95.
HCSO95-5B	*RHO5S326E-SkHIS3*	Sporulation and tetrad dissection of DCSO95.
DCSO96	*MATa/MATα; sch9::kanMX/SCH9; RHO5G12V-SkHIS3/ RHO5*	Crossing of HD56-R8 (*rho5::KanMX::[YIp RHO5p RHO5G12V]*) and HOD348-4D (*sch9::KanMX*).
HCSO96-1A	*MATa; RHO5G12V-SkHIS3*	Sporulation and tetrad dissection of DCSO96.
HCSO96-3D	*RHO5G12V-SkHIS3*	Sporulation and tetrad dissection of DCSO96.
HCSO96-4C	*RHO5G12V-SkHIS3*	Sporulation and tetrad dissection of DCSO96.
DCSO97	*MATa/MATα; sch9::KanMX/SCH9; RHO5pbrK6A SkHIS3/RHO5*	Crossing of HOD337-7D (*RHO5-6KtA SkHIS3*) and HOD348-4D (*sch9::KanMX*).
HCSO97-1B	*MATa*	Sporulation and tetrad dissection of DCSO97.
HCSO97-3B	*RHO5pbrK6A-SkHIS3*	Sporulation and tetrad dissection of DCSO97.
HCSO97-5C	*MATa; RHO5pbrK6A-SkHIS3*	Sporulation and tetrad dissection of DCSO97.
HCSO97-7C	*MATa*	Sporulation and tetrad dissection of DCSO97.
HCSO97-8A	*RHO5pbrK6A-SkHIS3*	Sporulation and tetrad dissection of DCSO97.
HCSO97-11B	*RHO5pbrK6A-SkHIS3*	Sporulation and tetrad dissection of DCSO97.
DCSO98	*MATa/MATα; sch9::KanMX/SCH9; rho5::SkHIS3/RHO5*	Crossing of HOD295-7D (*rho5::SkHIS3*) and HOD348-4D (*sch9::KanMX*).
HCSO98-2B	*MATa; rho5::SkHIS3*	Sporulation and tetrad dissection of DCSO98.
HCSO98-4A	*MATa; rho5::SkHIS3*	Sporulation and tetrad dissection of DCSO98.
DCSO99	*MATa/MATα; rho5::KanMX/ RHO5; rdi1::SkHIS3/RDI1*	Crossing of HAJ216-A (*rho5::KanMX*) und HOD355 (*rdi1::SkHIS3*).
HCSO99-1D	*rho5::KanMX; rdi1::SkHIS3*	Sporulation and tetrad dissection of DCSO99.
DCSO102	*MATa/MATα; bxi1::KanMX/BXI1; GFP-RHO5 SkHIS3/RHO5; GFPbinder-FIS1 LEU2::leu2-3,112 [pLAO12]/ leu2-3,112*	Crossing of HCSO68-9A (*bxi1::KanMX*) and HOD370-3B (*GFP-RHO5 SkHIS3; GB-FIS1 LEU2::leu2-3,112 [pLAO12]*).

HCSO102-2B	*leu2-3,112::pLAO12 (GB-FIS1TMD-LEU2)*	Sporulation and tetrad dissection of DCSO102.

[1] *MATα ura3-52 leu2-3,112 his3-11,15.*
[2] *MATα/MATα; ura3-52/ura3-52 leu2-3,112/leu2-3,112 his3-11,15/his3-11,15*

2.1.7 Bacterial strain

Bacterial strain	Genotype	Source
DH5α	*F– Φ80lacZΔM15 Δ(lacZYA-argF) U169 recA1 endA1 hsdR17 (rK–, mK+) phoA supE44 λ– thi-1 gyrA96 relA1*	GIBCO BRL (Gaithesburg MD USA)

2.1.8 Oligonucleotides used in this study

The oligonucleotides used in this work were supplied by Metabion International AG (Martinsried, Germany).

Number	Name	Sequence (3‘ – 5‘)
99.41	RHO5-44c	CCTACTGCACCATCACC
99.98	Reverse	CAGGAAACAGCTATGACCATG
04.19	GALpEco	CTGCATAACCACTTTAACTAATAC
04.36	YIp128	GAAGGGAGAAAGGCGGACAGG
13.099	ScRHO5GFPfor	AAATATTTATTAAATACAATATAGTATACTAATAAGTCTGATG TCTAAAGGTGAAGAATTATTC
13.100	ScRHO5GFPrev	CACCATCACCAATTATCACACATTTAATAGACCTCATAGCGGT ACCAGAACCAACACCAGCTTTGTACAATTCATCCATACC
13.183	SkHIS3raus3	GAGTGCGTTCAAGGCTTTGG
15.344	Rho5 BglII S326L	GACAAGAAGAAAAAGAAGTCAAAGCTTGTAATACTTTAAGAT CTAGGAGGCAGAAAAAG
15.345	Rho5 BglII C328A	GACAAGAAGAAAAAGAAGGCCAAGTGTGTAATACTTTAAGA TCTAGGAGGCAGAAAAAGT
16.003	Rho5 BglII C328S	GACAAGAAGAAAAAGAAGTCAAAGTCTGTAATACTTTAAGAT CTAGGAGGCAGAAAAAG
16.004	Rho5 BglII S326E	GACAAGAAGAAAAAGAAGGAAAAGTGTGTAATACTTTAAGA TCTAGGAGGCAGAAAAAG
16.237	POR1forXho	GAAGTTCTCCTCGAGGATTTAGG
16.238	POR1revHind	GAATATCAAAGCTTCCTGGAGTCAG
16.240	por1del5	AAACAGCCAAGCGTACCCAAAGCAAAAATCAAACCAACCTCT CAACTTCGTACGCTGCAGGTCGAC
16.241	por1del3	ATATATGGTATATAGTGAACATATATATATTAGATATATACGC ATAGGCCACTAGTGGATCTG
17.095	GFP_binderfor	AACAGCTATGACCATGATTACGCCAAGCTTGCATGCCTGCAT GGCCGATGTGCAGCTGGT
17.096	GFP_binderrev	TCTTCGCCATAGAGTATTCACCGAGTTTGTAGCAACCTATTGA GGAGACGGTGACCTGGG
17.124	pAFOforHind_PFK2p	TGGAATTGTGAGCGGATAACAATTTCACACAGGAAACAGCG ACAGTGAATTCTAGCTTCCAC
17.125	pAFO3rATG_PFK2p	TGCACCAAGGCTCCCCCAGACTCCACCAGCTGCACATCGGCC ATTGCGTATGGTTAGTTCTTGGCCAATGC

17.179	POR1_F4	AAAGAACCCCTTTTATAGCCAGCAGAGCACGAGTTGATCTGAATTCGAGCTCGTTTAAAC
17.180	POR1_R2	TGATATTTCTGGAGATATCGCTGTAAACTGGAGGAGACATCATTTTGAGATCCGGGTTTT
17.086	FIS1(90-155)_F_SalI	GATCGTCGACCCATAGGTTGCTACAAACTC
17.087	FIS1(90-155)_R_BamHI	GCGCGGATCCTCTCACAATACAGTATTACG
17.095	GFP_binderfor	AACAGCTATGACCATGATTACGCCAAGCTTGCATGCCTGCATGGCCGATGTGCAGCTGGT
17.096	GFP_binderrev	TCTTCGCCATAGAGTATTCACCGAGTTTGTAGCAACCTATTGAGGAGACGGTGACCTGGG
17.124	pAFOforHind_PFK2p	TGGAATTGTGAGCGGATAACAATTTCACACAGGAAACAGCGACAGTGAATTCTAGCTTCCAC
17.125	pAFO3rATG_PFK2p	TGCACCAAGGCTCCCCCAGACTCCACCAGCTGCACATCGGCCATTGCGTATGGTTAGTTCTTGGCCAATGC
17.178	RHO5(314-330)_PstI_f	GCACCTGCAGGCCAAAGACGAGAAACGACAA
18.085	hsRAC1_rev_GFP	CAGCACCATCACCAACAACAACACACTTAATGGCTTGCATTTTGTACAATTCATCCATAC
19.087	PBR(RHO5)_RAC1_for	TGTTTTCGATGAAGCTATCAGAGCTGTTTTGTGTCCACCACCAAAGACGAGAAACGACAA

2.1.9 Pre-existing plasmids used in this study

Name	Relevant Features	Source
pJJH455	*PFK2p GFP; LEU2; 2µm*	J. J. Heinisch
pJJH1637	*RHO5p RHO5; LEU2; CEN4/ARS1; bla*	(Sterk et al. 2019)
pJJH1639	*RHO5p GFP-RHO5; LEU2; CEN4/ARS1; bla*	(Schmitz et al. 2018)
pJJH2294	*PFK2p-hsRAC1; URA3; CEN4/ARS1; bla*	J. J. Heinisch
pJJH2334	*ScRHO5-G12V; LEU2; CEN4/ARS1; bla*	J. J. Heinisch
pJJH2562	*RHO5p GFP-RHO5C110; CEN4/ARS1; LEU2; bla*	J. J. Heinisch
pJJH2616	*RHO5p GFP-RHO5Δ222–314; URA3; CEN4/ARS1; bla*	J. J. Heinisch
pSH4	YEp352 *GAL1/10p RHO5*	(Schmitz et al. 2002)
pSH8	YEp352 *GAL1/10p RHO5Q91H*	(Schmitz et al. 2002)
pYM40 GFPchromo	*GFP binder-kanMX; bla*	(Busto et al. 2018)
YCplac33	*URA3; CEN4/ARS1; bla*	(Gietz and Sugino 1988)
YCplac111	*LEU2; CEN4/ARS1; bla*	(Gietz and Sugino 1988)
YIplac128	*LEU2; bla*	(Gietz and Sugino 1988)

2.1.10 Plasmids constructed in this study

Name	Relevant features	Construction	Source
pAFO1	*FIS1(83-155); URA3; CEN4/ARS1; bla*	PCR with 17.086 and 17.087 on genomic DNA from *S. cerevisiae*. Restriction of YCplac33 and 645bp PCR-product with SalI and BamHI, ligation, control restriction with PvuII	Aileen Faist
pAFO3	*GFPbinder-FIS1(83-155); URA3; CEN4/ARS1; bla*	PCR of GFPbinder from pYM40 with 17.095 and 17.096, linearization of pAFO1 with SalI,	Aileen Faist

		co-transformation in DHD5 for ivR, control restriction with PstI and EcoRI	
pAFO9	*PFK2p GFPbinder-FIS1(83-155); URA3; CEN4/ARS1; bla*	PCR of *PFK2p* from pJJH2076 with 17.124 and 17.125, linearization of pAFO3 with HindIII, co-transformation in DHD5 for ivR, control restriction with EcoRI	Aileen Faist
pCSO9	*RHO5p GFP; LEU2; CEN4/ARS1; bla*	Restriction of YCplac111 and pJJH1639 with EcoRI and KpnI, agarose electrophoresis of cut pJJH1639 and extraction of 1638bp band, ligation with cut YCplac111, blue-white-screen	this work
pCSO18	*RHO5p GFP-RHO5C328L; LEU2; CEN4/ARS1; bla*	PCR with 15.344 and 99.98 on pJJH1639, restriction of pJJH1639 with PaeI and co-transformation in DHD5 for ivR	this work
pCSO19	*RHO5p GFP-RHO5S326A; LEU2; CEN4/ARS1; bla*	PCR with 15.345 and 99.98 on pJJH1639, restriction of pJJH1639 with PaeI and co-transformation in DHD5 for ivR	this work
pCSO23	*GAL1p RHO5S326E; LEU2; CEN4/ARS1, bla*	PCR with 16.004 and 99.98 on pJJH1639, restriction of pJJH1635 with PaeI and co-transformation in DHD5 for ivR	this work
pCSO31	*RHO5p GFP-RHO5S326E; LEU2; CEN4/ARS1; bla*	PCR on pCSO23 with 99.41 and 04.36, restriction of pJJH1639 with PaeI and co-transformation in DHD5 for ivR	this work
pCSO35	*RHO5p GFP-RHO5pbrK6A; LEU2; CEN4/ARS1; bla*	PCR on pJJH2107 with 99.41 and 99.98, restriction of pJJH1639 with PaeI and co-transformation in DHD5 for ivR	this work
pCSO50	*PFK2p GFP-RHO5C110; LEU2; 2µ; bla*	PCR on pJJH1636 with 17.178 + 99.98, restriction of product and pJJH455 with SphI and PstI co-transformation in DHD5	this work
pCSO85	*TEF2p hsRAC1-RHO5; LEU2; CEN4/ARS1; bla*	Restriction of pJJH2295 and pJJH1239 with BamHI and SphI, ligation	this work
pCSO89	*RHO5p GFP-RAC1-RHO5C110; LEU2; CEN4/ARS1; bla*	Restriction of pCSO9 and pJJH2295 with BamHI and SphI, ligation	this work
pCSO91	*RHO5p RHO5(T17N); URA3; CEN4/ARS1; bla*	PCR on pAJ146 with 14.034 and 17.300, restriction of product and pJJH1636 with BamHI and KpnI, co-transformation in DHD5 for ivR	this work
pCSO92	*RHO5p GFP-RHO5(T17N); LEU2; CEN4/ARS1; bla*	Restriction pCSO9 and pCSO91 with BamHI and SphI, ligation	this work
pCSO94	*RHO5p 2xGFP-RHO5C17; LEU2; CEN4/ARS1; bla*	Restriction of pCSO9 and pCSO50 with BamHI and SphI, ligation	this work
pCSO95	*RHO5p 2xGFP-RHO5pbrK6AC17; LEU2; CEN4/ARS1; bla*	Restriction of pCSO9 and pCSO82 with BamHI and SphI, ligation	this work
pCSO98	*RHO5p RAC1-RHO5C110; URA3; CEN4/ARS1; bla*	Restriction of pJJH2295 and YCplac111 with EcoRI and SphI, ligation	this work

pCSO99	*RHO5p RAC1-RHO5C17; URA3; CEN4/ARS1; bla*	PCR on pJJH1636 with 19.087 and 99.98, restriction of pLAO4 with XhoI and co-transformation in DHD5 for ivR	this work
pCSO100	*RHO5p GFP-RAC1-RHO5C17; URA3; CEN4/ARS1; bla*	PCR with 19.087 and 99.98 on pJJH1636, restriction of pCSO99 with XhoI and co-transformation in DHD5 for ivR	this work
pLAO2	*RHO5p GFP-RHO5G12V; LEU2; CEN4/ARS1; bla*	Amplification of myeGFP from pJJH1619 with 13.099 and 13.100, restriction of pJJH2333 with BamHI, co-transformation in DHD5 for ivR	Lauren Graeber
pLAO4	*RHO5p hsRAC1; LEU2; CEN4/ARS1; bla*	Restriction of pJJH2293 and YCplac111 with EcoRI and HindIII, ligation	Lauren Graeber
pLAO5	*RHO5p GFP-RHO5Δ222–319; URA3; CEN4/ARS1; bla*	Amplification of myeGFP from pJJH1619 with 13.099 and 13.100, restriction of pJJH2300 with BamHI, co-transformation in DHD5 for ivR	Lauren Graeber
pLAO6	*RHO5p GFP-hsRAC1; URA3, CEN4/ARS1; bla*	Amplification of myeGFP from pJJH1619 with 13.099 and 18.085, restriction of pJJH2293 with BamHI, co-transformation in DHD5 ivR	Lauren Graeber
pLAO12	*PFK2p GFPbinder-FIS1TMD; LEU2; bla*	Restriction of pAFO9 with EcoRI and BamHI, ligation with YIp128	Lauren Graeber

2.2 Methods

2.2.1 Handling of *Escherichia coli*

2.2.1.1 Growth conditions and preparation of over-night culture

For an over-night culture of *E. coli*, 3 ml of LB_0 were mixed with ampicillin (0,1 mg/ml), inoculated with a sample of a bacterial colony and incubated on a rotator at 37 °C for 16 hours. Bacteria were centrifuged at 5.000 rpm (2400x g) for 3 minutes.

2.2.1.2 Competent *Escherichia coli* and Transformation with plasmid DNA

The transformation of the *E. coli* strain DH5α followed the rubidium chloride method of (Hanahan 1983).

2.2.2 Handling of yeast strains

2.2.2.1 Handling of *Saccharomyces cerevisiae*, preparation of an over-night culture

For a yeast over-night culture, 3 ml of the appropriate medium was inoculated with a probe of a yeast colony and incubated at 30 °C for 16 hours on a shaker set at 180 rpm. In case the strain harboured a plasmid, the medium was chosen for plasmid maintenance according to the auxotrophy. When selecting for a *kanMX* cassette, the corresponding medium was mixed with 0,2 µg/ml geneticin (G418). Yeast cells were centrifuged at 3.000 rpm (900x g) for 3 minutes. Yeast strains were stored at 4°C either

on agar plates or in liquid media for a maximum of two weeks. For long term storage, 750 ml overnight culture was mixed with 1 ml 33 % glycerine and stored at – 75 °C.

2.2.2.2 Construction of deletion mutants and gene tagging in *Saccharomyces cerevisiae*

In vivo recombination for gene substitutions and tagging in *S. cerevisiae* was done by one-step gene replacements using PCR-based gene-targeting methods. To obtain the correspondent cassettes, oligonucleotides were constructed with 18 to 22 base pairs homologous to plasmids from the Longtine collection (Longtine et al. 1998, Sheff and Thorn 2004) at their 3'-ends and with flanking sequences homologous to the targeted genomic locus of 40 base pairs at their 5'-ends, respectively. Deletion cassettes were designed to remove and replace the entire gene with the homologous sequence usually 50 to 100 bp up- and downstream of the open reading frame (ORF). Oligonucleotides for fusion cassette amplification were designed so that the homologous region for the forward primer is 40 base pairs upstream of the stop codon of the target gene. The reverse primer is separated by around 100 bp downstream of the forward primer for optimal recombination, also including a homologous region of 40 base pairs. The resulting PCR product was checked via agarose gel electrophoresis and integrated into *S. cerevisiae* following the lithium acetate method (Gietz et al. 1995) or the lithium acetate freeze method (Gietz and Schiestl 2007). To determine the correct integration of the DNA fragments, samples of single colonies of an agar plate, which selects for the respective genetic manipulation, were subjected to "Quick-and-dirty" genomic DNA extraction. Until noted otherwise, two PCR reactions were employed using two different primer pairs: For the first reaction the forward primer bound in the native locus upstream of the genetically manipulated gene and the reverse primer within the integration. In the second reaction the forward primer bound within and the reverse primer in the native locus downstream of the integration. The product sizes were confirmed via agarose gel electrophoresis. For oligonucleotide design and assembly of sequences the Clone Manager 9 program (Scientific and Educational Software, Denver, CO, USA) was employed. DNA concentration was measured using the NanoPhotometer NP80.

2.2.2.3 Sporulation, determination of the mating type and crossing

To induce sporulation of *S. cerevisiae*, an over-night culture of a diploid strain was grown in rich medium to stationary phase. In case the strain harboured a plasmid, selective complete medium lacking the corresponding marker was used. The probe was then centrifuged, the supernatant discarded, and the cell pellet resuspended in the remaining liquid. The sample was placed on solid medium with 1 % potassium acetate and incubated at 30 °C for sporulation for at least 2 days. Ascus formation was checked under a light microscope by mixing a small cell sample with water on a glass slide. The mating type of segregants was determined by spreading 50 µl of the yeast strains LD3R-7B

and SMC-19A separately in an ovoid area in the middle of full medium agar plates. After drying, 15 µl of an overnight culture from the correspondent segregant was dropped above the ovoid area and while still moist, mixed with the LD3R-7B or SMC-19A sample using a toothpick and pulled down in zigzag lines to obtain single colonies. The two plates were incubated for one night at 30 °C and subsequently replica-plated on synthetic medium agar plates lacking leucine. After another incubation of 2 days at 30 °C the selective plate was checked for complementation. For crossing of strains, 50 µl of each overnight culture were mixed in a reaction tube, supplied with 500 µl fresh full medium and incubated at 30 °C for 4 to 6 hours. The sample was centrifuged, supernatant discarded, cells mixed in the remaining medium and spread on medium selecting for markers of both parental strains.

2.2.2.4 Tetrad analysis

For tetrad analysis, diploid strains were subjected to sporulation. After microscopic confirmation of ascus formation, a sample was put in 100 µl of sterile water with 4 µl of Zymolyase 20T (10 mg/ml; MP Biomedicals, Germany) and incubated at room temperature for 7 to 10 minutes. 15 µl of the sample was placed on a YEPD plate and spores were separated using a Singer MSM400 micromanipulator. Plates were incubated at 30 °C for 3 days and the growth was documented by scanning. Resulting pictures were adjusted for brightness and contrast using CorelDraw 2019 (Corel, Canada) with the same settings for the entire plate. To determine the area of the tetrads, the area measurement function of ImageJ was employed.

2.2.2.5 Growth and sensitivity analysis by serial drop dilution assay

Cells were pre-grown in either rich medium or, in case the strain harboured a plasmid, in synthetic medium overnight at 30 °C. The OD_{600} of the culture was determined and an appropriate volume of culture was transferred to fresh medium and adjusted to an OD_{600} of 0.3. The samples were placed on a shaker and incubated at 180rpm and 30°C until at least two rounds of cell division were completed and the culture reached mid-logarithmic phase. A volume equivalent to 1 OD_{600} was than centrifuged, the supernatant carefully removed, the cell pellet resuspended in 1 ml fresh medium and diluted in 10^{-1}, 10^{-2}, 10^{-3} and 10^{-4} steps using a 96 well plate (Thermo Scientific, Bremen, Germany). 3 µl of each dilution including the undiluted sample (being 10^{0}) were transferred to an agar plate with or without a stressor. Plates were then incubated at 30 °C, scanned once a day for documentation and the pictures processed for contrast and brightness with CorelDraw 2019.

2.2.2.6 Growth analysis and sensitivity in a microwell plate scanner

To record growth curves, cells were pre-grown overnight in either rich or synthetic medium at 30 °C on a shaker set at 180 rpm. Cells were inoculated in fresh medium at an OD_{600} of 0.3, grown to mid-

logarithmic phase and diluted to an OD_{600} of 0.1 in fresh medium in 100 µL aliquots into 96-well plates (Thermo Scientific, Germany), with or without hydrogen peroxide. Growth was recorded in a Varioscan Lux plate reader following the increase in OD_{600} by measuring each well once every 30 minutes for at least 18 hours at 30 °C. Plates were shaken with 1024 rpm with 5 seconds intervals to avoid sedimentation. The setup was controlled by the SkanIt Software 4.1 for microplate readers, version 4.1.0.43. After data acquisition, a factor of 3.546 was used for normalization with standard 1 cm cuvettes, as the path length in the cell culture was 0.282 cm. A minimum of two biological replicates (usually different segregants with the same mutant alleles obtained from tetrad analyses) and two technical replicates were recorded, and data sets combined into one growth curve with the standard error bars given at each mean value of each time point, respectively.

2.2.3 Analysis of DNA

2.2.3.1 Polymerase chain reaction (PCR)

In order to construct yeast strains with a deletion or gene tagging the corresponding forward (F1 for deletion, F2 for tag) and reverse (R1 for deletion and tag) primer were used to amplify the correspondent cassette. Until mentioned otherwise, the template originated from the Longtine series (Longtine et al. 1998). Two separate 50 µl-PCR samples were mixed and included 0,2 µM of each primer, 200 µM dNTPs, 1 unit Phusion DNA polymerase, 10 µl 5x Phusion buffer and 2 µl plasmid preparation. The elongation time (t_{el}) was calculated with 30 seconds for 1 kb and, until noted otherwise, the annealing temperature (T_{An}) was 56 °C. The cycle steps were as followed: 1 x 5 minutes 98 °C, 32x [10 seconds 98 °C, 30 seconds T_{An}, 30 seconds/kb 72 °C], 1x 10 minutes 72 °C.

For a control PCR of a new yeast strain, the DreamTaq DNA polymerase was used. The 20 µl sample contained 0,2 µM of each primer, 200 µM dNTPs, 0.5 unit DreamTaq DNA polymerase and 2 µl 10x DreamTaq buffer. As template, genomic DNA (either 2 µl Q&D or 1 µl clean) was added. The elongation time (t_{el}) was calculated with 1 minute for products up to 2kb and 1 minute per 1 kb for products longer than 2 kb. The annealing temperature (T_{An}) was 56 °C and the cycle steps were as followed: 1 x 5 minutes 95 °C, 32x [10 seconds 95 °C, 30 seconds T_{An}, 1 minute/kb 72°C], 1x 10 minutes 72 °C. After the PCR, the samples were mixed with 10x sample buffer (FD Green Buffer) and applied into the wells of an agarose gel.

2.2.3.2 Separation of DNA fragments via agarose gel electrophoresis

DNA fragments were separated via electrophoresis in a 1 % (m/v) agarose gel. Agarose was put in 1x TAE and boiled in a microwave until completely dissolved (6 minutes) and subsequently poured into an agarose gel chamber with a comb to create wells. After cooling, the gel was covered with 1x TAE, the comb removed, and the sample(s) applied in the wells. Until mentioned otherwise, the

GeneRuler™ 1kb DNA Ladder (Thermo Scientific) was used as size marker. DNA separation was achieved by connecting the chamber to a power supply at 90 V for 40 to 60 minutes depending on the size of the fragment(s). After the electrophoresis, the gel was removed from the chamber and stained in an ethidium bromide solution (0.5 µg/ml in H_2O) for 20 to 30 min. For the visualization of the fragments, the gel was exposed to UV light (λ = 366nm) and documented via the BioImagingSystem GelDoc-IT Imaging System.

2.2.3.3 Extraction of DNA fragments from an agarose gel

DNA fragments were separated by agarose gel electrophoresis as described above and excised with a scalpel under UV light (λ = 312nm). The gel was placed in a reaction cup and the DNA was extracted using the GeneJET DNA Extraction Kit following the manufacturer's instructions (Thermo Scientific).

2.2.3.4 Plasmid extraction

2.2.3.4.1 From *E. coli*

For the extraction of plasmid DNA from *E. coli*, the GeneJET Plasmid MiniPrep Kit (Thermo Scientific) was used following the manufacturer's instructions. To screen larger numbers of *E. coli* colonies for correct integration of an insert, columns of the GeneJET Plasmid MiniPrep Kit were reprocessed by using the maxXbond MB007 DNA Binding Column Regeneration Kit (AppliChem GmbH, Germany) according to the manufacturer's instructions. For cell lysis, self-prepared buffers MPI1, MPI2 and MPI3 were employed following the protocol of the GeneJET Plasmid MiniPrep Kit. To determine the DNA concentration and purity, 1 µl of the resulting sample was measured with the NanoPhotometer NP80.

2.2.3.4.2 From *S. cerevisiae*

For the isolation of plasmid DNA from yeast cells, 5 ml of an overnight culture were centrifuged, and the pellet was resuspended in 400 µl MPI1. 0,4 ml glass beads were added, and the sample put on a Vibrax at 4 °C for 45 minutes for mechanical disruption of the yeast cells. 250 µl of the supernatant was transferred into a new reaction cup and further processed with the MPI solutions following the instructions of the GeneJET Plasmid MiniPrep Kit (Thermo Scientific) using regenerated tubes. The bound plasmid was eluted with 20 µl heated elution buffer and 10 µl of the eluted plasmid was subsequently used for *E. coli* transformation.

2.2.3.5 Sequencing of plasmid DNA

For sanger sequencing, samples of the constructed plasmids were sent either to Microsynth SeqLab (Göttingen, Germany) or the GATC Biotech AG (Konstanz, Germany) with the mixture corresponding to the respective supplier's instructions. The resulting data were analysed using the sequence assembly tool of the software Clone Manager 9, Professional Edition.

2.2.3.6 Restriction of DNA with endonucleases

To check the identity of plasmids, correct cloning or to prepare DNA for ligation, restriction with endonucleases from either Thermo Scientific or New England Biolabs (NEB) was employed. Identity of plasmids or correct cloning was verified using 20 µl samples containing 2 µl of the appropriate enzyme buffer mixed with 0,5 units of endonuclease. The respective volume of dH_2O was added up to the end volume.

2.2.3.7 Ligation of DNA fragments

For ligation of DNA fragments, 20 µl samples were prepared containing 1 µl T4 DNA-Ligase (5 units), 2 µl ligase buffer (40 mM Tris/HCl, 10 mM $MgCl_2$, 10 mM DTT und 0,5 mM ATP (pH 7,8)), 30 ng cut target vector and 90 ng original vector or insert DNA. The respective volume of dH_2O was added up to the final 20 µl. Incubation was carried out at room temperature for 1 hour. If necessary, inactivation was performed at the appropriate temperature depending on the endonuclease used. To determine the DNA concentration and purity, 1µl of the resulting sample was measured with the NanoPhotometer NP80.

2.2.3.8 Chromosomal DNA extraction from *Saccharomyces cerevisiae*

2.2.3.8.1 "Quick-and-dirty" DNA extraction

A pin head-sized cell sample was picked from an agar plate with a sterile toothpick and dissolved in 50 µl 20 mM NaOH. After the incubation at RT for 20 minutes, the sample was microwaved for 2 minutes and centrifuged briefly. The supernatant was subsequently used for PCR.

2.2.3.8.2 Pure DNA Extraction

1,5 ml of an overnight culture was centrifuged and the resulting cell pellet resuspended in 300 µl spheroblast buffer. The sample was incubated 1 hour at 37 °C in the presence of 4 µl Zymolyase (25 mg/ml) to enzymatically digest the cell wall. For cell lysis 50 µl 10 % (m/v) SDS and 50 µl 0,5M EDTA (pH 8,0) were added and the sample incubated at 65 °C for 30 minutes and cooled at RT for another 5 minutes. Proteins were precipitated by adding 5 M potassium acetate (pH 8,6) and incubation on ice for 1 hour. Cell debris and precipitated proteins were centrifuged at 10.000 rpm for 10 minutes at 4 °C. 500 µl of the supernatant was transferred into a new reaction cup, mixed with 340 µl 2-Propanol, incubated 5 minutes at RT and centrifuged at 13.000 rpm at 4 °C for another 15 minutes. To remove remaining salts, the pellet was washed with 1 ml 70 % (v/v) ethanol and centrifuged at 13.000 rpm for 5 minutes. The ethanol was decanted carefully and the pellet dried. The genomic DNA was dissolved in 50 µl dH_2O and stored at -20 °C.

2.2.3.9 Gene synthesis

For human *RAC1* and *RHO5*, string-DNA synthesis was ordered from GeneArt (Thermo Scientific, Germany) with the open reading frame optimized for *S. cerevisiae* codon usage. Before usage, the synthesised gene was first cloned into pUK1921 for sequence verification (see 2.2.3.5).

2.2.4 Cell Imaging and life-cell fluorescence microscopy

Fluorescence microscopy was performed with a Zeiss Axioplan 2 (Carl Zeiss, Jena, Germany) microscope equipped with a 100× alpha-Plan Fluor objective (numerical aperture 1.45) and differential-interference contrast (DIC), as described previously (Schmitz et al. 2015). Images were acquired using a Photometrics CoolSNAP HQ Camera (Roper Scientific, Tucson, AZ, USA). Fluorescence was excited with a SPECTRA X light engine (Lumencor, Beaverton, OR, USA). The setup was controlled by the Metamorph v6.2 program (Universal Imaging Corporation, Downingtown, PA, USA). Brightfield images were acquired as single planes using DIC. For standard microscopic examination cells were grown to mid logarithmic phase in SCD medium. For oxidative stress exposure, 4.4 mM hydrogen peroxide was added to the sample prior to image acquisition throughout all localization studies, and images were taken for 5 to 15 minutes post-stress exposure. Depending on the subcellular distributions of GFP-Rho5 signals, cells were categorized in three patterns: association of the signal with the plasma membrane (pm), being either cytosolic or associated with internal structures (int), and those co-localizing with the mitochondrial marker (mit). These numbers were divided by the total number of cells examined in each case and multiplied by 100 to calculate the percentages of cells showing the respective localization. Figures were chosen to depict representative examples of hundreds of images examined for each condition and strain. In case cells showed more than one signal localization, priority was set as follows: Mitochondria > plasma membrane > internal structures.

Deconvolution of fluorescent pictures was performed with the Huygens Remote Manager v3.5 (Scientific Volume Imaging B.V.). Scale bars were added using Metamorph's scale image command. In order to visualize colocalization of signals from the mCherry- and the GFP-channels from the same cell, the processed images were overlaid using Metamorph's overlay images command. For the arrangement of pictures Metamorph's stack and montage command was employed.

2.2.5 Abbreviations

ARS	Autonomously replicating sequence	**GTP**	Guanosine triphosphate
cAMP	Cyclic adenosine monophosphate	**HOG**	High osmolarity glycerol
CEN	centromere	**HVR**	Hypervariable region
CWI	Cell wall integrity	**ivR**	In vivo recombination
DHR	DOCK homology region	**LB**	Lysogeny broth medium

DIC	Differential interference contrast (microscopy)	**MAPK**	Mitogen-activated protein kinase
DNA	Deoxyribonucleic acid	**OD_{600}**	Optical density at a wavelength of 600 nm
DOCK	Dedicator of cytokinesis	**PBR**	Polybasic region
e.g.	Lat.: exempli gratia (= for example)	**PCR**	Polymerase chain reaction
ELMO	Engulfment and motility	**PIP_2**	Phosphatidylinositol-4,5-bisphosphate
ER	Endoplasmic reticulum	**PM**	Plasma membrane
FRAP	Fluorescence recovery after photobleaching	**PTM**	Posttranslational modification
GAP	GTPase-activating protein	**SCD**	Synthetic complete dextrose medium
GB	GFP-binding monomeric antibody	**SCGal**	Synthetic complete galactose medium
GDI	Guanine nucleotide dissociation inhibitor	**TAE**	Tris/acetate/EDTA buffer
GDP	Guanosine diphosphate	**TMD**	Transmembrane domain
GEF	GDP/GTP exchange factor	**WT**	Wild type
GFP	Green-fluorescent protein	**YEPD**	Yeast extract peptone dextrose (rich medium)
GPCR	G protein coupled receptor		

Nucleotides and amino acids are represented with the single letter code (IUPAC-IUB Commission on Biochemical Nomenclature).

3. Results

3.1 Importance of the C-terminal region for intracellular distributions of Rho5

The distribution of Rho-GTPases to a variety of different cellular compartments is known to depend on a range of stimuli (Philips et al. 1993, Fleming et al. 1996, Kranenburg et al. 1997). There are several common mechanisms to ensure the correct association with compartments, two of which are determined by the primary sequence of Rho proteins. First, the interaction with membranes is mediated by a lipid modification of the CAAX motif's cysteine. Secondly, a preceding polybasic region (PBR) was frequently shown to be essential for a proper compartmentalization.

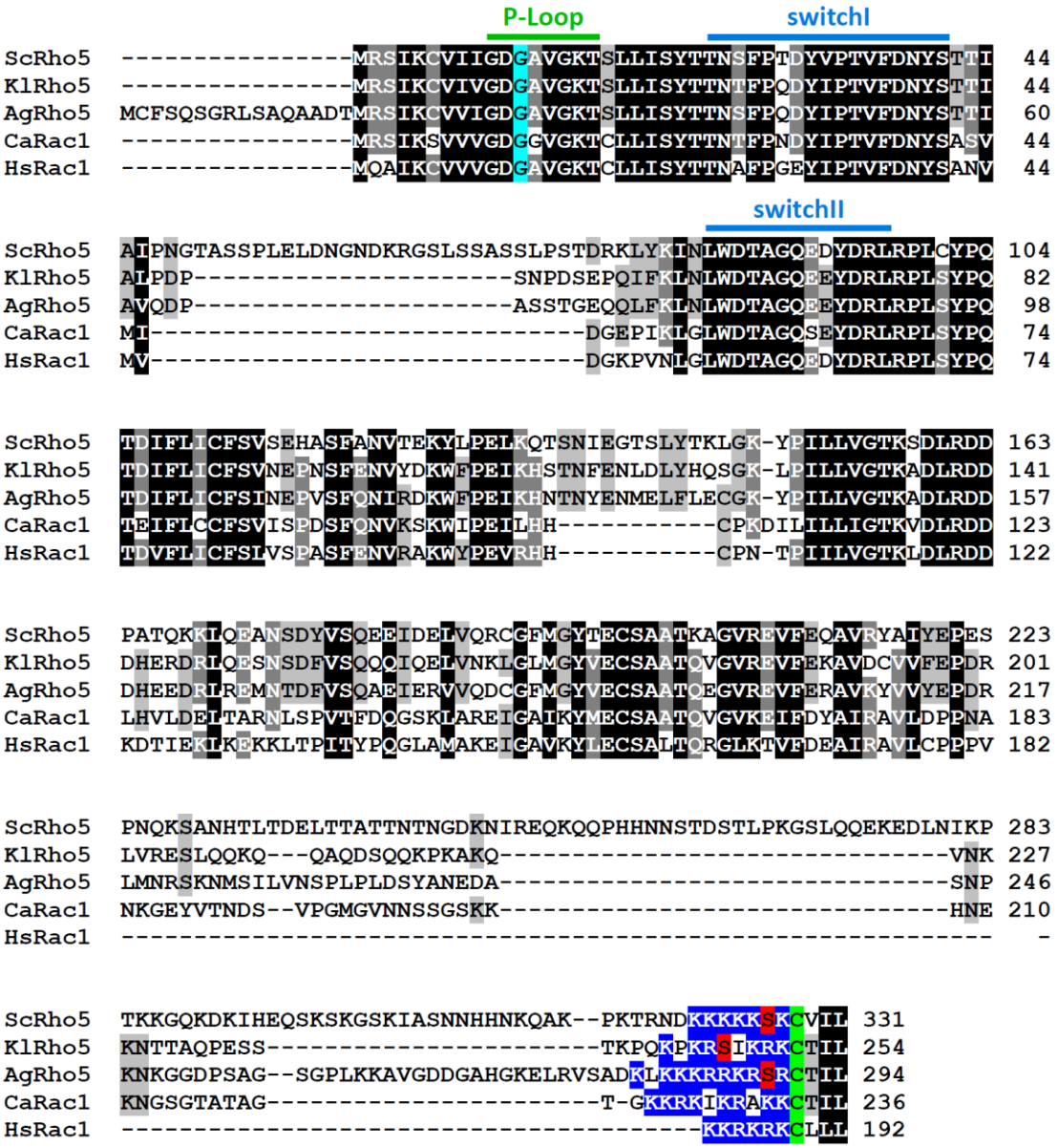

Figure 5: Alignment of Rho5 homologues from different species The multiple sequence alignment was performed online on the T-Coffee server website based on ClustalW (Thompson et al. 1994). Data were then imported into and designed with GeneDoc (version 2.5.000). Annotation of P-loop, switch I and II based on (Schaefer et al. 2014). Chosen Rho-GTPases: *Sc*Rho5 (*Saccharomyces cerevisiae*) – *Kl*Rho5 (*Kluyveromyces lactis*) – *Ag*Rho5 (*Ashbya gossypii*) – *Ca*Rac1 (*Candida albicans*) – *Hs*Rac1. Degree of conservation among the Rho proteins: Black = 100 %, grey with white letters = 80 %, grey with black letters = 60 %. Specific residues of interest are coloured: Turquoise = Conserved glycine essential for GTPase activity, blue = Polybasic region, red = serine residue in the polybasic region, green = cysteine of the CAAX motif.

These two motifs, together with additional amino acid residues, have also been designated as the "hypervariable region" of GTPases (Hancock et al. 1991, Choy et al. 1999, Michaelson et al. 2001).

3.1.1 *In silico* analysis of the primary sequence of Rho5 and its homologues

In order to determine whether the aforementioned structural features are conserved in Rho5, its primary sequence and the ones of four homologues from other organisms were analysed *in silico*. The resulting alignment of the five Rho proteins is depicted in Figure 5 and reveals two distinct features of the amino acid sequence situated at Rho5's C-terminal region: The last four amino acids "CVIL" are in accordance with the described CAAX motif and it is preceded by a sequence of six lysine residues meeting the PBR requirements. Furthermore, the alignment uncovers an insertion of 98 residues in Rho5 that is missing in the human Rac1 and precedes the PBR. It also seems to be truncated in Rho5 from *A. gossypii* and even more so in the closely related *K. lactis* with identities among the individual proteins being virtually absent. It is conceivable that this insertion is a specific extension in *S. cerevisiae*'s Rho5 and assumed to be part of the hypervariable region (Sterk et al. 2019). In accordance with that, no significant homologies with other motifs could be identified despite extensive research in databases.

3.1.2 Intracellular distribution of wild type Rho5

As a first step, a construct with an N-terminally GFP-tagged Rho5 on a low copy vector (pJJH1639) previously employed (Schmitz et al. 2015) was introduced into a *rho5* deletion strain with an *IDP1-mCherry* fusion construct at its native genomic locus as a mitochondrial marker (HCSO76-1A). Throughout this work, the strain HCSO76-1A was employed for the determinations of intracellular distribution of GFP-Rho5 and its derivatives. If not stated otherwise, GFP-fusions were introduced on a low-copy number *CEN/ARS* vector. Under standard growth conditions, the GFP signal of the wild type Rho5 was mainly located at the plasma membrane in 94 % of the examined cells (Figure 6B, upper two rows). Upon exposure to 4.4 mM hydrogen peroxide, the GFP signal almost entirely left the plasma membrane and showed a co-localization with the mitochondrial mCherry marker in 70 % of the cells as depicted in the overlay images (lower two rows, right columns). Only in 4 % of the cells the signal remained at the plasma membrane and 26 % showing the signal associated with non-specified intracellular structures. Because of Rho5's involvement in a number of signalling pathways, relocalization in response to glucose starvation was investigated next. To do so, cells were pre-grown in medium containing glucose and then transferred to a medium without a carbon source. As seen in the right panel of Figure 6C, a significant proportion of Rho5 relocated from the plasma membrane to the mitochondria upon carbon starvation, similar to the previously observed behaviour under

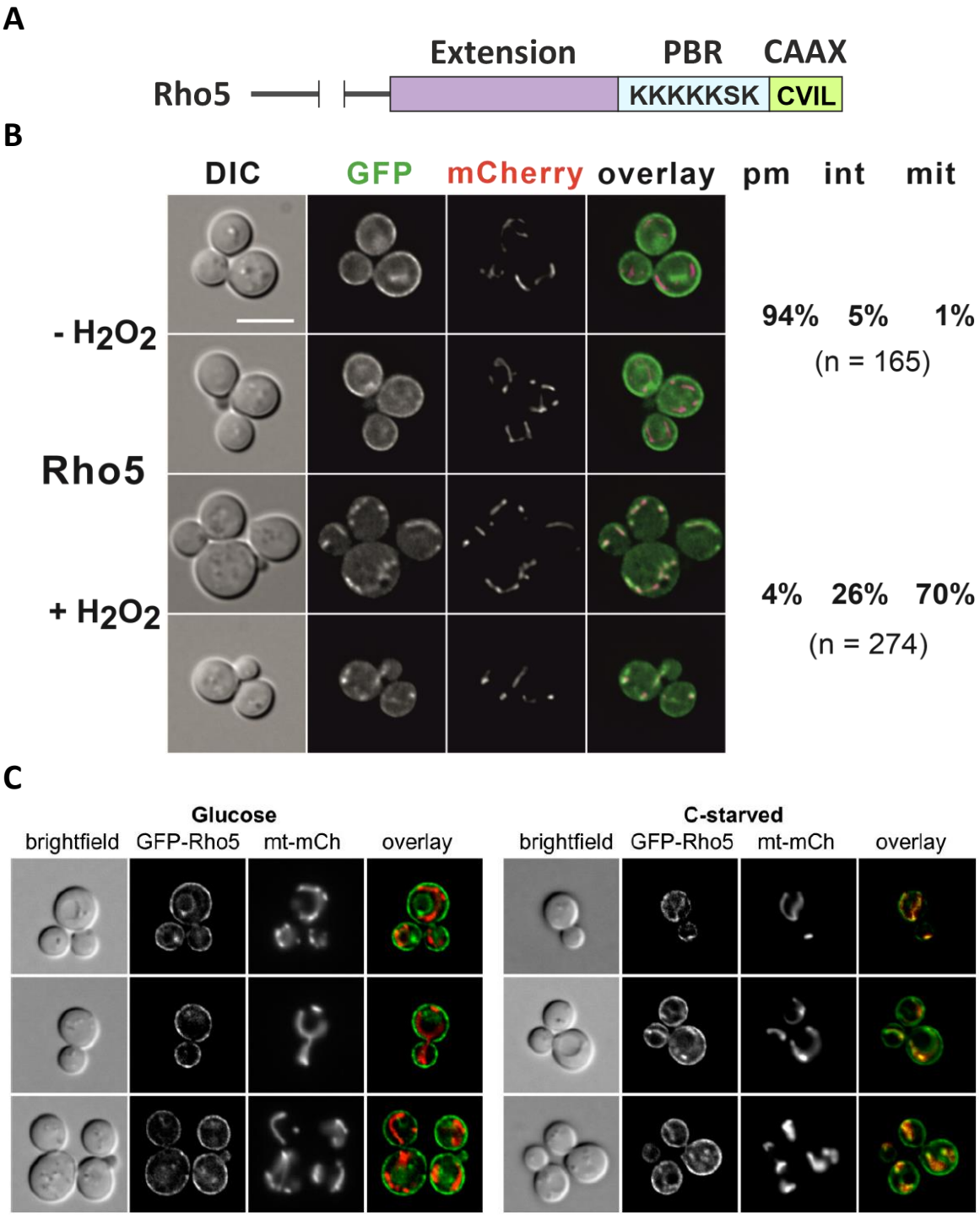

Figure 6: Localization of GFP-tagged Rho5 A: Schematic representation of the C-terminal domains of Rho5. **B:** Life-cell fluorescence microscopy of a *rho5* deletion strain with a mitochondrial mCherry marker (HCSO76-1A) carrying an N-terminally GFP-tagged Rho5 on a *CEN/ARS* vector (pJJH1639). Cells were grown to mid-logarithmic phase and examined under the fluorescence microscope. For induction of oxidative stress, the sample was exposed to 4.4 mM H_2O_2 and examined for 5 to 15 minutes. Cell counts of intracellular localization of the GFP signal are presented on the right-hand side of the microscope pictures. Co-localization of red and green signals is highlighted by a yellow to white pseudo-colorization in the overlay. pm = plasma membrane, int = non-specific internal localization, mit = mitochondrion. Exposure brightfield: 20 ms, excitation GFP channel: 2000 ms, Rhodamine channel: 400 ms. Scale bar indicates 5 µm. **C:** Life-cell fluorescence microscopy of a *rho5* deletion strain with a mitochondrial mCherry marker (HCSO76-1A) carrying the gene for an N-terminally GFP-tagged Rho5 encoded on a *CEN/ARS* vector (pJJH1639). Cells were grown in synthetic medium with 2 % glucose to mid-logarithmic phase and inspected under the microscope. The same sample was then washed twice with synthetic medium without carbon source and resuspended in this medium for carbon starvation ("C-starved"). Cells were observed under the microscope between 5 to 15 minutes after the transfer. Panel was published in (Schmitz et al. 2018).

oxidative stress. In order to investigate potential components involved in Rho5 relocalization, RhoGDIs, which are involved in Rho transport, were included in this study (Boulter et al. 2010). In the first step, a strain depleted of the only RhoGDI in *S. cerevisiae*, Rdi1, was constructed and crossed with a *rho5* deletion strain. Then, the plasmid pJJH1638 was introduced. Under logarithmic growth conditions GFP-Rho5 normally located at the PM (Figure 7, upper row). Exposure to 4.4 mM hydrogen peroxide lead to a reduction of the peripheral GFP signal and an increased association with intracellular tubular structures (lower row).

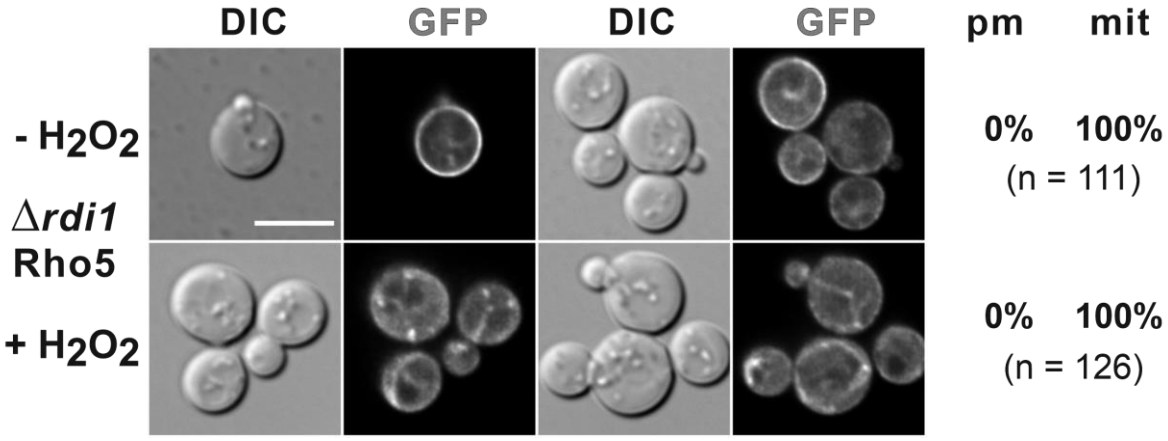

Figure 7: Localization of Rho5 in a Rdi1 depleted strain Life-cell fluorescence microscopy of a *rho5 rdi1* deletion strain (HCSO99-1D) carrying the *RHO5* allele with an N-terminal GFP on a *CEN/ARS* vector (pJJH1638). Cells were grown to mid-logarithmic phase in synthetic selective medium for plasmid maintenance and inspected under the fluorescence microscope. For induction of oxidative stress, the sample was exposed to 4.4mM H_2O_2 and examined for 15 minutes. Microscopy was performed once. Exposure brightfield: 20ms, excitation GFP channel: 2000ms, Rhodamine channel: 400ms. Bar indicates 5 µm.

3.1.3 Importance of Rho5's hypervariable region for its intracellular distribution under different growth conditions

The C-terminal 17 amino acid residues of human K-Ras4B were shown to be sufficient to direct the protein to the plasma membrane which was later also observed for several Rho-type GTPases (Hancock et al. 1991, Michaelson et al. 2001). In order to test whether this was also the case for yeast Rho5, the last 17 codons (codons 314 to 331) were amplified by PCR and cloned in frame to the GFP coding sequence at its C-terminus. The resulting construct was named "GFP-Rho5^{C17}", encoded on the plasmid pCSO94, introduced into the previously described *Δrho5* strain with the mitochondrial Idp1-mCherry marker (HCSO76-1A) and subjected to fluorescence microscopy. In Figure 8B, the first two rows depict representative cells grown to mid-logarithmic phase. Under non-stressed growth conditions, the GFP signal appears unevenly distributed along the plasma membrane in 88 % of the examined cells (upper two rows). Simultaneously, strong signals at intracellular structures could be observed. The addition of 4.4 mM H_2O_2 reduced the plasma membrane (PM) localization so that only 29 % of the cells displayed a peripheral GFP signal, whereas in 69 % of the cases an intracellular signal was still observed, but very rarely associated with the mitochondria (lower two rows). These findings differ from the

previous results of publications that found the last 17 amino acids of other GTPases to be sufficient to locate GFP to the plasma membrane and indicate that there are additional determinants involved (Hancock et al. 1991). To test whether the previously described Rho5-specific insert contributes to the intracellular distribution, in the next step the last 110 amino acids ($Rho5^{C110}$) were fused to the GFP tag on the plasmid pJJH2562 which was introduced in the tester strain for fluorescence microscopic inspection. The construct generated a GFP signal evenly distributed along the plasma membrane in 93 % of the cells akin to wild-type GFP-Rho5 (Figure 9B, upper two rows). It was also partly intracellular but with a lower intensity compared to $Rho5^{C17}$.

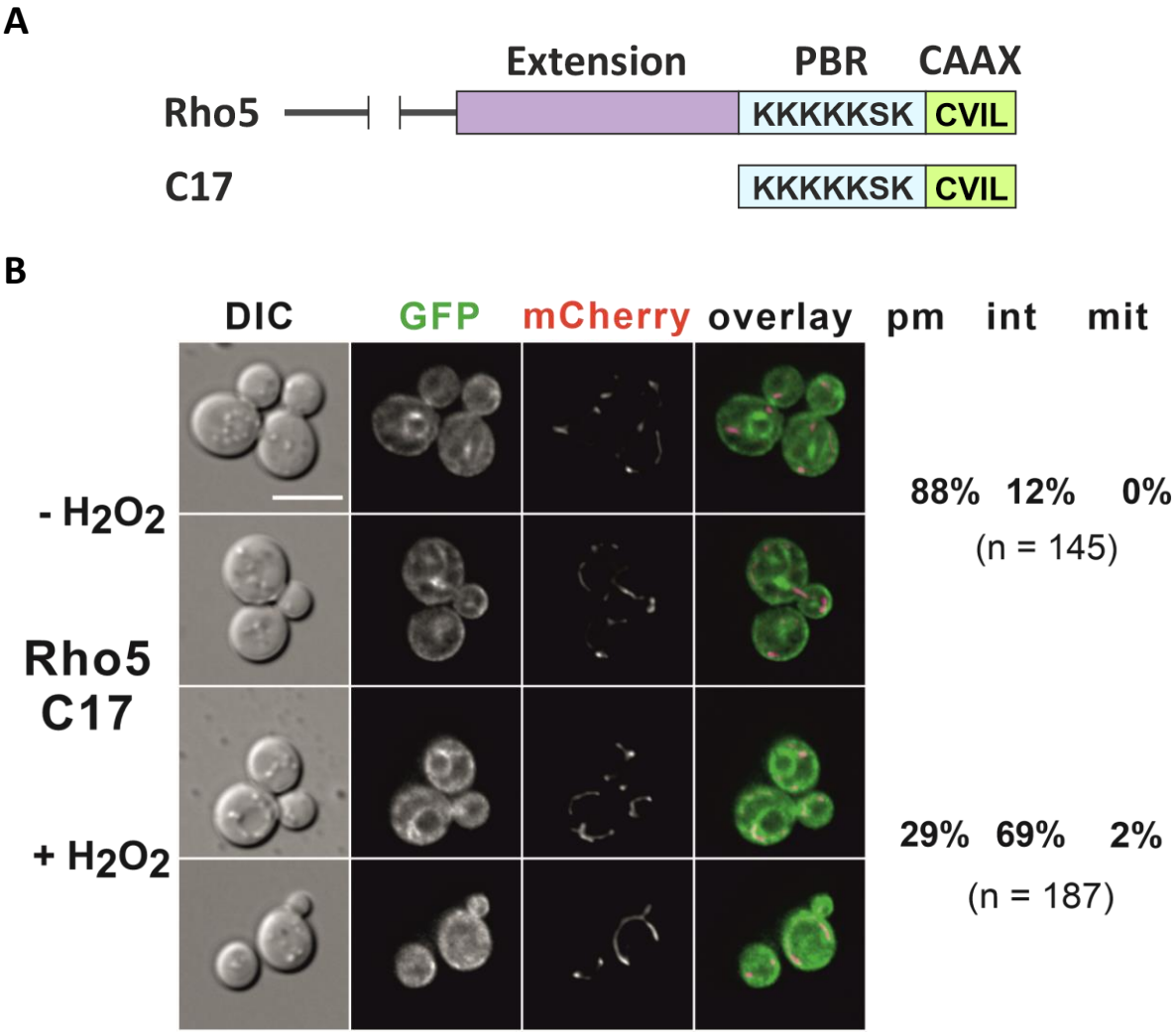

Figure 8: Localization of the hypervariable region of Rho5 A: Schematic representation of the $Rho5^{C17}$ construct. **B:** Life-cell fluorescence microscopy of a *rho5* deletion strain with a mitochondrial mCherry marker (HCSO76-1A) carrying the codons 314 to 331 of the *RHO5* gene, encompassing the PBR and the CAAX motif, fused with an N-terminal GFP on a *CEN/ARS* vector (pCSO94). Cells were grown in selective synthetic medium for plasmid maintenance to mid-logarithmic phase and examined under the fluorescence microscope. For induction of oxidative stress, the sample was exposed to 4.4 mM H_2O_2 and examined for 5 to 15 minutes post-exposure. Cell counts of localization of the GFP signal are presented on the right-hand side of the microscope pictures. Co-localization of the red and green signals is highlighted by a yellow to white pseudo-colorization in the overlay. pm = plasma membrane, int = non-specific internal localization, mit = mitochondrion. Exposure brightfield: 20 ms, excitation GFP channel: 2000 ms, Rhodamine channel: 400 ms. Scale bar indicates 5 µm.

Exposure to 4.4 mM hydrogen peroxide lead to a mild decrease in peripheral localization with 76 % of the cells exhibiting this arrangement (second to last row). A co-localization of the GFP signal and the mitochondrial mCherry marker could be observed in a relatively small number of cells (12 %, bottom row). The remaining 12 % of the cells displayed a GFP signal at unidentified intracellular compartments (not depicted).

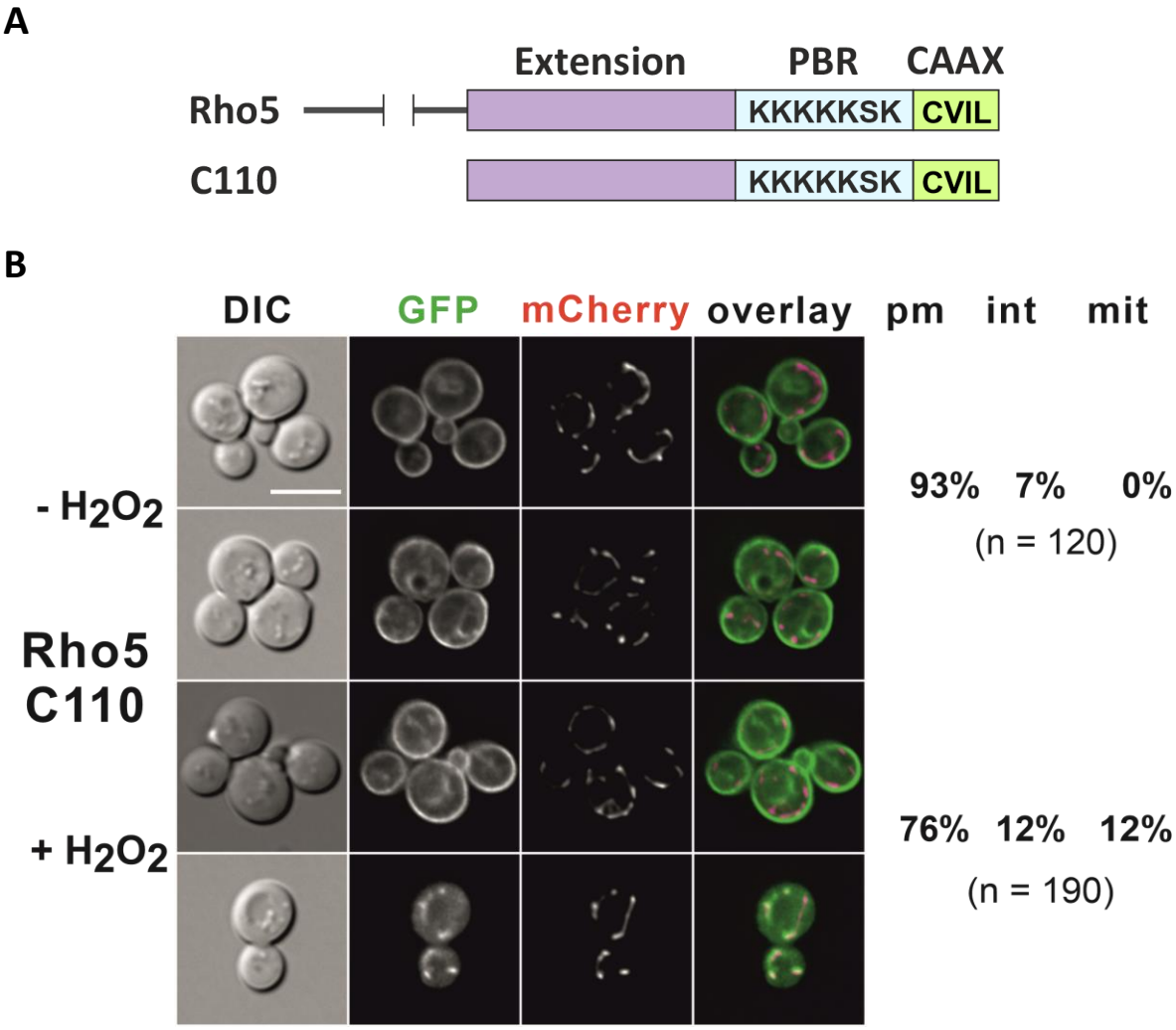

Figure 9: Localization of GFP-tagged extension and hypervariable region of Rho5 A: Schematic representation of the Rho5^{C110} construct. **B:** Life-cell fluorescence microscopy of a *rho5* deletion with a mitochondrial mCherry marker strain carrying the extension of the *RHO5* gene including the PBR and the CAAX motif (codons 203 to 331) with an N-terminal GFP on a *CEN/ARS* vector (pJJH2562). Cells were grown in synthetic selective medium for plasmid maintenance to mid-logarithmic phase and examined under the fluorescence microscope. For induction of oxidative stress, the sample was exposed to 4.4 mM H_2O_2 and examined for 5 to 15 minutes post-exposure. Cell counts of intracellular localization of the GFP signal are presented on the right-hand side of the microscope pictures. Co-localization of the red and green signals is highlighted by a yellow to white pseudo-colorization in the overlay. pm = plasma membrane, int = non-specific internal localization, mit = mitochondrion. Exposure brightfield: 20 ms, excitation GFP channel: 2000 ms, rhodamine channel: 400 ms. Scale bar indicates 5 µm.

3.1.4 Role of Rho5's extension in signalling and cellular distribution

To study the importance of the Rho5-specific extension described above, two truncated Rho5 variants were created either leaving out the entire residues 222 to 319 or including five additional amino acids preceding the PBR which were named *RHO5*$^{\Delta 222–319}$ and *RHO5*$^{\Delta 222–314}$, respectively (Figure 10).

```
Rho5          ATQAGVREVFEQAVRYAIYEPESPNQKSANHTLTDELTTATTNTNGDKNI 250
Rho5Δ222-319  ATQAGVREVFEQAVRYAIYEP---------------------------- 221
Rho5Δ222-314  ATQAGVREVFEQAVRYAIYEP---------------------------- 221

Rho5          REQKQQPHHNNSTDSTLPKGSLQQEKEALNIKPTKKGQKDKIHEQSKSKG 300
Rho5Δ222-319  ------------------------------------------------  -
Rho5Δ222-314  ------------------------------------------------  -

Rho5          SKIASNNHHNKQAKPKTRNDKKKKKSKCVIL 331
Rho5Δ222-319  ----------------LEDKKKKKSKCVIL 235
Rho5Δ222-314  --------------PKTRNDKKKKKSKCVIL 238
```

Figure 10: Alignment of Rho5's C-terminal primary sequence with two Rho5 constructs lacking the specific extension Residues 201 to 331 of Rho5. Highlighted in orange: Extension of Rho5, highlighted in green: Five amino acids additionally present in the *RHO5*$^{\Delta 222–314}$ construct. Designed with GeneDoc, version 2.5.000.

3.1.4.1 Rho5's extension is essential for its function in the oxidative stress response and vegetative growth

In order to shed light on the role of the Rho5-specific extension in response to oxidative stress and vegetative growth, the genomically integrated *RHO5*$^{\Delta 222–319}$ and *RHO5*$^{\Delta 222–314}$ were subjected to a growth assay in rich medium in a microwell plate scanner (see Materials & Methods). As shown in Figure 11B (left panel), the non-stressed samples grew almost identically with no phenotypical deviations among the three growth curves. All entered stationary phase after 8 hours of incubation at an OD_{600} of around 2.3. In medium containing hydrogen peroxide (right panel), the *Δrho5* strain (red squares) grew better with an OD_{600} of 3 at the 13-hour mark compared to that of wild-type *RHO5* (black rhombus) which reached this approximate OD_{600} after 18 hours. Strains carrying the *RHO5*$^{\Delta 222–319}$ construct (green rectangles) displayed a growth mimicking the *Δrho5* strain with an OD_{600} of 2.8 after 13 hours whereas retaining five residues of the extension (*RHO5*$^{\Delta 222–314}$) decreased the hyper-resistance, resulting in an OD_{600} of 2.9 at the 16-hour mark (blue crosses). The serial drop dilution assay confirmed the loss-of-function of *RHO5*$^{\Delta 222–319}$ from the growth curve. The strain grew to the fifth dilution step on rich medium containing 1.5 mM H_2O_2 like the *rho5* deletion strain whereas the wild type just grew up to the second dilution (Figure 11C).To test the functionality of the Rho5$^{\Delta 222–319}$ and Rho5$^{\Delta 222–314}$ constructs in glucose signalling, the synthetic lethality of a *rho5 sch9* double deletion was utilized in a tetrad analysis. For this, strains carrying either the *RHO5*$^{\Delta 222–319}$ or the *RHO5*$^{\Delta 222–314}$ allele were crossed with a strain lacking the *SCH9* gene, respectively. The resulting heterozygous diploid strains (DCSO94 and DHD5/dL+5) were submitted to tetrad dissection. None of the segregants that were expected to harbour either of the mutated *RHO5* alleles produced viable progeny in a *sch9*

deletion background (Figure 11D, yellow circles). This points to a failed complementation of the constructs due to non-functionality of both constructs.

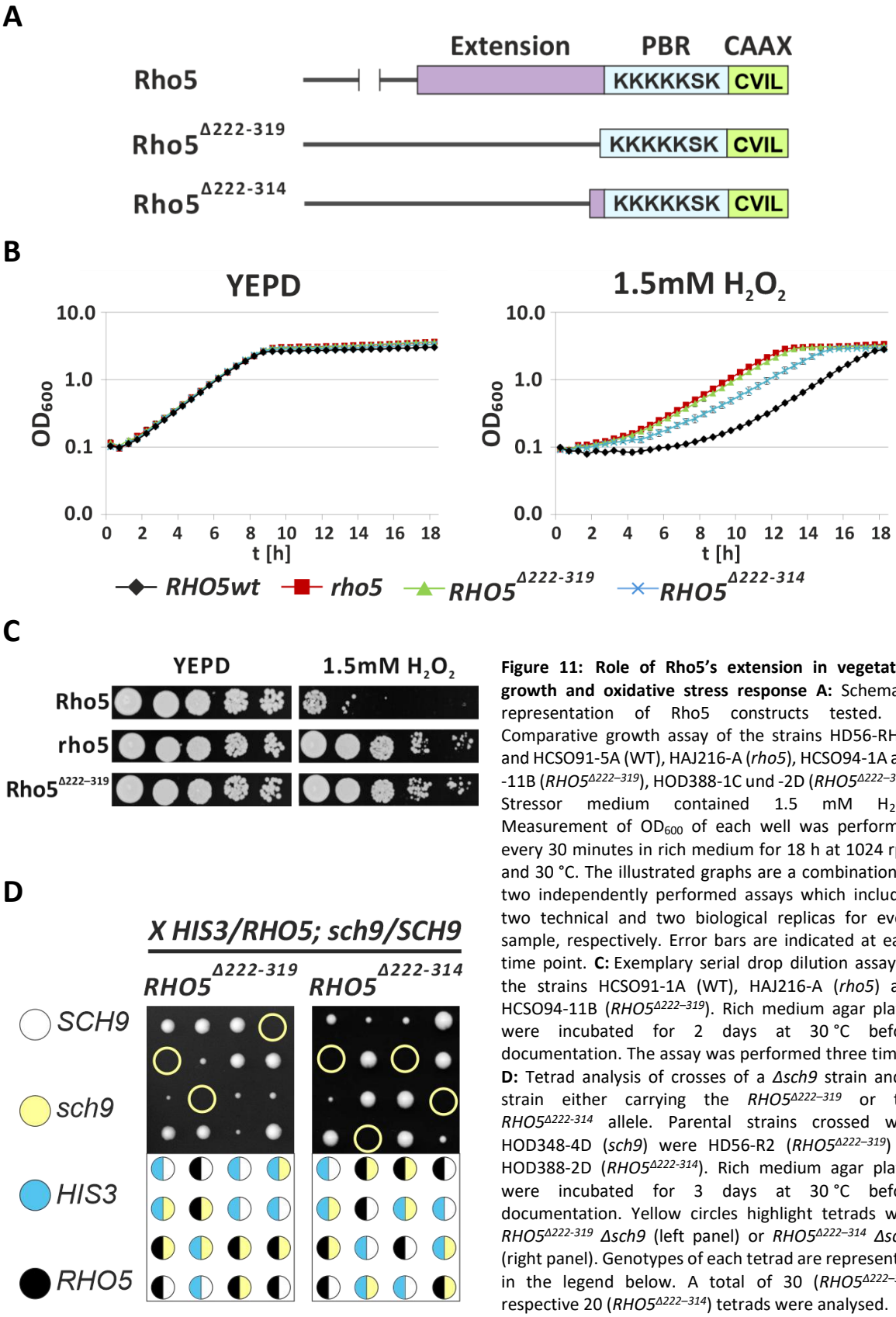

Figure 11: Role of Rho5's extension in vegetative growth and oxidative stress response A: Schematic representation of Rho5 constructs tested. **B:** Comparative growth assay of the strains HD56-RHwt and HCSO91-5A (WT), HAJ216-A (*rho5*), HCSO94-1A and -11B (*RHO5*$^{\Delta222–319}$), HOD388-1C und -2D (*RHO5*$^{\Delta222–314}$). Stressor medium contained 1.5 mM H_2O_2. Measurement of OD_{600} of each well was performed every 30 minutes in rich medium for 18 h at 1024 rpm and 30 °C. The illustrated graphs are a combination of two independently performed assays which included two technical and two biological replicas for every sample, respectively. Error bars are indicated at each time point. **C:** Exemplary serial drop dilution assay of the strains HCSO91-1A (WT), HAJ216-A (*rho5*) and HCSO94-11B (*RHO5*$^{\Delta222–319}$). Rich medium agar plates were incubated for 2 days at 30 °C before documentation. The assay was performed three times. **D:** Tetrad analysis of crosses of a *Δsch9* strain and a strain either carrying the *RHO5*$^{\Delta222–319}$ or the *RHO5*$^{\Delta222-314}$ allele. Parental strains crossed with HOD348-4D (*sch9*) were HD56-R2 (*RHO5*$^{\Delta222–319}$) or HOD388-2D (*RHO5*$^{\Delta222-314}$). Rich medium agar plates were incubated for 3 days at 30 °C before documentation. Yellow circles highlight tetrads with *RHO5*$^{\Delta222-319}$ *Δsch9* (left panel) or *RHO5*$^{\Delta222–314}$ *Δsch9* (right panel). Genotypes of each tetrad are represented in the legend below. A total of 30 (*RHO5*$^{\Delta222–319}$) respective 20 (*RHO5*$^{\Delta222–314}$) tetrads were analysed.

3.1.4.2 Inclusion of five amino acids partly re-establishes the PM localization of Rho5

To test the significance of the extension for the intracellular distribution of Rho5, the two constructs investigated in the last chapter were fused to GFP expressed from the plasmids pLAO5 (*GFP-RHO5*$^{\Delta 222\text{-}319}$) and pJJH2616 (*GFP-RHO5*$^{\Delta 222–314}$) that were transformed into the *Δrho5* strain with a genomic mitochondrial mCherry marker (HCSO76-1A). The upper two rows of Figure 12A show exemplary fluorescent pictures of yeast cells from a strain carrying the *RHO5*$^{\Delta 222–319}$. The GFP signal could not be detected at the PM but was rather exclusively found at internal structures. Treatment with 4.4 mM H_2O_2 resulted in a redistribution of the signal with 14 % of the cells showing co-localization with the mitochondrial marker while in 86 % the GFP signal remained at unidentified internal compartments (lower two rows). In contrast to that, 82 % of the cells harbouring the *RHO5*$^{\Delta 222\text{-}314}$ construct (Figure 12B, upper two rows) exhibited a GFP signal predominantly at the plasma membrane. The signal was also found to a higher degree at intracellular structures than compared to the wild-type Rho5 signal. Additionally, some bright spots were detected close to darker areas which are probably vacuoles (white arrows). Following hydrogen peroxide exposure, 18 % of the cells displayed a co-localization of the GFP signal with the mitochondrial marker (bottom row) and only 9 % were found at the plasma membrane suggesting a severely impeded mitochondrial relocation process. Taken together, these results confirm the importance of the extension for the *in vivo* function of Rho5 and indicate a participation in the oxidative stress response as well as in glucose signalling.

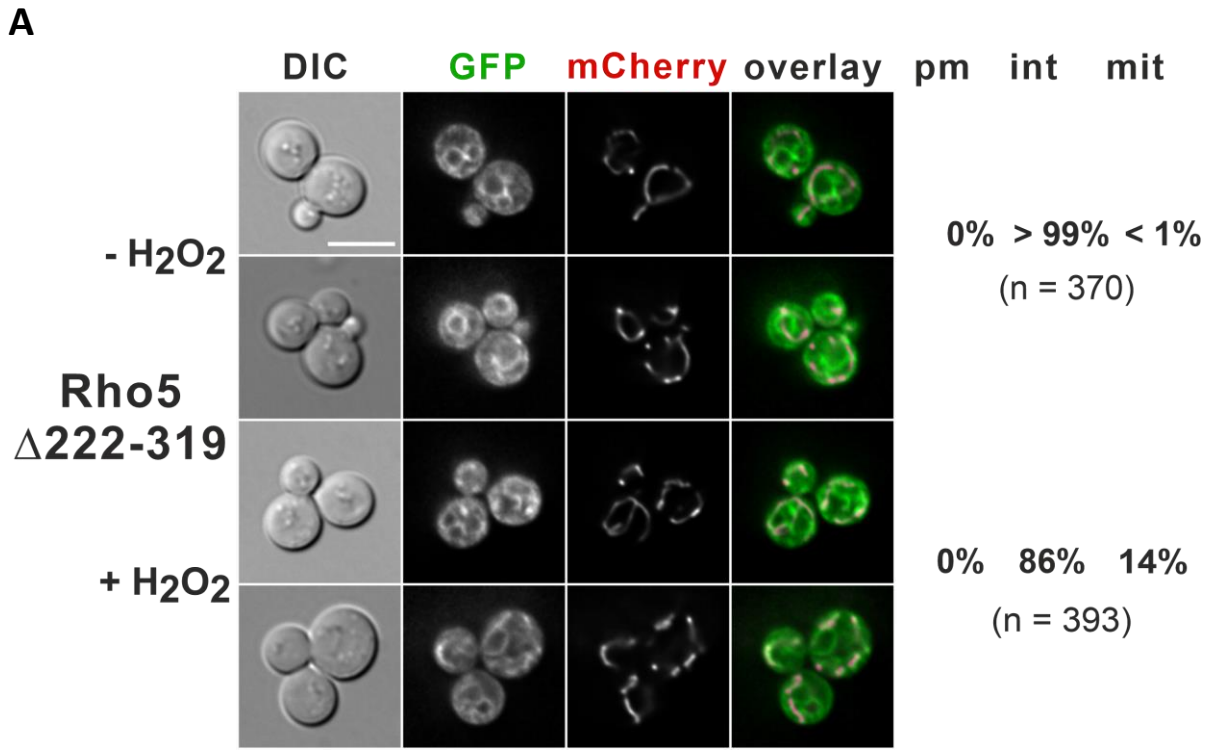

Figure 12 *Cont.*

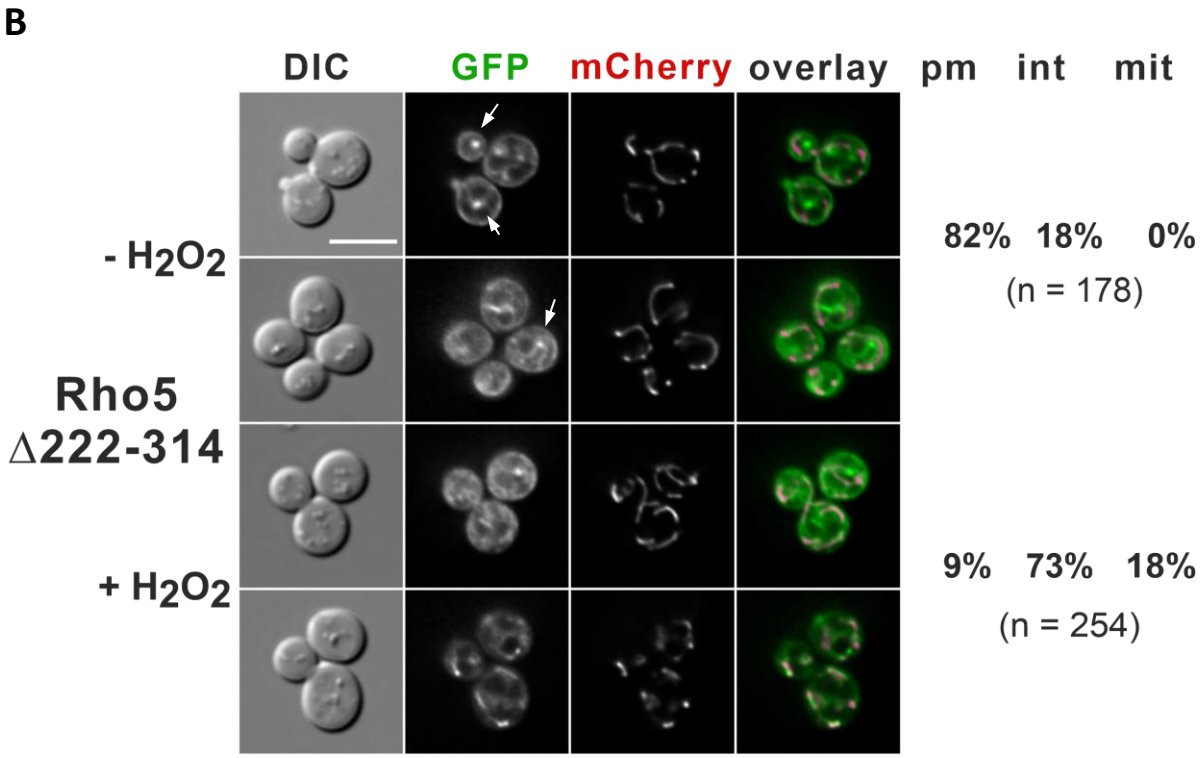

Figure 12: Localization Rho5 lacking the extension Life-cell fluorescence microscopy of a *rho5* deletion with a mitochondrial mCherry marker strain carrying the *RHO5*$^{\Delta 222–319}$ (A) or *RHO5*$^{\Delta 222–314}$ (B) allele with an N-terminal GFP on a CEN/ARS vector (pLAO5 or pJJH2616, respectively). For induction of oxidative stress, the sample was exposed to 4.4 mM H_2O_2 and examined for 5 to 15 minutes post-exposure. To assess intracellular localization, the GFP signals were counted and categorized. Results are presented on the right-hand side of the microscope pictures. White arrows point to bright intracellular spots. Co-localization of red and green signals is highlighted by a yellow to white pseudo-colorization in the overlay. pm = plasma membrane, int = non-specific internal localization, mit = mitochondrion. Exposure brightfield: 20 ms, excitation GFP channel: 2000 ms, Rhodamine channel: 400 ms. Scale bar indicates 5 µm.

3.1.5 The hypervariable region determines function and distribution of yeast Rho5

As proven by a number of publications, the C-terminal region of GTPases carries nearly all the information required for proper intracellular targeting under various conditions (Hancock et al. 1991, Michaelson et al. 2001, Williams 2003, Heo et al. 2006). In Rho proteins a dual code leads to the designated membranes.

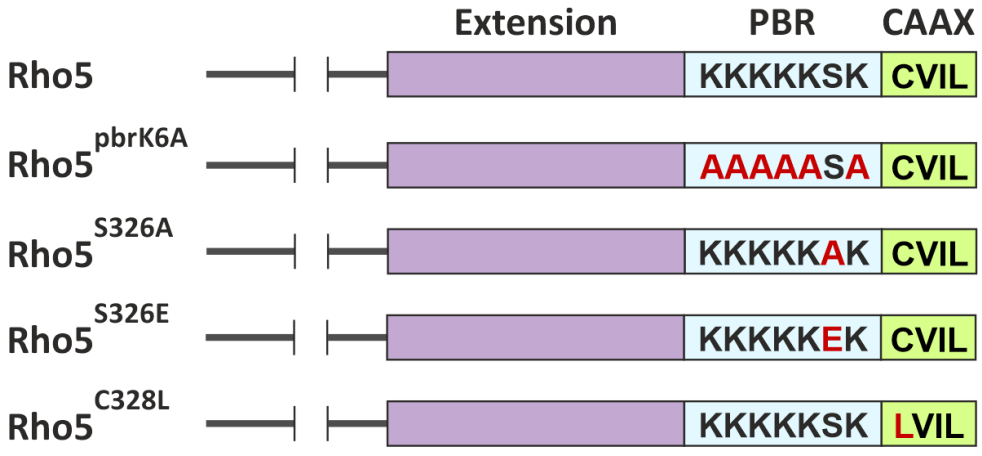

Figure 13: Schematic representation of Rho5 constructs studied in this section. Red letters indicate mutations.

The lipid moiety provided by the CAAX motif mediates the anchoring to membranes and the hypervariable region (HVR) functions as a protein binding side as well as a platform for the interaction with the lipid bilayer. In the following chapter the C-terminal region of Rho5 will be put under close inspection to pinpoint crucial primary sequences that ensure the correct function of this GTPase. The examined mutants are displayed in Figure 13.

3.1.5.1 Investigations of the hexa-lysine polybasic region of Rho5

Despite the high degree of amino acid identities in some Rho isoforms, small disparities within the hyper-variable region (HVR) frequently entail profound differences in signalling specificity. This is impressively demonstrated by the three mammalian GTPases Rac1, Rac2 and Rac3 which share a sequence identity of about 90 % with the differences mainly situated in 10 residues within the PBR. Ultimately, this region was proven to be responsible for the different order of temporal accumulation of the Rho proteins to their target compartment (Ueyama et al. 2005). Besides the targeting of Rho-GTPases, the PBR also mediates the interaction with complexes and adaptor proteins (Tolias et al. 1998, van Hennik et al. 2003) and ensures signalling specificity (Filippi et al. 2004). As evident from Figure 5, Rho5 also possesses a PBR (blue) consisting of six lysins interrupted by a serine at the penultimate position. To examine the importance of Rho5's PBR, the six positively charged lysins were replaced with nonpolar alanine residues (see Figure 13) by string-DNA synthesis. The mutated allele was named *RHO5*^{pbrK6A} and integrated into the genome of *S. cerevisiae*. The growth of the strain, together with a *Δrho5* and a wild-type strain as controls, was documented in the presence and absence of H_2O_2 (Figure 14A).

While under non-stressed conditions all three strains grew similarly (left chart) while in medium containing hydrogen peroxide (right chart), the *rho5* deletion strain (red squares) demonstrated a better growth compared to the wild-type control (black rhombus). The strain harbouring the *RHO5*^{pbrK6A} allele showed a growth that lay between the two controls (green triangles). The drop dilution assay presented in Figure 14B supports these results: On rich media without stressors, the *RHO5* wild type, the *Δrho5* and the *RHO5*^{pbrK6A} strain grew normal to the fifth dilution step (left panel). However, while the growth of Rho5-depleted cells was barely affected on medium containing 1.5 mM hydrogen peroxide, the wild type only grew to the second dilution. The strain with the mutated PBR extended to the third dilution step thus, again, showing an intermediate growth (bottom row). To investigate the potential impact of the mutated PBR on glucose signalling, the strain carrying the *RHO5*^{pbrK6A} allele was crossed with a *sch9* deletion strain to create a diploid heterozygote strain (DCSO97-4D). The dissection and successive tetrad analysis led to a total of 29 segregants allegedly carrying both the *sch9* deletion and the gene for *RHO5*^{pbrK6A} as depicted in the exemplary section in Figure 14C. 22 of these 29 segregants were viable and colonies were diminutive.

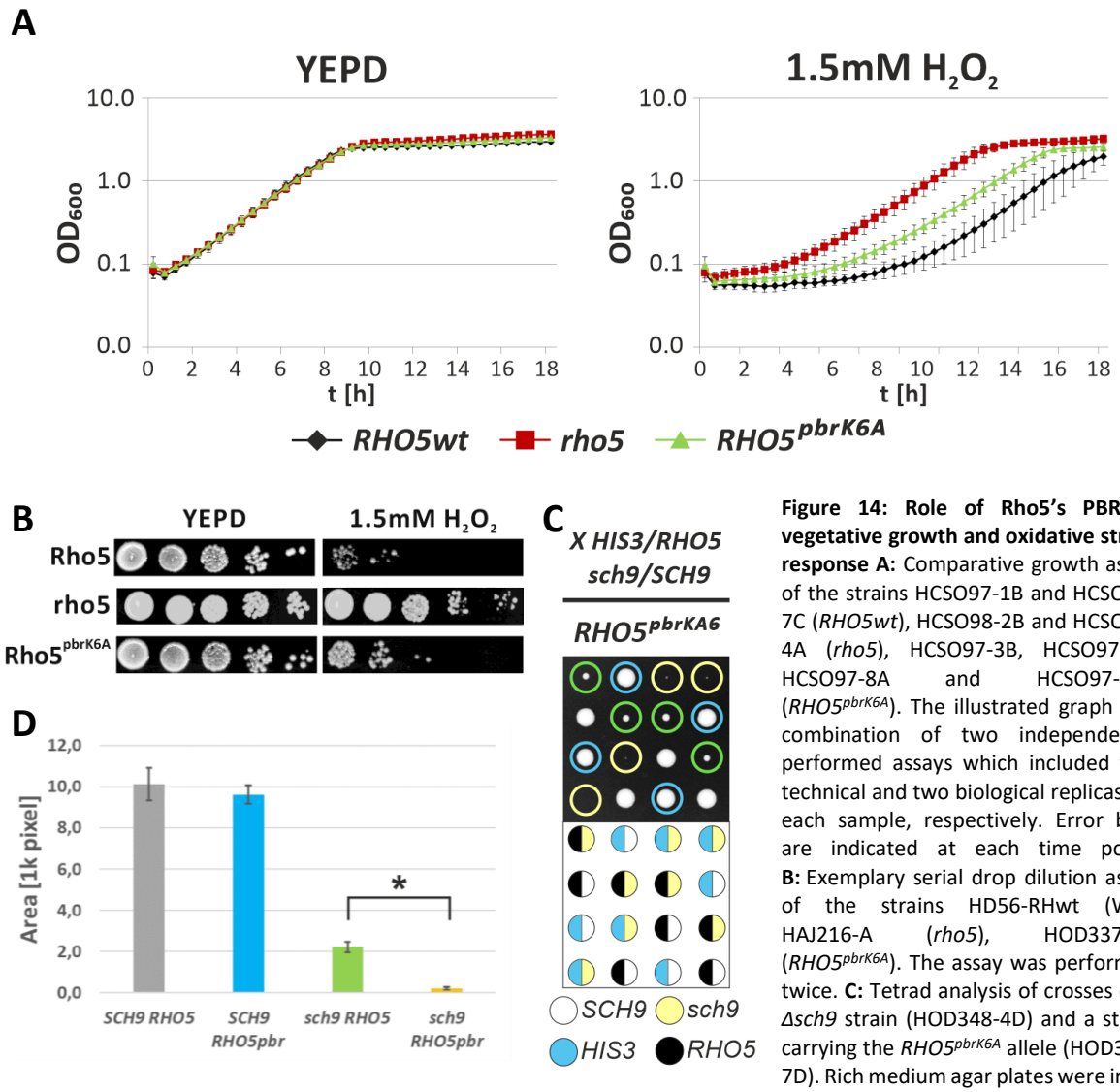

Figure 14: Role of Rho5's PBR in vegetative growth and oxidative stress response A: Comparative growth assay of the strains HCSO97-1B and HCSO97-7C (*RHO5wt*), HCSO98-2B and HCSO98-4A (*rho5*), HCSO97-3B, HCSO97-5C, HCSO97-8A and HCSO97-11B (*RHO5^{pbrK6A}*). The illustrated graph is a combination of two independently performed assays which included two technical and two biological replicas for each sample, respectively. Error bars are indicated at each time point. **B:** Exemplary serial drop dilution assay of the strains HD56-RHwt (WT), HAJ216-A (*rho5*), HOD337-7D (*RHO5^{pbrK6A}*). The assay was performed twice. **C:** Tetrad analysis of crosses of a *Δsch9* strain (HOD348-4D) and a strain carrying the *RHO5^{pbrK6A}* allele (HOD337-7D). Rich medium agar plates were incubated for 3 days at 30 °C before documentation. Yellow circles highlight tetrads with *Δsch9 RHO5^{pbrK6A}*, blue circles mark tetrads with *SCH9 RHO5^{pbrK6A}* and green circles highlight segregants with *Δsch9 RHO5*. Unmarked segregants are wild type. Genotypes of each segregant are represented in the legend below. A total of 30 tetrads were analysed. **D:** Area of segregants from DCSO97-4D in pixels. Each bar is the result of at least 9 measurements of single segregants. Error bars are indicated for each data set. Comparison of colony sized of *sch9 RHO5^{pbrK6A}* and *sch9 RHO5* gave a P-value of $0{,}7*10^{-19}$ (marked by asterisk). Segregants with *SCH9* and *RHO5* or *RHO5^{pbrK6A}* did not show significant differences in size.

While a wild-type *SCH9* allele in combination with either the *RHO5* wild type or the *RHO5^{pbrK6A}* allele did not influence the colony size of segregants (Figure 14C, unmarked and blue circles), the *Δsch9 RHO5^{pbrK6A}* segregants reached only about 10 % of the size of *Δsch9 RHO5* segregants. Taken together, these results indicate that the mutated PBR led to a malfunction of Rho5 in the reaction to hydrogen peroxide and even more severe in glucose signalling. The use of the PBR as a determinant for membrane identification and a temporal regulator for Rho proteins seems to be a highly conserved mechanism since it was found in Rho-GTPases from yeast (Haupt and Minc 2017) to mammalian cells (Yeung et al. 2008). In order to examine the influence of Rho5's PBR on its localization and intracellular behaviour, the allele of the lysine-to-alanine exchange mutant *RHO5^{pbrK6A}* was tagged with GFP expressed from the plasmid pCSO35.

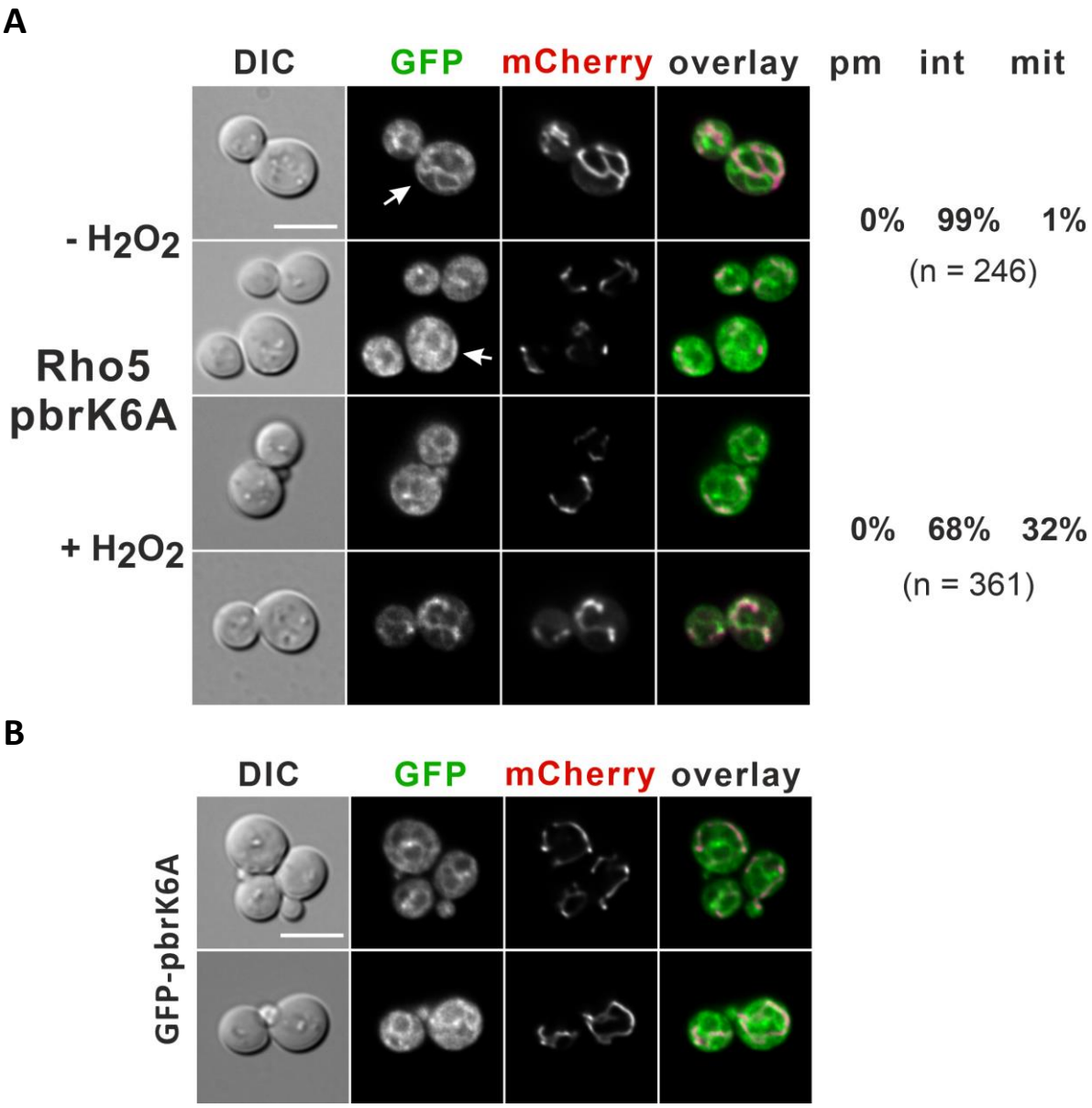

Figure 15: Localization of Rho5 with mutated PBR A: Life-cell fluorescence microscopy of a *rho5* deletion with a mitochondrial mCherry marker strain carrying the *RHO5*^{pbrK6A} allele with an N-terminal GFP on a *CEN/ARS* vector (pCSO35). For induction of oxidative stress, the sample was exposed to 4.4 mM H_2O_2 and examined for 5 to 15 minutes. Cell counts of intracellular localization of the GFP signal are presented on the right-hand side of the microscope pictures. Co-localization of the red and green signals is highlighted by a yellow to white pseudo-colorization. pm = plasma membrane, int = non-specific internal localization, mit = mitochondrion. Exposure brightfield: 20 ms, excitation GFP channel: 2000 ms, Rhodamine channel: 400 ms. Scale bar indicates 5 µm. **B:** Life-cell fluorescence microscopy a strain with a mitochondrial mCherry marker carrying the mutated PBR of *RHO5* with an N-terminal GFP on a *CEN/ARS* vector (pCSO95).

The upper two rows of Figure 15A depict cells with a representative GFP signal distribution. It was almost exclusively detected at intracellular structures and in the cytosol in 99 % of the cells missing any GFP-Rho5 at the plasma membrane (compare Figure 6). Fusing the last 17 residues of Rho5^{pbrK6A} to GFP resulted in the same subcellular distribution in logarithmically growing cells (Figure 15B).The addition of 4.4 mM H_2O_2 to the logarithmic cells triggered a moderate redistribution of the GFP signal towards co-localization with the mitochondrial mCherry marker (lower two rows) which occurred in

32 % of the cells. The remaining 68 % of the cells still exhibited a localization confined to the non-specified subcellular compartments.

3.1.5.2 Role of the serine 326 for Rho5 function and distribution

The Ras-GTPase KRas-4B has been extensively studied due to its involvement in a number of diseases (Quatela et al. 2008, Schmick et al. 2014). It carries a serine residue at the position 181 within the PBR that was disclosed to be phosphorylated by the Protein kinase C triggering the GTPase to shift from the plasma membrane to endomembranes (Bivona et al. 2006). Interestingly, Rho5 also harbours a serine residue at position 326 while Rac1 does not (Figure 5, red). A valuable tool to study the effects of a potential phosphorylation is the exchange of the correspondent residue to a phosphomimetic or a non-phosphorylatable amino acid. This strategy was employed in the following chapter by introducing a phosphomimetic exchange of serine 326 to the basic glutamate (S326E) and a non-phosphorylatable one with the replacement to a hydrophobic alanine (S326A). Both variants were integrated into the genome of *S. cerevisiae* and the resulting haploid strains were tested for their growth under stressed and non-stressed conditions. A wild-type and a *Δrho5* strain were included as controls.

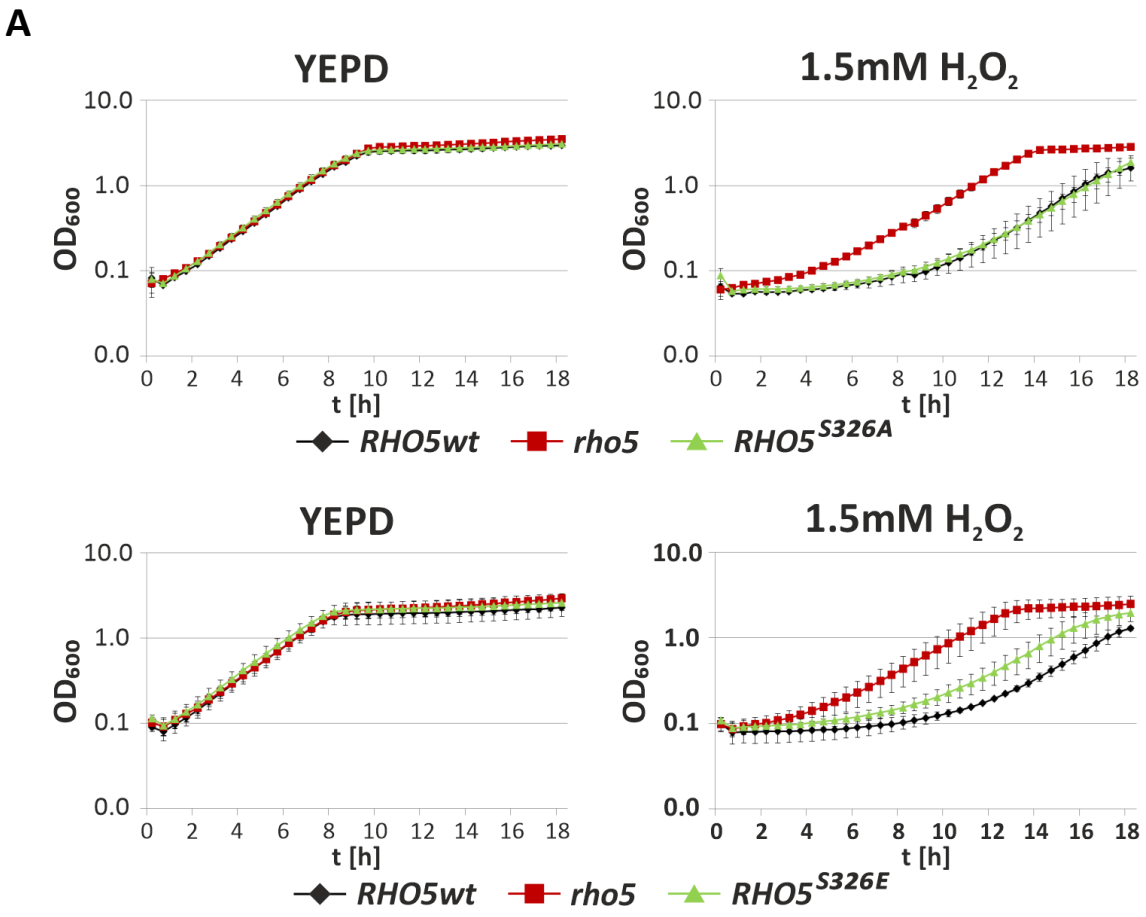

Figure 16 *Cont.*

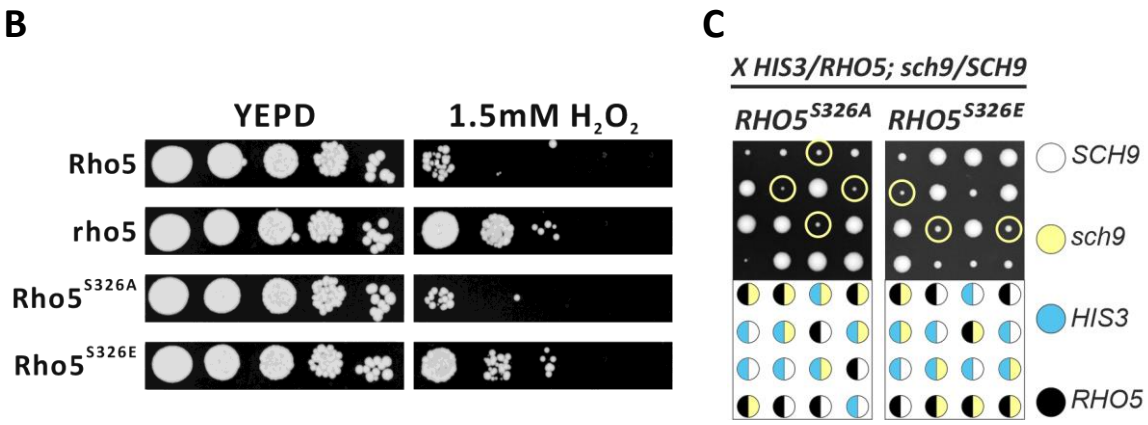

Figure 16: Effect of a phosphomimetic and a non-phosphorylatable mutation of Rho5's serine 326 A: Comparative growth assay of the strains HD56-RHwt and HCSO91-3C (*RHO5wt*), HAJ216-A und HCSO98-2B (*Δrho5*), HD56-RHS326A, HCSO90-3D, HCSO90-5A, HCSO90-7B (*RHO5^{S326A}*), HCSO92-3A and HCSO92-5A (upper panel) and HCSO91-3C and HD56-RHwt (*RHO5wt*), HCSO98-2B und HAJ216-A (*Δrho5*), HCSO95-1C and HCSO95-5B (*RHO5^{S326E}*) (lower panel). For oxidative stress, 1.5 mM hydrogen peroxide was added to rich medium. The depicted graphs are a combination of two independently performed assays which included two technical and two biological replicas for each sample, respectively. Error bars are indicated at every time point. **C:** Exemplary serial drop dilution assay of the strains HCSO91-7A (WT), HCSO98-2B (*Δrho5*), HCSO90-3D (*RHO5^{S326A}*) and HCSO95-5B (*RHO5^{S326E}*). The assay was performed twice and included two biological replicas for both serine mutants. **C:** Tetrad analysis of crosses of a *sch9* deletion strain (HOD348-4D) and a strain carrying either the *RHO5^{S326A}* (HD56-RHS326A #9) or the *RHO5^{S326E}* allele (HD56-R7). Rich medium agar plates were incubated for 3 days at 30 °C before documentation. Yellow circles highlight tetrads with *Δsch9 RHO5^{S326A}* or *Δsch9 RHO5^{S326E}*. Genotypes of each segregant are represented in the legend below. A total of 30 tetrads were analysed.

As can be taken from Figure 16A (left panels), in both assays all strains grew similarly. In media containing 1.5 mM H_2O_2 (right panels), both the wild-type control (black rhombus, upper panel) and the *RHO5^{S326A}* strain (green triangles,) exhibited a very similar growth while the phosphomimetic exchange (green triangles, lower panel) led to a growth between the *Δrho5* control (red squares) and the wild type. These results are in accordance with the serial drop dilution assay depicted in Figure 16B. To examine the role of the serine residue in glucose signalling, strains carrying the *RHO5^{S326A}* or *RHO5^{S326E}* allele were crossed with a *Δsch9* strain and subjected to tetrad analyses (Figure 16C). All segregants with a *sch9* deletion also harbouring either the *RHO5^{S326A}* (third panel) or *RHO5^{S326E}* (forth panel) allele produced viable progeny with remarkably similar sizes (yellow circles) when compared to *Δsch9 RHO5* segregants suggesting that the residue at position 326 does not have a prominent role in glucose signalling. To better understand the nature of the serine residue, the intracellular distribution of the two mutants was examined using GFP fusions. Figure 17 depicts the results of the microscopic examination. The upper two rows show representative pictures of the subcellular distribution of the GFP signal in both mutants. It is mainly present at the plasma membrane in 95 % of the cells from the *RHO5^{S326A}* strain (Figure 17A) and 90 % of those carrying the *RHO5^{S326E}* allele (Figure 17B), similar to the wild type (compare Figure 6).

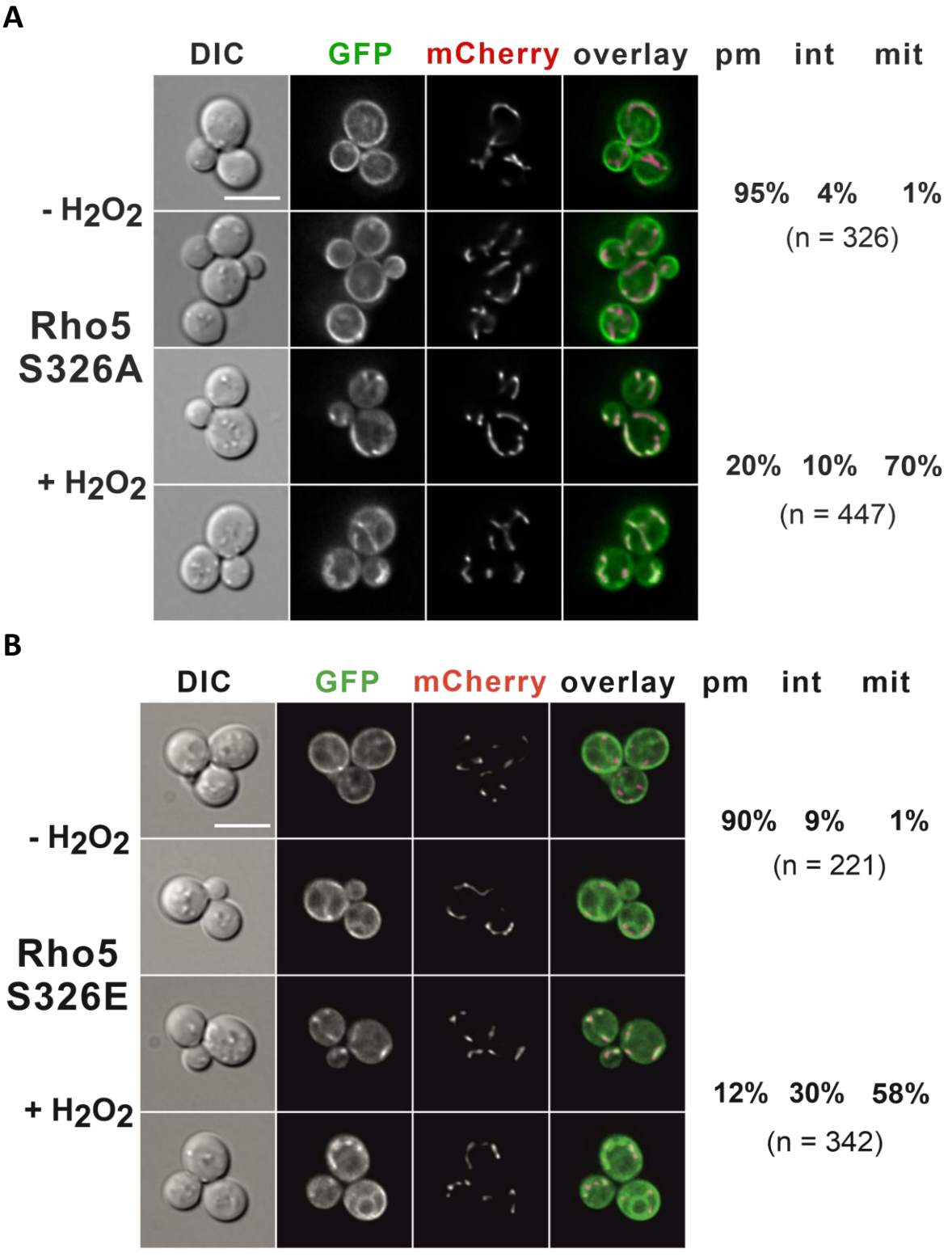

Figure 17: Localization of non-phosphorylatable and phosphomimetic mutation of Rho5's serine 326 Life-cell fluorescence microscopy of a *Δrho5* strain with a mitochondrial mCherry marker (HCSO76-1A) carrying a *CEN/ARS* vector encoding for either $RHO5^{S326A}$ (**A**, pCSO19) or $RHO5^{S326E}$ (**B**, pCSO31) allele with an N-terminal GFP. For induction of oxidative stress, the sample was exposed to 4.4 mM H_2O_2 and examined for 5 to 15 minutes post-exposure. Cell counts of intracellular localization of the GFP signal are presented on the right-hand side of the microscope pictures. Co-localization of the red and green signals is highlighted by a yellow to white pseudo-colorization in the overlay. pm = plasma membrane, int = non-specific internal localization, mit = mitochondrion. Exposure brightfield: 20 ms, excitation GFP channel: 2000 ms, Rhodamine channel: 400 ms. Scale bar indicates 5 µm.

Treatment with 4.4 mM H_2O_2 caused a redistribution of the peripheral GFP signal to mitochondria in both mutants in 70 % of the Rho5S326A cells (Figure 17A, lower two rows) but only 58 % of the cells containing the Rho5S326E phosphomimetic mutant (Figure 17B, lower two rows). Furthermore, the GFP signal associated with non-specified cellular structures ("int") is found more often in both mutants (20 % for Rho5S326E and 12 % for Rho5S326A) compared to the wild type. Hence, it appears that the mutant proteins are less prone to be removed from the plasma membrane.

3.1.5.3 The role of the CAAX motif for Rho5 function

The sequence of Rho5's last amino acids, C-V-I-L, qualifies as a CAAX motif: A cysteine, two aliphatic amino acids valine and isoleucine and leucine as the final, arbitrary residue. In the next step of this work the essential cysteine at position 328 was exchanged to a leucine in order to disrupt the prenylation process. The constructed mutant allele *RHO5*^{C328L} was genomically integrated and the resulting strain subjected to a growth assay in a microwell plate scanner together with a wild-type and a *Δrho5* strain serving as controls. As can be seen in the left panel of Figure 18A, *RHO5*^{C328L} and the two control strains did not show any differences in their growth under non-stressed conditions. Exposure to 1.5 mM hydrogen peroxide (right panel) resulted in a severely impeded growth of the wild-type control (black rhombus) as opposed to both the *rho5* deletion (red squares) and the *RHO5*^{C328L} strain (green triangles) that were only mildly affected and grew almost identically. These results agree with the serial drop dilution assay depicted in Figure 18B, rich medium neither of the strains diverged from one another (left panel). On medium with 1.5 mM hydrogen peroxide however (right panel), the wild-type control only grew up to the second dilution while both the *rho5* deletion and the *RHO5*^{C328L} mutant strain showed hyper-resistance growing up to the fourth dilution step. Both assays hint towards the *RHO5*^{C328L} allele encoding a protein defective in the oxidative stress response. Tetrad analysis of a cross of a strain carrying the *RHO5*^{C328L} allele and a *sch9* deletion strain demonstrated that the mutated Rho5 is non-functional since no viable progeny was produced of the CAAX mutant in a *sch9* deletion background (Figure 18C, yellow circles).In order to test whether the hyper-resistance can be suppressed by a constitutively active mutation, the *RHO5*^{C328L} allele was equipped with the G12V exchange (Figure 18D). While no difference in growth was observed in the absence of a stressor (left panel), under 1.5 mM H_2O_2 the growth of the strain carrying the *RHO5*^{G12V} allele (right panel, yellow circles) was severely impeded compared to the wild type (black rhombus). The strain expressing *RHO5*^{G12VC328L} (blue crosses) showed hyper-resistance towards the oxidative stress and grew similarly to the *rho5* deletion (red squares) as well as the *RHO5*^{C328L} strain (green triangles). This implies that the constitutively active mutation was not able to restore the functionality of the unprenylated Rho5.

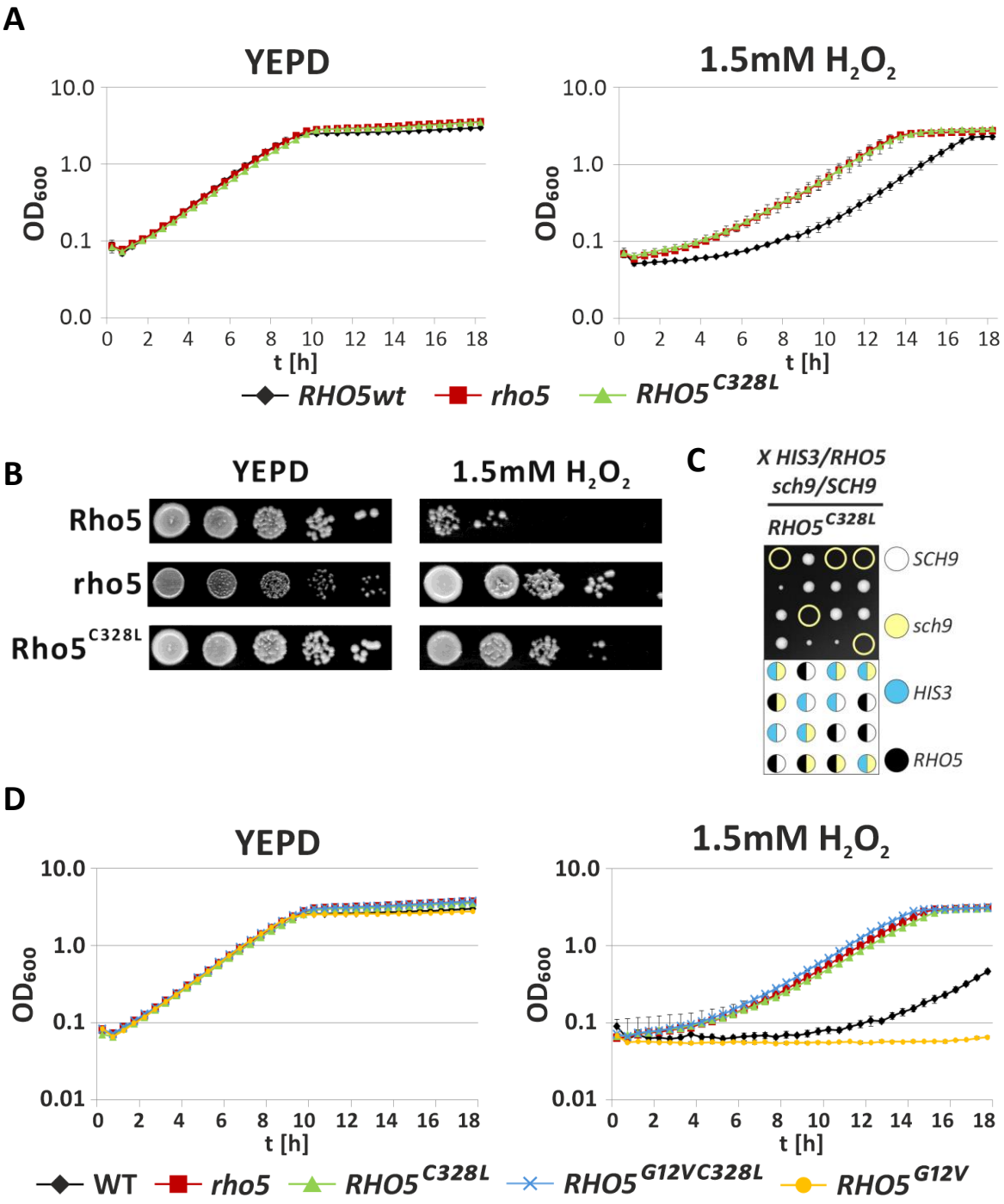

Figure 18 Effect of disruption of Rho5's CAAX motif on growth and oxidative stress response A: Comparative growth assay of the strains HD56-RHwt, HCSO91-3C and -7A (*RHO5wt*), HAJ216-A (*rho5*), HD56-RHC328L#4 and #5 ($RHO5^{C328L}$). The depicted graphs are a combination of two independently performed assays which included two technical and two biological replicas for each sample, respectively. Error bars are indicated at each time point. **B:** Exemplary serial drop dilution assay. Rich medium agar plates were incubated for 3 days at 30 °C before documentation. Strains used: HD56-RHwt (*RHO5wt*), HAJ216-A (*rho5*) and HD56-RHC328L#4 ($RHO5^{C328L}$). The assay was performed two times and included two biological replicas. **C:** Tetrad analysis of a heterozygote strain carrying a *sch9* deletion and the $RHO5^{C328L}$ allele. Parental strains were HOD348-4D (*sch9*) and HD56-RHC328L #4 ($RHO5^{C328L}$). Rich medium agar plates were incubated for 3 days at 30 °C prior to documentation. Yellow circles highlight tetrads with *sch9* $RHO5^{C328L}$. Genotypes of each tetrad is represented in the legend below. A total of 30 tetrads were analysed. **D:** Effect of a constitutively active mutation on a prenylation-depleted Rho5, strains employed: HD56-RHwt#2 (WT), HAJ216-A (*rho5*), HD56-RHC328L#4 ($RHO5^{C328L}$), HD56-R8D ($RHO5^{G12VC328L}$) and HD56-R8 ($RHO5^{G12V}$). Stressor medium contained 1.5mM H_2O_2. The assay was performed once and included two replicas for each sample, respectively. Error bars are indicated at each time point

To examine the effect of the defective CAAX motif on Rho5's subcellular distribution, the cysteine mutant was fused with GFP for subsequent examination under the fluorescence microscope. The upper two rows of Figure 19 depict representative cells. In 99 % of the cells the signal of the fluorescently labelled Rho5^{C328L} was detected evenly distributed within the cytosol. No distinct structures could be identified except for regions with reduced signal intensity, which are most likely the vacuole and the nucleus. Exposure to 4.4 mM H_2O_2 triggered a partial relocalization to the mitochondria in 36 % of the examined cells (Figure 19, bottom row). The signal of the remaining 64 % remained distributed in the cytosol (third row). This clearly deviates from the wild type which showed an association of the GFP signal with mitochondria in 70 % of the cells. Yet, the prenylation does not appear to be essential for mitochondrial relocalization.

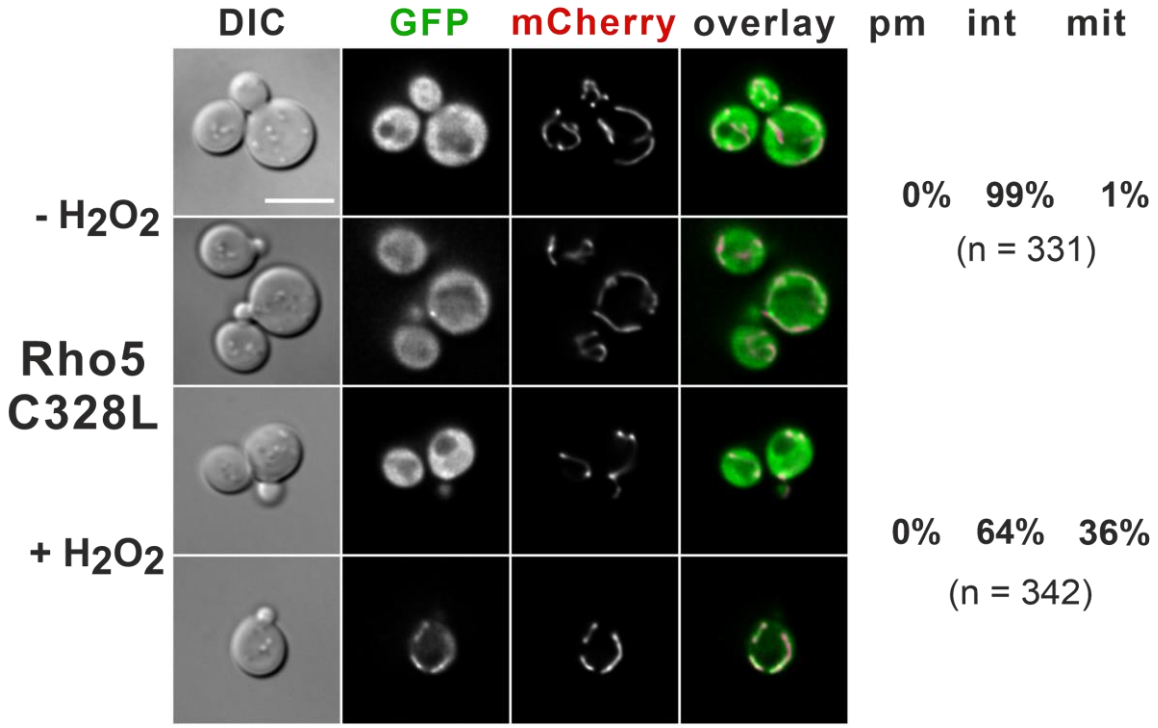

Figure 19: Localization of Rho5 with mutated essential cysteine of the CAAX motif Life-cell fluorescence microscopy of a *rho5* deletion with a mitochondrial mCherry marker strain carrying the *RHO5^{C328L}* allele with an N-terminal GFP on a *CEN/ARS* vector (pCSO18). For induction of oxidative stress, the sample was exposed to 4.4 mM H_2O_2 and examined for 5 to 15 minutes. Cell counts of intracellular localization of the GFP signal are presented on the right-hand side of the microscope pictures. Co-localization of the red and green signals is highlighted by a yellow to white pseudo-colorization.pm = plasma membrane, int = non-specific internal localization, mit = mitochondrion. Exposure brightfield: 20 ms, excitation GFP channel: 2000 ms, Rhodamine channel: 400 ms. Scale bar indicates 5 µm.

1.3. GTPase activity

For many Rho proteins an intracellular stimulus has been shown to induce a translocation from an inactive cytosolic pool to membranes (Philips et al. 1993, Boivin and Beliveau 1995, Fleming et al. 1996, Kranenburg et al. 1997). This allows the interaction with their guanine exchange factor and the subsequent switch from a GDP to a GTP-bound state (DerMardirossian and Bokoch 2005). As previously shown, Rho5 rapidly relocalizes from the plasma membrane to mitochondria upon oxidative

stress. The mechanisms involved in this resettlement are still largely unclear but a dependence on both components of the bipartite GEF (namely Dck1 and Lmo1) could be determined (Schmitz et al. 2015). One could assume that the relocation was initiated by the conversion of the nucleotide binding status, i.e. its activation. A frequently used mutation to lock Rho-GTPases in their active state is the exchange of a conserved glycine (often found at the position 12) to valine. This renders the protein constitutively active by inhibiting its GTPase activity (reviewed in (Aspenstrom 2018)). The physiological ramifications of this constitutively active mutation can be devastating in a cell or organism as evident from the fact that those exchanges are frequently found as the cause of neurodegenerative disorders, inflammation and various types of cancer (reviewed in (Zhao and Pothoulakis 2003, Alan and Lundquist 2013)). In contrast to that, Rho GTPases with mutations at position 17 (e.g. $Rac1^{T17N}$) have a reduced affinity for guanine nucleotides and as a result are either locked in their inactive GDP-bound state or remain nucleotide free (Feig 1999). Both modifications are valuable tools to study the roles of Rho proteins in certain signalling pathways. The following chapter will address the influence of the described exchanges in Rho5.

3.1.6 Constitutively active Rho5

Figure 5 depicts the conserved glycine at position 12 highlighted in turquoise which is frequently found to be mutated in human cancer cells in Ras- and Rho-type GTPases, including Rac1 (reviewed in (Rajasekharan and Raman 2013, Aspenstrom 2018)). This common exchange was introduced into Rho5 via PCR and the mutated allele was subsequently integrated into the genome of *S. cerevisiae*. The effect of a constitutive activity on the localization of Rho5 ought to be investigated under physiological and stressed conditions. A GTP-locked Rho5 has already been included in the study of Schmitz and colleagues who exchanged glutamine 91 to histidine. The mutant allele caused a hypersensitivity towards cell wall stressors like CFW, caffeine, Congo red and heat (Schmitz et al. 2002). Additionally, Singh and co-workers demonstrated that the growth of a G12V mutant on media containing the oxidizing agents paraquat or diethyl maleate was severely impaired. This was accompanied by an increase in apoptotic markers (Singh et al. 2008). As a first step, the hypersensitivity of the strain expressing $Rho5^{G12V}$ was to be confirmed by testing the growth in the presence and absence of H_2O_2. A wild-type and a *Δrho5* strain were included as controls. The left graph of Figure 20A shows the growth under non-stressed conditions in rich medium and, as evident, all three strains demonstrated a similar growth.

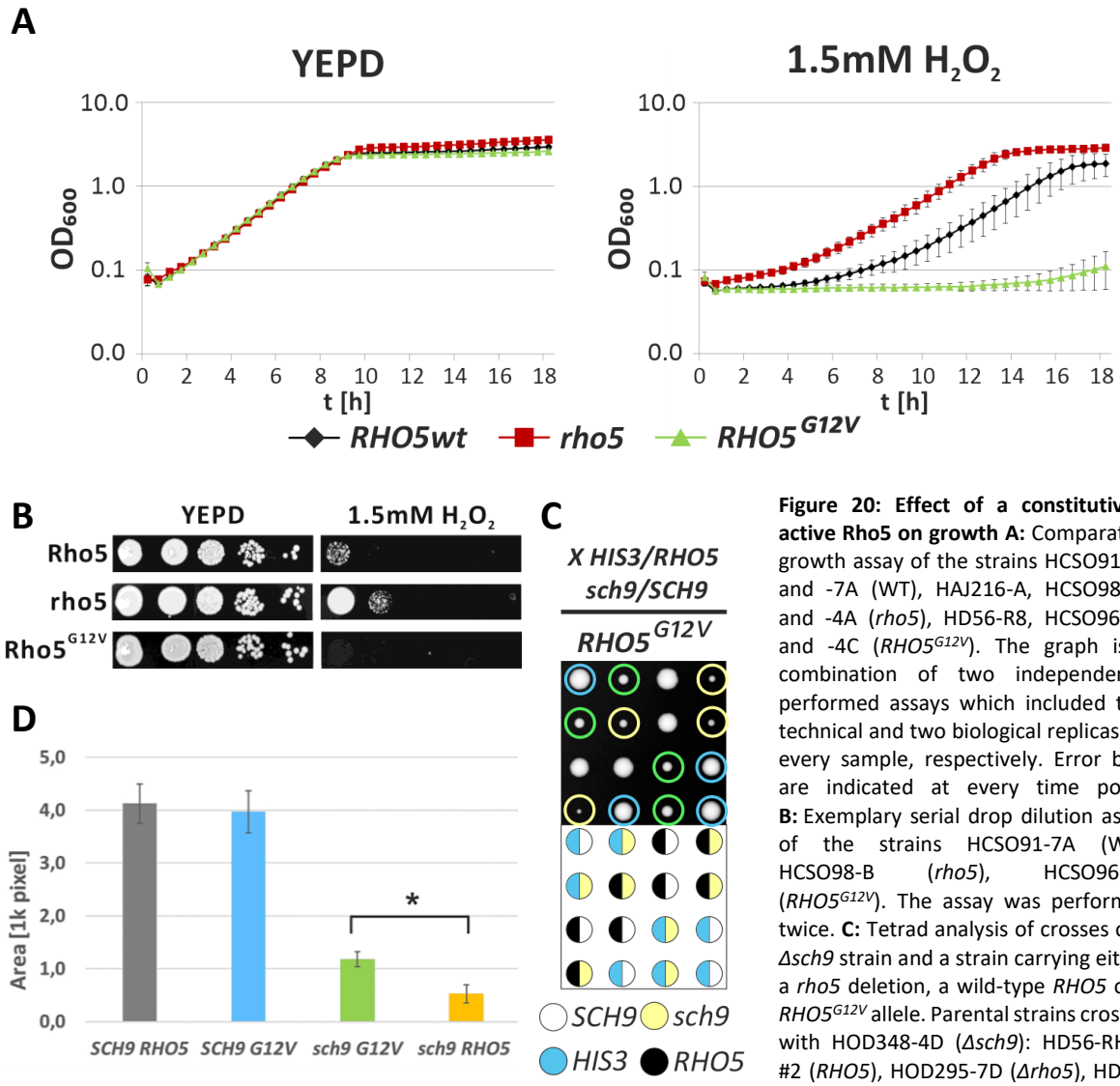

Figure 20: Effect of a constitutively active Rho5 on growth A: Comparative growth assay of the strains HCSO91-3C and -7A (WT), HAJ216-A, HCSO98-2B and -4A (*rho5*), HD56-R8, HCSO96-1A and -4C (*RHO5*^{G12V}). The graph is a combination of two independently performed assays which included two technical and two biological replicas for every sample, respectively. Error bars are indicated at every time point. **B:** Exemplary serial drop dilution assay of the strains HCSO91-7A (WT), HCSO98-B (*rho5*), HCSO96-3D (*RHO5*^{G12V}). The assay was performed twice. **C:** Tetrad analysis of crosses of a *Δsch9* strain and a strain carrying either a *rho5* deletion, a wild-type *RHO5* or a *RHO5*^{G12V} allele. Parental strains crossed with HOD348-4D (*Δsch9*): HD56-RHwt #2 (*RHO5*), HOD295-7D (*Δrho5*), HD56-R8 (*RHO5*^{G12V}). Rich medium agar plates were incubated for 3 days at 30 °C before documentation. Yellow circles highlight tetrads with *Δsch9 RHO5*, blue circles mark tetrads with *SCH9 RHO5*^{G12V} and green circles highlight tetrads with *Δsch9RHO5*^{G12V}. Genotypes of each tetrad are represented in the legend below. A total of 30 tetrads were analysed. **D:** Area of tetrads from DCSO96-4D in pixels. Each bar is the result of at least 13 measurements of single tetrads. Error bars are indicated for each data set. Comparison of tetrads areas of *Δsch9 RHO5*^{G12V} and *Δsch9 RHO5* gave a P-value of 0,3*10^{-9} (marked by asterisk).

On the other hand, in medium containing 1.5 mM hydrogen peroxide growth progressions differentiated from one another: As expected, the strain lacking *RHO5* (red squares) grew better compared to the wild-type strain (black rhombus). In stark contrast to that, the strain harbouring the *RHO5*^{G12V} allele (green triangles) did not reach logarithmic growth up to the end of the measurement corroborating the assumption of a hypersensitivity. These results are supported by the drop dilution assay presented in Figure 20B, where all strains grew normally on rich media without stressors lacking any differences to the control strains. On a plate containing 1.5 mM H_2O_2 (right panel) the controls exhibited reduced growth with the wild type growing to the first and the *rho5* deletion strain to the second dilution (first and second row). The *RHO5*^{G12V} mutant did not grow at all (bottom row), thus mimicking the hypersensitivity of the *RHO5*^{Q91H} mutant observed by Schmitz and co-workers (Schmitz

et al. 2002). To expand the investigations on glucose signalling, a haploid strain bearing a genomic integration of the *RHO5*^{G12V} allele was crossed with a *Δsch9* strain and the resulting heterozygote diploid strain was subjected to tetrad analyses. The dissection of 30 tetrads produced viable progeny harbouring the *RHO5*^{G12V} allele in a *sch9* deletion background (Figure 20C, green circles). Surprisingly, the respective colonies showed an increased diameter compared to the tetrads with a wild-type *RHO5* allele and a *sch9* deletion (yellow circles). Bearing just the *RHO5*^{G12V} mutation (blue circles) did not result in any conspicuous variations compared to the wild type (non-marked colonies). This observation is reflected in the diameter measurement of 30 colonies depicted in Figure 20D that were arranged in four categories depending on their *SCH9* and *RHO5* locus. Eventually, it revealed that the size of the *Δsch9 RHO5*^{G12V} tetrads was 2.4 times that of the *Δsch9 RHO5* tetrads. This observation suggests that a constitutively active Rho5 is advantageous in the *sch9* deletion background. In the next investigation the GTP-locked mutant Rho5^{G12V} was fused with GFP in order to examine the mutant's subcellular location. The upper two rows of Figure 21 show exemplary cells of *S. cerevisiae*. During physiological growth, the signal of the GTP-locked Rho5 exhibits a localization pattern corresponding to the wild type with nearly all the analysed cells showing the GFP signal at the plasma membrane.

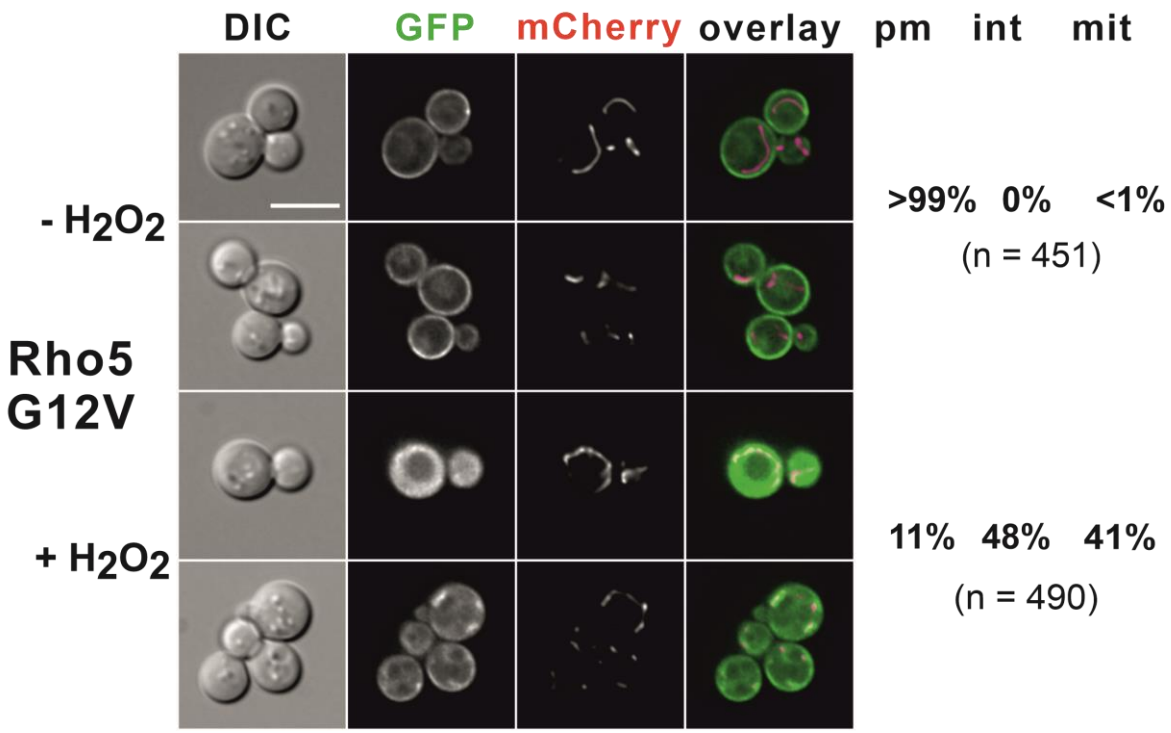

Figure 21: Localization of constitutively active Rho5 Life-cell fluorescence microscopy of a *rho5* deletion with a mitochondrial mCherry marker strain carrying the *RHO5*^{G12V} allele with an N-terminal GFP on a *CEN/ARS* vector (pLAO2). Cells were grown to mid-logarithmic phase in synthetic selective medium for plasmid maintenance and inspected under the fluorescence microscope. For induction of oxidative stress, the sample was exposed to 4.4 mM H_2O_2 and examined for 5 to 15 minutes. Cell counts of intracellular localization of the GFP signal are presented on the right-hand side of the microscope pictures. Co-localization of the red and green signals is highlighted by a yellow to white pseudo-colorization. pm = plasma membrane, int = non-specific internal localization, mit = mitochondrion. Exposure brightfield: 20 ms, excitation GFP channel: 2000 ms, Rhodamine channel: 400 ms. Scale bar indicates 5 µm.

This observation favours a model in which activation of Rho5 is insufficient for the relocalization of Rho5. Exposure to hydrogen peroxide was followed by a change in distribution with 41 % of the cells showing a co-localization of the GFP and the mitochondrial mCherry signal. An even higher number of cells displayed a different distribution with the signal at intercellular compartments or in the cytoplasm (48 %) or still at the plasma membrane (11 %).

3.1.7 Intracellular location of a dominant negative Rho5 variant

Dominant negative mutants of Rho-GTPases were shown to be either GDP-locked or devoid of any nucleotide (Feig 1999). Such a variant of Rho5 with the exchange of lysine 16 to asparagine has already been reported to be resistant to oxidative stress (Singh et al. 2008). This variant also failed to interact with its putative target Trr1. In this work, the similar dominant negative mutant Rho5^{T17N} was investigated for its subcellular distribution using a GFP fusion (Figure 22). As with the constitutively active mutant, the GFP signal from the fusion Rho5^{T17N} resided at the plasma membrane in 98 % of the analysed non-stressed yeast cells (upper two rows). Treatment with 4.4 mM hydrogen peroxide led to a redistribution of the GFP signal in 73 % of the cells that displayed co-localization with the mitochondrial mCherry marker (lower two rows). This observation mimics the results obtained in Rho5

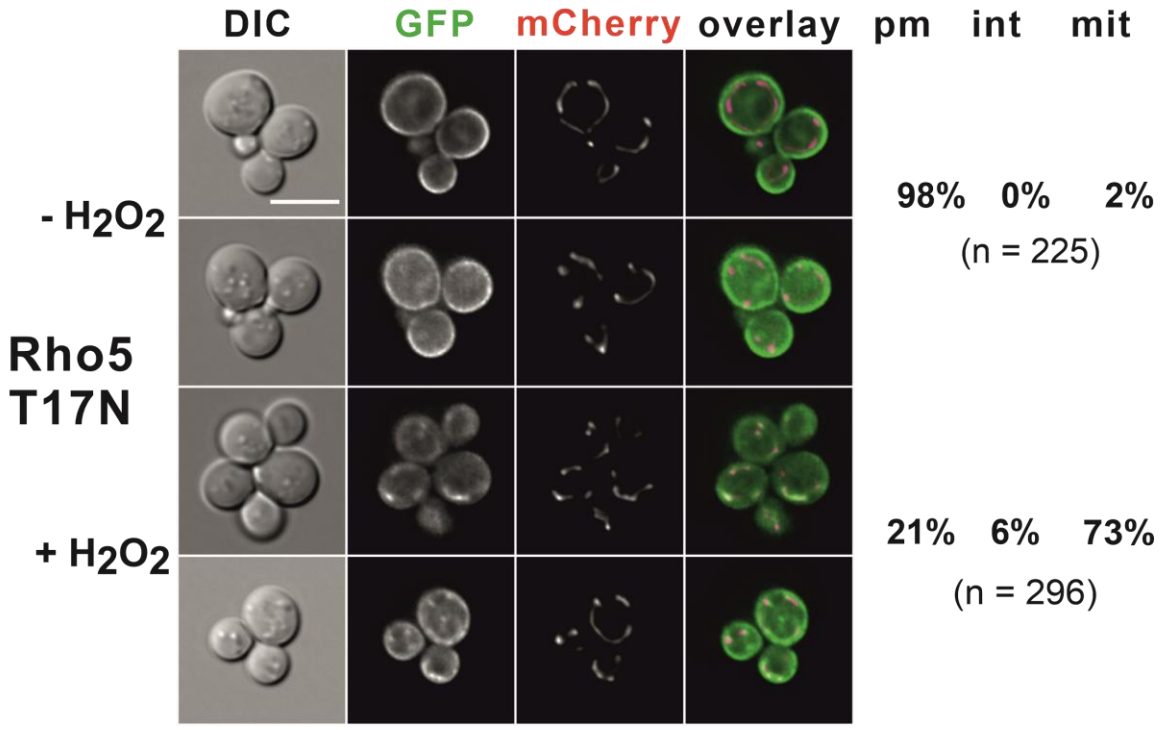

Figure 22: Localization of dominant negative Rho5 Life-cell fluorescence microscopy of a *rho5* deletion with a mitochondrial mCherry marker strain carrying the *RHO5^{T17N}* allele with an N-terminal GFP on a *CEN/ARS* vector (pCSO92). Cells were grown in synthetic selective medium for plasmid maintenance to mid-logarithmic phase and examined under the fluorescence microscope. For induction of oxidative stress, the sample was exposed to 4.4 mM H_2O_2 and examined for 5 to 15 minutes. Cell counts of intracellular localization of the GFP signal are presented on the right-hand side of the microscope pictures. Co-localization of the red and green signals is highlighted by a yellow to white pseudo-colorization. pm = plasma membrane, int = non-specific internal localization, mit = mitochondrion. Exposure brightfield: 20 ms, excitation GFP channel: 2000 ms, Rhodamine channel: 400 ms. Scale bar indicates 5 µm.

wild-type cells. However, in contrast to the wild type, 21 % of the Rho5^{T17N} cells still exhibited a peripheral GFP signal after oxidative stress exposure, thus presenting a slight but significant deviation.

3.2 Artificial recruitment of a GFP-tagged Rho5 and the components of its dimeric GEF to specific membranes

Rho5 exhibits a rapid relocation from the plasma membrane to mitochondria under oxidative stress starting within seconds (Schmitz et al. 2015). Yet, the exact role of the redistribution as well as the underlying molecular mechanisms have remained elusive. In order to shed light on the process, an antigen-binding region of a special antibody that recognizes GFP (henceforth abbreviated with "GB" for "GFP-binder") was employed as molecular tool to specifically trap GFP-tagged proteins *in vivo* and monitor the effects this artificial recruitment has on the fitness of the cells (Rothbauer et al. 2006). The chimeric construct was to be targeted to the mitochondrial outer membrane (Figure 23A).

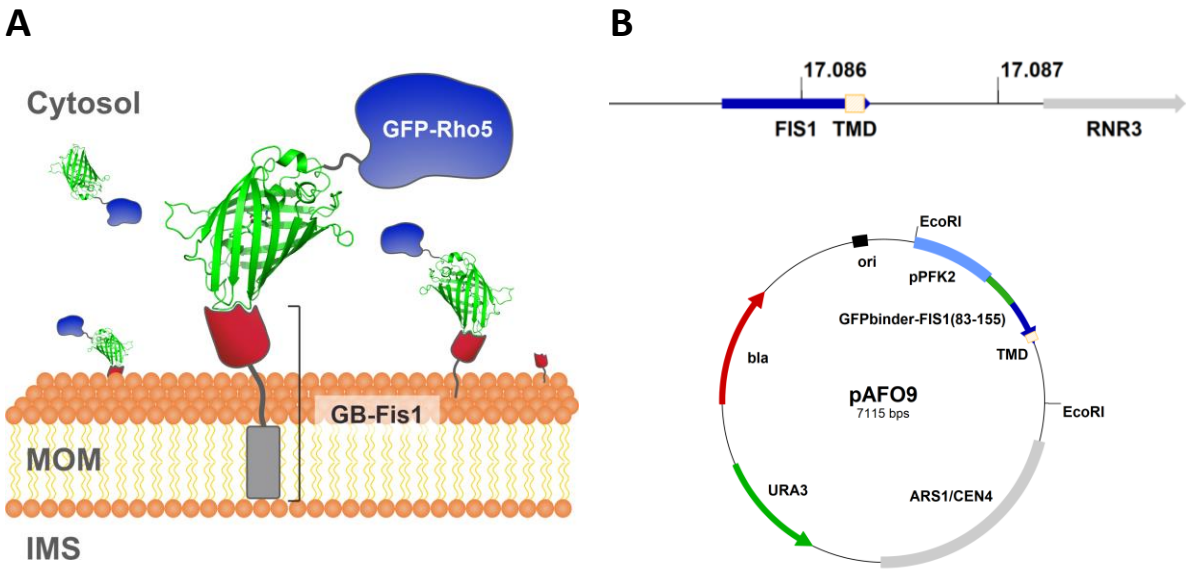

Figure 23: Construction of a mitochondrial GFP-binder A: Schematic representation of GFP-Rho5 recruitment via GFP-binder **B:** Construction of a plasmid-encoded mitochondrial GFP-binder (provided by Aileen Faist). MOM = mitochondrial outer membrane; IMS = intermembrane space. *Top*: Binding sites of oligonucleotides 17.086 and 17.087 for the amplification of codons 83 to 155 of *FIS1*. *Bottom:* Final plasmid of the *GB-FIS1* construct under the control of the *PFK2* promoter.

3.2.1 GFP-recruitment to mitochondria

For mitochondrial recruitment of GFP-tagged proteins the mitochondrial fission protein Fis1 was selected as fusion partner for the chimeric construct. To avoid a potential enhanced fission of mitochondria caused by the additional copy of Fis1, only the residues 83 to 155 were included because a correspondent peptide was the shortest fragment that was non-functional yet still located at mitochondria in human cells (Yoon et al. 2003). Hence, as a first step the respective codons were amplified by PCR from genomic yeast DNA and cloned into a low copy *CEN/ARS* vector (Figure 23B,

top). The GFP-binder gene under the control of the constitutive *PFK2* promoter was then fused to 5'-end of the shortened *FIS1* open reading frame by *in vivo* recombination. The *PFK2p GFP-binder-FIS1(83-155)*, henceforth referred to as *GB-FIS1*, was expressed from the plasmid pAFO9 (Figure 23B, bottom). To assess the binding capacity of this construct, pAFO9 was co-transformed with a plasmid encoding a cytosolic form of GFP (pJJH455) into a strain harbouring an mCherry mitochondrial marker (HJH11-2B). Cells were grown to mid-logarithmic phase and inspected under the fluorescence microscope. Figure 24 depicts representative cells of this culture and the majority of the cells (82 %) displayed a co-localization of the GFP and the mCherry signal. This observation suggests that the cytosolic GFP is efficiently recruited to the mitochondrion and furthermore proofs that GB-Fis1 is i) anchored to the mitochondrial surface and ii) properly folded and sufficiently protrudes into the cytosol to bind its antigen.

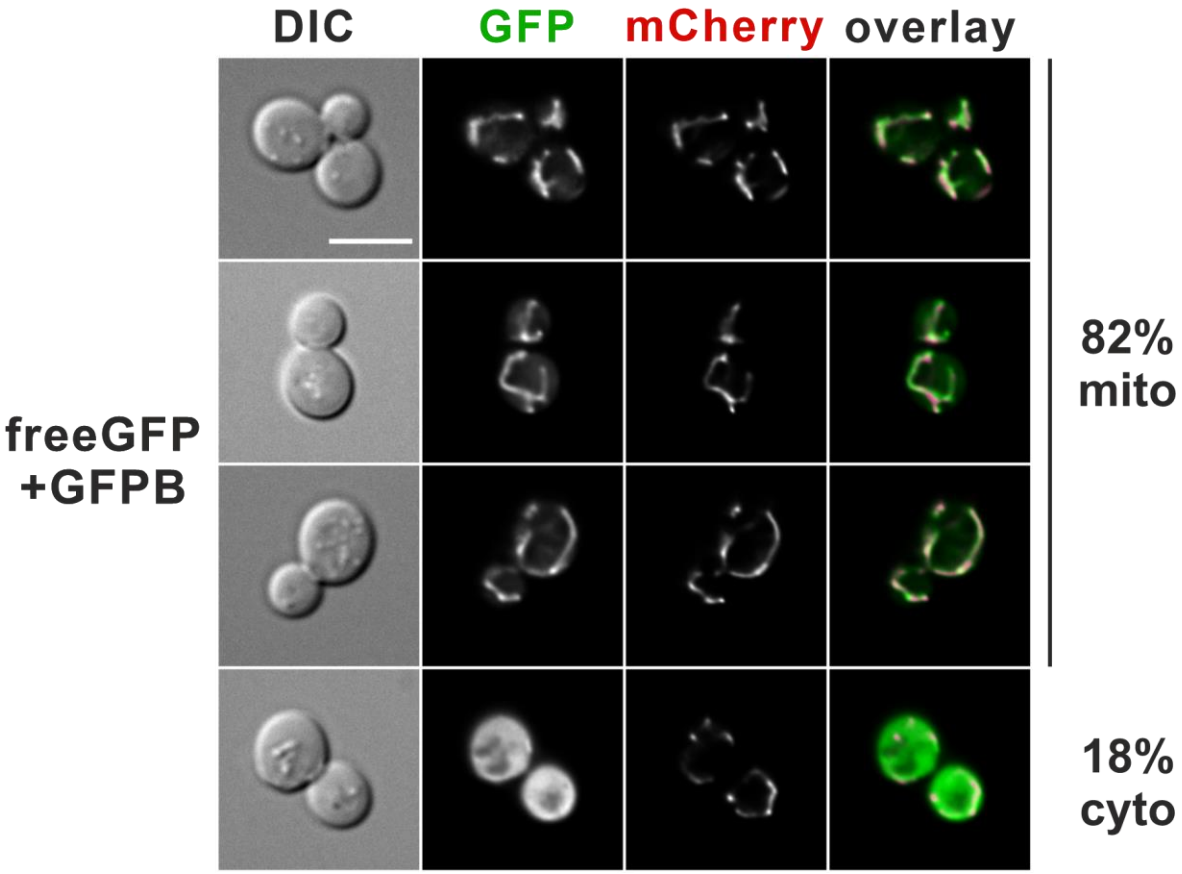

Figure 24: Recruitment of cytosolic GFP by the mitochondrial GFP-binder Life-cell fluorescence microscopy of a strain harbouring *IDP1-mCherry* fusion serving as mitochondrial marker (HJH11-2B) and two plasmids encoding for cytosolic GFP (pJJH455) and the mitochondrial GFP-binder (pAFO9). Cell counts of intracellular location of the GFP signal are presented on the right-hand side of the microscope pictures (n = 34). Co-localization of the red and green signals is reflected by a yellow to white pseudo-colorization in the overlay. Micrographs were taken from the Bachelor thesis of Aileen Faist. mito = mitochondrion, cyto = cytosol. Exposure brightfield: 20 ms, excitation GFP channel: 2000 ms, Rhodamine channel: 500 ms. Scale bar indicates 5 µm.

3.2.2 Trapping of GFP-Rho5 to mitochondria by stably inherited GFP-binder

To ensure stable inheritance, the *GB-FIS1* sequence from pAFO9 was cloned into the integrative vector YIp128 as an EcoRI/BamHI-fragment yielding pLAO12. Integration into the *leu2-3,112* locus was achieved by linearization of pLAO12 with EcoRV within the *LEU2* gene (Figure 25A, upper panel), transformed into DHD5 and grown on selective media (Figure 25A, lower panel). Three separate control PCRs were performed with purified genomic DNA as template. After confirmation of the correct integration (Figure 25B), the segregant named HCSO102-2B was chosen for further analyses. In order to investigate the mitochondrial trapping of Rho5, two independent strains bearing a genomic *GFP-RHO5* fusion expressed from the native *RHO5* promoter were crossed with HCSO102-2B and again

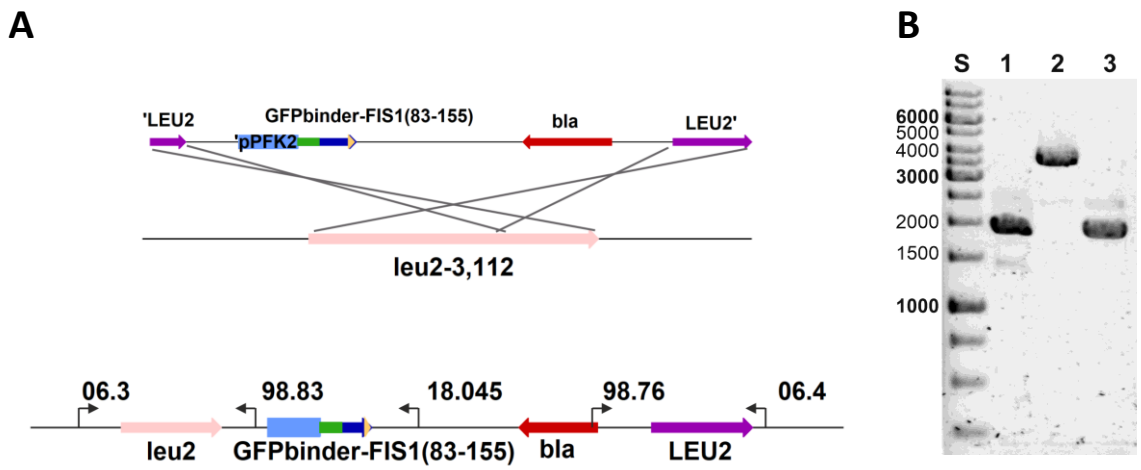

Figure 25: Construction of an integrative vector for a genomic mitochondrial GFP-binder Genomic integration of pLAO12 into the *leu2-3,112* locus of DHD5 to create HCSO102-2B. *Upper left panel:* Schematic representation of the homologous recombination between the linearized integrative plasmid pLAO12 and the *leu2-3,112* locus. pLAO12 was digested with the single cut endonuclease EcoRV before transformation. *Lower left panel*: Schematic overview of oligonucleotide binding sites for three separate control PCRs. *Right panel*: 1 % agarose gel with three separate control PCRs depicted on the lower left. 1: Oligonucleotides 06.3 and 98.83 with a predicted product of 1973 bp; 2: Oligonucleotides 06.3 and 18.045 with a predicted product of 3786 bp; 3: Oligonucleotides 98.76 and 06.4 with a predicted product of 1924 bp. S = size marker (GeneRuler™ 1 kb DNA Ladder)

subjected to tetrad dissection. Haploid segregants carrying both the *GB-FIS1* and *GFP-RHO5* were examined under the microscope to inspect the distribution of the GFP signal (Figure 26). All of the inspected cells showed tubular-shaped GFP signals (upper row) assumed to be mitochondria because of the striking similarity observed in previous microscopy (Figure 24). Segregants merely expressing the *GFP-RHO5* allele showed the expected peripheral signal (bottom row). The tubular GFP-location in the *GFP-RHO5 GB-FIS1* strain remained unaltered after 4.4 mM hydrogen peroxide exposure (middle row). These observations confirm the successful expression of the integrated *GB-FIS1* and recruitment of GFP-Rho5.

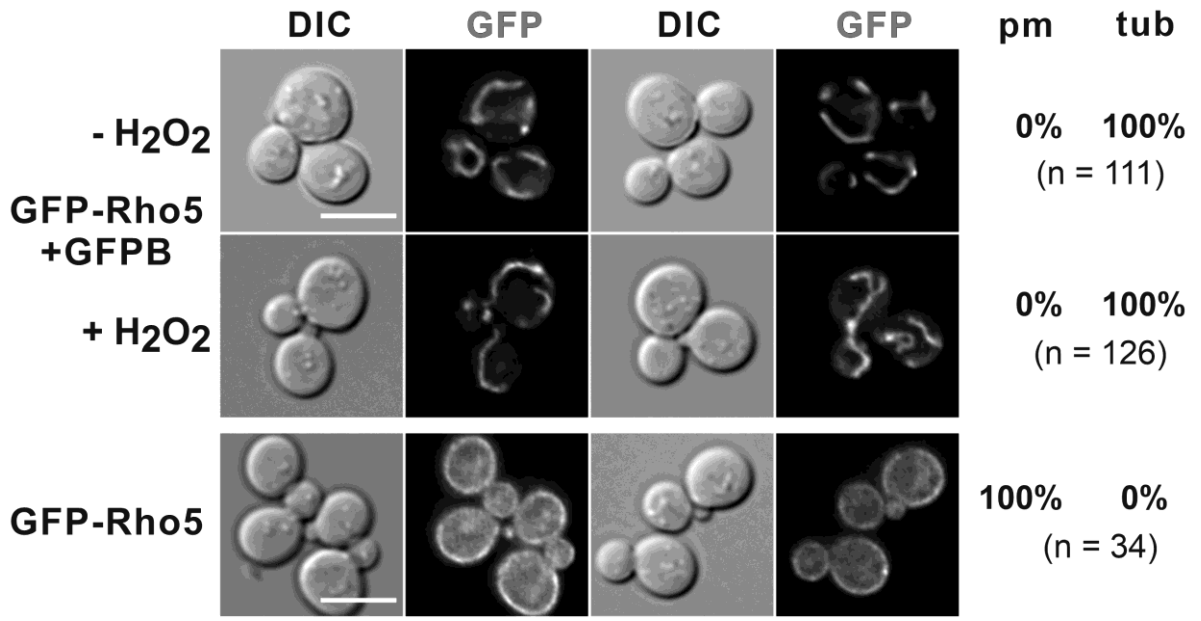

Figure 26: Recruitment of GFP-tagged Rho5 by the mitochondrial GFP-binder Life-cell fluorescence microscopy of a strain harbouring a genomically encoded GFP-Rho5 and the mitochondrial GFP-binder (HOD370-2A, upper two rows) as well as a strain exclusively carrying genomic *GFP-RHO5* (HOD365-9A, bottom row). Oxidative stress was induced by adding hydrogen peroxide to the sample to a final concentration of 4.4 mM. Cell counts of mitochondrial or plasma membrane localization of the GFP signal are presented on the right-hand side of the microscope pictures. pm = plasma membrane, tub = tubular structure. Exposure brightfield: 20 ms, excitation GFP channel: 2000 ms. Scale bar indicates 5 µm.

3.2.3 *In vivo* trapping of GFP-Rho5 at the mitochondrial surface results in a hyper-resistance towards hydrogen peroxide

To examine the physiological effect of the *in vivo* trapping of GFP-Rho5, strains carrying *GFP-RHO5* (HOD365-7B), *Δrho5* (HAJ216-A), *GB-FIS1* (HCSO102-2B) and a wild-type strain (HCSO90wt) were used as controls to be compared to a strain carrying *GFP-RHO5 GB-FIS1* derived from two independent crossings (HOD370-3B and HOD371-4A). They were subjected to a growth assay and as can be seen on the left panel of Figure 27A, all strains exhibit similar growth curves in rich medium. The presence of 1.5 mM hydrogen peroxide in the medium on the other hand had a diverging influence on the strains' growth behaviour: The wild type (black rhombus) as well as the strain carrying the genomically integrated *GFP-RHO5* (green triangles) showed similarly impeded growth while the *GB-FIS1* strain (blue crosses) grew a little bit better exhibiting a mild hyper-resistance compared to the wild. As expected, the *Δrho5* strain (red squares) showed hyper-resistance. Slightly below runs the graph of the strains carrying both the *GB-FIS1* and *GFP-RHO5* (yellow circles), thus clearly showing hyper-resistance to H_2O_2. The serial drop dilution assay using the same strains confirmed these results (Figure 27B). While the wild-type, the *GFP-RHO5* and the *GB-FIS1* strain all grew to the third dilution, the strain expressing both *GFP-RHO5* and *GB-FIS1* showed growth to the fourth dilution step, like the *rho5* deletion. Therefore, the mitochondrial *in vivo* trapping is established as a potent molecular tool to manipulate cellular processes.

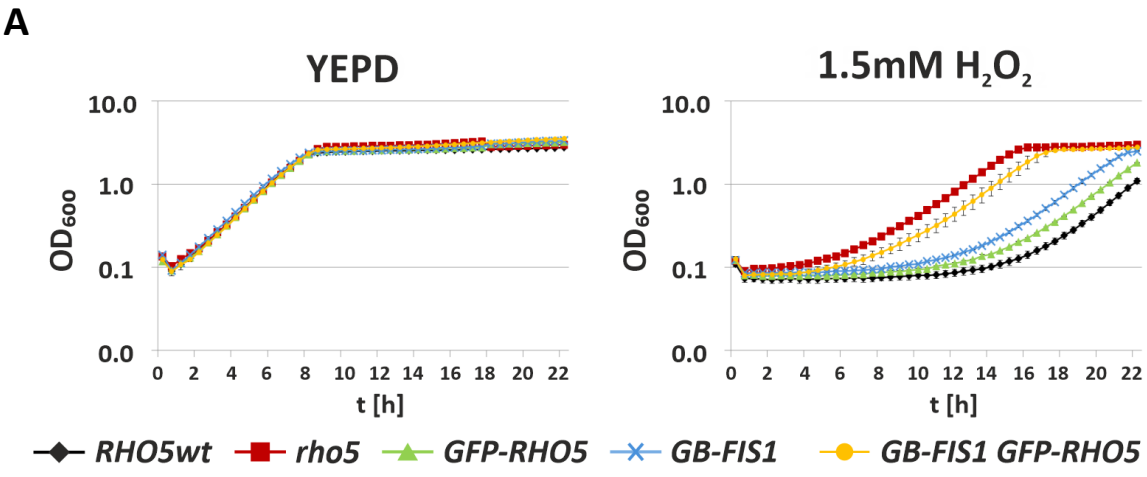

Figure 27: Effect of *in vivo* trapping of GFP-tagged Rho5 to mitochondria on growth A: Comparative growth analysis of the strains HCSO90wt (WT), HOD365-7B (*GFP-RHO5*), HAJ216-A (*Δrho5*), HCSO102-2B (*GB-FIS1*), HOD370-3B and HOD371-4A (*GFP-RHO5*, *GB*-FIS1. For oxidative stress, hydrogen peroxide was added to rich medium to a final concentration of 1.5 mM. Each graph included two technical and two biological replicas for each sample, respectively. Error bars are indicated at each time point. The assay was performed twice. **B:** Exemplary serial drop dilution assay of the strains HCSO90wt (WT), HAJ216-A (*rho5*), HOD365-7B (*GFP-RHO5*), HCSO102-2B (*GB-FIS1*), HOD370-3B and HOD371-4A (*GFP-RHO5*, *GB-FIS1*). Rich medium agar plates were incubated for 2 days at 30 °C before documentation. The assay was performed three times.

3.2.4 *In vivo* trapping of GFP-tagged, constitutively active Rho5 exhibits wild-type sensitivity towards oxidative stress

The experiments outlined in the previous chapter revealed the hyper-resistance resulting from the Rho5 recruitment to mitochondria. This raises the question whether the hyper-resistance of the *in vivo* trapping is due to a general non-functionality of the Rho protein or a failure to be activated by its dimeric GEF when associated with the plasma membrane. To test this, a GFP-tagged constitutively active variant of Rho5 was integrated into the genome of *Saccharomyces cerevisiae* and the transformants crossed with the *GB-FIS1* strain. From the resulting diploid strain, two independent segregants of a wild type, a strain carrying the *GB-FIS1* allele, the *GFP-RHO5*^{G12V} allele and both *GB-FIS1 GFP-RHO5*^{G12V} were chosen, respectively, and tested for their growth behaviour under oxidative stress. Additionally, to represent the hyper-resistance phenotype, a *Δrho5* strain was included. The results are shown in Figure 28. In rich medium all strains exhibit similar growth behaviour. Under 1.5 mM hydrogen peroxide, the *rho5* deletion (red squares) showed its expected hyper-resistance phenotype with a better growth compared to the wild type (black rhombus). The same outcome was observed with the *GB-FIS1* strain (blue crosses) resembling the progression of the wild type. In stark contrast to that, the *GFP-RHO5*^{G12V} strain (green triangles) exhibited a distinct hyper-sensitivity towards H_2O_2 which changed when the strain also carried the *GB-FIS1* construct (yellow circles).

Growth significantly improved almost reaching wild-type level. This indicates that it was indeed the lack of activation at the plasma membrane that caused the non-functional phenotype of the mitochondrially trapped wild-type GFP-Rho5 in the previous section.

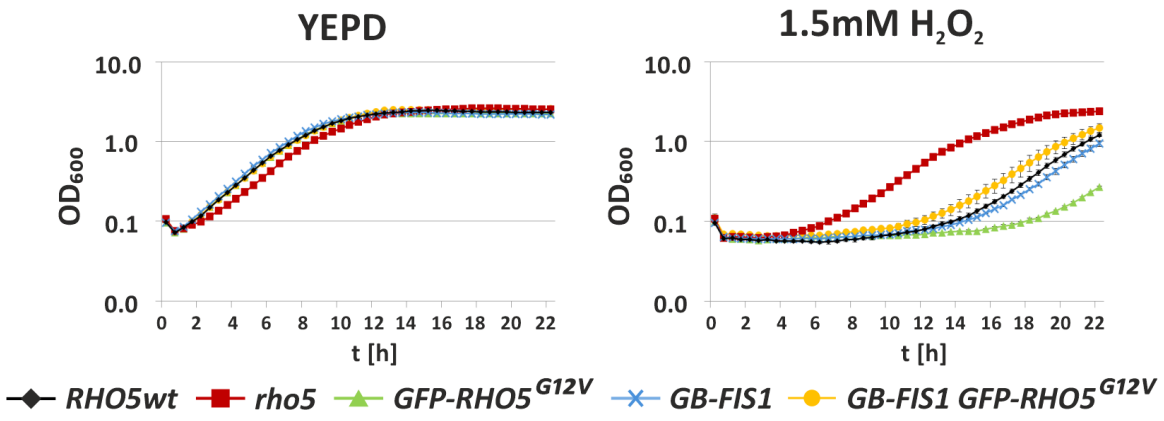

Figure 28: Effect of *in vivo* trapping of GTP-locked GFP-Rho5 to mitochondria on growth Comparative growth analysis of the strains HOD410-1B and HOD410-3D (WT), HAJ216-A (*rho5*), HOD410-1A and HOD410-3A (*GB-FIS1*), HOD410-1C and HOD410-3B (*GFP-RHO5^{G12V}*), HOD410-1D and HOD410-3C (*GB-FIS1 GFP-RHO5^{G12V}*). For oxidative stress, 1.5 mM hydrogen peroxide was added to the medium. Each graph included two technical replicas and two biological ones for each sample, respectively. Error bars are indicated at every time point. The assay was performed once.

3.2.5 Trapping of Dck1 and Lmo1, the subunits of the dimeric GEF, to mitochondria

Dck1 and Lmo1 have been identified as subunits of the putative dimeric GEF for yeast Rho5. They are also required for the GTPase's translocation to mitochondria under oxidative stress (Schmitz et al. 2015). Consequently, in the next step the *in vivo* trapping of the two subunits was tested. To do so, strains carrying triple GFP fusions of the proteins were crossed with the *GB-FIS1* strain and the resulting diploids subjected to tetrad dissection, respectively. Proper recruitment of the GFP-tagged proteins to mitochondria was confirmed via fluorescence microscopy in segregants obtained from the dissection (Figure 29). Similar to the *in vivo* trapping of GFP-Rho5, Dck1 and Lmo1 were successfully removed from their native distribution. Next, the effect of the mitochondrial trapping of Dck1 and Lmo1 on physiological growth as well as the response to H_2O_2 exposure was to be investigated. As controls two wild-type strains, a *Δdck1* or *Δlmo1* strain, a strain encoding for the mitochondrial GFP-binder and two triple-GFP tagged *DCK1* or *LMO1* strains were included. As can be seen on the left panel in Figure 30A and B, all strains exhibited a similar growth. In the presence of 1.7 mM H_2O_2 the growth of the wild-type control (black rhombus) and the *GB-FIS1* strain (blue crosses) showed an almost congruent progression, while the *Δdck1* (Figure 30A) and *Δlmo1* (B) strain (red squares) exhibited the hyper-resistance already demonstrated in previous works (Schmitz et al. 2015).

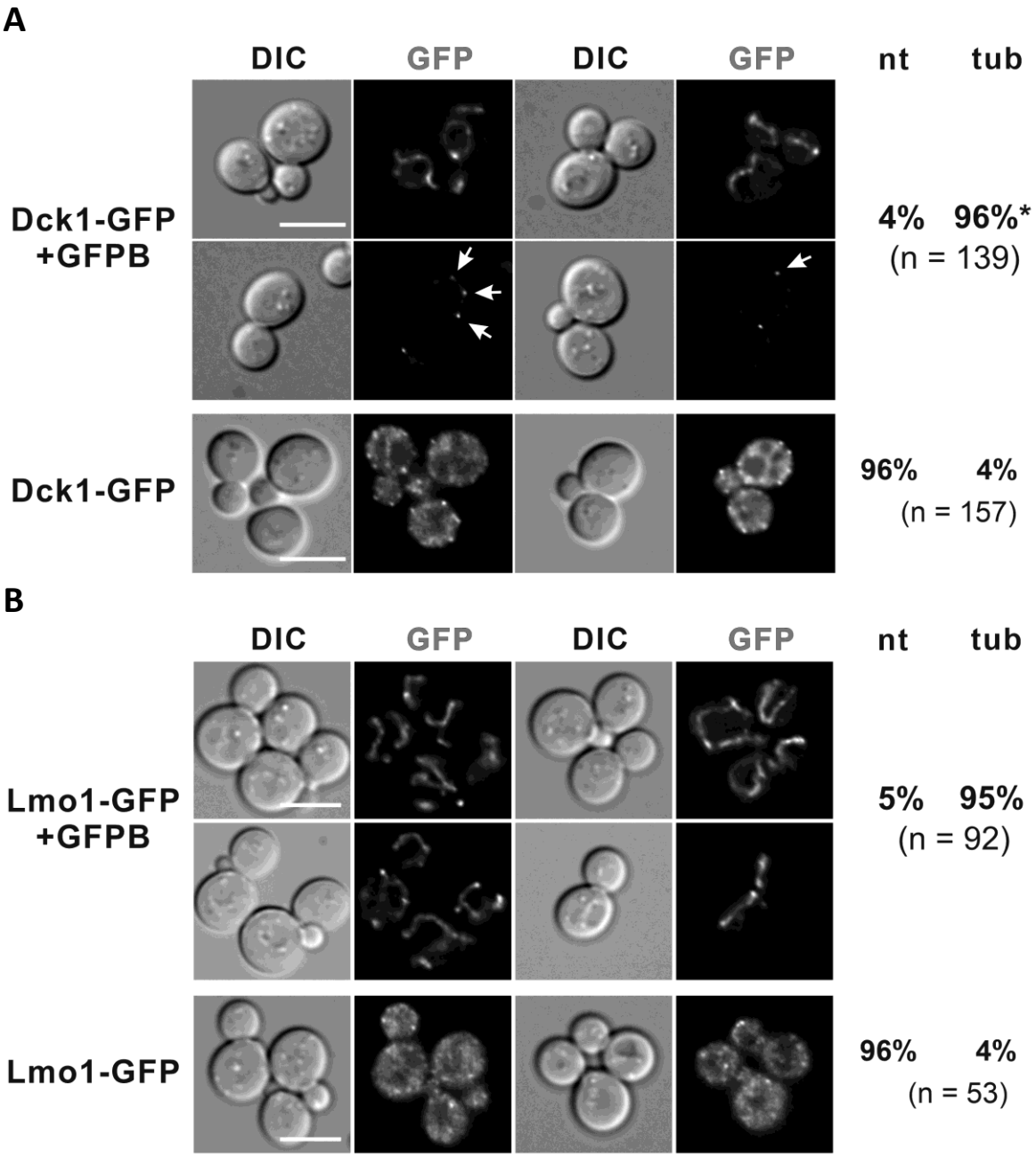

Figure 29: In *vivo* trapping of GFP-tagged Dck1 and Lmo1 by the mitochondrial GFP-binder A: Life-cell fluorescence microscopy of a strain harbouring a genomically encoded, triple GFP-tagged Dck1 and the mitochondrial GFP-binder (HOD405-3C and HOD406-8C, upper two rows) and a strain only carrying genomic *DCK1-3GFP* (HAJ152-A, bottom row). White arrows point at exemplary puncta of high GFP signal intensity located at the cell periphery. Asterisk: From the 96 % of cells exhibiting a mitochondrial signal, 43 % showed puncta as depicted in the second row. **B:** Life-cell fluorescence microscopy of a strain harbouring a genomically encoded, triple GFP-tagged Lmo1 and the mitochondrial GFP-binder (HOD415-11C, upper two rows) and a strain carrying only *LMO1-3GFP* (HOD415-1C, bottom row). nt = non-tubular signal, tub = tubular signal. Exposure brightfield: 20 ms, excitation GFP channel: 2000 ms. Scale bar indicates 5 µm.

Unexpectedly, growth of the triple GFP-tagged *DCK1* (green triangles, A) was severely impeded suggesting a hyper-sensitivity towards oxidative stress. In contrast to that, when *DCK1-3GFP* was co-expressed with the *GB-FIS1* (yellow circles), growth was significantly improved and only slightly less pronounced than the *dck1* deletion. In the Lmo1-assay (Figure 30B), treatment with 1.7 mM H_2O_2 revealed a hyper-resistance of the triple GFP-tagged *LMO1* strain (green triangles) as well as the *LMO1-3GFP* in the *GB-FIS1* background making the growth of both strains indistinguishable.

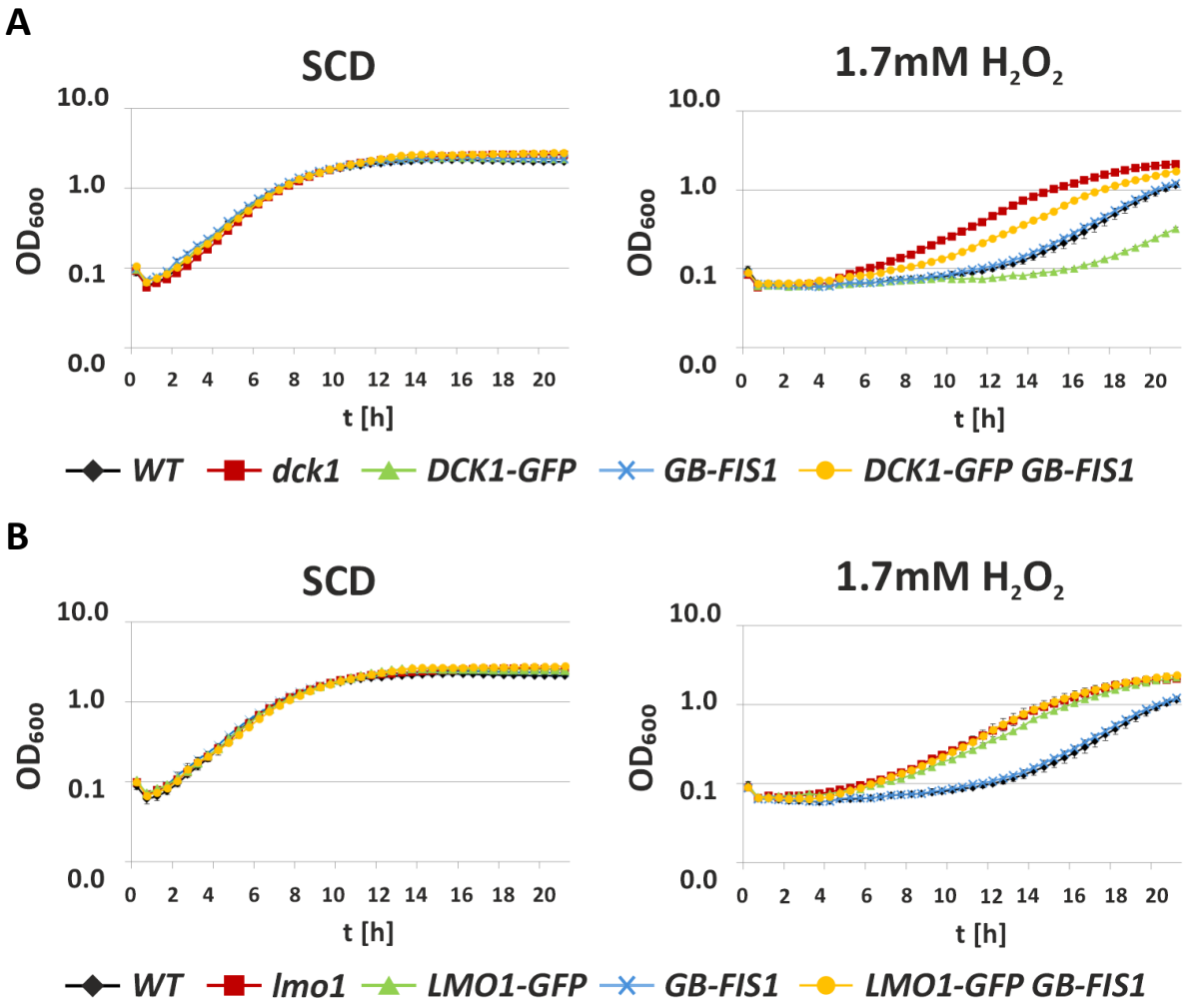

Figure 30: Effect of *in vivo* trapping of GFP-tagged Dck1 to mitochondria on growth Comparative growth analysis of the strains **A:** HOD405-3B and HOD406-8B (WT), HAJ03-B (*Δdck1*), HOD405-3A and -3D (*GB-FIS1*), HOD405-3D and HOD405-3A (*DCK1-3GFP*), HOD406-8C (*GB-FIS1 DCK1-3GFP*) or **B:** HOD405-3B and HOD406-8B (WT), HAJ201-B (*Δlmo1*), HOD405-3A and -3D (*GB-FIS1*), HOD415-11C (*LMO1-3GFP*), and HOD415-11D (*GB-FIS1 LMO1-3GFP*). For oxidative stress, 1.7 mM hydrogen peroxide was added to the medium. Each graph included two technical replicas for every sample, respectively. Error bars are indicated at every time point. The assay was performed once.

3.3 Dck1 and Lmo1 relocation

The mitochondrial redistribution of Rho5 depends on the presence of both components of the dimeric GEF, Dck1/Lmo1 (Schmitz et al. 2015). In order to further investigate the dependency of redistribution, the subcellular distribution of Lmo1 and Dck1 was followed in strains lacking the respective other component as well as on Rho5 itself. Figure 31 shows representative cells grown to mid-logarithmic phase, respectively. Under normal growth conditions, Dck1 and Lmo1 show a diffuse cytoplasmic distribution which frequently form foci that transiently co-localize. This was observed in the *rho5* deletion background indicating that the Rho protein is dispensable for this relocalization. In the absence of the other GEF component however, this punctate location of Dck1 or Lmo1 is abolished (Figure 31, third and fourth panel, first row) confirming previously published results (Schmitz et al. 2015). Nevertheless, exposing the cell to 4.4 mM H_2O_2 still lead to a redistribution in a solid portion of cells indicating that the translocation process of Dck1 and Lmo1 is independent of the respective other.

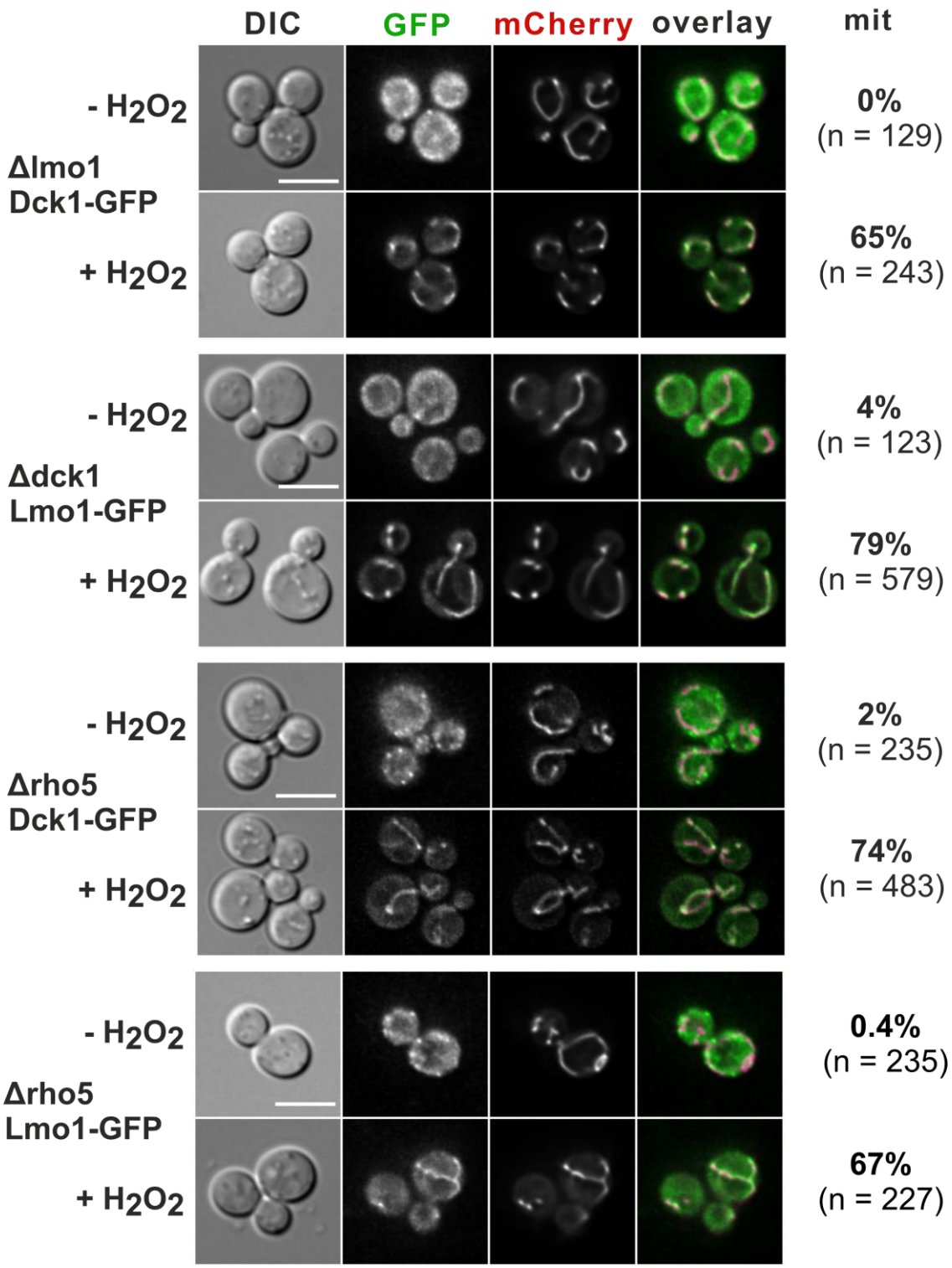

Figure 31: Effect of different deletions on the distribution of Dck1- and Lmo1-GFP. Life-cell fluorescence microscopy of strains with the indicated combinations of deletions and GFP fusions, all expressed from the respective native loci, and a plasmid-encoded mitochondrial mCherry marker (pJJH1408). Total cell counts (n) and the percentages of cells showing colocalization of the GFP and mCherry signals are given at the right. Microscopy was performed at least twice and with two biological replicas. Oxidative stress was applied by addition of 4.4 mM hydrogen peroxide and images were taken within 5 to 15 minutes post-exposure. Strains used were: HCSO26 = *Δlmo1 DCK1-GFP*; HCSO33 = *Δdck1 LMO1-GFP*; HCSO20 = *Δrho5 DCK1-GFP*; HCSO25 = *Δrho5 LMO1-GFP*. Scale bar indicates 5 µm.

3.4 *POR1*, encoding the main VDAC in *S. cerevisiae*, genetically interacts with *RHO5*

The targeted translocation of Rho5 to mitochondria upon oxidative stress suggests that it may interact with a mitochondrial surface protein as a local downstream effector. The mitochondrial surface is populated by a varying number of proteins one of which is the voltage dependant anion channel (VDACs) Por1 which is considered an anti-apoptotic factor (Pereira et al. 2007, Morgenstern et al. 2017). Due to its involvement in apoptosis and the position at the mitochondrial outer membrane (MOM) Por1 was examined in preliminary studies. As a first approach to check for a possible connection between Por1 and Rho5, a strain lacking both genes was constructed by crossing the single deletion strains and subjecting them to tetrad dissection. Two segregants of each genotype were chosen to document growth, including the single deletions and wild type as controls and the *rho5 por1* deletion background. On the left panel of Figure 32A, the results of growth in rich medium is depicted. Both *por1* (green triangles) and *rho5 por1* (blue crosses) deletion strains grew a bit slower compared to wild type (black rhombus) and *rho5* deletion (red squares). In the presence of 1.5 mM H_2O_2 growth of the *Δrho5* strain was not as severely impeded as the wild type.

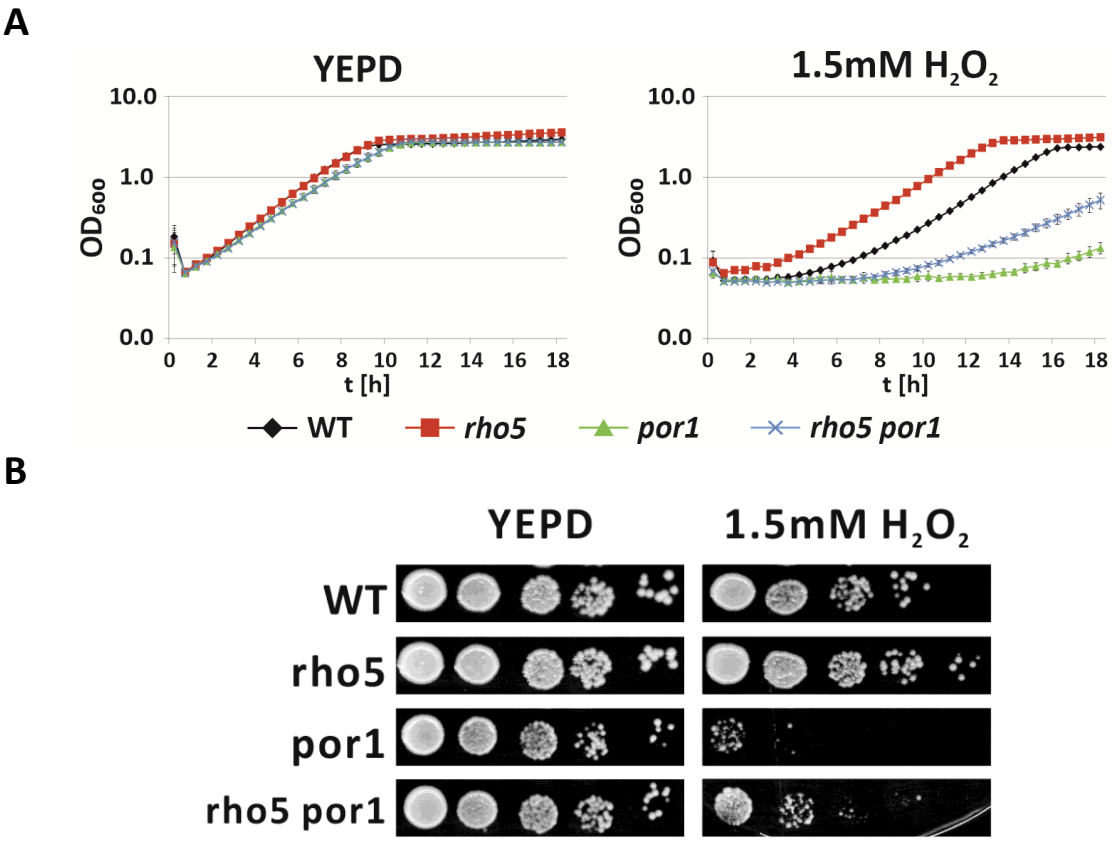

Figure 32: A: Comparative growth assay via plate reader of the strains HCSO87-2B and -5B (WT), HCSO87-1B and -6A (*rho5*), HCSO87-1A and -4A (*por1*), HCSO87-2D and -7A (*rho5 por1*). For oxidative stress, 1.5 mM hydrogen peroxide was added to rich medium. The assay was performed twice. Each graph included two technical and two biological replicas for every sample, respectively. Error bars are indicated at every time point. **B:** Exemplary serial drop dilution assay of the

As expected, the *por1* deletion background exhibits heavily impaired growth but in the *rho5 por1* double deletion strain, growth was improved. These results were consistent with the serial drop dilution assay conducted with the same strains (Figure 32B). The *por1* and the *rho5 por1* deletion produced slightly smaller colonies on rich medium (left panel, bottom two rows) indicating impaired growth as previously observed. On medium containing 1.5 mM H_2O_2 the wild type grew to the fourth dilution step while the strain lacking *RHO5* did so to the fifth step (right panel, first two rows). The *Δpor1* strain showed colony formation merely to the second dilution step (third row) conveying the expected hypersensitivity towards the stressor. The simultaneous deletion of *RHO5* and *POR1* however significantly improved growth and the strain grew to the fourth dilution (bottom row). Nevertheless, the colony sizes were less pronounced compared to the wild type so that the vitality clearly improved yet was not completely restored.

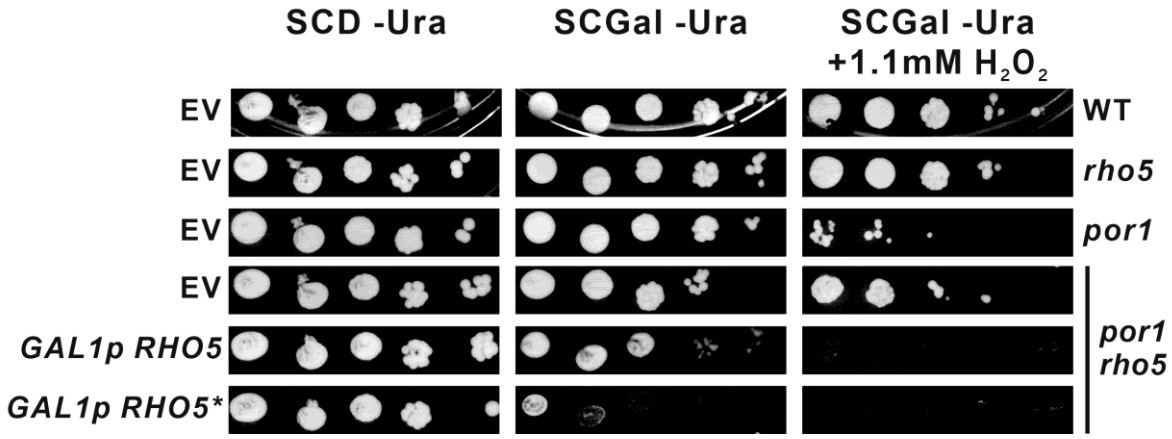

Figure 33: Effect of overexpressed *RHO5* Exemplary serial drop dilution assay of a *rho5 por1* double deletion strain (HAFO1) transformed with the following plasmids, respectively: YCplac33 (empty vector = EV), pSH4 (*GAL1p RHO5*) and pSH8 (*GAL1p RHO5^{Q91H}*, abbreviated with an asterisk). As control, a wild-type (HD56-5A), a *rho5* deletion (HAJ218-A) and a *por1* deletion strain (HOD266-1B) were employed, carrying the empty vector, respectively. Strains were pre-grown in synthetic selective medium with glucose to mid-logarithmic phase, calibrated to OD_{600} of 1.0, diluted in decimal steps and a respective volume of 3 µl of each dilution step placed on the solid medium. Synthetic selective medium plates with either glucose (non-inducive) or galactose (inducive) as carbon source were incubated for 3 days at 30 °C before documentation. The assay was performed four times. The drop dilution assay was performed by Aileen Faist during her Bachelor thesis.

Genetic interactions between *RHO5* and *POR1* were also substantiated by overexpressing a constitutively active *RHO5* allele in the background of a *por1* deletion. For this purpose, a *Δrho5 Δpor1* strain (HAFO1) was transformed with the plasmids YCplac33 serving as empty vector, pSH4 encoding for the wild-type *RHO5* and pSH8 with a constitutively active *RHO5* allele (*RHO5^{Q91H}*) both under the expression control of the inducible *GAL1* promoter. As additional controls a wild-type, a *Δrho5* and a *Δpor1* strain were chosen and transformed with the empty vector, respectively. Figure 33 depicts the results of this assay. On non-inducive medium with glucose, all transformants exhibit a similar growth pattern growing up to the 10^{-4} dilution step. On medium containing galactose the *Δpor1 Δrho5* strain expressing *RHO5* showed a slightly impaired growth apparent from the smaller colonies on the medium (second to last row). Expression of the constitutive active *RHO5* allele in the same background

however had a severe impact so that growth only reached the 10^{-1} dilution step (bottom row). This indicates that the GTP-locked variant has a hazardous effect in a *por1* deletion strain as opposed to the wild type as previously reported (Schmitz et al. 2002). While addition of 1.1 mM H_2O_2 to the galactose medium (right panel) only mildly affected the WT and *Δrho5* strain (first and second row) growth of the *Δpor1* strain was significantly impacted only reaching the second dilution, hence displaying hypersensitivity. On the other hand, the *por1 rho5* deletion (fourth row) demonstrated a reduced hypersensitivity as already shown in the previous assay (Figure 32). In contrast to that, the *Δpor1 Δrho5* strain expressing either *RHO5* or *RHO5*^{Q91H} grew not at all on 1.1 mM H_2O_2 (fifth and bottom row) thus being significantly more sensitive than a *POR1* depleted strain. Next, the question ought to be answered whether an increased number of Por1 can counteract the higher number of Rho5. For this, *POR1* was placed under the control of the *GAL1* promoter. The resulting strain (HCSO72-1C) was transformed with YCplac33 as empty vector control, pSH4 expressing the wild-type *RHO5* and pSH8 with *RHO5*^{Q91H} encoding the constitutively active variant also under the control of the *GAL1* promoter, respectively. The previously employed *por rho5* double deletion (HAFO1) was included in the test integrating the same plasmids.

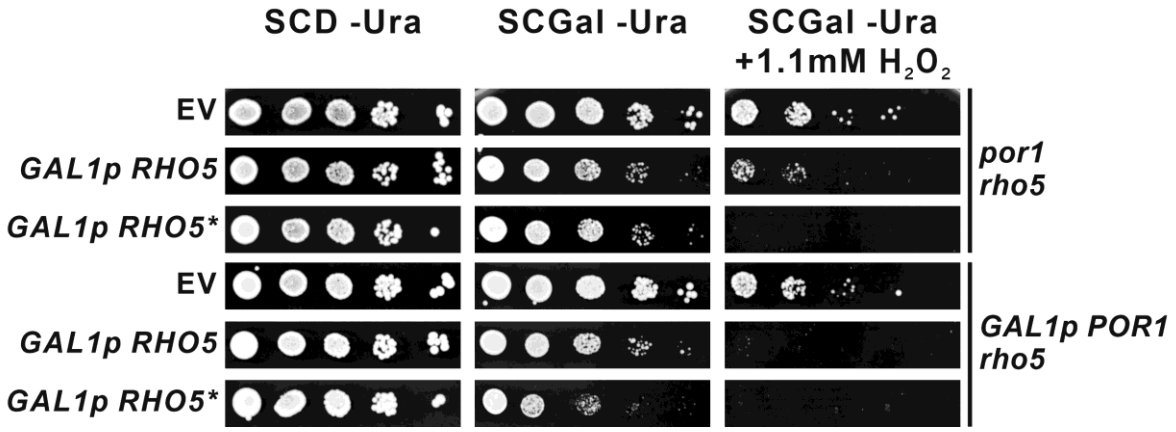

Figure 34: Effect of simultaneous overexpression of *RHO5* and *POR1* Exemplary serial drop dilution assay of a *rho5 por1* double deletion strain (HAFO1) as well as the *rho5 GAL1p POR1* strain (HCSO72-1C) transformed with the following plasmids, respectively: YCplac33 (empty vector = EV), pSH4 (*GAL1p RHO5*) and pSH8 (*GAL1p RHO5*^{Q91H}, abbreviated with an asterisk). Synthetic selective medium plates with either glucose (non-inducive) or galactose (inducive) as carbon source were incubated for 3 days at 30 °C before documentation. The assay was performed once.

On non-inducive, synthetic medium no difference could be observed in growth between the strains (Figure 34, left panel). On galactose medium (middle panel) growth was impeded in both strain backgrounds expressing either *RHO5* or *RHO5*^{Q91H} (second, third and fifth row) but was most affected in the *Δrho5 GAL1p POR1* strain carrying *RHO5*^{Q91H} (bottom row). The discrepancies exacerbated on galactose medium with 1.1 mM hydrogen peroxide (right panel): While the *rho5 por1* double deletion and the *Δrho5 GAL1p POR1* strain carrying the empty vector (first and fourth row, respectively) grew up to the fourth dilution step, *Δrho5 Δpor1* expressing wild-type *RHO5* (second row) only grew to the second dilution (third row). Under these conditions, no growth was shown by the *Δrho5 Δpor1* double

deletion carrying the *RHO5*^{Q91H} allele and *Δrho5 GAL1p POR1* strain expressing either *RHO5* or *RHO5*^{Q91H}. These results suggest that the co-overexpression of *RHO5* and *POR1* exhibits a higher sensitivity towards stress compared to a strain with a *por1* deletion overexpressing solely *RHO5*.

3.5 Human Rac1 in the yeast *Saccharomyces cerevisiae*

Rac1 is one of the central Rho-GTPases in virtually all eukaryotes. Yet, many aspects of its function are still unknown. In order to aid these investigations, *Saccharomyces cerevisiae* may serve as a suitable model organism to establishing a Rac1-based model. For this purpose, the *RAC1* gene was synthesized with optimized yeast codon usage and cloned into the *CEN/ARS* vector YCplac111. The gene was put under the control of the native yeast *RHO5* promoter expressed from the plasmid pLAO4. A *Δrho5* strain (HAJ216-A) was employed as recipient for pLAO4 and derivatives and tested under various growth conditions.

3.5.1 Wild-type *HsRAC1* does not complement a *rho5* deletion and does not associate with the plasma membrane

To test whether *HsRAC1* can complement a yeast *rho5* deletion, the plasmid pLAO4 (*RHO5p HsRAC1*, for construction details 2.1.9) was introduced into the strain HAJ216-A (*rho5*) and transformants were grown under standard and stressed conditions. As controls, cells carrying an empty vector (YCplac111) or one harbouring the *RHO5* wild-type allele (pJJH1637) were employed. Figure 35A shows the resulting growth curves under non-stressed conditions (left panel) and treatment with 1.2 mM H_2O_2 (right panel). The measurement of the non-stressed samples did not show significant growth differences. By contrast, under hydrogen peroxide treatment the *rho5* deletion (right panel, red squares) displayed hyper-resistance compared to that of wild-type *RHO5* (black rhomboids). The growth of the *RAC1* samples (green triangles) on the other hand resembled the vector control. These results were confirmed by the drop dilution assay in Figure 35B: In the presence of 1.2 mM hydrogen peroxide (right), the strain expressing wild-type *RHO5* hardly grew to the second (top row) while the *Δrho5* strain solidly reached the first second dilution (second row). The sample strain expressing *HsRAC1* grew slightly better than the *rho5* deletion control up to the third dilution verifying the lack of complementation (bottom row). To analyse the complementation capacity of Rac1 in glucose signalling, the synthetically lethal phenotype of a *sch9 rho5* double deletion of *S. cerevisiae* was employed by integrating the previously used plasmids into a heterozygote diploid *Δsch9 Δrho5* strain (DAJ138) and subjecting the transformants to tetrad analyses. Figure 35C depicts the results with the left and the middle panel depicting representative tetrads of the vector and the wild-type control, respectively. As expected, the vector control did not produce any viable progeny with the segregant predicted to carry the *sch9 rho5* deletion and the plasmid.

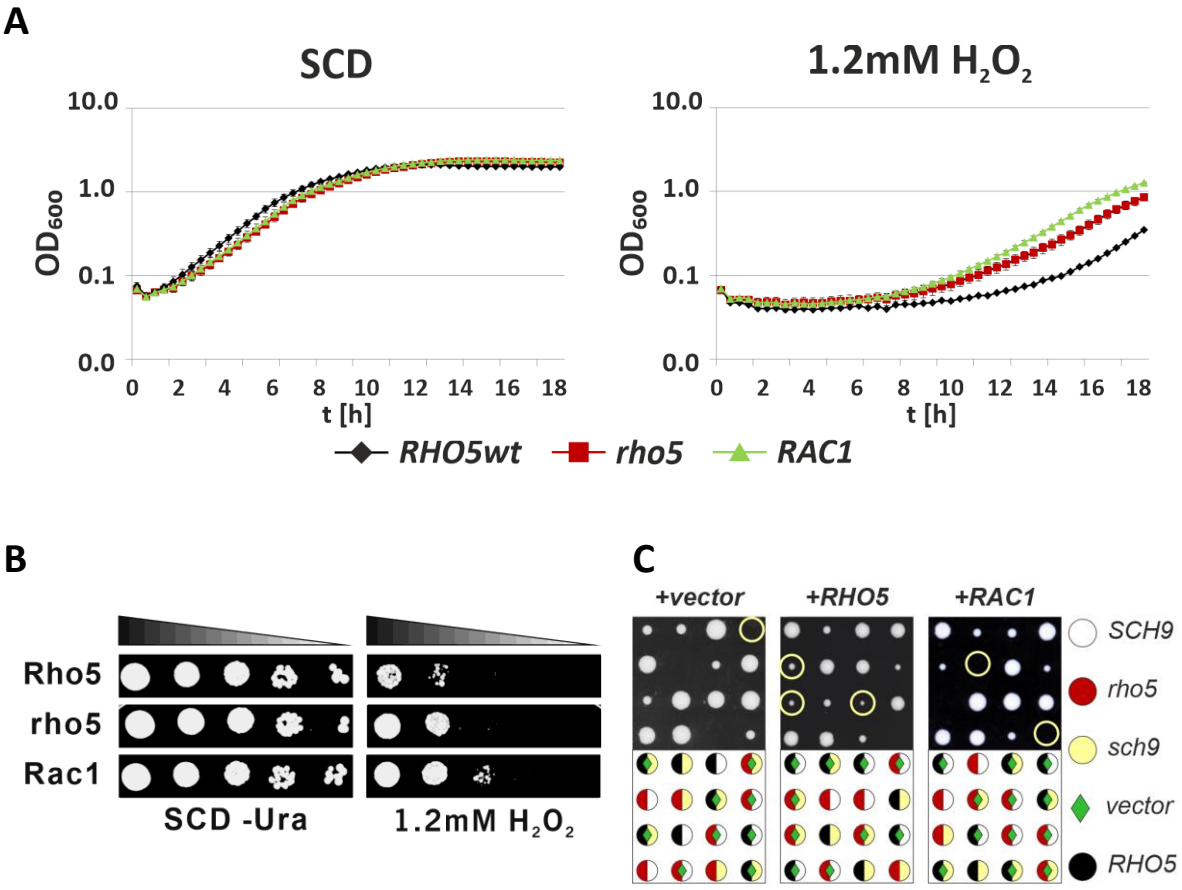

Figure 35: Effect of human Rac1 on growth of a *Δrho5* strain A: Comparative growth assay via microwell plate scanner of a strain depleted of *RHO5* (HAJ216-A) transformed with the plasmids harbouring *RHO5* (pJJH1637), *rho5* (empty vector; YCplac111), *RAC1* (pLAO4), respectively. Samples were grown in synthetic medium lacking uracil to mid-logarithmic phase, calibrated to OD_{600} = 1.0, diluted to OD_{600} = 0.1 into the wells of the microwell plate. Stressor medium contained 1.2 mM H_2O_2. The assay included two technical and two biological replicas for every sample. Error bars are indicated at each time point. **B:** Serial drop dilution assay. Plates were incubated for 3 days at 30 °C before documentation. Samples contained same plasmids listed in A. **C:** Tetrad analysis of a *sch9 rho5* heterozygotes deletion strain (DAJ138) transformed with the corresponding vectors listed in A. Rich medium agar plates were incubated for 3 days at 30 °C before documentation. Light yellow circles mark tetrads with a *sch9 rho5* double harbouring a plasmid. Genotypes of each tetrad are represented in the legend below. A total of 30 tetrads were analysed.

On the other hand, every segregant with this background that also expressed wild-type *RHO5* showed colony formation (yellow circles). Regarding *RAC1*, no segregants predicted to harbour a *sch9 rho5* double deletion while also expressing *HsRAC1* were obtained (right panel, light yellow circles). Low expression or low activity as cause for the absent complementation was excluded by placing *HsRAC1* under the control of the strong *PFK2* promoter or exchanging the conserved glycine 12 for valine to generate a constitutively active variant (Figure 36). The results of these growth assays and the tetrad dissection correlate with the wild-type Rac1 confirming the notion that the protein is not functional.

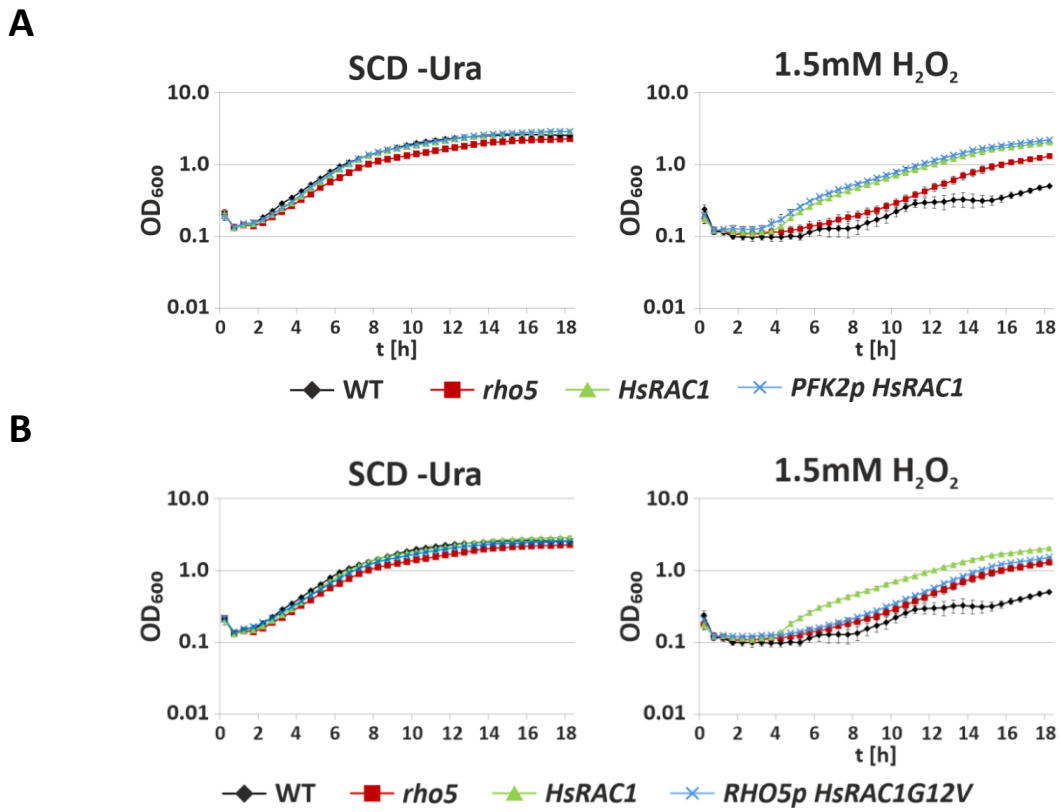

Figure 36: Effect of different human Rac1 constructs on growth A: Comparative growth assay via microwell plate scanner of a *Δrho5* strain (HAJ216-A) harbouring the plasmids *RHO5p RHO5* (pJJH1637), *rho5* (empty vector; YCplac111), *RHO5p HsRAC1* (pLAO4) and *PFK2p HsRAC1* (pJJH2294) respectively. **B:** Comparative growth assay via microwell plate scanner of a *Δrho5* strain (HAJ216-A) harbouring the plasmids *RHO5p RHO5* (pJJH1637), *rho5* (empty vector; YCplac111), *RHO5p HsRAC1* (pLAO4) and *RHO5p HsRAC1^{G12V}* (pJJH2334). Samples were grown in synthetic medium lacking uracil to mid-logarithmic phase, calibrated to OD_{600} = 1.0, diluted to OD_{600} = 0.1 into the wells of the microwell plate. Stressor medium contained 1.2 mM H_2O_2. Error bars are indicated at each time point.

3.5.2 GFP-*Hs*Rac1 localizes in the cytosol and at intracellular structures

One reason for the lack of complementation could be a mis-localization of the heterologous human Rac1. To address this question, an N-terminal fusion with GFP was constructed, expressed from the plasmid pLAO6. It was introduced into the *Δrho5* tester strain carrying a genomic mitochondrial mCherry marker (HCSO76-1A) and analysed under the fluorescence microscope. The upper two rows of Figure 37 show representative cells of *S. cerevisiae* during mid-logarithmic growth. Evidently, the majority of the signal appeared evenly distributed throughout the cytosol. A certain fraction can be detected at distinct intracellular structures, sometimes in a circular shape (second row). Quantification revealed that 99 % of the cells showed this localization labelled as “int” for a non-specific intracellular site. After treatment with 4.4 mM hydrogen peroxide (lower two rows), the signal showed a similar distribution to the untreated samples, except for 11 % of the cells that exhibited a co-localizing of the GFP signal and the mitochondrial mCherry marker (third row).

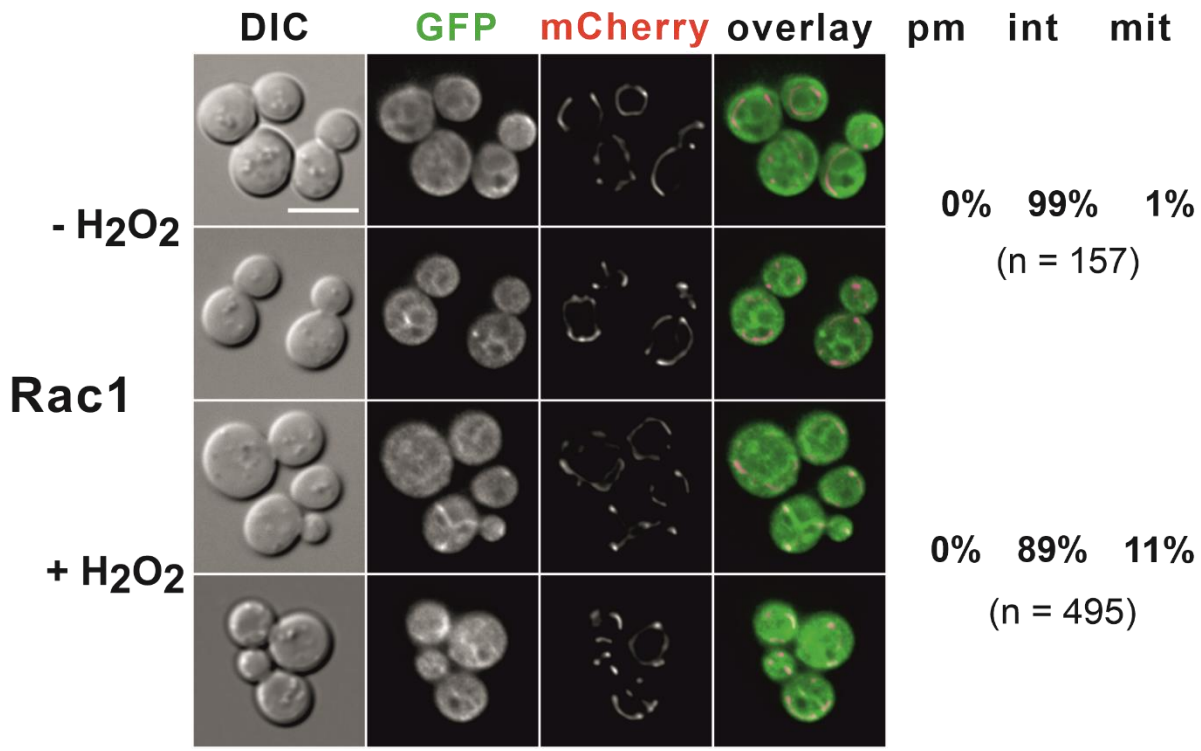

Figure 37: Localization of GFP-tagged human Rac1 in *S. cerevisiae* Life-cell fluorescence microscopy of a *rho5* deletion strain with a mitochondrial mCherry marker (HCSO76-1A) carrying the *RAC1* gene with an N-terminal GFP on a *CEN/ARS* vector (pLAO6). Cells were grown to mid-logarithmic phase in synthetic selective medium lacking uracil for plasmid maintenance and examined under the fluorescence microscope. For induction of oxidative stress, the sample was exposed to 4.4 mM H_2O_2 and examined for 5 to 15 minutes post-exposure. Cell counts of intracellular localization of the GFP signal are presented on the right-hand side of the microscope pictures. Co-localization of the red and green signals is highlighted by a yellow to white pseudo-colorization in the overlay. pm = plasma membrane, int = non-specific internal localization, mit = mitochondrion. Exposure brightfield: 20 ms, excitation GFP channel: 2000 ms, Rhodamine channel: 400 ms. Scale bar indicates 5 µm.

3.5.3 Function and localization of chimeric *Hs*Rac1 constructs

*Hs*Rac1 and *Sc*Rho5 differ in their primary sequence, especially in their C-terminal part (Figure 5). Since human *RAC1* cannot complement a *rho5* deletion as demonstrated in the previous chapter, consequently, the next step was to investigate whether the C-terminal region of Rho5 influences Rac1's functionality. In order to do so, two chimeric Rac1 constructs were created, one comprising of Rho5's PBR and CAAX motif and the other of the last 110 residues substituting the last 13 amino acids of Rac1, respectively (Figure 38A). Both constructs were placed under the control of the *RHO5* promoter and expressed from pCSO99 (*RAC1-RHO5*^{C17}) and pCSO98 (*RAC1-RHO5*^{C110}). Additionally, *RAC1-RHO5*^{C110} was placed under the control of the strong *TEF2* promoter expressed from pCSO85 (construction details, see 2.1.10). All three plasmids were introduced into the *Δrho5* strain alongside with an empty vector (YCplac111) and one carrying the wild-type *RHO5* allele (pJJH1637) to serve as controls. The serial drop dilution assays depicted in Figure 38B show that all three backgrounds grew equally well on standard synthetic medium. In the presence of 1.2 mM hydrogen peroxide the *RHO5* control barely grew to the second dilution (first row) while the *rho5* deletion (empty vector, second row) solidly grew to the same step.

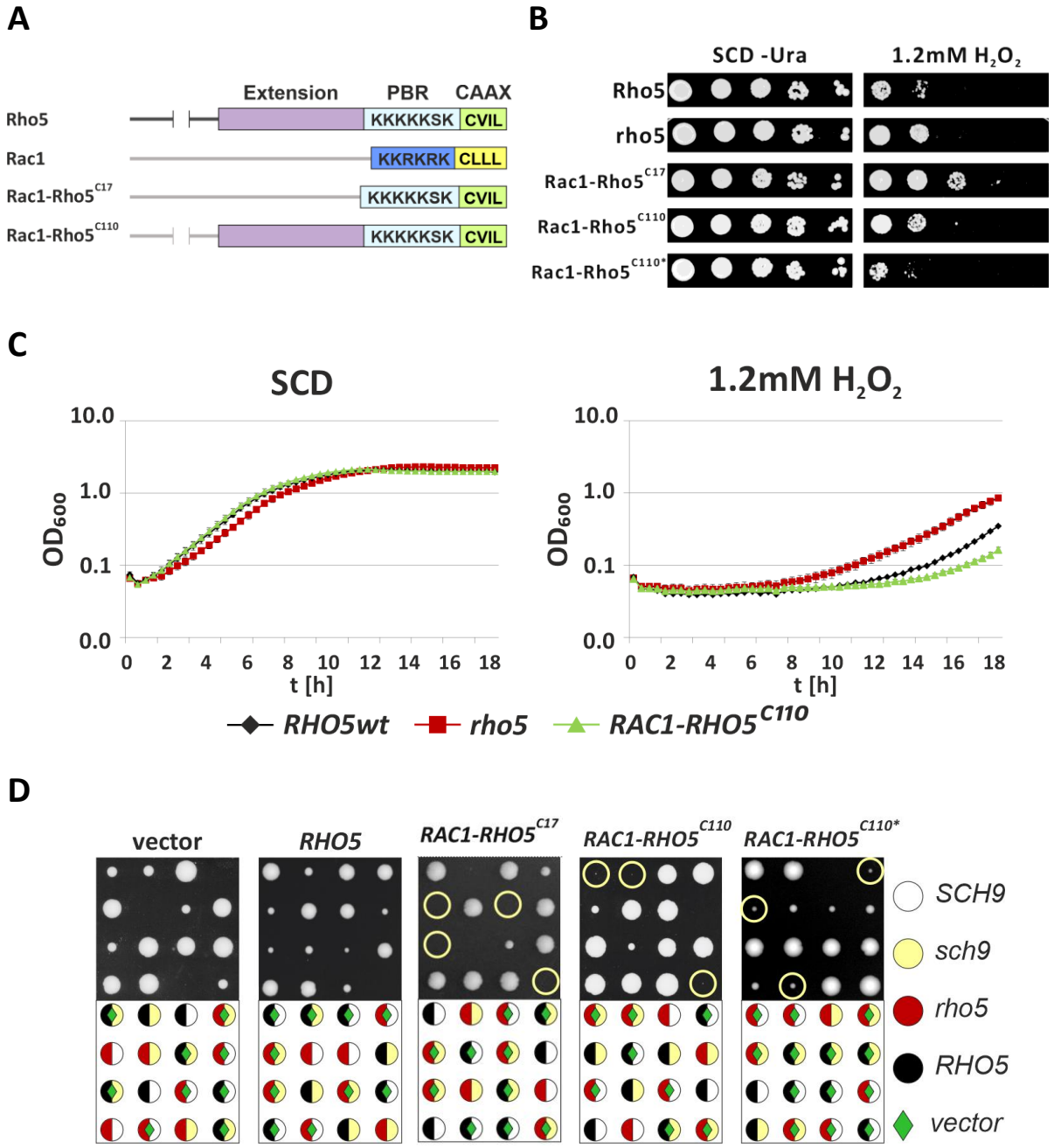

Figure 38: Effect of chimeric *Hs*Rac1 with Rho5's PBR and CAAX motif on growth of a *rho5* deletion strain A: Schematic representation of Rac1 constructs used in this chapter. **B:** Serial drop dilution assay of a *Δrho5* strain (HAJ216-A) separately transformed with plasmids harbouring *RHO5* (pJJH1637), *rho5* (empty vector; YCplac111), *RAC1-RHO5^{C17}* (pCSO99), *RAC1-RHO5^{C110}* (pCSO98) or overexpressed *RAC1-RHO5^{C110}* (marked with*, pCSO85). Plates were subsequently incubated for 3 days at 30 °C before documentation. **C:** Comparative growth assay in the microwell plate scanner of transformants with plasmids harbouring *RHO5* (pJJH1637), *rho5* (empty vector; YCplac111), *TEF2p RAC1-RHO5^{C110}* (pCSO85) transformed into a strain depleted of *RHO5* (HAJ216-A). The assay included two technical replicas and two biological ones. Error bars are indicated at each time point. **D:** Tetrad analysis of a *sch9 rho5* heterozygotes deletion strain (DAJ138) transformed with the corresponding plasmids listed in B. Rich medium agar plates were incubated for 3 days at 30 °C before documentation. Yellow circles highlight tetrads with a *sch9 rho5* double deletion harbouring the respective a plasmid. Genotypes of each tetrad are represented in the legend below. A total of 30 tetrads were analysed.

When carrying the plasmid with the *RAC1-RHO5^{C17}* construct, colony formation could be detected up to the fourth dilution (bottom row). The sample with *RHO5p RAC1-RHO5^{C110}* also shows growth up to the second dilution conferring an intermediate growth between the hyper-resistant *rho5* deletion and the wild-type control. *TEF2p RAC1-RHO5^{C110}* showed growth just about to the second dilution thus

resembling the wild-type control (bottom row). The functionality of the *TEF2p RAC1-RHO5^{C110}* construct was also confirmed in a growth assay in the microwell plate scanner. As can be seen on the left chart of Figure 38C, all three growth progressions of the untreated samples are similar and do not betray any phenotype under growth in synthetic selective medium. Under exposure to 1.2 mM hydrogen peroxide (right chart), the hyper-resistance of the *rho5* deletion (red squares) was observed by a better growth compared to that of *RHO5* (black rhombus), reaching a final OD_{600} of a little less than 1 compared to 0.35 of the wild-type control, respectively. With respect to *TEF2p RAC1-RHO5^{C110}* (green triangles), the samples grew to a final OD_{600} of 0.2 therefore resembling the wild type.

In order to test for complementation in glucose signalling, the heterozygote diploid *Δsch9 Δrho5* strain (DAJ138) was transformed with the plasmids used in the drop dilution assay and subjected to tetrad analyses. In a *sch9 rho5* double deletion background segregants expected to harbour *RAC1-RHO5^{C17}* did not produce viable progeny (Figure 38D, yellow circles). As with the wild-type *RAC1*, this points to a non-functional protein. In contrast to that, the *RHO5p RAC1-RHO5^{C110}* construct seemed to partially elevate the synthetic lethality but colonies were diminutive and only detectable after 3 days of incubation (Figure 38D, third panel, light yellow circles). In contrast to that, segregants expressing *TEF2p RAC1-RHO5^{C110}* showed a better growth compared to the expression of the construct under the *RHO5* promoter (second panel, highlighted by yellow circles). These results indicate that the construct Rac1-Rho5^{C110} is not fully functional and thus the expression level provided by the native *RHO5* promoter was not sufficient to grant thorough complementation of the synthetic lethality.

3.5.4 The C-terminal half of yeast Rho5 improves peripheral distribution of *Hs*Rac1

To investigate the influence of Rho5's C-terminus on Rac1's subcellular location, the chimeric constructs Rac1-Rho5^{C17} and Rac1-Rho5^{C110} were fused with GFP on the plasmids pCSO99 and pCSO100, respectively. They were introduced into the *rho5* strain with a genomic mCherry-labelled Idp1, allowing the detection of mitochondria (HCSO76-1A). The upper two rows of Figure 39A depict representative cells from the microscopic inspection of Rac1-Rho5^{C17}. Quantification of the distribution patterns revealed that in 99 % of the analysed cells the GFP signal predominantly occurred at the cell periphery. Many cells simultaneously exhibited a strong signal at non-specified intracellular structures. Treatment with 4.4 mM hydrogen peroxide (Figure 39A, lower two rows) reduced the PM localization of the GFP signal in 30 % cells while in 68 % the GFP signal appeared mainly in the non-specific internal fraction.

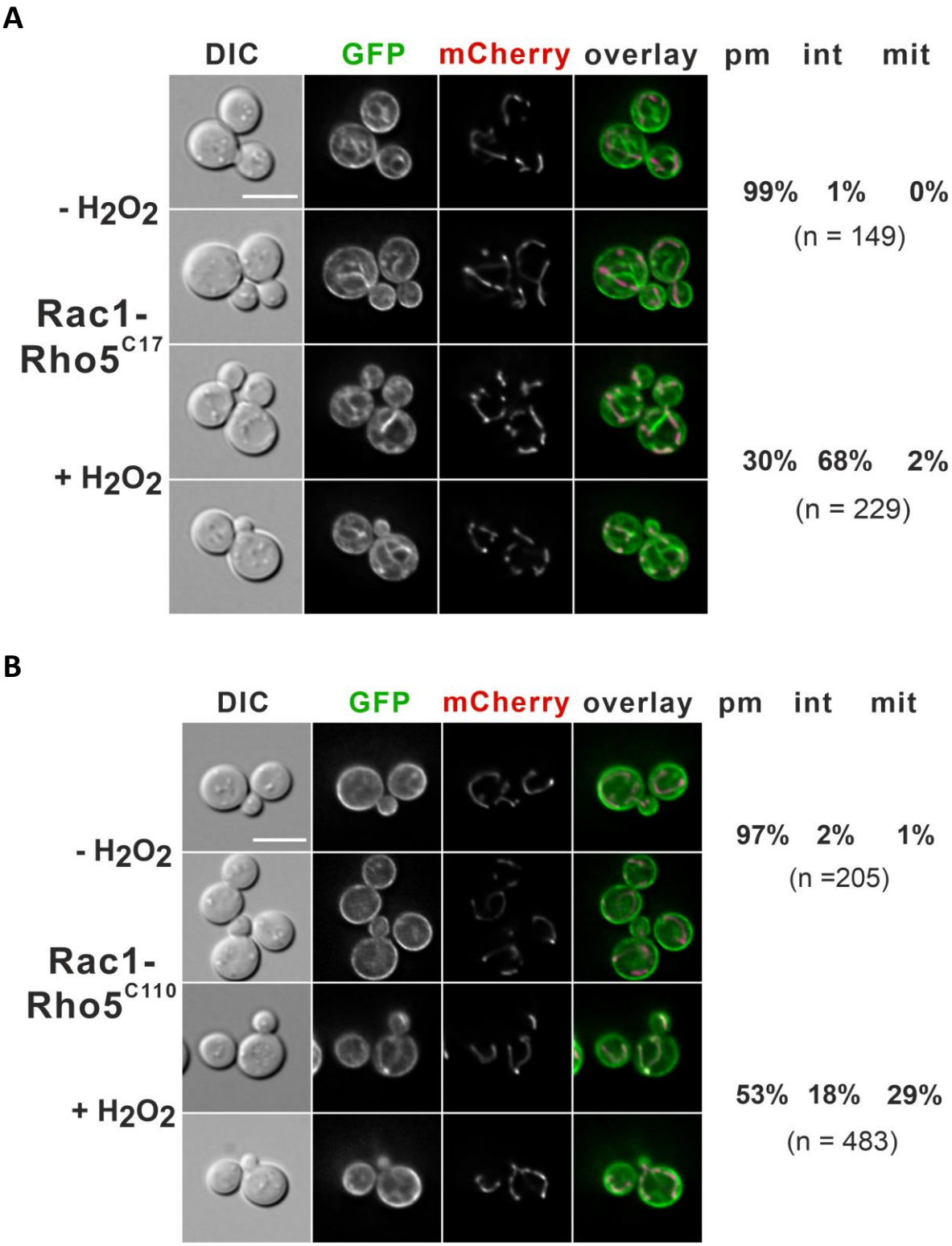

Figure 39: Localization of GFP-tagged chimeric constructs of human Rac1 Life-cell fluorescence microscopy of a *rho5* deletion strain with a mitochondrial mCherry marker (HCSO76-1A) carrying **A:** the *RAC1-RHO5*^{C17} gene with an N-terminal GFP on a *CEN/ARS* vector (pCSO100) or **B:** the *RAC1-RHO5*^{C110} gene with an N-terminal GFP on a *CEN/ARS* vector (pCSO89). Cells were grown in synthetic selective medium for plasmid maintenance to mid-logarithmic phase and examined under the fluorescence microscope. For induction of oxidative stress, the sample was exposed to 4.4 mM H_2O_2 and examined for 5 to 15 minutes post exposure. Cell counts of intracellular localization of the GFP signal are presented on the right-hand side of the microscope pictures. Co-localization of the red and green signals is highlighted by a yellow to white pseudo-colorization in the overlay. pm = plasma membrane, int = non-specific internal localization, mit = mitochondrion. Exposure brightfield: 20 ms, excitation GFP channel: 2000 ms, Rhodamine channel: 400 ms. Scale bar indicates 5 µm.

Only in 2 % of the cells the GFP signal co-localized with the mitochondrial marker (not shown). Under standard growth conditions the GFP signal of Rac1-Rho5^{C110} appeared enhanced and more evenly dispersed compared to GFP-Rac1-Rho5^{C17} (Figure 39B). Simultaneously, the association with unidentified intracellular structures was reduced which is not reflected in the cell counts because the signal's position at the plasma membrane was given priority. Treatment with 4.4 mM H_2O_2 resulted in a mild redistribution of the GFP signal so that it was associated with internal structures in 18 % of the cells while 53 % still displayed a localization at the cell membrane (Figure 39B, bottom row). Nevertheless, a striking difference between Rac1-Rho5^{C17} and Rac1-Rho5^{C110} was found in the co-localization of the GFP signal with that of the mitochondrial mCherry marker: 29 % of the H_2O_2 treated cells showed this overlap (third row), in contrast to 2 % of Rac1-Rho5^{C17}. For a better visual representation of the signal distribution, fluorescence intensity line scans were conducted using two exemplary cells of Rac1, Rac1-Rho^{C17} and Rac1-Rho^{C110}, respectively (Figure 40). The scan of GFP-Rac1 showed low intensities at the cell borders reflecting the lack of association with the plasma membrane. Higher intensities were restricted to the middle parts of the graphs representing the unidentified intracellular structures. While the diagrams of both Rac1-Rho^{C17} and Rac1-Rho^{C110} displayed peaks at the outer borders of the graph illustrating the association with the plasma membrane, the signal intensity of the intracellular structures was significantly higher in the Rac1-Rho^{C17} graph consistent with the previously described observation for the respective GFP fusion of Rac1-Rho^{C17} (Figure 39). This result is in accordance with the GFP constructs depicted in Figure 8 and Figure 9 where the extension of Rho5 conferred a distribution more similar to that of the wild type compared to only including the PBR and the CAAX motifs. In summary, a chimeric Rac1-Rho5 protein with the extended C-terminus of Rho5 was shown to be partially functional in yeast.

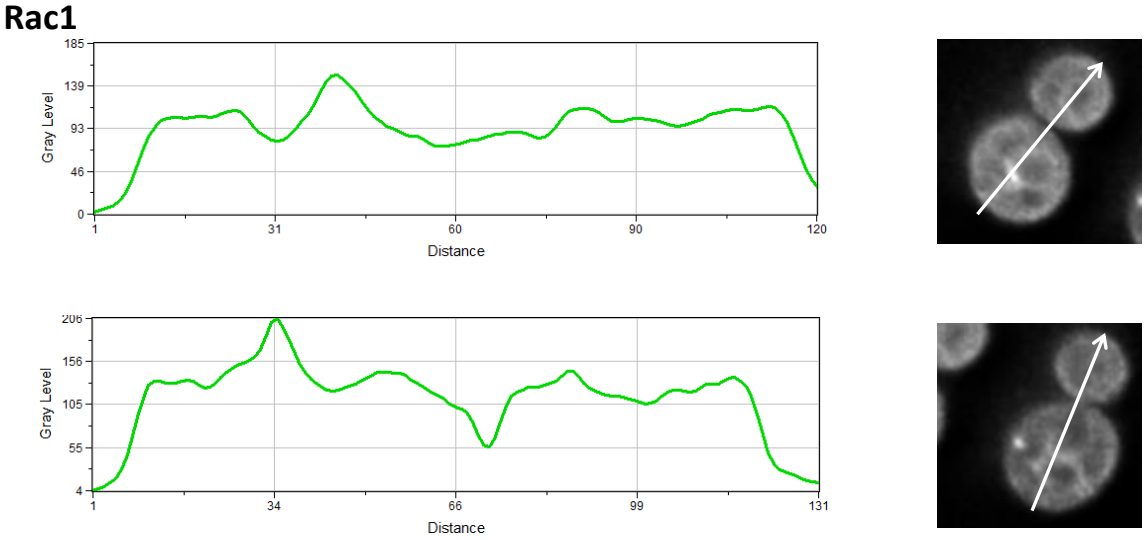

Figure 40 *Cont.*

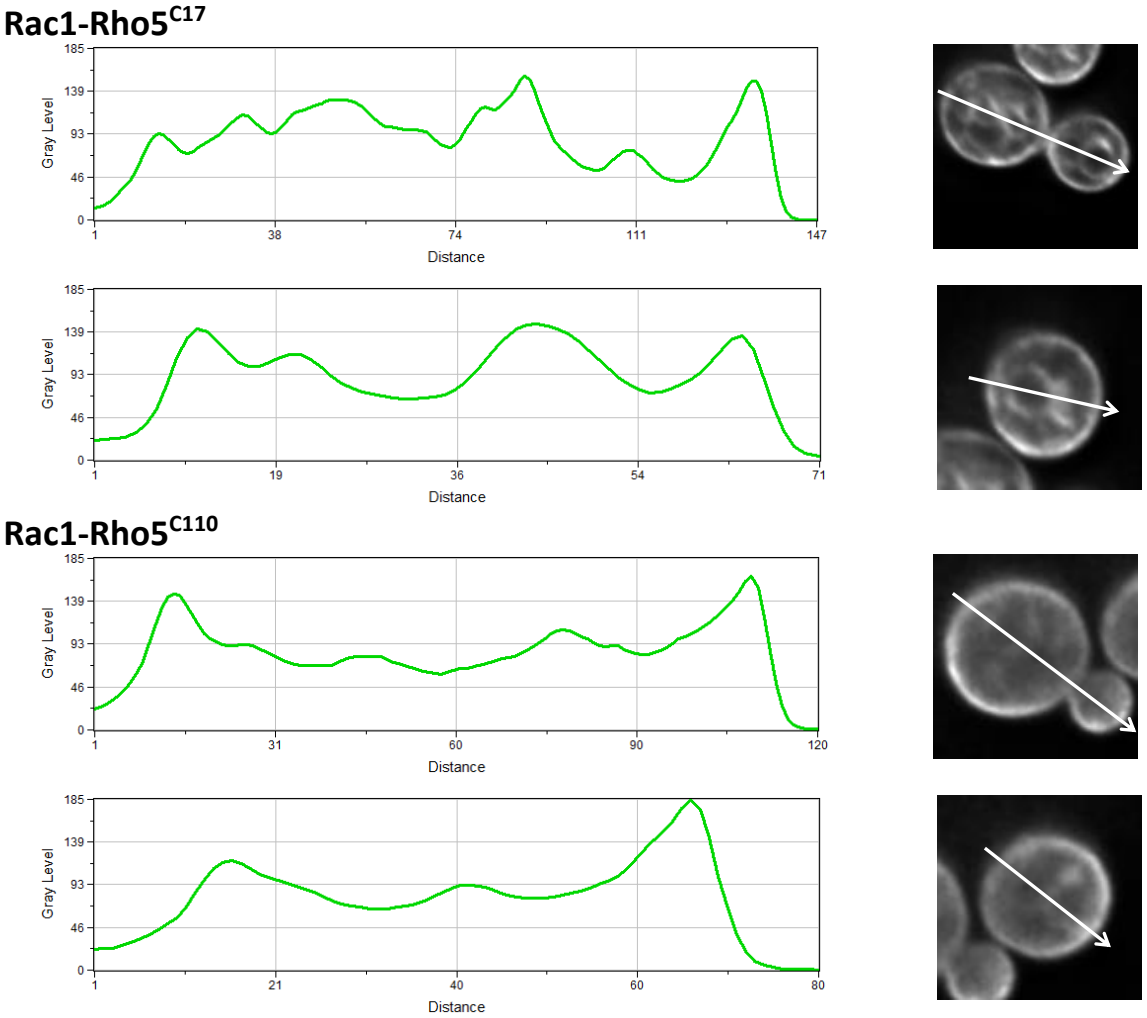

Figure 40: Exemplary fluorescence intensity line scan from Rac1 and its chimeric constructs Two exemplary cell of GFP-Rac1, GFP-Rac1-Rho5^{C17} and GFP-Rac1-Rho5^{C110} were chosen for a grey level line scan. White arrows mark the direction in the fluorescent pictures. Generated with line scan tool of Metamorph.

4. Discussion

Rho-GTPases are essential signalling molecules involved in a multitude of central cellular processes and are subjected to a complex network of regulatory mechanisms. Despite extensive studies and substantial knowledge gained over the last decades, many aspects are still unclear. Misregulation of certain Rho-GTPases, including Rac1, was shown to be the cause for a variety of diseases. This makes the investigation of the structural components that contribute to spatio-temporal regulation an important topic. The Rac1 homologue in *S. cerevisiae*, Rho5, emerged as a hub for a multitude of signalling pathways, including the cell wall integrity pathway, oxidative stress response, high osmolarity glycerol pathway, mitophagy and glucose signalling. Due to the extensive participation in such central cellular processes, Rho5 was chosen as subject for this work which aimed to elucidate physiological functions and molecular mode-of-action of this signalling protein. To do so, the first approach was to examine the differences of specific Rho5 domains and their role in oxidative stress and glucose sensing. The obtained insights were then employed to achieve a functional expression of human *RAC1* in *S. cerevisiae*. The following discussion will therefore critically evaluate the experimental setups and conclusions drawn from the results to put them in a broader context in order to expand the knowledge of monomeric GTPases from yeast to humans.

4.1 Role of Rho5's extension in signalling and cellular distribution as compared to human Rac1 in *Saccharomyces cerevisiae*

The alignment analysis of five homologous Rho-GTPases from different organisms strikingly revealed a section preceding the carboxyterminal end with a high variation in length and similarities (Figure 5). This region ranges from proline 221 to aspartate 320 in *Sc*Rho5. Since extensive search for similarities with other functional domains did not yield any homologies, the region was classified as "yeast-specific extension". The results presented in chapter 3.1.4.1 point towards a crucial participation of Rho5's extension in its function both in oxidative stress response and glucose signalling. These findings are consistent with the observation that when Rho5 is deprived of the extension it does not reach the plasma membrane, the presumed site of its activation (Figure 12). In a second approach a computational analysis of Rho5 was conducted using the MINNOU protein transmembrane domain prediction server. No specific secondary structure was assigned to the extension encompassing the residues from tryptophan 219 to asparagine 310 (Figure 41, highlighted in blue). Due to the lack of specific secondary structures this section can be classified as an intrinsically disordered region (IDR). IDRs are sections of various length in proteins characterized by a high degree of disorder thereby defying the classical "sequence determines structure determines function" paradigm (reviewed in (van der Lee et al. 2014)). This provides a reasonable explanation for the absence of similarities to other

functional domains. IDRs provide conformational plasticity and thereby increase the functional versatility of proteins which may explain Rho5's ability to regulate a multitude of pathways requiring this very flexibility (Schmitz et al. 2002, Annan et al. 2008, Singh et al. 2008, Schmitz et al. 2015). This, amongst others, is achieved by the circumstance that IDRs are frequently subjected to posttranslational modifications further contributing to the protein's complexity of states. For instance, clusters of phosphorylation tend to be found in regions of intrinsic sequence disorder (Iakoucheva et al. 2004, Collins et al. 2008, Holt et al. 2009, Tyanova et al. 2013). Large scale phosphoproteome analyses have already identified seven phosphorylation sites within the extension of Rho5 (Holt et al. 2009, Swaney et al. 2013). By employing an *in silico* analysis using the NetPhosYeast server, five additional potential sites were determined in this region (Figure 41). It is of note, that these analyses were neither performed under oxidative stress conditions nor under glucose deprivation. Since phosphorylation sites outside of the extension of Rho5 have also been determined by whole proteomic analyses (Figure 41), it is probable that the postulated code is not restricted to this region. A systematic mutational approach surveying potential phosphorylation sites in Rho5 and inspecting their impact on location and functionality would answer a lot of open questions.

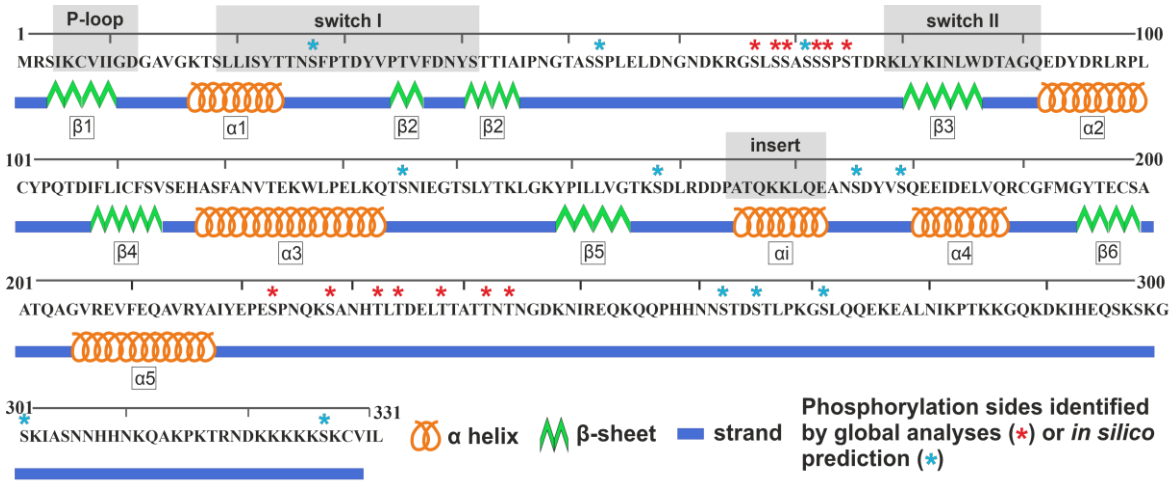

Figure 41: Prediction of Rho5's secondary structures *First row*: Annotation of functional regions, *second row*: Position marker, intervals mark ten residues; *third row*: Primary sequence, phosphorylation sites highlighted with red asterisks when identified in large scale analyses and blue asterisks mark additional *in silico* predicted phosphorylation sites; *fourth row*: Secondary structures colour coded: orange = α-helix, green = β-sheet, blue = strand; *fifth row*: Annotation of secondary structures. Prediction is based on analysis made with MINNOU server (**M**embrane protein **I**de**N**tificatio**N** with**OU**t explicit use of hydropathy profiles and alignments). Annotation of secondary structures and functional regions taken from (Schaefer et al. 2014). Phosphorylation sites identified via *in vivo* analyses were taken from (Holt et al. 2009) and (Swaney et al. 2013). Prediction of phosphorylation sites was performed on the NetPhosYeast 1.0 Server (Ingrell et al. 2007). Identified residues had a score of ≥ 0.5.

Furthermore, IDRs are prone to a higher frequency of mutations due to their lack of structural order, in contrast to the regions coding for α-helices and β-sheets (reviewed in (van der Lee et al. 2014), Figure 41). This leads to a faster evolution and subsequent sequence divergence even between homologues of closely related organisms. In this regard, Rac1 as the human Rho5 homologue is a compelling subject (Elias and Klimes 2012). Due to the Rac-GTPases' involvement in various human

diseases, there is a strong interest in Rac1 and its regulatory key associates as therapeutic targets (review in (Marei and Malliri 2017)). Importantly, Rac1 was also shown to interact *in vitro* with the catalytic DHR2 domain of yeast Dck1, a prerequisite for GEF activity which opens up the possibility to use *S. cerevisiae* as a model to study molecular interactions (Brugnera et al. 2002). However, the complementation assays performed herein revealed, that human Rac1 does neither abolish the hyper resistance of a *rho5* deletion (Figure 35) nor the synthetic lethality of the *sch9 rho5* double deletion, even when overproduced (Figure 36A). This raises the question, what causes the lack of complementation. The subcellular placement in the cytoplasm and at intracellular structures might be a hint (Figure 37), since some GTPases are activated at the plasma membrane (Bivona et al. 2006, Zhou et al. 2013, van Unen et al. 2015). Thus, the heterologously expressed Rac1 was equipped with a constitutively activating mutation to examine whether Rac1 fails to undergo nucleotide exchange. However, no complementation could be observed again neither under oxidative stress (Figure 36B) nor in the *sch9 rho5* test strain (data not shown). Hence, it is conceivable that an aberrant nucleotide exchange may not be the cause of the missing complementation and other factors may be involved. Since the C-terminal region is of major importance for Rho-GTPases (Michaelson et al. 2001, Heo et al. 2006) the HVR of Rac1 might not be sufficient for proper plasma membrane localization despite the similarity of the last amino acids (Figure 5). Although a chimeric construct replacing this section with the last 17 residues of Rho5 (Rac1-Rho5^{C17}) could not confer biological function (Figure 38B), it did improve the PM localization (Figure 39A, upper rows). This corresponds with the distribution of GFP fused to the last 17 amino acids of Rho5 confirming that Rho5's PBR in combination with the CAAX motif are indeed the origin of this positioning (Figure 8B). The tagged Rac1-Rho5^{C17} was also found at intracellular structures in a higher amount compared to Rho5 and the relocalization to mitochondria upon stress was virtually absent (Figure 39A, lower rows). It stands to reason that it requires more than these 17 residues of Rho5 to establish proper localization and function. Interestingly, Vauchelles and colleagues as well introduced human Rac1 in the opportunistic pathogenic yeast *Candida albicans* (included in alignment of Figure 5) and also found that it was unable to complement the deletion of *CaRAC1* (Vauchelles et al. 2010). A chimeric construct replacing the last 12 amino acids with the last 14 residues of *Ca*Rac1 (*Hs*Rac1-*Ca*Rac1CT) did not invoke functionality which is analogous to the results obtained from the Rac1-Rho5^{C17} construct in this work (Vauchelles et al. 2010). In the sequence alignment in Figure 5, *Ca*Rac1 shows a similar region upstream of the polybasic region lacking any explicit similarity with other homologous Rho proteins. It is tempting to assume that *Ca*Rac1's extension is also an IDR and thus has a similarly crucial significance as observed for Rho5.

To test whether functionality can be conferred by inclusion of the Rho5-specific extension, a second chimeric Rac1 variant was constructed encompassing Rho5's last 110 residues. Three major differences resulted from the expanded construct (Rac1-Rho5^{C110}) compared to Rac1-Rho5^{C17}: Firstly, the plasma

membrane location of GFP-Rac1-Rho5^{C110} was more similar to GFP-Rho5 compared to the shorter construct (Figure 39B). Secondly, expression of *RAC1-RHO5^{C110}* under the *RHO5* promoter granted a minimal complementation in growth assays (Figure 38D) which was improved by enhanced expression (Figure 38C+D). Thirdly, the microscopic inspection revealed a moderately increased relocalization to mitochondria under oxidative stress in cells expressing *RAC1-RHO5^{C110}* (Figure 39B). The information taken from the experiments in this work support the notion that Rho5's expansion plays a major role in directing the Rho protein to its subcellular destination and point towards this section as source of the versatility. Thus, it is believable that it could also mediate downstream effector binding. This was shown for *Sc*Rho4, another of the six Rho-GTPases in *S. cerevisiae*. *Sc*Rho4 possesses a unique N-terminal extension that is 69 residues longer than the one of Rho5. It was demonstrated to be important for *Sc*Rho4 functionality. Furthermore, Rho4 homologues from other fungi also harbour unusually long regions at their amino-terminal end with their respective sequence widely differing depending on the organism (Gong et al. 2013). This is a compelling similarity to the C-terminal extension of Rho5 and its homologues (Figure 5). It further emphasizes the versatility of Rho proteins even in an allegedly simple organism like *S. cerevisiae*. The identification of potential interaction partners of Rho5's extension will be an exciting objective of future studies.

4.2 GTPase activity and nutrient signalling

The physiological role of GTPases is frequently examined by employing mutations that lock the protein in an active, GTP-bound state. For Rho5, two such mutants, Q91H and G12V, have already been assessed in previous works and G12V was included in this study (Schmitz et al. 2002, Singh et al. 2008). The hypersensitive phenotype towards oxidants could be reproduced herein as was the wild type-like subcellular distribution of a GFP-tagged Rho5^{G12V} under physiological conditions (Figure 21, upper rows). However, the exposure to oxidative stress revealed a subcellular redistribution diverting from the wild type where in a larger fraction of cells the tagged Rho5 variant remained at the plasma membrane or in the cytosol (Figure 21, lower rows). This suggests a hampered membrane extraction. GTP-locked Rho-GTPases including Rac1 have previously been shown to abrogate interaction with their respective RhoGDI (Michaelson et al. 2001). In higher eukaryotes, members of this protein family normally serve as chaperones storing prenylated GTPases in the cytosol as a soluble complex and delivering it to the plasma membrane when needed (reviewed in (Garcia-Mata et al. 2011), Figure 4). However, Rho5 does not interact with *S. cerevisiae*'s only RhoGDI *Sc*Rdi1 *in vitro* (Tiedje et al. 2008). This is consistent with the observation that GFP-tagged Rho5 resides at the plasma membrane in a *Δrdi1* mutant like in the wild type and that the Rho protein was still able to relocate to mitochondria under oxidative stress (Figure 7). Consequently, one has to assume that there is an alternative, RhoGDI-independent mechanism that transports Rho5 to the plasma membrane (Figure 42e). Interestingly, in

C. albicans the cortical location of Rac1 is also not subordinated to Rdi1. Furthermore, *Ca*Rac1's shuttling to the nucleus was independent of this prenyl binding protein and the authors postulated the existence of another transport factor (Vauchelles et al. 2010). This tempts the idea that the dimeric GEF Dck1/Lmo1 mediates the extraction process of Rho5 and its mitochondrial relocalization. Accordingly, the GTP-bound Rho5 variant may interact poorly with the bipartite GEF which may ultimately obstruct the association with Rho5. This is supported by the fact that Rho5 translocation depends on the cellular presence of Dck1 as well as Lmo1 (Schmitz et al. 2015) but, as was confirmed herein, the mere GTP binding and activation of the Rho protein does not (Figure 21). The notion that Lmo1 and Dck1 may be the driving force of the relocalization process is supported by the fact that both redistribute not independent from one another but also despite the absence of Rho5 (Figure 31). Finally, the region between the DHR1 and DHR2 domain of Dock proteins is speculated to harbour armadillo (ARM) repeats (Rossman et al. 2005), α-helical hairpins that are well-suited for protein-protein interactions. They regularly occur in transport proteins as is the case in SmgGDSs that entirely compose of this structure (Peifer et al. 1994). This might also be the case for Dck1 region which enables it to engage in Rho5 transport. It is of note that relocation of Rho5 as well as $Rho5^{G12V}$ after H_2O_2

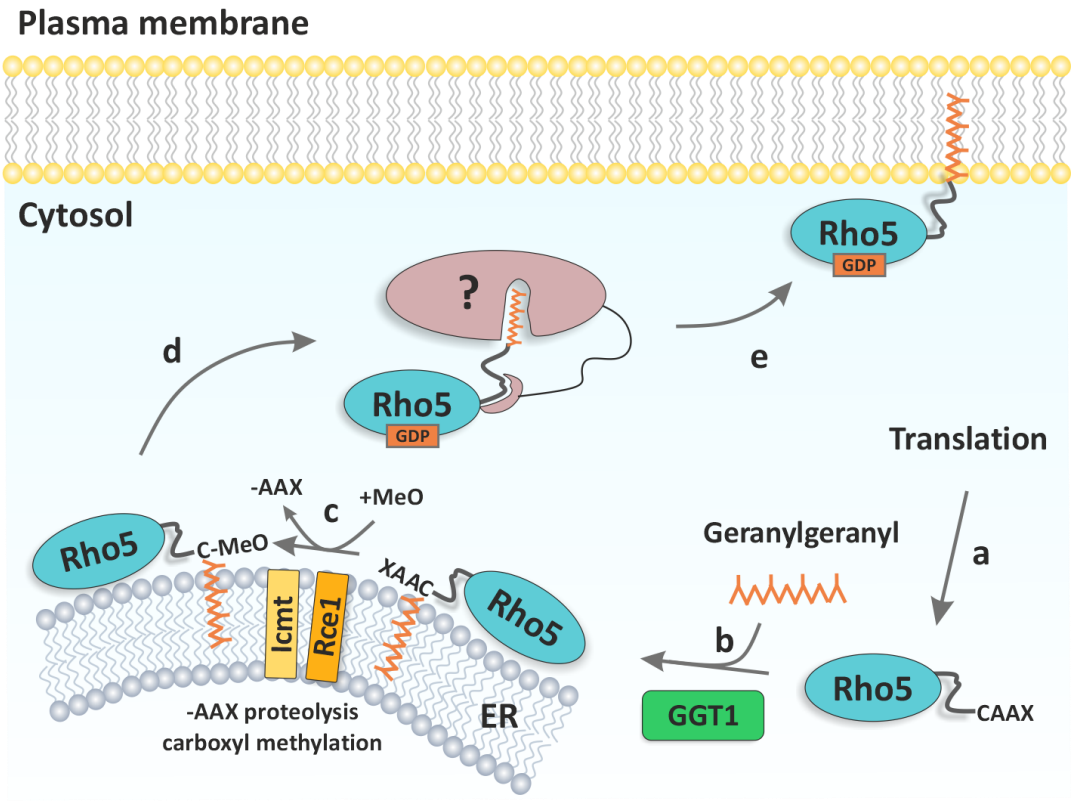

Figure 42: Schematic working model of Rho5's synthesis and relocation a - After translation, the Rho5 is released into the cytosol in an unprocessed soluble form. **b** – The native Rho-GTPase is modified by the geranylgeranyl- which adds geranylgeranyl moiety to the cysteine of the CVIL motif and is then transported to the outer leaflet of the endoplasmic reticulum (ER). **c** – On the ER surface, the two enzymes Rce1 and Icmt further process Rho5 by cleaving off the VIL tripeptide and adding a methyl group to the cysteine. **d** – An unknown chaperone recognizes Rho5's PBR, extracts the fully processed Rho5 from the ER membrane and transports it to the plasma membrane. **e** – The chaperone releases the Rho protein at the plasma membrane

treatment has also been observed in a previous study. However, the protein was detected at intracellular patches that are speculated to be endosomes rather than mitochondria (Singh et al. 2008). In order to inspect the subcellular location of Rho5, the authors replaced the residues 248 to 316 to integrate GFP. These residues however lie in the extension which was shown to be important for proper relocation herein. So, the discrepancies could be a result from an impeded signalling that disrupts the mitochondrial relocation process. In contrast to the GTP-bound Rho5, a dominant negative variant, which permanently carries a GDP, demonstrated wild-type distribution, under physiological growth and under oxidative stress except for a more frequent presence at the PM (Figure 22). Ultimately, the gathered results support the notion that the guanidine triphosphate is the cause of the altered relocalization.

In contrast to other Ras-GTPases in higher eukaryotes, the transport of *Sc*Ras2 in yeast cells to the plasma membrane turned out to be independent of the classical secretory pathway (Dong et al. 2003). Unexpectedly, it seems to depend on components of the class C Vps complex that is involved in regulating vesicle fusion (Wang and Deschenes 2006). The absence of any one of the complex subunits resulted in an accumulation of Ras2 at the mitochondrion suggesting that i) the Vps components play a role distinct of endosome and vacuole vesicle fusion and ii) mitochondria are involved in Ras trafficking (Wang and Deschenes 2006). Hence, the alternative route for Rho5's distribution could involve the class C Vps complex which could be analysed by following the subcellular distribution of GFP-Rho5 in a strain deficient for the respective component (e.g. Vps33) under various conditions. Nevertheless, one question remains: How does the reduced translocation of $Rho5^{G12V}$ fit into the hypothesis that the oxidative stress response mediated by Rho5 is exerted at the mitochondrial outer membrane? The reduced efficiency of translocation should then repeal the hypersensitivity caused by the constitutive activation. It is possible that the proportion of the GTPase that reached the mitochondrion suffices to transmit the signal as a result of the hyperactive state. A more detailed study of the redistribution dynamics, e.g. by employing FRAP analyses, could help shed some light on the situation.

The effect of a constitutively active Rho5 on glucose signalling was even more puzzling: A $RHO5^{G12V}$ allele partially reversed the inhibited growth caused by a *sch9* deletion compared to a wild-type *RHO5* strain depleted of *SCH9* (Figure 20C und D). The latter has been attributed to a larger portion of cells that enter the G_0 phase of the cell cycle (Urban et al. 2007). In order to explain this phenotype, it is helpful to have a closer look on Sch9 in yeast. Sch9 is a major target of the TOR1 complex in the signalling of nutrient availability and is inactivated under nutrient restriction. This serves to maintain cell survival by conserving resources which ultimately leads to an increased chronological lifespan (Fabrizio et al. 2001). Hence, a *Δsch9* background basically imitates an inactive Sch9. *Vice versa*, in a study originally investigating the accumulation of storage carbohydrates, a deletion of *RHO5* had a

decreased chronological lifespan indicating that Rho5 is involved in long-term survival (Cao et al. 2016). However, these findings could not be reproduced in our laboratory, even in the same genetic background of the yeast BY strain series (J. Heinisch, personal communication). Since the depletion of Rho5 and Sch9 by themselves are viable, it indicates that both components act in parallel pathways in an essential biological function, which is probably nutrient signalling (Boone et al. 2007). Glucose as the most important carbohydrate for yeast is a likely candidate.

Three main signalling pathways have been described for *S. cerevisiae* that mediate the cellular response to the presence of glucose, namely the Ras/cAMP/PKA, the Gpr1/Gpa2/cAMP and the SNF1 pathway (reviewed in (Santangelo 2006)). While mostly known for nitrogen signalling, there is accumulating evidence that Sch9 also serves a role in glucose regulated growth (Jorgensen et al. 2004, Zaman et al. 2009). Schmitz and co-workers provided evidence that Rho5 works in parallel to the Sch9 signalling (Schmitz et al. 2018). Moreover, in bimolecular fluorescence complementation (BiFC) assays Rho5 interacts with other components of the glucose metabolism including the glucose transporters Hxt1 and Hxt3 as well as the hexokinase isoenzyme Hxk2. This encourages the hypothesis that Rho5 acts as part of the intracellular section of glucose sensing ((Singh et al. 2019), Figure 1). It has been proposed that the adenylate cyclase needs to be sensitized by glucose uptake via the Ras1/2 branch before it can be fully activated by the Gpr1/Gpa2 branch (Rolland et al. 2000, Colombo et al. 2004). The synthetical sickness of a *Δrho5 Δgpr1* double deletion strain insinuates that Rho5 acts in the Ras1/2 branch and that both branches act in parallel (Boone et al. 2007). Consistent with this, a *rho5* deletion also shows a synthetic growth defect with *ras1* but not with a *ras2* deletions (Schmitz et al. 2018). Another connection point to Ras to is the fact that, similar to Rho5, Ras2-depleted cells are hyper-resistant towards cell wall stressors and Ras2 localizes to mitochondria upon apoptotic stimuli. This line of evidence backs up the notion that both GTPases may work in more than one stress response (Amigoni et al. 2013). Interestingly, GTP-locked Ras2 was also found to localize to mitochondria in yeast cells lacking the major kinase Hxk2. This is accompanied by an increase of apoptotic cells after exposure to acetic acid (Amigoni et al. 2013). Hence, the authors suggest that the mitochondrial translocation of Ras2 is triggered by an apoptotic stimulus enhanced by the absence of Hxk2 which not only suggests a connection of the two proteins but also reveals possible correlations between Ras2 and Rho5 (Schmitz et al. 2015). Cyr1 and the RasGAP Ira2 as components of the Ras/cAMP/PKA pathway were also found at the mitochondrial surface in exponentially growing yeast cells with the help of fluorescence microscopy and cellular fractionation (Belotti et al. 2012) while Ira1 co-purifies with mitochondria (Ho et al. 2002, Sickmann et al. 2003). Thus, one could assume that Rho5 utilizes mitochondria as a signalling platform which allows it to interact with respective downstream effects. This is reminiscent of K-Ras-4B interacting with the anti-apoptotic protein Bcl-X_L on the mitochondrial surface (Bivona et al. 2006). The possible involvement of Rho5 in glucose signalling would also explain

the partial suppression of the growth defect of the *sch9* deletion by the constitutively active Rho5, as it would amplify the signal output of the Ras1/2-branch on glucose activation.

As a plausible alternative Ras2 and Rho5 may also work in parallel on a common downstream target in the same signalling pathway. The fact that up to now only genetic interactions rather than a physical one has been detected favours this model. A possible converging point could be the serine/threonine kinase Rim15 as has already been proven for the longevity regulatory network controlled by Tor, Sch9, and Ras (Wei et al. 2008). If glucose is available, signalling by Sch9 and cAMP/PKA sequester Rim15 in the cytoplasm (Figure 43A). Consequently, Msn2/4, the central transcription factors which respond to general stress conditions like nutrient starvation and oxidative stress (Thevelein and de Winde 1999, Morano et al. 2012), cannot be phosphorylated and are exported from the nucleus. It is tempting to speculate that plasma membrane-associated Rho5 could play a similar role in a parallel glucose-responsive pathway, for instance in contributing to sequestration of Rim15 in the cytoplasm. The observed switch of the trimeric Rho5/Dck1/Lmo1 complex to mitochondria upon glucose starvation

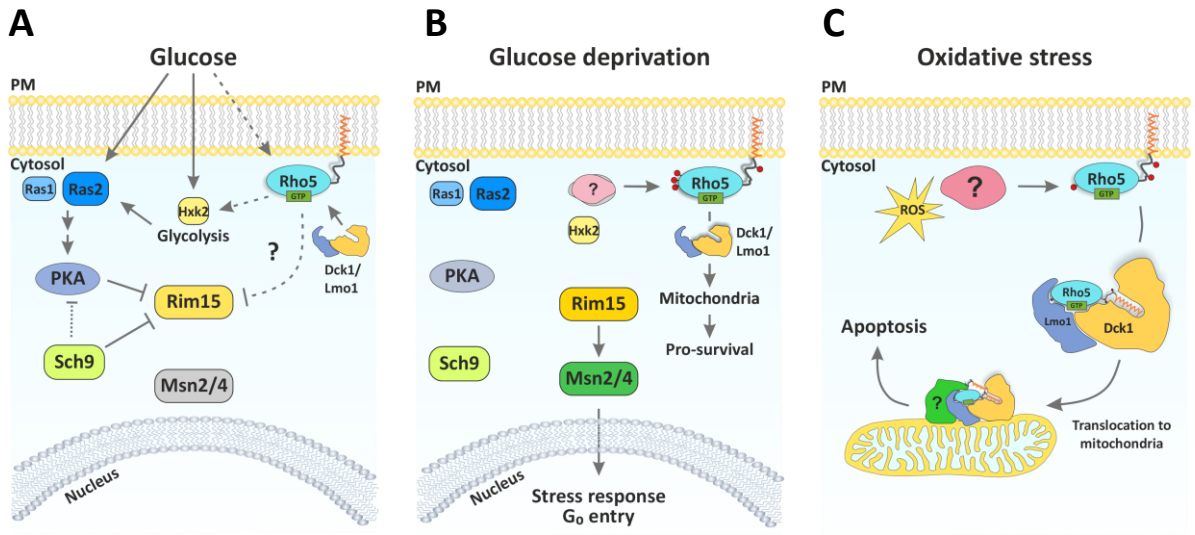

Figure 43: Schematic working model of response of Rho5 to glucose and oxidative stress A: When glucose is available, the kinase Rim15 is retained in the cytosol by PKA, Sch9 and activated, PM-bound Rho5. **B:** Under glucose deprivation, PKA and Sch9 no longer retain Rim15. Additionally, an unknown kinase phosphorylates Rho5 triggering mitochondrial relocation which also abolishes Rho5's influence on Rim15. Hence, Rim15 can transfer into the nucleus and phosphorylate Msn2/4 to induce transcriptional stress response and G_0 entry. **C:** Under oxidative stress, PM-bound Rho5 is phosphorylated by another unknown kinase at specific residues summoning the dimeric GEF Dck1/Lmo1 to extract Rho5. The trimeric complex transfers to mitochondria where Rho5 interacts with an unknown effector resulting in the induction of apoptosis.

would then relieve this regulation. As a result, Rim15 and Msn2/4 can trigger the responses to sugar depletion and other stresses (Figure 43B). That way, growth of a *sch9* deletion could be enhanced by constitutively active Rho5 because it partially compensates Sch9's Rim15 retention. While further studies are required to shed light into the exact engagement of Rho5 in the Ras/cAMP/PKA pathway, the gathered results substantiate that like Ras2, Rho5 might utilize the same components for glucose signalling as it does for the induction of apoptosis (Amigoni et al. 2013). Thus, Rho5 could be seen as a

Janus-faced molecule whose benefit or detriment for the single cell entirely depends on the physiological context. Both glucose starvation and oxidative stress trigger relocalization of Rho5 to mitochondria (Schmitz et al. 2015, Schmitz et al. 2018) which raises the question how Rho5 conveys the information of two different signals. The key structural feature to mediate the specific signal of the different conditions could be the yeast-specific extension of the Rho-GTPase discussed above. As an intrinsically disordered region it was proven to be crucial under both assessed conditions. The yeast cell might employ a signal-specific phosphorylation pattern as an encryption code. How the phosphorylation code of an IDR can have antagonistic effects was demonstrated for the protein phosphatase Cdc25. In response to DNA damage phosphorylation of one kinase prevented Cdc25-medated initiation of mitosis while phosphorylation of another kinase activated the phosphatase (reviewed in (Cohen 2000)). This does not have to rely on a single modified residue as demonstrated by the atypical Rho protein Rnd3: Only the simultaneous mutations of six potential phosphorylation sites to nonphosphorylatable residues had an impact on the protein's subcellular localization (Madigan et al. 2009). Hence, a systematic mutational approach surveying potential phosphorylation sites in Rho5 and inspecting their impact on location and functionality would answer a lot of open questions.

4.3 The CAAX motif

Ras-type GTPases employ a bipartite signal to ensure accurate spatio-temporal distribution which is vital for proper function. The signal consists of the CAAX motif and the preceding polybasic region (PBR) which will be discussed in the next chapter (Hancock et al. 1991, Michaelson et al. 2001). An exchange of the key residue cysteine 328 to leucine was employed in Rho5 to prevent the conjugation with the lipid moiety. Thus, the transition from a soluble cytoplasmic to a hydrophobic membrane-bound protein was abolished (Figure 42b) which lead to the expected intracellular distribution: As already demonstrated for other GTPases (Hancock et al. 1991, Kato et al. 1992, Roberts et al. 2008, Schmick et al. 2014), the non-prenylated Rho5 variant remained in the cytosol and was accompanied by a complete loss-of-function in the oxidative stress response and the reaction to glucose (Figure 18A to C). Intriguingly, in Rac1 from *C. albicans* a similar exchange of the cysteine of the CAAX motif to a non-prenylatable residue displays a mis-localization to the nucleus instead of the plasma membrane which also results in physiological inactivity (Vauchelles et al. 2010). In contrast to this study, Rho5^{C328L} did not show any hint of a nuclear appearance. In human cells, both *Hs*Cdc42 and *Hs*Rac1 failed to be activated by their GEF DOCK7 in their non-prenylated variants but when provided with an artificial anchor to a synthetic bilayer, robust activation of both small GTPases was restored (Zhou et al. 2013). Hence, a proper passage to the plasma membrane seems to be mandatory for this activation and the biological inactivity of Rho5^{C368L} is presumably owed to an inability to interact with its GEF Dck1/Lmo1.

Although essential for activity, the prenylation of Rho5 was, unexpectedly, not absolutely required for its interaction with mitochondria since Rho5^{C328L} still relocated under oxidative stress, although at a lower abundance (Figure 19). On the other hand, it cannot be ruled out that the mutated protein only exerts a transient contact to the organelle with a fast attachment and detachment cycle prohibiting a proper signal transduction. However, the fact that an activated Rho5^{G12V,C328L} double mutant cannot restore the function of the non-prenylatable Rho5 further points to a requirement of interaction with the dimeric GEF for efficient translocation (Figure 18D). A closer look at the dynamics of GFP-Rho5 and its mutants at the mitochondrial surface could reveal possible changes in the attachment, for example by employing FRAP analyses. Substituting Rho5's prenyl group with an alternative membrane attachment, e.g. Num1's PH domain, could give a more detailed picture of the moiety's function and answer whether the Rho-GTPase maintains its physiological activity (Tang et al. 2009).

4.4 The polybasic region

The studies on the function of Rho5's PBR conducted herein focused on two types of mutants: i) Substitution of six lysine residues to alanines (Rho5^{pbrK6A}) and ii) mutation of the serine residue 326, a putative phosphorylation site, to either a phosphomimic (Rho5^{S326E}) or a non-phosphorylatable (Rho5^{S326A}) residue, respectively. Interestingly, the Rho5 homolog *Hs*Rac1 does not possess a serine at a comparable position (Figure 5). Mutating the PBR showed that Rho5 was confined to endomembranes and the cytoplasm instead of the plasma membrane (Figure 15A). This shows striking similarities to the results from a study in *C. albicans*, where the exchange of five basic residues in the PBR of *Ca*Rac1 showed a distribution at internal membranes and in the cytoplasm rather than associating with the plasma membrane and the mutant was non-functional (Vauchelles et al. 2010). Furthermore, in a recent study in yeast the exchange of all four lysines of the *Sc*Cdc42's PBR to non-polar residues lead to a mis-localization of the GTPase to intracellular structures instead of polarized domains of the plasma membrane. The mutant *Sc*Cdc42 was non-functional which was associated with a lethal phenotype (Meca et al. 2019). Fusing GFP to the last 17 amino acids from Rho5^{pbrK6A} mutant demonstrated an identical subcellular distribution validating that the mis-localization is attributed to the perturbed sequence (Figure 15B). These observations are analogous to the results obtained from Rho5 that unambiguously underlines the significance of the PBR for Rho-GTPases in *S. cerevisiae* and other fungi. Furthermore, they support published data illustrating the PBR as conductor to target GTPases to specific subcellular membranes whose identity is defined by their charge and lipid composition (reviewed in (Casares et al. 2019)). Apparently, Ras-type proteins with a mutated PBR cannot be properly extracted from the ER surface and sequestered into the cytosol, suggesting that the mutant Rho5 is trapped at this compartment. This however could not be verified herein (Apolloni

et al. 2000, Heo et al. 2006). The nature of the transport machinery to distribute newly synthesized Rho5 to the plasma membrane has already been discussed in a previous section.

By employing different charged biosensors in human cells, Magalhaes and Glogauer were able to demonstrate that the net positive charge of the C-terminal end of Rho-GTPases is a key determinant for target membrane recognition via negatively charged phospholipids (Magalhaes and Glogauer 2010). In their work the distribution of biosensors with a net charge of +6 and +8 were situated at the plasma membrane and moderate-to-low charged constructs with +2 and +3 exclusively localized to endomembranes (Magalhaes and Glogauer 2010). While Rho5 has a net charge of +9 within the 17 C-terminal residues, the human homolog Rac1 has only +7. It is doubtful, that this difference causes the absence of plasma membrane localization of the GFP-tagged human Rac1 in yeast. Data from other fungal Rho-GTPases are also inconsistent and only give limited answers: *Sc*Rho1's PBR for instance has a net charge of +10. Exchanging five of ten lysines lead to an aberrant, diffuse distribution of the Rho protein (Hatakeyama et al. 2017) while five positive charges were sufficient for *Sc*Rho4 to properly locate to the plasma membrane (Tiedje et al. 2008). Likewise, there are inconsistencies with the extension-depleted constructs: Like *Sc*Rho4, Rho5$^{\Delta 222\text{-}319}$ carries a net charge of +5 but is still completely absent from the plasma membrane, while the chimeric Rac1-Rho5^{C17} and Rho5$^{\Delta 222\text{-}314}$ with a net charge of +8 are significantly more abundant at the cell periphery (Figure 39A and Figure 12). It is questionable if three positive charges have such an impact on subcellular distribution. Besides the charge, the difference between the constructs is the inclusion of five additional residues from the extension in Rac1-Rho5^{C17} and Rho5$^{\Delta 222\text{-}314}$. Hence, it stands to reason that these five residues are an important part of the yeast-specific extension and that the conformation of Rho5 may be significantly altered by the presence or absence of this penta-peptide. On the one hand, a systematic survey that investigates the intracellular distribution could help to uncover *S. cerevisiae*'s "charge code" for example by employing fluorescently labelled, differently charged probes, and follow their subcellular distribution. On the other hand, the inconsistency supports the notion that net charge is not the only factor determining the subcellular location of Rho proteins in *S. cerevisiae*. It is conceivable that other proteins are involved that recognize specific C-terminal regions and mediate the transfer to endomembranes similar to SmgGDS (Berg et al. 2010). Such a participation however remains speculative.

A conspicuous part of Rho5's PBR is a serine residue at the position 326 which intermits the sequence of six lysins (Figure 5, highlighted in red). A similar arrangement can be found in many GTPases like the Ras-type GTPases K-Ras4B and RalA. The serine residues of both proteins were shown to be phosphorylated triggering a relocalization from the plasma membrane to endomembranes (Bivona et al. 2006, Lim et al. 2010). The authors proposed that it is an electrostatic switch initiating the redistribution process. Inserting a negatively charged phosphate into the positively charged

environment of the PBR creates a repulsion from the likewise negatively charged phosphate head groups of the plasma membrane. This is believed to initiate the relocation process. In Rho5 however, neither the nonphosphorylatable nor the phosphomimetic mutation exerted comparable effects to the previously described examples of KRas-4B and RalA. When exposed to hydrogen peroxide, the phosphomimetic exchange showed a hyper-resistance pointing to a certain degree of malfunction (Figure 16A, bottom). The growth of the nonphosphorylatable exchange to alanine on the other hand proved to be quite unstable which is reflected in the broad error bars in the growth curves (Figure 16A, top). Also, a higher number of cells were detected with the protein still located at the cell periphery which suggests a disturbance in the detachment process from the plasma membrane. Interestingly, Rho5^{S326E} also exhibited a lower mitochondrial relocalization rate tempting the idea that this might be the reason for the mild hyper-resistance in the growth assays (Figure 17B). In any case, both results point towards an impeded relocation process. This seems paradox, because an additional negative charge was expected to weaken the attachment to the likewise negative plasma membrane due to electrostatic repulsion. It would therefore have been followed by enhanced downstream effects (Zhang et al. 2017). The contrary result obtained herein may point to a relocation model where a redistribution is triggered by a multi-side phosphorylation like in the already mentioned atypical Rho-GTPase Rnd3: The serine residue within the GTPase's PBR alone was insufficient to influence its function. Only the exchange of six potential phosphorylation sites to nonphosphorylatable residues rendered Rnd3 non-functional and the Rho protein failed to detach from the plasma membrane (Madigan et al. 2009). Hence, systematic mutational analyses of Rho5's putative phosphorylation sides could reveal the influence of phosphorylation patterns on growth and subcellular distribution. Condition-specific phosphorylations could be uncovered by homologous protein purification and subsequent mass spectrometry from yeast cells exposed to various stressors. Up to the date of this work, the only kinase known to presumably phosphorylate Rho5 is Npr1 which seems to direct the Rho-GTPase to ubiquitin-dependent proteasomal degradation (Annan et al. 2008). Therefore, the identification of the serine/threonine kinase responsible for certain phosphorylations would be highly advantageous and could be achieved by chemical stimulation of a subset of kinases as done by Madigan and colleagues.

Possibly, the serine residue 326 may not serve in Rho5's subcellular redistribution but rather influence activity, like in RhoA. When phosphorylated at a serine 188 within its PBR, RhoA's affinity to its downstream effectors ROK was reduced whereas unphosphorylated GTP-RhoA normally associated with the kinase (Nusser et al. 2006). This overwriting of the activation status by phosphorylation was proposed as a novel secondary switch. Hence, phosphorylation of Rho5's serine 326 may not serve as initiator for the redistribution but rather influence the affinity to the given binding partner resulting in reduced function. Conclusively, the non-phosphorylated state may represent the status quo which

explains why the nonphosphorylatable exchange does not exhibit a clear phenotype. Nevertheless, the reason for the altered subcellular distribution of both variants remains puzzling.

Despite the functional aberration of Rho5^{pbrK6A}, mitochondrial localization and activity still occurred (Figure 15) which raises the question by which mechanism this is done. As previously discussed, Rho5 needs to be associated with the plasma membrane to be activated and properly translocated to the mitochondrion. A microscopic time lapse conducted in the work of Schmitz and co-workers revealed that after exposure to hydrogen peroxide GFP-tagged Rho5 at first translocates to mitochondrial sections close to the cell surface (Schmitz et al. 2015). This encourages the hypothesis that contact sides play a role in the rapid relocation since they mediate general diffusional exchange of proteins and lipids between compartments (Phuyal and Farhan 2019). In a deletion mutant depleted of Num1, a component of a tethering complex attaching mitochondria to the plasma membrane (Klecker et al. 2013), GFP-Rho5 demonstrated wild-type relocalization to mitochondria under oxidative stress arguing against the necessity of a membrane contact side (data not shown). An alternative mechanism for the subcellular redistribution of Rho5 may be provided by the work of Silvius and colleagues: The authors employed a rapamycin-induced relocation of different chimeric lipid-modified proteins to mitochondria in order to investigate the dynamics of prenylated proteins. The triggered intercompartmental transfer of a KRas-4B construct was therein speculated to travel through the cytoplasm by diffusion rather than by a controlled chaperone-mediated transport. The authors argue that no transport of membrane proteins is known between the plasma membrane and mitochondria (Silvius et al. 2006). Accordingly, the relocalization of Rho5 initially occurring at the cellular cortex would merely stem from the physical proximity of the tethered mitochondria to the plasma membrane where the GTPase detaches from (Schmitz et al. 2015). Notwithstanding, this does not provide an adequate solution of how the lipid moiety is concealed from the hydrophilic environment. No matter the underlying transport machinery, the question remains how the activation of Rho5^{pbrK6A} takes place, since both components of the bipartite GEF Dck1/Lmo1 are found at the plasma membrane. Determining the nucleotide binding status of the PBR mutant would provide an answer in this matter.

4.5 *In vivo* trapping of Rho5, Dck1 and Lmo1

As with many classical Rho-GTPases, Rho5 normally resides at the plasma membrane under physiological conditions where the interaction with GEFs is believed to take place (Roberts et al. 2008). Hence, not reaching the plasma membrane abrogates the interaction with the respective exchange factors and prevents activation of the Rho proteins (Zhou et al. 2013). Members of the Dock family of GEFs were shown to be specifically recruited to membranes enriched in certain phosphatidylinositols promoting the local attachment of the Dock/ELMO complex and facilitating locally restricted Rac1 activity (Premkumar et al. 2010). A first clear hint that this may also hold true for Rho5 was revealed

by the severely impeded function of the mislocalized Rho5^{pbrK6A}. As subsequently shown in chapter 3.2.3, *in vivo* trapping of GFP-Rho5 succeeded to abrogate proper reaction to H_2O_2 exposure which may be attributed to an obstructed apoptotic induction. One can conclude this as a consequence of Rho5´s removal from the plasma membrane so it cannot interact with and be activated by its putative GEF Dck1/Lmo1, ultimately preventing the transmission of signals to downstream effectors. It is also conceivable that GFP-Rho5 may be trapped prior to its prenylation, directly after its translation (Figure 42a). In this scenario, the premature GTPase would exist in an inactive state that is non-functional, as was the case in the trapping experiment. This suspicion however is unlikely, as *in vivo* trapping of the constitutively active mutant of GFP-Rho5^{G12V} reinstated wild-type growth but only if it is able to be prenylated (Figure 18). The gathered information further supports the notion that wild-type Rho5 needs to be associated with the plasma membrane prior to mitochondrial translocation in order to gain a GTP-bound state (Figure 42B). Additionally, at least a part of Rho5's signalling is destined for the mitochondrial surface as proven by the PBR mutant, where signal transduction from any other membrane is severely impeded. Alternatively, *in vivo* trapping of Rho5 may avert the interaction of Rho5 with the reductase Trr1 which occurs at endocytic and vacuolar membranes (Singh et al. 2008). The authors postulated that Rho5 inhibits Trr1's reduction of the thioredoxin system, namely Trx1, ultimately causing an accumulation of reactive oxygen species (ROS). Trapping Rho5 at the mitochondrion could therefore prevent interaction of the Rho protein and Trr1 thereby abrogating downstream effects. As already proposed by the authors, the inhibition of Trr1 is likely just one signalling target of Rho5. In a recent genome wide screen, the autophagy related protein Atg21 was identified as another interaction partner and putative downstream effector suggesting an overlap of components of the autophagy machinery to promote apoptosis (Singh et al. 2019).

As a follow up study, the *in vivo* trapping of the GEF subunit Dck1 confirmed that the triple-GFP tagged variant by itself exhibited a hypersensitivity towards oxidative stress that has previously been observed for other stressors ((Schmitz et al. 2015), Figure 30A). The cause of this phenotype may be found in a perturbation of Dck1's autoinhibitory intramolecular folding where under non-stimulated circumstances the N-terminal SH3 domain of DOCK proteins masks and thereby inhibits the C-terminal DHR2 (or "docker") domain ((Cote and Vuori 2002, Lu et al. 2005), Figure 3). Thus, the triple-GFP tag of Dck1 may cause a more frequent opening confirmation of Dck1 with an increased activation of downstream effectors. Notwithstanding, the effect of the *in vivo* trapping becomes all the more obvious with the abrogation of the sensitivity towards hydrogen peroxide exposure (Figure 30A). As an appropriate follow-up experiment, the *in vivo* trapping of Lmo1 was conducted. Unfortunately, the likewise triple-GFP tagged Lmo1 exhibited a hyper-resistance similar to the *Δlmo1* strain and consequently a loss-of-function could not be proven (Figure 30B). To overcome this obstacle, the

future assignment will be the integration of a single GFP tagged Lmo1 which was shown to be functional by Schmitz and colleagues.

Under physiological conditions, Dck1 and Lmo1 are mainly located in punctate foci near the yeast cell periphery while Rho5 resides evenly distributed at the plasma membrane ((Schmitz et al. 2015), Figure 29). All three components are efficiently redistributed to mitochondria by the GFP-binder when tagged adequately. Combining the findings from the *in vivo* trapping of Rho5 with the ones from the Dck1-trapping once more support the hypothesis that Rho5 has to reach the plasma membrane to be activated. Thus, the current working model of mitochondrial translocation includes a two-step process in which only after a signal-specific phosphorylation the bipartite GEF Dck1/Lmo1 interacts and redistributes Rho5 so it can fulfil its role in the oxidative stress response (Figure 43C). A portion of microscopically inspected cells from the Dck1-trapping showed high-intensity puncta along the cell periphery that were neither observed in the Rho5- nor the Lmo1-trapping (Figure 29A, white arrows). They may be attributed to contact sides of the alleged mitochondria with the periphery. One could assume that the GB accumulates Dck1 in the cellular perimeters resulting in a considerably brighter signal compared to the one solely expressing GFP-tagged Dck1 (Figure 29A, bottom row). Accordingly, this accumulation seems to impede Dck1's alleged nucleotide exchange of Rho5 causing the hyper-resistance. It is of note that the complementary approach to retain GFP-Rho5 at the plasma membrane via GB has failed so far. Both GB-constructs consisting of the plasma membrane ATPase Pma1 (personal communication Wedlich-Söldner) as well as an attachment to the CWI sensor Mid2 (Kock et al. 2015), did not properly prevent the translocation of the tagged Rho protein to mitochondria when cells were exposed to hydrogen peroxide. Due to time limitations, the mitochondrial trapping of Rho5 and the dimeric GEF in glucose signalling, e.g. by assessing the complementation of the synthetic lethality of the *sch9 rho5* double deletion, could not be assessed.

4.6 Interaction of Rho5 with the VDAC Por1

As discussed above the mitochondrial surface serves as a major interaction platform and connects many different signalling pathways (Tait and Green 2012). So, it seems plausible that Rho5 changes its membrane location to engage in a specific protein-protein interaction mediated by the mitochondrial surface. A prominent protein of the mitochondrial outer membrane is Por1. The baker's yeast homologue of VDAC1 ("voltage dependant anion channel") has diverse functions including the exchange of small molecules like adenine nucleotides with the surrounding cytoplasm. Furthermore, Por1 also seems to function as an anti-apoptotic factor in the response to oxidants and acetic acid (Guaragnella et al. 2012). Due to the functional coincidence, a potential connection with Rho5 signalling was investigated herein. As the first step, epistatic analyses were conducted using comparative growth assays. The partial repression of the hypersensitivity of the *por1* deletion by the

additional depletion of Rho5 suggests a genetic interaction between the two components. This notion is supported by further studies, where a constitutively active Rho5, in contrast to the wild type, caused strongly reduced growth in a *rho5 por1* deletion background, even in the absence of a stressor (Figure 33). There are several ways to explain the genetic interaction at a physiological level: One is a physical protein-protein interaction between Por1 and Rho5 after the Rho5's translocation to mitochondria overcoming the spatial separation. Since Por1 is seen as a pro-survival regulator of stress-induced apoptosis, it is tempting to speculate that it directly blocks Rho5 from passing a "death signal" to its downstream effectors. In this scenario the absence of Por1 would allow Rho5 to transmit the hazardous signal unrestrictedly and thus explain the profound increase of apoptotic markers and hypersensitivity of a *por1* deletion strain when exposed to stressors (Pereira et al. 2007). Although Por1 seems to be needed for maintaining the cytosol redox state as part of the oxidant defence (Galganska et al. 2010) and Rho5 is proposed to inhibit Trr1 to promote ROS accumulation (Singh et al. 2008), a reasonable hypothesis cannot be drawn from the results obtained herein. A second explanation for the observed genetic interaction would require the inclusion of additional components downstream of Rho5 that would engage in the crosstalk of the Rho5 and Por1. Promising downstream candidates were identified as interaction partners in a recent genome wide study screening for Rho5 interaction partners, two of which are the AAA-ATPase Msp1 and the translocator Tom70. Both proteins reside at the mitochondrion and are proposed as a target of H_2O_2-activated Rho5 (Singh et al. 2019). The respective deletion mutants are currently investigated to determine whether relocation of GFP-Rho5 still occurs under oxidative stress. Finally, as the third possibility Rho5 and Por1 are not directly linked at all. The genetic interaction would therefore be the result of the profound physiological perturbations caused by a depletion of Por1 resulting in reduced mitochondrial outer membrane permeability, health and activity which makes the cell more prone to undergo apoptosis (Pereira et al. 2007, Magri et al. 2016). In the *rho5 por1* double deletion on the other hand, apoptosis cannot be exerted properly due to a lack in Rho5. Hence, the quantification of apoptotic markers in the double deletion compared to the single deletions would be a logical step in future studies to unveil this interesting connection.

5. Summary

Rho-GTPases are essential signalling proteins which regulate a multitude of central cellular processes that are vital for organisms to thrive and adapt to changing environments. Many regulatory networks involving Rho proteins have first been elucidated in the model yeast *Saccharomyces cerevisiae*, in which Rho5 emerges as a central hub connecting different signalling pathways, such as the responses to cell wall stress, high medium osmolarity, and oxidative stress. In this work, the rapid translocation of Rho5 to mitochondria as reaction to oxidants and glucose starvation was thoroughly investigated. The studies on structure-function relationships was focussed on the C-terminal region of the Rho5 which in other Rho-type GTPases determines their spatio-temporal distribution and contributes to their physiological function. The C-terminal end of these GTPases is considered to be a hypervariable region (HPR) that consists of a polybasic region (PBR) and its preceding amino acid residues, followed by the CAAX motif which becomes prenylated at its cysteine residue. These motifs are conserved in the yeast Rho5 where the PBR contains a serine residue as a putative phosphorylation target. Moreover, Rho5 of *S. cerevisiae* is characterized by an extension preceding the PBR that comprises 98 amino acid residues. While substitutions of the serine residue within the PBR for either phosphomimetic or non-phosphorylatable residues indicate that it is of minor physiological importance, deletion analyses of the yeast-specific extension showed that it is required for proper localization of Rho5 to the plasma membrane. As expected, substitution of the cysteine residue within the CAAX motif also prevented proper plasma membrane localization, accompanied by a loss of function both with respect to oxidative stress response and glucose starvation. Results from studies employing a trapping-device of GFP-Rho5 to the mitochondrial surface indicate that the GTPase needs to be activated at the plasma membrane by its dimeric GDP/GTP exchange factor (GEF) which is composed of Dck1 and Lmo1, in response to stress conditions. The trimeric DLR complex is then capable of rapidly translocate to mitochondria and fulfil its functions at the organelle. This view was supported by the finding that a constitutively active Rho5 variant restored function when trapped to mitochondria. Interestingly, Rho5 requires the dimeric GEF for the translocation process under oxidative stress while Dck1 and Lmo1 can reach the mitochondria independent from each other. Finally, the human Rho5 homolog Rac1 cannot complement the defects of a *rho5* deletion and does not show a proper intracellular distribution, unless its C-terminal end is equipped with the yeast-specific extension. Taken together, the results of this thesis contributed to a better understanding of the structure-function relationships of Rho5 and its human homolog Rac1.

6. References

Abo, A., M. R. Webb, A. Grogan and A. W. Segal (1994). "Activation of NADPH oxidase involves the dissociation of p21rac from its inhibitory GDP/GTP exchange protein (rhoGDI) followed by its translocation to the plasma membrane." *Biochem J* **298 Pt 3**: 585-591.

Adamo, J. E., G. Rossi and P. Brennwald (1999). "The Rho GTPase Rho3 has a direct role in exocytosis that is distinct from its role in actin polarity." *Molecular Biology of the Cell* **10**(12): 4121-4133.

Alan, J. K. and E. A. Lundquist (2013). "Mutationally activated Rho GTPases in cancer." *Small GTPases* **4**(3): 159-163.

Amigoni, L., E. Martegani and S. Colombo (2013). "Lack of HXK2 induces localization of active Ras in mitochondria and triggers apoptosis in the yeast Saccharomyces cerevisiae." *Oxid Med Cell Longev* **2013**: 678473.

Amin, E., M. Jaiswal, U. Derewenda, K. Reis, K. Nouri, K. T. Koessmeier, P. Aspenstrom, et al. (2016). "Deciphering the Molecular and Functional Basis of RHOGAP Family Proteins: A SYSTEMATIC APPROACH TOWARD SELECTIVE INACTIVATION OF RHO FAMILY PROTEINS." *J Biol Chem* **291**(39): 20353-20371.

Annan, R. B., C. Wu, D. D. Waller, M. Whiteway and D. Y. Thomas (2008). "Rho5p is involved in mediating the osmotic stress response in Saccharomyces cerevisiae, and its activity is regulated via Msi1p and Npr1p by phosphorylation and ubiquitination." *Eukaryot Cell* **7**(9): 1441-1449.

Apolloni, A., I. A. Prior, M. Lindsay, R. G. Parton and J. F. Hancock (2000). "H-ras but not K-ras traffics to the plasma membrane through the exocytic pathway." *Mol Cell Biol* **20**(7): 2475-2487.

Arvanitidis, A. and J. J. Heinisch (1994). "Studies on the Function of Yeast Phospofructokinase Subunits by in-Vitro Mutagenesis." *Journal of Biological Chemistry* **269**(12): 8911-8918.

Ashby, M. N. (1998). "CaaX converting enzymes." *Curr Opin Lipidol* **9**(2): 99-102.

Aspenstrom, P. (2018). "Activated Rho GTPases in Cancer-The Beginning of a New Paradigm." *International Journal of Molecular Sciences* **19**(12).

Belotti, F., R. Tisi, C. Paiardi, M. Rigamonti, S. Groppi and E. Martegani (2012). "Localization of Ras signaling complex in budding yeast." *Biochim Biophys Acta* **1823**(7): 1208-1216.

Berg, T. J., A. J. Gastonguay, E. L. Lorimer, J. R. Kuhnmuench, R. Li, A. P. Fields and C. L. Williams (2010). "Splice variants of SmgGDS control small GTPase prenylation and membrane localization." *J Biol Chem* **285**(46): 35255-35266.

Bivona, T. G., S. E. Quatela, B. O. Bodemann, I. M. Ahearn, M. J. Soskis, A. Mor, J. Miura, et al. (2006). "PKC regulates a farnesyl-electrostatic switch on K-Ras that promotes its association with Bcl-XL on mitochondria and induces apoptosis." *Mol Cell* **21**(4): 481-493.

Boguski, M. S. and F. McCormick (1993). "Proteins regulating Ras and its relatives." *Nature* **366**(6456): 643-654.

Boivin, D. and R. Beliveau (1995). "Subcellular distribution and membrane association of Rho-related small GTP-binding proteins in kidney cortex." *Am J Physiol* **269**(2 Pt 2): F180-189.

Boone, C., H. Bussey and B. J. Andrews (2007). "Exploring genetic interactions and networks with yeast." *Nat Rev Genet* **8**(6): 437-449.

Boulter, E., R. Garcia-Mata, C. Guilluy, A. Dubash, G. Rossi, P. J. Brennwald and K. Burridge (2010). "Regulation of Rho GTPase crosstalk, degradation and activity by RhoGDI1." *Nat Cell Biol* **12**(5): 477-483.

Brugnera, E., L. Haney, C. Grimsley, M. Lu, S. F. Walk, A. C. Tosello-Trampont, I. G. Macara, et al. (2002). "Unconventional Rac-GEF activity is mediated through the Dock180-ELMO complex." *Nat Cell Biol* **4**(8): 574-582.

Brzostowski, J. A., P. Fey, J. Yan, N. Isik and T. Jin (2009). "The Elmo family forms an ancient group of actin-regulating proteins." *Commun Integr Biol* **2**(4): 337-340.

Buck, L. and R. Axel (1991). "A novel multigene family may encode odorant receptors: a molecular basis for odor recognition." *Cell* **65**(1): 175-187.

Bustelo, X. R., V. Sauzeau and I. M. Berenjeno (2007). "GTP-binding proteins of the Rho/Rac family: regulation, effectors and functions in vivo." *Bioessays* **29**(4): 356-370.

Busto, J. V., A. Elting, D. Haase, F. Spira, J. Kuhlman, M. Schafer-Herte and R. Wedlich-Soldner (2018). "Lateral plasma membrane compartmentalization links protein function and turnover." *EMBO J* **37**(16).

Butty, A. C., N. Perrinjaquet, A. Petit, M. Jaquenoud, J. E. Segall, K. Hofmann, C. Zwahlen, et al. (2002). "A positive feedback loop stabilizes the guanine-nucleotide exchange factor Cdc24 at sites of polarization." *Embo Journal* **21**(7): 1565-1576.

Cao, L., Y. Tang, Z. Quan, Z. Zhang, S. G. Oliver and N. Zhang (2016). "Chronological Lifespan in Yeast Is Dependent on the Accumulation of Storage Carbohydrates Mediated by Yak1, Mck1 and Rim15 Kinases." *PLoS Genet* **12**(12): e1006458.

Casares, D., P. V. Escriba and C. A. Rossello (2019). "Membrane Lipid Composition: Effect on Membrane and Organelle Structure, Function and Compartmentalization and Therapeutic Avenues." *Int J Mol Sci* **20**(9).

Chhatriwala, M. K., L. Betts, D. K. Worthylake and J. Sondek (2007). "The DH and PH domains of Trio coordinately engage Rho GTPases for their efficient activation." *J Mol Biol* **368**(5): 1307-1320.

Choy, E., V. K. Chiu, J. Silletti, M. Feoktistov, T. Morimoto, D. Michaelson, I. E. Ivanov, et al. (1999). "Endomembrane trafficking of ras: the CAAX motif targets proteins to the ER and Golgi." *Cell* **98**(1): 69-80.

Chuang, T. H., B. P. Bohl and G. M. Bokoch (1993). "Biologically active lipids are regulators of Rac.GDI complexation." *J Biol Chem* **268**(35): 26206-26211.

Clarke, S. (1992). "Protein isoprenylation and methylation at carboxyl-terminal cysteine residues." *Annu Rev Biochem* **61**: 355-386.

Cohen, P. (2000). "The regulation of protein function by multisite phosphorylation--a 25 year update." *Trends Biochem Sci* **25**(12): 596-601.

Collins, M. O., L. Yu, I. Campuzano, S. G. Grant and J. S. Choudhary (2008). "Phosphoproteomic analysis of the mouse brain cytosol reveals a predominance of protein phosphorylation in regions of intrinsic sequence disorder." *Mol Cell Proteomics* **7**(7): 1331-1348.

Colombo, S., D. Ronchetti, J. M. Thevelein, J. Winderickx and E. Martegani (2004). "Activation state of the Ras2 protein and glucose-induced signaling in Saccharomyces cerevisiae." *J Biol Chem* **279**(45): 46715-46722.

Cote, J. F., A. B. Motoyama, J. A. Bush and K. Vuori (2005). "A novel and evolutionarily conserved PtdIns(3,4,5)P3-binding domain is necessary for DOCK180 signalling." *Nat Cell Biol* **7**(8): 797-807.

Cote, J. F. and K. Vuori (2002). "Identification of an evolutionarily conserved superfamily of DOCK180-related proteins with guanine nucleotide exchange activity." *J Cell Sci* **115**(Pt 24): 4901-4913.

Cote, J. F. and K. Vuori (2007). "GEF what? Dock180 and related proteins help Rac to polarize cells in new ways." *Trends Cell Biol* **17**(8): 383-393.

Crechet, J. B., E. Jacquet, A. Bernardi and A. Parmeggiani (2000). "Analysis of the role of the hypervariable region of yeast Ras2p and its farnesylation in the interaction with exchange factors and adenylyl cyclase." *J Biol Chem* **275**(23): 17754-17761.

DerMardirossian, C. and G. M. Bokoch (2005). "GDIs: central regulatory molecules in Rho GTPase activation." *Trends Cell Biol* **15**(7): 356-363.

DerMardirossian, C., A. Schnelzer and G. M. Bokoch (2004). "Phosphorylation of RhoGDI by Pak1 mediates dissociation of Rac GTPase." *Mol Cell* **15**(1): 117-127.

Dong, X., D. A. Mitchell, S. Lobo, L. Zhao, D. J. Bartels and R. J. Deschenes (2003). "Palmitoylation and plasma membrane localization of Ras2p by a nonclassical trafficking pathway in Saccharomyces cerevisiae." *Mol Cell Biol* **23**(18): 6574-6584.

Elias, M. and V. Klimes (2012). "Rho GTPases: deciphering the evolutionary history of a complex protein family." *Methods Mol Biol* **827**: 13-34.

Estravis, M., S. A. Rincon, E. Portales, P. Perez and B. Santos (2017). "Cdc42 activation state affects its localization and protein levels in fission yeast." *Microbiology* **163**(8): 1156-1166.

Fabrizio, P., F. Pozza, S. D. Pletcher, C. M. Gendron and V. D. Longo (2001). "Regulation of longevity and stress resistance by Sch9 in yeast." *Science* **292**(5515): 288-290.

Fairn, G. D. and S. Grinstein (2012). "Cell biology. Precursor or charge supplier?" *Science* **337**(6095): 653-654.

Fairn, G. D., M. Hermansson, P. Somerharju and S. Grinstein (2011). "Phosphatidylserine is polarized and required for proper Cdc42 localization and for development of cell polarity." *Nat Cell Biol* **13**(12): 1424-1430.

Feig, L. A. (1999). "Tools of the trade: use of dominant-inhibitory mutants of Ras-family GTPases." *Nat Cell Biol* **1**(2): E25-27.

Feltham, J. L., V. Dotsch, S. Raza, D. Manor, R. A. Cerione, M. J. Sutcliffe, G. Wagner, et al. (1997). "Definition of the switch surface in the solution structure of Cdc42Hs." *Biochemistry* **36**(29): 8755-8766.

Filippi, M. D., C. E. Harris, J. Meller, Y. Gu, Y. Zheng and D. A. Williams (2004). "Localization of Rac2 via the C terminus and aspartic acid 150 specifies superoxide generation, actin polarity and chemotaxis in neutrophils." *Nat Immunol* **5**(7): 744-751.

Fleming, I. N., C. M. Elliott and J. H. Exton (1996). "Differential translocation of rho family GTPases by lysophosphatidic acid, endothelin-1, and platelet-derived growth factor." *J Biol Chem* **271**(51): 33067-33073.

Forget, M. A., R. R. Desrosiers, D. Gingras and R. Beliveau (2002). "Phosphorylation states of Cdc42 and RhoA regulate their interactions with Rho GDP dissociation inhibitor and their extraction from biological membranes." *Biochem J* **361**(Pt 2): 243-254.

Freeman, J. L., A. Abo and J. D. Lambeth (1996). "Rac ''insert region'' is a novel effector region that is implicated in the activation of NADPH oxidase, but not PAK65." *Journal of Biological Chemistry* **271**(33): 19794-19801.

Galganska, H., A. Karachitos, M. Baranek, M. Budzinska, J. Jordan and H. Kmita (2010). "Viability of Saccharomyces cerevisiae cells following exposure to H2O2 and protective effect of minocycline depend on the presence of VDAC." *Eur J Pharmacol* **643**(1): 42-47.

Garcia-Mata, R., E. Boulter and K. Burridge (2011). "The 'invisible hand': regulation of RHO GTPases by RHOGDIs." *Nat Rev Mol Cell Biol* **12**(8): 493-504.

Gietz, R. D. and R. H. Schiestl (2007). "Frozen competent yeast cells that can be transformed with high efficiency using the LiAc/SS carrier DNA/PEG method." *Nature Protocols* **2**(1): 1-4.

Gietz, R. D., R. H. Schiestl, A. R. Willems and R. A. Woods (1995). "Studies on the transformation of intact yeast cells by the LiAc/SS-DNA/PEG procedure." *Yeast* **11**(4): 355-360.

Gietz, R. D. and A. Sugino (1988). "New Yeast-Escherichia-Coli Shuttle Vectors Constructed with Invitro Mutagenized Yeast Genes Lacking 6-Base Pair Restriction Sites." *Gene* **74**(2): 527-534.

Gong, T., Y. Liao, F. He, Y. Yang, D. D. Yang, X. D. Chen and X. D. Gao (2013). "Control of polarized growth by the Rho family GTPase Rho4 in budding yeast: requirement of the N-terminal extension of Rho4 and regulation by the Rho GTPase-activating protein Bem2." *Eukaryot Cell* **12**(2): 368-377.

Grimsley, C. M., J. M. Kinchen, A. C. Tosello-Trampont, E. Brugnera, L. B. Haney, M. Lu, Q. Chen, et al. (2004). "Dock180 and ELMO1 proteins cooperate to promote evolutionarily conserved Rac-dependent cell migration." *J Biol Chem* **279**(7): 6087-6097.

Guaragnella, N., M. Zdralevic, L. Antonacci, S. Passarella, E. Marra and S. Giannattasio (2012). "The role of mitochondria in yeast programmed cell death." *Front Oncol* **2**: 70.

Hanahan, D. (1983). "Studies on transformation of Escherichia coli with plasmids." *J Mol Biol* **166**(4): 557-580.

Hancock, J. F., K. Cadwallader, H. Paterson and C. J. Marshall (1991). "A CAAX or a CAAL motif and a second signal are sufficient for plasma membrane targeting of ras proteins." *EMBO J* **10**(13): 4033-4039.

Hart, M. J., A. Eva, T. Evans, S. A. Aaronson and R. A. Cerione (1991). "Catalysis of guanine nucleotide exchange on the CDC42Hs protein by the dbl oncogene product." *Nature* **354**(6351): 311-314.

Hatakeyama, R., K. Kono and S. Yoshida (2017). "Ypk1 and Ypk2 kinases maintain Rho1 at the plasma membrane by flippase-dependent lipid remodeling after membrane stresses." *J Cell Sci* **130**(6): 1169-1178.

Haupt, A. and N. Minc (2017). "Gradients of phosphatidylserine contribute to plasma membrane charge localization and cell polarity in fission yeast." *Mol Biol Cell* **28**(1): 210-220.

Heinisch, J. J., A. Lorberg, H. P. Schmitz and J. J. Jacoby (1999). "The protein kinase C-mediated MAP kinase pathway involved in the maintenance of cellular integrity in Saccharomyces cerevisiae." *Mol Microbiol* **32**(4): 671-680.

Heo, W. D., T. Inoue, W. S. Park, M. L. Kim, B. O. Park, T. J. Wandless and T. Meyer (2006). "PI(3,4,5)P3 and PI(4,5)P2 lipids target proteins with polybasic clusters to the plasma membrane." *Science* **314**(5804): 1458-1461.

Herrmann, A., B. A. Tillmann, J. Schurmann, M. Bolker and P. Tudzynski (2014). "Small-GTPase-associated signaling by the guanine nucleotide exchange factors CpDock180 and CpCdc24, the GTPase effector CpSte20, and the scaffold protein CpBem1 in Claviceps purpurea." *Eukaryot Cell* **13**(4): 470-482.

Hilger, D., M. Masureel and B. K. Kobilka (2018). "Structure and dynamics of GPCR signaling complexes." *Nature Structural & Molecular Biology* **25**(1): 4-12.

Ho, Y., A. Gruhler, A. Heilbut, G. D. Bader, L. Moore, S. L. Adams, A. Millar, et al. (2002). "Systematic identification of protein complexes in Saccharomyces cerevisiae by mass spectrometry." *Nature* **415**(6868): 180-183.

Hodge, R. G. and A. J. Ridley (2016). "Regulating Rho GTPases and their regulators." *Nature Reviews Molecular Cell Biology* **17**(8): 496-510.

Holt, L. J., B. B. Tuch, J. Villen, A. D. Johnson, S. P. Gygi and D. O. Morgan (2009). "Global analysis of Cdk1 substrate phosphorylation sites provides insights into evolution." *Science* **325**(5948): 1682-1686.

Hope, H., S. Bogliolo, R. A. Arkowitz and M. Bassilana (2008). "Activation of Rac1 by the guanine nucleotide exchange factor Dck1 is required for invasive filamentous growth in the pathogen Candida albicans." *Mol Biol Cell* **19**(9): 3638-3651.

Hope, H., C. Schmauch, R. A. Arkowitz and M. Bassilana (2010). "The Candida albicans ELMO homologue functions together with Rac1 and Dck1, upstream of the MAP Kinase Cek1, in invasive filamentous growth." *Mol Microbiol* **76**(6): 1572-1590.

Iakoucheva, L. M., P. Radivojac, C. J. Brown, T. R. O'Connor, J. G. Sikes, Z. Obradovic and A. K. Dunker (2004). "The importance of intrinsic disorder for protein phosphorylation." *Nucleic Acids Res* **32**(3): 1037-1049.

Imai, J., A. Toh-e and Y. Matsui (1996). "Genetic analysis of the Saccharomyces cerevisiae RHO3 gene, encoding a rho-type small GTPase, provides evidence for a role in bud formation." *Genetics* **142**(2): 359-369.

Ingrell, C. R., M. L. Miller, O. N. Jensen and N. Blom (2007). "NetPhosYeast: prediction of protein phosphorylation sites in yeast." *Bioinformatics* **23**(7): 895-897.

Isomura, M., K. Kaibuchi, T. Yamamoto, S. Kawamura, M. Katayama and Y. Takai (1990). "Partial purification and characterization of GDP dissociation stimulator (GDS) for the rho proteins from bovine brain cytosol." *Biochem Biophys Res Commun* **169**(2): 652-659.

Jorgensen, P., I. Rupes, J. R. Sharom, L. Schneper, J. R. Broach and M. Tyers (2004). "A dynamic transcriptional network communicates growth potential to ribosome synthesis and critical cell size." *Genes Dev* **18**(20): 2491-2505.

Karnoub, A. E., C. J. Der and S. L. Campbell (2001). "The insert region of Rac1 is essential for membrane ruffling but not cellular transformation." *Mol Cell Biol* **21**(8): 2847-2857.

Kato, K., A. D. Cox, M. M. Hisaka, S. M. Graham, J. E. Buss and C. J. Der (1992). "Isoprenoid addition to Ras protein is the critical modification for its membrane association and transforming activity." *Proc Natl Acad Sci U S A* **89**(14): 6403-6407.

Kirchrath, L., A. Lorberg, H. P. Schmitz, U. Gengenbacher and J. J. Heinisch (2000). "Comparative genetic and physiological studies of the MAP kinase Mpk1p from Kluyveromyces lactis and Saccharomyces cerevisiae." *Journal of Molecular Biology* **300**(4): 743-758.

Klecker, T., D. Scholz, J. Fortsch and B. Westermann (2013). "The yeast cell cortical protein Num1 integrates mitochondrial dynamics into cellular architecture." *J Cell Sci* **126**(Pt 13): 2924-2930.

Kock, C., Y. F. Dufrene and J. J. Heinisch (2015). "Up against the wall: is yeast cell wall integrity ensured by mechanosensing in plasma membrane microdomains?" *Appl Environ Microbiol* **81**(3): 806-811.

Kranenburg, O., M. Poland, M. Gebbink, L. Oomen and W. H. Moolenaar (1997). "Dissociation of LPA-induced cytoskeletal contraction from stress fiber formation by differential localization of RhoA." *J Cell Sci* **110 (Pt 19)**: 2417-2427.

Lanning, C. C., J. L. Daddona, R. Ruiz-Velasco, S. H. Shafer and C. L. Williams (2004). "The Rac1 C-terminal polybasic region regulates the nuclear localization and protein degradation of Rac1." *J Biol Chem* **279**(42): 44197-44210.

Lanning, C. C., R. Ruiz-Velasco and C. L. Williams (2003). "Novel mechanism of the co-regulation of nuclear transport of SmgGDS and Rac1." *J Biol Chem* **278**(14): 12495-12506.

Leventis, P. A. and S. Grinstein (2010). "The distribution and function of phosphatidylserine in cellular membranes." *Annu Rev Biophys* **39**: 407-427.

Lim, K. H., D. C. Brady, D. F. Kashatus, B. B. Ancrile, C. J. Der, A. D. Cox and C. M. Counter (2010). "Aurora-A phosphorylates, activates, and relocalizes the small GTPase RalA." *Mol Cell Biol* **30**(2): 508-523.

Longtine, M. S., A. McKenzie, 3rd, D. J. Demarini, N. G. Shah, A. Wach, A. Brachat, P. Philippsen, et al. (1998). "Additional modules for versatile and economical PCR-based gene deletion and modification in Saccharomyces cerevisiae." *Yeast* **14**(10): 953-961.

Lu, M., J. M. Kinchen, K. L. Rossman, C. Grimsley, M. Hall, J. Sondek, M. O. Hengartner, et al. (2005). "A Steric-inhibition model for regulation of nucleotide exchange via the Dock180 family of GEFs." *Curr Biol* **15**(4): 371-377.

Madaule, P. and R. Axel (1985). "A novel ras-related gene family." *Cell* **41**(1): 31-40.

Madigan, J. P., B. O. Bodemann, D. C. Brady, B. J. Dewar, P. J. Keller, M. Leitges, M. R. Philips, et al. (2009). "Regulation of Rnd3 localization and function by protein kinase C alpha-mediated phosphorylation." *Biochem J* **424**(1): 153-161.

Magalhaes, M. A. and M. Glogauer (2010). "Pivotal Advance: Phospholipids determine net membrane surface charge resulting in differential localization of active Rac1 and Rac2." *J Leukoc Biol* **87**(4): 545-555.

Magri, A., M. C. Di Rosa, M. F. Tomasello, F. Guarino, S. Reina, A. Messina and V. De Pinto (2016). "Overexpression of human SOD1 in VDAC1-less yeast restores mitochondrial functionality modulating beta-barrel outer membrane protein genes." *Biochim Biophys Acta* **1857**(6): 789-798.

Marei, H. and A. Malliri (2017). "Rac1 in human diseases: The therapeutic potential of targeting Rac1 signaling regulatory mechanisms." *Small GTPases* **8**(3): 139-163.

Matsui, Y. and A. Tohe (1992). "Yeast Rho3 and Rho4 Ras Superfamily Genes Are Necessary for Bud Growth, and Their Defect Is Suppressed by a High-Dose of Bud Formation Genes-Cdc42 and Bem1." *Molecular and Cellular Biology* **12**(12): 5690-5699.

Meca, J., A. Massoni-Laporte, D. Martinez, E. Sartorel, A. Loquet, B. Habenstein and D. McCusker (2019). "Avidity-driven polarity establishment via multivalent lipid-GTPase module interactions." *EMBO J* **38**(3).

Michaelson, D., W. Abidi, D. Guardavaccaro, M. Zhou, I. Ahearn, M. Pagano and M. R. Philips (2008). "Rac1 accumulates in the nucleus during the G2 phase of the cell cycle and promotes cell division." *J Cell Biol* **181**(3): 485-496.

Michaelson, D., J. Silletti, G. Murphy, P. D'Eustachio, M. Rush and M. R. Philips (2001). "Differential localization of Rho GTPases in live cells: Regulation by hypervariable regions and RhoGDI binding." *Journal of Cell Biology* **152**(1): 111-126.

Miller, T. E., K. M. Henkels, M. Huddleston, R. Salisbury, S. M. Hussain, A. T. Sasaki and K. J. Cho (2019). "Depletion of phosphatidylinositol 4-phosphate at the Golgi translocates K-Ras to mitochondria." *J Cell Sci* **132**(16).

Mitchell, L., G. A. Hobbs, A. Aghajanian and S. L. Campbell (2013). "Redox regulation of Ras and Rho GTPases: mechanism and function." *Antioxid Redox Signal* **18**(3): 250-258.

Morano, K. A., C. M. Grant and W. S. Moye-Rowley (2012). "The response to heat shock and oxidative stress in Saccharomyces cerevisiae." *Genetics* **190**(4): 1157-1195.

Morgenstern, M., S. B. Stiller, P. Lubbert, C. D. Peikert, S. Dannenmaier, F. Drepper, U. Weill, et al. (2017). "Definition of a High-Confidence Mitochondrial Proteome at Quantitative Scale." *Cell Rep* **19**(13): 2836-2852.

Nordmann, D., M. Lickfeld, V. Warnsmann, J. Wiechert, A. Jendretzki and H. P. Schmitz (2014). "The small GTP-binding proteins AgRho2 and AgRho5 regulate tip-branching, maintenance of the growth axis and actin-ring-integrity in the filamentous fungus Ashbya gossypii." *PLoS One* **9**(8): e106236.

Nusser, N., E. Gosmanova, N. Makarova, Y. Fujiwara, L. Yang, F. Guo, Y. Luo, et al. (2006). "Serine phosphorylation differentially affects RhoA binding to effectors: implications to NGF-induced neurite outgrowth." *Cell Signal* **18**(5): 704-714.

Olson, M. F. (2018). "Rho GTPases, their post-translational modifications, disease-associated mutations and pharmacological inhibitors." *Small GTPases* **9**(3): 203-215.

Osborn-Heaford, H. L., A. J. Ryan, S. Murthy, A. M. Racila, C. He, J. C. Sieren, D. R. Spitz, et al. (2012). "Mitochondrial Rac1 GTPase import and electron transfer from cytochrome c are required for pulmonary fibrosis." *J Biol Chem* **287**(5): 3301-3312.

Palczewski, K. (2006). "G protein-coupled receptor rhodopsin." *Annu Rev Biochem* **75**: 743-767.

Park, H. O. and E. Bi (2007). "Central roles of small GTPases in the development of cell polarity in yeast and beyond." *Microbiol Mol Biol Rev* **71**(1): 48-96.

Patel, M., Y. Margaron, N. Fradet, Q. Yang, B. Wilkes, M. Bouvier, K. Hofmann, et al. (2010). "An evolutionarily conserved autoinhibitory molecular switch in ELMO proteins regulates Rac signaling." *Curr Biol* **20**(22): 2021-2027.

Patel, M., A. Pelletier and J. F. Cote (2011). "Opening up on ELMO regulation: New insights into the control of Rac signaling by the DOCK180/ELMO complex." *Small GTPases* **2**(5): 268-275.

Peeters, K., F. Van Leemputte, B. Fischer, B. M. Bonini, H. Quezada, M. Tsytlonok, D. Haesen, et al. (2017). "Fructose-1,6-bisphosphate couples glycolytic flux to activation of Ras." *Nat Commun* **8**(1): 922.

Peifer, M., S. Berg and A. B. Reynolds (1994). "A repeating amino acid motif shared by proteins with diverse cellular roles." *Cell* **76**(5): 789-791.

Pereira, C., N. Camougrand, S. Manon, M. J. Sousa and M. Corte-Real (2007). "ADP/ATP carrier is required for mitochondrial outer membrane permeabilization and cytochrome c release in yeast apoptosis." *Mol Microbiol* **66**(3): 571-582.

Perez, P. and S. A. Rincon (2010). "Rho GTPases: regulation of cell polarity and growth in yeasts." *Biochem J* **426**(3): 243-253.

Philips, M. R., M. H. Pillinger, R. Staud, C. Volker, M. G. Rosenfeld, G. Weissmann and J. B. Stock (1993). "Carboxyl methylation of Ras-related proteins during signal transduction in neutrophils." *Science* **259**(5097): 977-980.

Phuyal, S. and H. Farhan (2019). "Multifaceted Rho GTPase Signaling at the Endomembranes." *Front Cell Dev Biol* **7**: 127.

Premkumar, L., A. A. Bobkov, M. Patel, L. Jaroszewski, L. A. Bankston, B. Stec, K. Vuori, et al. (2010). "Structural basis of membrane targeting by the Dock180 family of Rho family guanine exchange factors (Rho-GEFs)." *J Biol Chem* **285**(17): 13211-13222.

Prouzet-Mauleon, V., F. Lefebvre, D. Thoraval, M. Crouzet and F. Doignon (2008). "Phosphoinositides affect both the cellular distribution and activity of the F-BAR-containing RhoGAP Rgd1p in yeast." *J Biol Chem* **283**(48): 33249-33257.

Quatela, S. E., P. J. Sung, I. M. Ahearn, T. G. Bivona and M. R. Philips (2008). "Analysis of K-Ras phosphorylation, translocation, and induction of apoptosis." *Methods Enzymol* **439**: 87-102.

Rajasekharan, S. K. and T. Raman (2013). "Ras and Ras mutations in cancer." *Central European Journal of Biology* **8**(7): 609-624.

Ridley, A. J. and A. Hall (1992). "The small GTP-binding protein rho regulates the assembly of focal adhesions and actin stress fibers in response to growth factors." *Cell* **70**(3): 389-399.

Robbe, K., A. Otto-Bruc, P. Chardin and B. Antonny (2003). "Dissociation of GDP dissociation inhibitor and membrane translocation are required for efficient activation of Rac by the Dbl homology-pleckstrin homology region of Tiam." *J Biol Chem* **278**(7): 4756-4762.

Roberts, P. J., N. Mitin, P. J. Keller, E. J. Chenette, J. P. Madigan, R. O. Currin, A. D. Cox, et al. (2008). "Rho Family GTPase modification and dependence on CAAX motif-signaled posttranslational modification." *J Biol Chem* **283**(37): 25150-25163.

Rolland, F., J. H. De Winde, K. Lemaire, E. Boles, J. M. Thevelein and J. Winderickx (2000). "Glucose-induced cAMP signalling in yeast requires both a G-protein coupled receptor system for extracellular glucose detection and a separable hexose kinase-dependent sensing process." *Mol Microbiol* **38**(2): 348-358.

Rolli-Derkinderen, M., V. Sauzeau, L. Boyer, E. Lemichez, C. Baron, D. Henrion, G. Loirand, et al. (2005). "Phosphorylation of serine 188 protects RhoA from ubiquitin/proteasome-mediated degradation in vascular smooth muscle cells." *Circ Res* **96**(11): 1152-1160.

Ron, D., M. Zannini, M. Lewis, R. B. Wickner, L. T. Hunt, G. Graziani, S. R. Tronick, et al. (1991). "A region of proto-dbl essential for its transforming activity shows sequence similarity to a yeast cell cycle gene, CDC24, and the human breakpoint cluster gene, bcr." *New Biol* **3**(4): 372-379.

Rossman, K. L., C. J. Der and J. Sondek (2005). "GEF means go: turning on RHO GTPases with guanine nucleotide-exchange factors." *Nat Rev Mol Cell Biol* **6**(2): 167-180.

Rothbauer, U., K. Zolghadr, S. Tillib, D. Nowak, L. Schermelleh, A. Gahl, N. Backmann, et al. (2006). "Targeting and tracing antigens in live cells with fluorescent nanobodies." *Nat Methods* **3**(11): 887-889.

Santangelo, G. M. (2006). "Glucose signaling in Saccharomyces cerevisiae." *Microbiol Mol Biol Rev* **70**(1): 253-282.

Sasaki, T., M. Kato and Y. Takai (1993). "Consequences of weak interaction of rho GDI with the GTP-bound forms of rho p21 and rac p21." *J Biol Chem* **268**(32): 23959-23963.

Schacherer, J., D. M. Ruderfer, D. Gresham, K. Dolinski, D. Botstein and L. Kruglyak (2007). "Genome-wide analysis of nucleotide-level variation in commonly used Saccharomyces cerevisiae strains." *PLoS One* **2**(3): e322.

Schaefer, A., N. R. Reinhard and P. L. Hordijk (2014). "Toward understanding RhoGTPase specificity: structure, function and local activation." *Small GTPases* **5**(2): 6.

Scheffzek, K., M. R. Ahmadian, W. Kabsch, L. Wiesmuller, A. Lautwein, F. Schmitz and A. Wittinghofer (1997). "The Ras-RasGAP complex: structural basis for GTPase activation and its loss in oncogenic Ras mutants." *Science* **277**(5324): 333-338.

Schmick, M., N. Vartak, B. Papke, M. Kovacevic, D. C. Truxius, L. Rossmannek and P. I. H. Bastiaens (2014). "KRas localizes to the plasma membrane by spatial cycles of solubilization, trapping and vesicular transport." *Cell* **157**(2): 459-471.

Schmitz, H. P., S. Huppert, A. Lorberg and J. J. Heinisch (2002). "Rho5p downregulates the yeast cell integrity pathway." *J Cell Sci* **115**(Pt 15): 3139-3148.

Schmitz, H. P., A. Jendretzki, C. Sterk and J. J. Heinisch (2018). "The Small Yeast GTPase Rho5 and Its Dimeric GEF Dck1/Lmo1 Respond to Glucose Starvation." *Int J Mol Sci* **19**(8).

Schmitz, H. P., A. Jendretzki, J. Wittland, J. Wiechert and J. J. Heinisch (2015). "Identification of Dck1 and Lmo1 as upstream regulators of the small GTPase Rho5 in Saccharomyces cerevisiae." *Mol Microbiol* **96**(2): 306-324.

Sharmeen, N., T. Sulea, M. Whiteway and C. Wu (2019). "The adaptor protein Ste50 directly modulates yeast MAPK signaling specificity through differential connections of its RA domain." *Mol Biol Cell* **30**(6): 794-807.

Sheff, M. A. and K. S. Thorn (2004). "Optimized cassettes for fluorescent protein tagging in Saccharomyces cerevisiae." *Yeast* **21**(8): 661-670.

Shinjo, K., J. G. Koland, M. J. Hart, V. Narasimhan, D. I. Johnson, T. Evans and R. A. Cerione (1990). "Molecular cloning of the gene for the human placental GTP-binding protein Gp (G25K): identification of this GTP-binding protein as the human homolog of the yeast cell-division-cycle protein CDC42." *Proc Natl Acad Sci U S A* **87**(24): 9853-9857.

Sickmann, A., J. Reinders, Y. Wagner, C. Joppich, R. Zahedi, H. E. Meyer, B. Schonfisch, et al. (2003). "The proteome of Saccharomyces cerevisiae mitochondria." *Proc Natl Acad Sci U S A* **100**(23): 13207-13212.

Silvius, J. R., P. Bhagatji, R. Leventis and D. Terrone (2006). "K-ras4B and prenylated proteins lacking "second signals" associate dynamically with cellular membranes." *Mol Biol Cell* **17**(1): 192-202.

Singh, K., P. J. Kang and H. O. Park (2008). "The Rho5 GTPase is necessary for oxidant-induced cell death in budding yeast." *Proc Natl Acad Sci U S A* **105**(5): 1522-1527.

Singh, K., M. E. Lee, M. Entezari, C. H. Jung, Y. Kim, Y. Park, J. D. Fioretti, et al. (2019). "Genome-Wide Studies of Rho5-Interacting Proteins That Are Involved in Oxidant-Induced Cell Death in Budding Yeast." *G3 (Bethesda)* **9**(3): 921-931.

Slaughter, B. D., A. Das, J. W. Schwartz, B. Rubinstein and R. Li (2009). "Dual modes of cdc42 recycling fine-tune polarized morphogenesis." *Dev Cell* **17**(6): 823-835.

Smith, G. R., S. A. Givan, P. Cullen and G. F. Sprague, Jr. (2002). "GTPase-activating proteins for Cdc42." *Eukaryot Cell* **1**(3): 469-480.

Sterk, C., L. Graber, H. P. Schmitz and J. J. Heinisch (2019). "Analysis of Functional Domains in Rho5, the Yeast Homolog of Human Rac1 GTPase, in Oxidative Stress Response." *Int J Mol Sci* **20**(22).

Swaney, D. L., P. Beltrao, L. Starita, A. Guo, J. Rush, S. Fields, N. J. Krogan, et al. (2013). "Global analysis of phosphorylation and ubiquitylation cross-talk in protein degradation." *Nat Methods* **10**(7): 676-682.

Tait, S. W. and D. R. Green (2012). "Mitochondria and cell signalling." *J Cell Sci* **125**(Pt 4): 807-815.

Tang, X., J. J. Punch and W. L. Lee (2009). "A CAAX motif can compensate for the PH domain of Num1 for cortical dynein attachment." *Cell Cycle* **8**(19): 3182-3190.

Tcherkezian, J. and N. Lamarche-Vane (2007). "Current knowledge of the large RhoGAP family of proteins." *Biol Cell* **99**(2): 67-86.

Thevelein, J. M. and J. H. de Winde (1999). "Novel sensing mechanisms and targets for the cAMP-protein kinase A pathway in the yeast Saccharomyces cerevisiae." *Mol Microbiol* **33**(5): 904-918.

Thompson, J. D., D. G. Higgins and T. J. Gibson (1994). "CLUSTAL W: improving the sensitivity of progressive multiple sequence alignment through sequence weighting, position-specific gap penalties and weight matrix choice." *Nucleic Acids Res* **22**(22): 4673-4680.

Tiedje, C., I. Sakwa, U. Just and T. Hofken (2008). "The Rho GDI Rdi1 regulates Rho GTPases by distinct mechanisms." *Mol Biol Cell* **19**(7): 2885-2896.

Tolias, K. F., A. D. Couvillon, L. C. Cantley and C. L. Carpenter (1998). "Characterization of a Rac1- and RhoGDI-associated lipid kinase signaling complex." *Mol Cell Biol* **18**(2): 762-770.

Tyanova, S., J. Cox, J. Olsen, M. Mann and D. Frishman (2013). "Phosphorylation variation during the cell cycle scales with structural propensities of proteins." *PLoS Comput Biol* **9**(1): e1002842.

Ueyama, T., M. Eto, K. Kami, T. Tatsuno, T. Kobayashi, Y. Shirai, M. R. Lennartz, et al. (2005). "Isoform-specific membrane targeting mechanism of Rac during Fc gamma R-mediated phagocytosis: positive charge-dependent and independent targeting mechanism of Rac to the phagosome." *J Immunol* **175**(4): 2381-2390.

Urban, J., A. Soulard, A. Huber, S. Lippman, D. Mukhopadhyay, O. Deloche, V. Wanke, et al. (2007). "Sch9 is a major target of TORC1 in Saccharomyces cerevisiae." *Mol Cell* **26**(5): 663-674.

Valencia, A., P. Chardin, A. Wittinghofer and C. Sander (1991). "The ras protein family: evolutionary tree and role of conserved amino acids." *Biochemistry* **30**(19): 4637-4648.

van der Lee, R., M. Buljan, B. Lang, R. J. Weatheritt, G. W. Daughdrill, A. K. Dunker, M. Fuxreiter, et al. (2014). "Classification of intrinsically disordered regions and proteins." *Chem Rev* **114**(13): 6589-6631.

van Hennik, P. B., J. P. ten Klooster, J. R. Halstead, C. Voermans, E. C. Anthony, N. Divecha and P. L. Hordijk (2003). "The C-terminal domain of Rac1 contains two motifs that control targeting and signaling specificity." *J Biol Chem* **278**(40): 39166-39175.

van Unen, J., N. R. Reinhard, T. Yin, Y. I. Wu, M. Postma, T. W. Gadella and J. Goedhart (2015). "Plasma membrane restricted RhoGEF activity is sufficient for RhoA-mediated actin polymerization." *Sci Rep* **5**: 14693.

Vauchelles, R., D. Stalder, T. Botton, R. A. Arkowitz and M. Bassilana (2010). "Rac1 dynamics in the human opportunistic fungal pathogen Candida albicans." *PLoS One* **5**(10): e15400.

Wang, G. and R. J. Deschenes (2006). "Plasma membrane localization of Ras requires class C Vps proteins and functional mitochondria in Saccharomyces cerevisiae." *Mol Cell Biol* **26**(8): 3243-3255.

Wang, N., M. Wang, Y. H. Zhu, T. W. Grosel, D. Sun, D. S. Kudryashov and J. Q. Wu (2015). "The Rho-GEF Gef3 interacts with the septin complex and activates the GTPase Rho4 during fission yeast cytokinesis." *Mol Biol Cell* **26**(2): 238-255.

Wei, M., P. Fabrizio, J. Hu, H. Ge, C. Cheng, L. Li and V. D. Longo (2008). "Life span extension by calorie restriction depends on Rim15 and transcription factors downstream of Ras/PKA, Tor, and Sch9." *PLoS Genet* **4**(1): e13.

Wennerberg, K. and C. J. Der (2004). "Rho-family GTPases: it's not only Rac and Rho (and I like it)." *J Cell Sci* **117**(Pt 8): 1301-1312.

Williams, C. L. (2003). "The polybasic region of Ras and Rho family small GTPases: a regulator of protein interactions and membrane association and a site of nuclear localization signal sequences." *Cell Signal* **15**(12): 1071-1080.

Woods, B., C. C. Kuo, C. F. Wu, T. R. Zyla and D. J. Lew (2015). "Polarity establishment requires localized activation of Cdc42." *J Cell Biol* **211**(1): 19-26.

Wu, H. and P. Brennwald (2010). "The function of two Rho family GTPases is determined by distinct patterns of cell surface localization." *Mol Cell Biol* **30**(21): 5207-5217.

Xue, C., Y. P. Hsueh and J. Heitman (2008). "Magnificent seven: roles of G protein-coupled receptors in extracellular sensing in fungi." *FEMS Microbiol Rev* **32**(6): 1010-1032.

Yang, Y., M. Park, M. Maekawa and G. D. Fairn (2019). "Enforced expression of phosphatidylinositol 4-phosphate 5-kinase homolog alters PtdIns(4,5)P2 distribution and the localization of small G-proteins." *Sci Rep* **9**(1): 14789.

Yeung, T., G. E. Gilbert, J. Shi, J. Silvius, A. Kapus and S. Grinstein (2008). "Membrane phosphatidylserine regulates surface charge and protein localization." *Science* **319**(5860): 210-213.

Yoon, Y., E. W. Krueger, B. J. Oswald and M. A. McNiven (2003). "The mitochondrial protein hFis1 regulates mitochondrial fission in mammalian cells through an interaction with the dynamin-like protein DLP1." *Mol Cell Biol* **23**(15): 5409-5420.

Yoshida, S., S. Bartolini and D. Pellman (2009). "Mechanisms for concentrating Rho1 during cytokinesis." *Genes Dev* **23**(7): 810-823.

Zaman, S., S. I. Lippman, L. Schneper, N. Slonim and J. R. Broach (2009). "Glucose regulates transcription in yeast through a network of signaling pathways." *Mol Syst Biol* **5**: 245.

Zhang, S. Y., B. Sperlich, F. Y. Li, S. Al-Ayoubi, H. X. Chen, Y. F. Zhao, Y. M. Li, et al. (2017). "Phosphorylation Weakens but Does Not Inhibit Membrane Binding and Clustering of K-Ras4B." *ACS Chem Biol* **12**(6): 1703-1710.

Zhao, D. and C. Pothoulakis (2003). "Rho GTPases as therapeutic targets for the treatment of inflammatory diseases." *Expert Opin Ther Targets* **7**(5): 583-592.

Zhou, Y., J. L. Johnson, R. A. Cerione and J. W. Erickson (2013). "Prenylation and membrane localization of Cdc42 are essential for activation by DOCK7." *Biochemistry* **52**(25): 4354-4363.

Zong, H., K. Kaibuchi and L. A. Quilliam (2001). "The insert region of RhoA is essential for Rho kinase activation and cellular transformation." *Mol Cell Biol* **21**(16): 5287-5298.

7. Acknowledgements/Danksagung

First of all, I want to thank Professor Jürgen Heinisch for the opportunity to work on my PhD thesis, for helping me throughout the years (even on his 60. birthday), and for being a nice supervisor.

Secondly, I want to thank Professor Joost Holthuis for taking a part in my dissertation as second supervisor.

Thanks also to Prof. Achim Paululat and Heiko Harten for joining the dissertation committee.

I want to thank PD Dr. Hans-Peter Schmitz for the invaluable help and impulses over the last years, on a scientific and on a technical level and pretty much everything concerning the fluorescence microscope.

I also want to thank Christian and Severin a lot for the much needed help especially at the beginning of my thesis and all the hilarious moments and discussions that made lab work enjoyable and **SO** much less frustrating. Likewise, thanks to Julia and Marius for supporting me during my lab time and dissertation, for the funny talks and for being cool colleagues. Thanks also to Anne, Dorthe, Doris and Sascha and the rest of the genetic department for having been great and supporting colleagues.

I am very thankful for all my friends who supported me and cheered me on, especially on the finishing straight. Thanks also to those who bravely battled through my dissertation.

Special thanks to my husband Axel, who over the last years has been supporting, encouraging and cheering me up over and over again even in difficult times. I cannot thank him enough and without him I would not be where I am now.

A big thank you for my parents Norbert and Doris who made studying possible and who over the last years have been very supportive along the way.

Thanks to the bouldering hall “Zenit” for the much needed physical and my DSA group for mental balance and distraction.

My rabbits Krümel, Flöckchen, Nulli and Finchen who were and always have been there for a cuddle.

8. Statutory declaration

Erklärung über die Eigenständigkeit der erbrachten wissenschaftlichen Leistung

Ich erkläre hiermit, dass ich die vorliegende Arbeit ohne unzulässige Hilfe Dritter und ohne Benutzung anderer als der angegebenen Hilfsmittel angefertigt habe. Die aus anderen Quellen direkt oder indirekt übernommenen Daten und Konzepte sind unter Angabe der Quelle gekennzeichnet. Bei der Auswahl und Auswertung folgenden Materials haben mir die nachstehend aufgeführten Personen in der jeweils beschriebenen Weise unentgeltlich geholfen. Im Rahmen von Abschlussarbeiten wurde ein Teil der Laborarbeiten gemeinsam mit Studenten durchgeführt:

- Der Stamm HLAO2, der für den Stamm HCSO102-B verwendet wurde, wurde von Lauren Gräber konstruiert. Die Wachstumskurven aus Figure 36 wurden in Zusammenarbeit mit Lauren Gräber erstellt. Zudem wurde ein Teil der von ihr erstellten mikroskopischen Aufnahmen zur statistischen Auswertung in Figure 21 verwendet.
- Der Tropftest in Figure 33 ist in Zusammenarbeit mit Aileen Faist entstanden und im Tropftest Figure 34 wurde HAFO1, ein von Aileen Faist konstruierter Stamm, verwendet.

Weitere Personen waren an der inhaltlichen materiellen Erstellung der vorliegenden Arbeit nicht beteiligt. Insbesondere habe ich hierfür nicht die entgeltliche Hilfe von Vermittlungs- bzw. Beratungsdiensten (Promotionsberater oder andere Personen) in Anspruch genommen. Niemand hat von mir unmittelbar oder mittelbar geldwerte Leistungen für Arbeiten erhalten, die im Zusammenhang mit dem Inhalt der vorgelegten Dissertation stehen. Die Arbeit wurde bisher weder im In- noch im Ausland in gleicher oder ähnlicher Form einer anderen Prüfungsbehörde vorgelegt.

_____ _____

(Ort, Datum) (Unterschrift)

9. Curriculum vitae

Name: **Carolin Christin Sterk**
Date of birth: **10/07/1984**
Place of birth: **Nordhorn**
Nationality: **German**

University Education

04/2014 – 08/2020	**Doctoral studies** University of Osnabrück (Germany) Department of Genetics Supervisor: Prof. Dr. rer. nat. Jürgen J. Heinisch Dissertation: „The role of Rho5 in oxidative stress response and glucose signalling in *Saccharomyces cerevisiae*“ Presumed degree: Doctor rerum naturalium (Dr. rer. nat.)
01/2014 – 03/2014	Research assistant University of Osnabrück (Germany)
10/2011 – 09/2013	**M.Sc. Biology – Cell- and Molecular biology** University of Osnabrück (Germany) Master thesis: „Charakterisierung der Chitinsynthasen in *Ashbya gossypii*“ Department of Genetics Supervisor: Priv. Doz. Dr. rer. nat. Hans-Peter Schmitz
10/2008 – 09/2011	**B.Sc. Biology of the cell** University of Osnabrück (Germany) Bachelor thesis: „Klonierung, Reinigung und Expression des cytosolischen Loops von Mitgliedern der SLC45-Familie“ Department of Animal Physiology Supervisor: Prof. Dr. rer. nat. Helmut Wieczorek

Work practice

02/2007 – 09/2008	Employment as Pharmaceutical technical assistant

Apprenticeship

08/2004 – 01/2007	School-based education to Pharmaceutical technical assistant (PTA) Völkerschule Osnabrück Osnabrück, Germany

School Education

1997-2004	Gymnasium am Stadtring, Nordhorn, Germany

Publications

- **„The Small Yeast GTPase Rho5 and Its Dimeric GEF Dck1/Lmo1 Respond to Glucose Starvation“** H.-P. Schmitz, A. Jendretzki, **C. Sterk** and J. J. Heinisch; *Int. J. Mol. Sci.* 2018, 19, 2186; doi:10.3390/ijms19082186

- **„Analysis of Functional Domains in Rho5, the Yeast Homolog of Human Rac1 GTPase, in Oxidative Stress Response“ C. Sterk**, L. Gräber, H.-P. Schmitz and J. J. Heinisch; *Int. J. Mol. Sci.* 2019, 20(22), 5550; https://doi.org/10.3390/ijms20225550

Conferences

- **12th International Meeting on Yeast Apoptosis (IMYA)**, Bari, Italy 14 – 18/05/2017
  Poster presentation (Poster price)

- **13th International Meeting on Yeast Apoptosis (IMYA)**, Leuven, Belgium, 26 – 30/08/2018
  Presentation